Activity-based proteomics of the endocannabinoid system

Rooden, E.J. van

Activity-based proteomics of the endocannabinoid system

PROEFSCHRIFT

ter verkrijging van
de graad van Doctor aan de Universiteit Leiden,
op gezag van Rector Magnificus prof. mr. C. J. J. M. Stolker,
volgens het besluit van het College voor Promoties
te verdedigen op 11 september 2018
klokke 15.00 uur

door

Eva Jacoba van Rooden

Geboren te Leiden in 1990

Promotiecommissie

Promotoren	Prof. dr. M. van der Stelt
	Prof. dr. H. S. Overkleeft
Overige leden	Prof. dr. J. M. F. G. Aerts
	Prof. dr. J. Brouwer
	Prof. dr. F. J. Dekker
	Prof. dr. G. A. van der Marel
	Dr. L. Willems

Printed by Gildeprint

Table of contents

Abbreviations 6

Chapter 1 9

General introduction

Chapter 2 19

Activity-based protein profiling

Chapter 3 35

Chemical proteomic analysis of endocannabinoid hydrolase activity in Niemann-Pick type C mouse brain

Chapter 4 49

Mapping *in vivo* target interaction profiles of covalent inhibitors using chemical proteomics with label-free quantification

Chapter 5 **81**

Design and synthesis of quenched activity-based probes
for diacylglycerol lipase and α/β-hydrolase domain containing protein 6

Chapter 6 **101**

Two-step activity-based protein profiling of diacylglycerol lipase

Chapter 7 **119**

Summary and future prospects

Samenvatting **135**

List of publications **138**

Curriculum Vitae **140**

Abbreviations

AA	arachidonic acid
ABP	activity-based probe
ABPP	activity-based protein profiling
ACN	acetonitrile (CH_3CN)
AEA	anandamide
2-AG	2-arachidonoylglycerol
aq.	aqueous
BOC	bioorthogonal chemistry
BODIPY	boron-dipyrromethene
BSA	bovine serum albumin
CB	cannabinoid receptor
CE-LIF	capillary electrophoresis - laser-induced fluorescence
CNS	central nervous system
CuAAC	copper(I)-catalyzed azide-alkyne [2 + 3] cycloaddition
DAGL	diacylglycerol lipase
Da	dalton
DCE	1,2-dichloroethane
DCM	dichloromethane (CH_2Cl_2)
DDA	data-dependent acquisition
DDQ	2,3-dichloro-5,6-dicyano-p-benzoquinone
DFT	density functional theory
DIA	data-independent acquisition
DIPEA	*N*,*N*-diisopropylethylamine
DMAP	4-(dimethylamino)pyridine
DMF	*N*,*N*-dimethylformamide
DMSO	dimethyl sulfoxide ($(CH_3)_2SO$)
DNA	deoxyribonucleic acid
DTT	1,4-dithiothreitol
ECS	endocannabinoid system
EDC	1-ethyl-3-(3-dimethylaminopropyl)carbodiimide
ESI	electrospray ionization
EtOAc	ethyl acetate
FA	formic acid (HCOOH)
FAAH	fatty acid amide hydrolase
FDR	false discovery rate
FluoPol	fluorescence polarization
FP	fluorophosphonate
g	g force (relative centrifugal force)
GluFib	[Glu^1]-fibrinopeptide B
h	hour
HEPES	4-(2-hydroxyethyl)piperazine-1-ethanesulfonic acid
HPLC	high-performance liquid chromatography
HRMS	high-resolution mass spectrometry
HRP	horseradish peroxidase
IAA	iodoacetamide

IEDDA	inverse electron-demand Diels-Alder
IMS	ion mobility separation
KO	knockout
l	liquid
LC	liquid chromatography
MAGL	monoacylglycerol lipase
min	minutes
MS	mass spectrometry
m/z	mass divided by charge number
NAAA	N-acylethanolamine-hydrolyzing acid amidase
NAE	N-acyl ethanolamide
NAPE	N-arachidonoyl phosphatidylethanolamine
NMR	nuclear magnetic resonance
NPC	Niemann-Pick type C
o/n	overnight
PAGE	polyacrylamide gel electrophoresis
PBS	phosphate buffered saline
PE	phosphatidylethanolamine
PEI	polyethylenimine
PLA2G4E	phospholipase A2 group IVE
PLA/AT	phospholipase A/acyltransferase
PLC	phospholipase C
PLD	phospholipase D
PTM	post-translational modification
PTPN22	protein-tyrosine phosphatase non-receptor type 22
qTOF	quadrupole time-of-flight
R_f	retardation factor
rpm	revolutions per minute
rt	room temperature (18 - 24 °C)
sat.	saturated
SDS	sodium dodecyl sulfate
sec	seconds
SHIP1	SH2 domain-containing inositol 5'-phosphatase
sPLA2	secretory phospholipase A2
TBS	tris buffered saline
TFA	trifluoroacetic acid (CF_3COOH)
THC	Δ^9-tetrahydrocannabinol
THF	tetrahydrofuran
THL	tetrahydrolipstatin
TLC	thin-layer chromatography
TMS	trimethylsilyl (CH_3Si-)
tris	2-amino-2-(hydroxymethyl)propane-1,3-diol
v	volume
w	weight
WT	wildtype

Chapter 1

General introduction

The endocannabinoid system (ECS) consists of the cannabinoid receptors CB_1 and CB_2, their endogenous ligands and the enzymes that regulate the levels of these ligands.[1] The cannabinoid receptors were discovered as the targets of Δ^9-tetrahydrocannabinol (THC), the psychoactive constituent in marijuana. The main endogenous ligands of these receptors are the lipid signaling molecules 2-arachidonoylglycerol (2-AG) and anandamide (AEA). Numerous neurological processes are regulated by the ECS, including learning, memory, pain perception, feeding and reward behaviors.

The medicinal use of preparations of the plant *Cannabis sativa* has a long history. Currently, the endocannabinoid system is viewed as a promising target for the discovery of novel therapeutics.[2–5] However, the psychoactive properties of THC and other CB_1 agonists are undesirable for patients, and these as well as the addictive properties have led to their regulated use and restricted access. The adverse side-effects can potentially be avoided if the CB_1 receptor is not activated, by using antagonists or inverse agonists instead. Rimonabant was the first (and only) inverse agonist on the CB_1 receptor that was approved as an anti-obesity drug. Due to severe psychiatric side effects Rimonabant was removed from the market. The case of Rimonabant illustrates that targeting the ECS is a delicate balancing act due to its involvement in many physiological processes.[6] Therefore, an alternative approach to modulate CB_1 receptor activity is to target the endocannabinoid metabolizing enzymes. Small molecule inhibitors can block the activity of enzymes temporarily and change the levels of the receptor's endogenous ligands. This approach is promising for more controlled tuning of the ECS and finding a suitable therapeutic window.

Activity-based protein profiling (ABPP) is an excellent method for the discovery and optimization of drug candidates to target the ECS.[1] ABPP has benefitted from the tremendous developments in proteomics technology over the last twenty years.[7] ABPP can be used to map the interactions between small molecules and enzymes in living systems.[8] The fundamental biological role of the endocannabinoid enzymes can be studied by measuring when and where these proteins are active *in vivo* by using ABPP.[9] Additionally, a comparison of endocannabinoid enzyme activity can be made between healthy and diseased states.[10] Potential inhibitors can be screened for potency and selectivity simultaneously.[11] ABPP

also has the potential to be used for personalized medicine by guiding the drug and dose selection after measuring the level of enzyme activity in an individual patient.

Endocannabinoid enzymes

A variety of enzymes are involved in the biosynthesis and degradation of both 2-AG and AEA and are therefore potential targets for therapeutic intervention strategies aimed at modulating endocannabinoid levels. 2-AG is mainly generated by the hydrolysis of diacylglycerols, as catalyzed by two diacylglycerol lipases (DAGLα and DAGLβ) (**Fig. 1**).[12] Diacylglycerols are generated by phospholipases C-β (PLC-β) from phosphatidylinositol 4,5-bisphosphate (PIP2).[13,14]

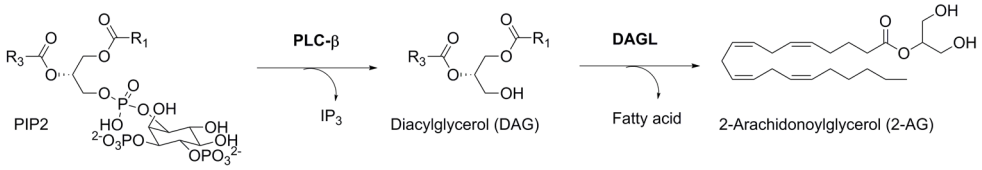

Figure 1 | Biosynthesis of 2-AG. DAGL: diacylglycerol lipase. IP3: inositol 1,4,5-trisphosphate. PIP2; phosphatidylinositol 4,5-bisphosphate. PLC: phospholipase C.

Anandamide is generated by N-acyl transferases that transfer arachidonic acid from the *sn*-1 position of membrane phospholipids to the primary amine of phosphatidylethanolamine (PE) to form N-arachidonoyl phosphatidylethanolamine (NAPE) (**Fig. 2**).[15] Several enzymes can catalyze this transfer: phospholipase A2 group IVE (PLA2G4E) is a calcium-dependent N-acyl transferase[16,17] and the phospholipase A/acyltransferase (PLA/AT) family are calcium-independent N-acyl transferases.[18] From NAPEs, several enzymatic routes can generate N-acyl ethanolamides (NAEs), including AEA.[19] The main route is hydrolysis by N-arachidonoyl phosphatidylethanolamine phospholipase D (NAPE-PLD).[20] Alternative pathways for anandamide synthesis are also proposed, such as via a phospholipase C to form phospho-anandamide, which is subsequently dephosphorylated by phosphatases SH2 domain-containing inositol 5'-phosphatase 1 (SHIP1) or protein-tyrosine phosphatase non-receptor type 22 (PTPN22).[21,22] Another possible route is via two hydrolysis steps by α/β-hydrolase domain containing protein 4 (ABHD4)[23] and one by glycerophosphodiester phosphodiesterase 1 (GDE1)[24] or GDE4.[25] A fourth proposed route goes from NAPE to NAE via secretory phospholipase A2 (sPLA2)[26] or ABHD4 and subsequent hydrolysis to NAE and phosphatidic acid by GDE4[25] or GDE7.[27]

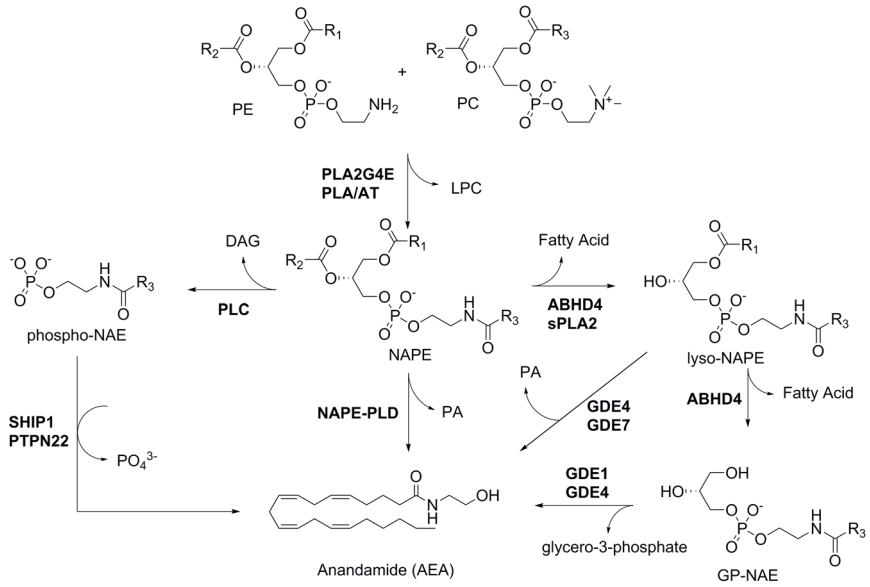

Figure 2 | Biosynthesis of anandamide. $R_{1/2}$: alkyl, R_3 = arachidonoyl. ABHD4: α/β-hydrolase domain containing protein 4. DAG: diacylglycerol. GDE: glycerophosphodiester phosphodiesterase. GP-NAE: *sn*-glycero-3-phospho-N-acylethanolamine . LPC: lysophosphatidylcholine. NAE: N-acylethanolamide. NAPE: N-arachidonoyl phosphatidylethanolamine. PA: phosphatidic acid. PC: phosphatidylcholine. PE: phosphatidylethanolamine. PLA/AT: phospholipase A/acyltransferase. PLA2G4E: phospholipase A2 group IVE. PLC: phospholipase C. PLD: phospholipase D. PTPN22: protein-tyrosine phosphatase non-receptor type 22. SHIP1: SH2 domain-containing inositol 5'-phosphatase 1. sPLA2: secretory phospholipase A2.

Both 2-AG and AEA are hydrolyzed to form arachidonic acid (AA) (**Fig. 3**). 2-AG is mainly hydrolyzed by monoacylglycerol lipase (MAGL),[28] and can also be hydrolyzed by ABHD6 and ABHD12 to form AA and glycerol.[29] Anandamide is hydrolyzed by fatty acid amide hydrolase (FAAH) to AA and ethanolamine.[30] At acidic pH, N-acylethanolamine-hydrolyzing acid amidase (NAAA) also hydrolyzes NAEs, including anandamide.[31]

Activity-based probes for the endocannabinoid system

ABPP relies on chemical probes that react with the catalytic nucleophile of target enzymes in their native biological environment.[32] These probes form a covalent and irreversible bond with the target enzyme and report on the abundance of active enzymes. Therefore, these chemical probes are called activity-based probes (ABPs). ABPP has been successfully applied to discover new enzymes involved in the ECS,[16,29,33] develop selective inhibitors for ECS enzymes[1,34–39] and compare the activity of ECS enzymes in healthy and diseased states.[10]

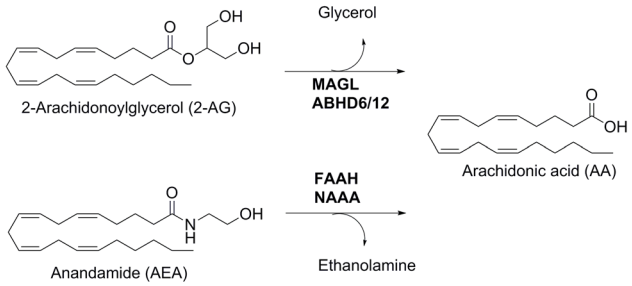

Figure 3 | Hydrolysis of 2-AG and anandamide. ABHD: α/β-hydrolase domain containing protein. FAAH: fatty acid amide hydrolase. MAGL: monoacylglycerol lipase. NAAA: N-acylethanolamine-hydrolyzing acid amidase.

The majority of enzymes involved in the endocannabinoid system are serine hydrolases (**Table 1**). A few enzymes have a catalytic cysteine residue: the PLA/AT family and NAAA. The phosphatase PTNP22 also has a cysteine in the active site, but it is as yet unclear if this cysteine acts as a nucleophile during catalysis. Several other enzymes employ active site histidines for an acid/base mechanism with water in the active site as nucleophile (PLCβ1, PLCβ4, sPLA2[40]). GDE1, GDE4, GDE7 and NAPE-PLD are metallohydrolases and therefore these enzymes cannot be targeted with classical ABPs. The exact identity of some of the proposed ECS enzymes is still unknown (PLC).

Most of the serine hydrolases of the ECS are targeted by broad-spectrum probes with a fluorophosphonate electrophilic trap, such as FP-TAMRA (**Table 2**).[32] FP-TAMRA inhibits DAGLβ, but not DAGLα. MB064 was the first fluorescent probe reported for DAGLα. MB064 is based on the inhibitor tetrahydrolipstatin and has a β-lactone as electrophilic trap.[44] MB064 targets several other enzymes from the α,β-hydrolase fold family. The triazole urea DH379 is a more selective fluorescent probe for diacylglycerol lipases.[45] The carbamate JW912 is a dual ABHD6/MAGL probe.[41] For the cysteine hydrolase NAAA, a fluorescent probe with a β-lactam electrophilic trap is reported.[43]

Table 1 | Human endocannabinoid enzymes and reported activity-based probes.

Enzyme	Uniprot accession	Catalytic nucleophile	Probe	Route
DAGLα[12]	Q9Y4D2	S	MB064, DH379	2-AG biosynthesis
DAGLβ[12]	Q8NCG7	S	MB064, DH379	
PLCβ1[13]	Q9NQ66			
PLCβ4[14]	Q15147			
MAGL[28]	Q99685	S	FP, carbamates	2-AG hydrolysis
ABHD6[29]	Q9BV23	S	FP, carbamates,[41] MB064, DH379	
ABHD12[29]	Q8N2K0	S	FP, MB064	
NAPE-PLD[20]	Q6IQ20			Anandamide biosynthesis
PLA2G4E[16]	Q3MJ16	S	FP	
PLA/AT1-5[18]	Q9HDD0, Q9NWW9, P53816, Q9UL19, Q96KN8	C		
ABHD4[23]	Q8TB40	S	FP, MB064	
GDE1[24]	Q9NZC3			
GDE4[25]	Q8N9F7			
GDE7[27]	Q7L5L3			
PLC				
PTPN22[21]	Q9Y2R2	C?		
SHIP1[22]	Q92835			
sPLA2[26]	P04054			
FAAH[30]	O00519	S	FP	Anandamide hydrolysis
FAAH2	Q6GMR7	S	FP	
NAAA[31]	Q02083	C	β-lactam[42,43]	

Table 2 | The reported fluorescent activity-based probes for endocannabinoid metabolizing enzymes feature distinct chemotypes.

Name	Chemotype	Structure
FP-TAMRA	fluorophosphonate	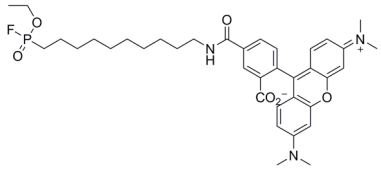
MB064	β-lactone	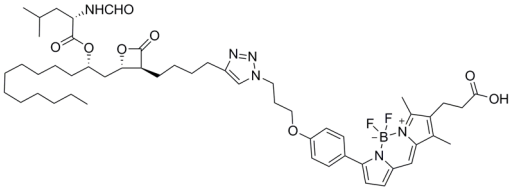
DH379	triazole urea	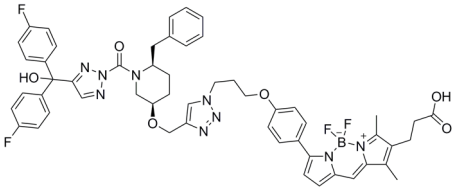
JW912	carbamate	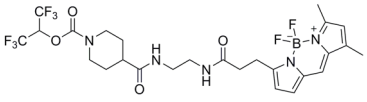
NAAA-probe	β-lactam	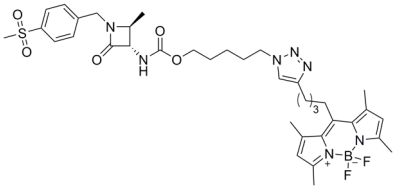

Aim and outline

The aim of this thesis is to use activity-based proteomics to further our understanding of the endocannabinoid system. This thesis describes the development of a method for the label-free quantification of enzyme activity using proteomics. Furthermore, the development of new activity-based probes for the endocannabinoid enzymes DAGL and ABHD6 is described.

In **Chapter 2**, the activity-based protein profiling method is explained. An overview of available probes, analytical techniques and applications is given. ABPP is applied in **Chapter 3** to study the role of the ECS in the lysosomal storage disorder Niemann-Pick Type C. Both gel-based and mass-spectrometry-based ABPP is used to compare serine hydrolase activity between healthy and diseased brain tissue from a transgenic mouse model. In this study, both dimethyl-labeling and label-free quantitative mass spectrometry is used. This led to the development of an ABPP method with label-free quantification for which a protocol is described in **Chapter 4**. The well-characterized DAGLα inhibitor DH376, which was previously studied using dimethyl-labeling techniques,[45] was studied with this new method. **Chapters 5 and 6** describe the design and synthesis of new probes. In **Chapter 5**, the synthesis and characterization of quenched activity-based probes for DAGL and ABHD6 is described. In **Chapter 6**, the design and synthesis of new two-step probes for DAGL is described. **Chapter 7** provides a summary and points at directions for future research.

References

1. Blankman, J. L. & Cravatt, B. F. Chemical probes of endocannabinoid metabolism. *Pharmacol. Rev.* **65**, 849–71 (2013).
2. Pacher, P. The Endocannabinoid System as an Emerging Target of Pharmacotherapy. *Pharmacol. Rev.* **58**, 389–462 (2006).
3. Chiurchiù, V., van der Stelt, M., Centonze, D. & Maccarrone, M. The endocannabinoid system and its therapeutic exploitation in multiple sclerosis: Clues for other neuroinflammatory diseases. *Prog. Neurobiol.* **160**, 82–100 (2017).
4. Scotter, E. L., Abood, M. E. & Glass, M. The endocannabinoid system as a target for the treatment of neurodegenerative disease. *Br. J. Pharmacol.* **160**, 480–498 (2010).
5. Marzo, V. Di, Bifulco, M. & Petrocellis, L. De. The endocannabinoid system and its therapeutic exploitation. *Nat. Rev. Drug Discov.* **3**, 771–784 (2004).
6. Di Marzo, V. Targeting the endocannabinoid system: To enhance or reduce? *Nat. Rev. Drug Discov.* **7**, 438–455 (2008).
7. Cravatt, B. F., Wright, A. T. & Kozarich, J. W. Activity-Based Protein Profiling: From Enzyme Chemistry to Proteomic Chemistry. *Annu. Rev. Biochem.* **77**, 383–414 (2008).
8. Speers, A. E. & Cravatt, B. F. Profiling Enzyme Activities In Vivo Using Click Chemistry Methods. *Chem. Biol.* **11**, 535–546 (2004).
9. Wright, A. T. & Cravatt, B. F. Chemical Proteomic Probes for Profiling Cytochrome P450 Activities and Drug Interactions In Vivo. *Chem. Biol.* **14**, 1043–1051 (2007).
10. Nomura, D. K. *et al.* Monoacylglycerol Lipase Regulates a Fatty Acid Network that Promotes Cancer Pathogenesis. *Cell* **140**, 49–61 (2010).
11. Bachovchin, D. A., Brown, S. J., Rosen, H. & Cravatt, B. F. Identification of selective inhibitors of uncharacterized enzymes by high-throughput screening with fluorescent activity-based probes. *Nat. Biotechnol.* **27**, 387–394 (2009).
12. Bisogno, T. *et al.* Cloning of the first sn1-DAG lipases points to the spatial and temporal regulation of endocannabinoid signaling in the brain. *J. Cell Biol.* **163**, 463–468 (2003).
13. Hashimotodani, Y. *et al.* Phospholipase Cβ serves as a coincidence detector through its Ca2+dependency for triggering retrograde endocannabinoid signal. *Neuron* **45**, 257–268 (2005).
14. Maejima, T. Synaptically Driven Endocannabinoid Release Requires Ca2+-Assisted Metabotropic Glutamate Receptor Subtype 1 to Phospholipase C 4 Signaling Cascade in the Cerebellum. *J. Neurosci.* **25**, 6826–6835 (2005).
15. Rahman, I. A. S., Tsuboi, K., Uyama, T. & Ueda, N. New players in the fatty acyl ethanolamide metabolism. *Pharmacol. Res.* **86**, 1–10 (2014).
16. Ogura, Y., Parsons, W. H., Kamat, S. S. & Cravatt, B. F. A calcium-dependent acyltransferase that produces N-acyl phosphatidylethanolamines. *Nat. Chem. Biol.* **12**, 1–5 (2016).

17. Natarajan, V., Schmid, P. C., Reddy, P. V, Zuzarte-Augustin, M. Lou & Schmid, H. H. Biosynthesis of N-Acylethanolamine Phospholipids by Dog Brain Preparations. *J. Neurochem.* **41**, 1303–1312 (1983).
18. Uyama, T. *et al.* Generation of N-acylphosphatidylethanolamine by members of the phospholipase A/acyltransferase (PLA/AT) family. *J. Biol. Chem.* **287**, 31905–31919 (2012).
19. Hussain, Z., Uyama, T., Tsuboi, K. & Ueda, N. Mammalian enzymes responsible for the biosynthesis of N-acylethanolamines. *Biochim. Biophys. Acta - Mol. Cell Biol. Lipids* **1862**, 1546–1561 (2017).
20. Okamoto, Y., Morishita, J., Tsuboi, K., Tonai, T. & Ueda, N. Molecular Characterization of a Phospholipase D Generating Anandamide and Its Congeners. *J. Biol. Chem.* **279**, 5298–5305 (2004).
21. Liu, J. *et al.* A biosynthetic pathway for anandamide. *Proc. Natl. Acad. Sci.* **103**, 13345–50 (2006).
22. Liu, J. *et al.* Multiple pathways involved in the biosynthesis of anandamide. *Neuropharmacology* **54**, 1–7 (2008).
23. Simon, G. M. & Cravatt, B. F. Endocannabinoid biosynthesis proceeding through glycerophospho-N-acyl ethanolamine and a role for α/β-hydrolase 4 in this pathway. *J. Biol. Chem.* **281**, 26465–26472 (2006).
24. Simon, G. M. & Cravatt, B. F. Anandamide biosynthesis catalyzed by the phosphodiesterase GDE1 and detection of glycerophospho-N-acyl ethanolamine precursors in mouse brain. *J. Biol. Chem.* **283**, 9341–9349 (2008).
25. Tsuboi, K. *et al.* Glycerophosphodiesterase GDE4 as a novel lysophospholipase D: A possible involvement in bioactive N-acylethanolamine biosynthesis. *Biochim. Biophys. Acta - Mol. Cell Biol. Lipids* **1851**, 537–548 (2015).
26. Sun, Y.-X. *et al.* Biosynthesis of anandamide and N-palmitoylethanolamine by sequential actions of phospholipase A2 and lysophospholipase D. *Biochem. J.* **380**, 749–56 (2004).
27. Ohshima, N. *et al.* New members of the mammalian glycerophosphodiester phosphodiesterase family: GDE4 and GDE7 produce lysophosphatidic acid by lysophospholipase D activity. *J. Biol. Chem.* **290**, 4260–4271 (2015).
28. Dinh, T. P. *et al.* Brain monoglyceride lipase participating in endocannabinoid inactivation. *Proc. Natl. Acad. Sci.* **99**, 10819–10824 (2002).
29. Blankman, J. L., Simon, G. M. & Cravatt, B. F. A Comprehensive Profile of Brain Enzymes that Hydrolyze the Endocannabinoid 2-Arachidonoylglycerol. *Chem. Biol.* **14**, 1347–1356 (2007).
30. Cravatt, B. F. *et al.* Molecular characterization of an enzyme that degrades neuromodulatory fatty-acid amides. *Nature* **384**, 83–87 (1996).
31. Tsuboi, K. *et al.* Molecular characterization of N-acylethanolamine-hydrolyzing acid amidase, a novel member of the choloylglycine hydrolase family with structural and functional similarity to acid ceramidase. *J. Biol. Chem.* **280**, 11082–11092 (2005).
32. Liu, Y., Patricelli, M. P. & Cravatt, B. F. Activity-based protein profiling: The serine hydrolases. *Proc. Natl. Acad. Sci.* **96**, 14694–14699 (1999).
33. Barglow, K. T. & Cravatt, B. F. Activity-based protein profiling for the functional annotation of enzymes. *Nat. Methods* **4**, 822–827 (2007).
34. Ahn, K. *et al.* Discovery of a Selective Covalent Inhibitor of Lysophospholipase-like 1 (LYPLAL1) as a

Tool to Evaluate the Role of this Serine Hydrolase in Metabolism. *ACS Chem. Biol.* **11**, 2529–2540 (2016).

35. Adibekian, A. *et al.* Click-generated triazole ureas as ultrapotent in vivo-active serine hydrolase inhibitors. *Nat. Chem. Biol.* **7**, 469–478 (2011).
36. Bachovchin, D. A. *et al.* Discovery and optimization of sulfonyl acrylonitriles as selective, covalent inhibitors of protein phosphatase methylesterase-1. *J. Med. Chem.* **54**, 5229–5236 (2011).
37. Baggelaar, M. P. *et al.* A highly selective, reversible inhibitor identified by comparative chemoproteomics modulates diacylglycerol lipase activity in neurons. *J. Am. Chem. Soc.* **137**, 8851–8857 (2015).
38. Hsu, K. L. *et al.* Discovery and optimization of piperidyl-1,2,3-triazole ureas as potent, selective, and in vivo-active inhibitors of alpha/beta-hydrolase domain containing 6 (ABHD6). *J. Med. Chem.* **56**, 8270–8279 (2013).
39. Janssen, F. J. *et al.* Discovery of glycine sulfonamides as dual inhibitors of sn-1-diacylglycerol lipase a and a/b-hydrolase domain 6. *J. Med. Chem.* **57**, 6610–6622 (2014).
40. Burke, J. E. & Dennis, E. Phospholipase A2 Biochemistry. *Cardiovasc. Drugs Ther.* **23**, 49 (2009).
41. Chang, J. W., Cognetta, A. B., Niphakis, M. J. & Cravatt, B. F. Proteome-wide reactivity profiling identifies diverse carbamate chemotypes tuned for serine hydrolase inhibition. *ACS Chem. Biol.* **8**, 1590–1599 (2013).
42. Romeo, E. *et al.* Activity-based probe for N-acylethanolamine acid amidase. *ACS Chem. Biol.* **10**, 2057–2064 (2015).
43. Petracca, R. *et al.* Novel activity-based probes for N-acylethanolamine acid amidase. *Chem. Commun.* **53**, 11810–11813 (2017).
44. Baggelaar, M. P. *et al.* Development of an activity-based probe and in silico design reveal highly selective inhibitors for diacylglycerol lipase-α in brain. *Angew. Chem. Int. Ed.* **52**, 12081–12085 (2013).
45. Ogasawara, D. *et al.* Rapid and profound rewiring of brain lipid signaling networks by acute diacylglycerol lipase inhibition. *Proc. Natl. Acad. Sci.* **113**, 26–33 (2016).

Chapter 2

Activity-based protein profiling[1]

Introduction

Activity-based protein profiling (ABPP) is a method to study the abundance of active enzymes in complex proteomes. ABPP uses chemical tools, termed activity-based probes (ABPs), which covalently and irreversibly react with a nucleophile in the active site of targeted proteins. Because only active enzymes are labeled by a probe, ABPP measures the abundance of active enzymes. This can differ from the total abundance of an enzyme, considering the activity of enzymes is regulated by post-translational modifications. This makes ABPP a unique and powerful method. Increasingly, ABPP is called activity-based or chemical proteomics,[2] complementing abundance-based proteomics. ABPP can be used to compare activity of certain enzymes between different proteomes, for example between healthy and diseased tissue, which enables drug target discovery. Furthermore, ABPP can be applied to characterize inhibitors and drug candidates for both potency and selectivity in a native physiological context, aiding the selection of therapeutically relevant compounds.

Every ABPP experiment consists of two parts: an activity-dependent labeling part and an analytical part to visualize and characterize this labeling event. This general view of ABPP shows it is a multidisciplinary endeavor: organic chemistry is needed to synthesize and characterize ABPs, analytical chemistry to provide the read-out of the labeling event, and biology to understand the proteomes being studied.

In this chapter, first the labeling of active proteins using an activity-based probe is described. The design of an ABP will be explained and several examples of probes and their enzyme targets will be discussed. In the second section, an overview is provided of the analytical platforms available to visualize the labeled proteome. Finally, in the third section, the applications of ABPP will be reviewed, focusing on comparative ABPP and competitive ABPP experiments.

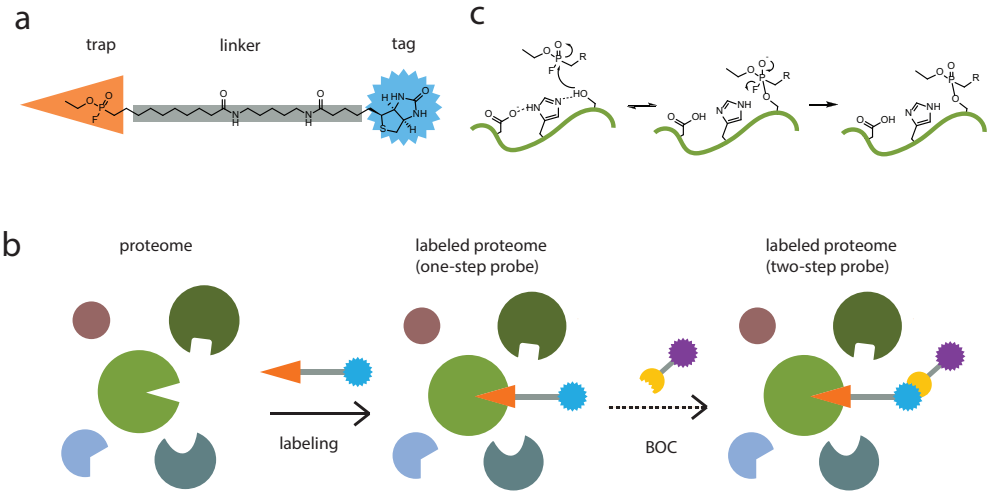

Figure 1 | Labeling enzymes with an activity-based probe. (**a**) General activity-based probe design, with fluorophosphonate-biotin as example. (**b**) Probe labeling cartoon: two-step labeling using bioorthogonal chemistry (BOC) is optional for probes equipped with a suitable tag. (**c**) Mechanism of serine hydrolase labeling: catalytic triad reacting with the fluorophosphonate trap.

Labeling

An activity-based probe generally consists of three main parts (**Fig. 1a**): the first part is the trap, also called warhead, which is able to form a covalent bond with the target enzyme. Usually, the trap is an electrophilic group,[3] as is the case for the fluorophosphonate probe shown in **Figure 1a**, which forms a covalent bond with nucleophilic serine residues. The second part is the linker, which can be changed to fine-tune chemical properties of the probe such as cell permeability, solubility, affinity and selectivity towards specific enzymes. The third part of the probe is the tag, which enables the detection of enzyme(s) labeled by the probe. This tag can be a fluorophore for visualization, an affinity tag (often biotin, **Fig. 1a**) that is used to enrich or purify probe-labelled enzymes (pulldown), a radioactive label or a ligation handle for a two-step labeling procedure.[4]

In the labeling part (**Fig. 1b**), the activity-based probe binds covalently to the target enzyme. This labeling event can take place in lysates, intact cells, tissues or living organisms.[5] There are two types of probes for the detection of active proteins (**Fig. 1b**): 1) one-step probes make use of a compound with a detection tag already installed, and 2) two-step probes rely on a ligation handle, which can be used to install the detection tag after the probe has reacted with the protein. One-step labeling is fast and efficient, but the large tag can decrease the affinity and selectivity of the probe for the target enzymes and/or may

interfere with cell permeability. Two-step probes may circumvent these issues, but are less efficient in the workflow. Key is that the ligation handle and the detection tag react in a bioorthogonal manner, which means that the biological system does not interfere with the coupling reaction.[6] The most commonly used bioorthogonal reaction is the 'click' reaction where an alkyne moiety reacts with an azide moiety in a copper(I)-catalyzed cyclization.[7] For an extensive review on different types of bioorthogonal chemistry, see reference.[8]

In **Table 1** several examples of activity-based probes for different enzyme classes are depicted. For a comprehensive overview the reader is referred to excellent reviews.[9,10] Here, predominantly ABP design will be discussed using enzyme class specific examples to explain the different methods of probe design.

Serine hydrolases. Probe **1** (**Table 1**) is a broad-spectrum probe which is designed to react with any serine hydrolase. The hydrophobic linker between the electrophilic trap and the biotin group does not contain any side chains that can provide extra interactions with selected members of the hydrolases, thus providing no specificity for a particular serine hydrolase. The mechanism of covalent bond formation between a fluorophosphonate probe and the catalytic triad of a serine hydrolase is depicted in **Figure 1c**.[11] The aspartic acid and histidine residues form a charge relay system with the serine, increasing its nucleophilicity. The catalytically active serine nucleophile of the hydrolase attacks the electrophilic fluorophosphonate, which results in expulsion of a fluoride ion and concurrent covalent binding of the enzyme with the probe. The formed covalent bond is stable and the active site is occupied, rendering the enzyme inactive. Probe **2** is an example of a tailored probe, used for profiling of the lipase DAGLα and other related proteins.[12] The design of this probe is based on the anti-obesity drug Orlistat, which has an irreversible covalent binding mechanism, with a lactone as electrophilic trap. This example highlights one method of activity-based probe design: using a known covalent inhibitor as a template. The tag used for probe **2** is a fluorophore.

Cysteine proteases. Activity-based probes for the family of cysteine proteases have also been extensively described.[13] For example, probes **3** and **4** are based on the natural substrates of their target enzymes (a peptide for caspases and ubiquitin for the deubiquitinases) and have an electrophilic trap. Cysteine proteases use a catalytic cysteine residue, and owing to the soft nature of the nucleophile, can be trapped by soft electrophiles. These traps include reactive groups such as vinyl sulfones, iodoacetamides and epoxides. Cysteine proteases ignore harder electrophilic traps like fluorophosphonates and sulfonyl fluorides. Caspases, a subfamily of cysteine proteases, can be labeled selectively and efficiently by using a low-reactive fluoromethylketone trap (probe **3**, **Table 1**). The peptidic linker element is required for selective caspase specific recognition.[14] The reaction of a terminal alkyne trap with the active site cysteines in deubiquinating enzymes is an example of the importance of the recognition element in the

Table 1 | Enzyme classes and reported activity-based probes specific to that class (orange trap and blue tag as in **Figure 1**).

Entry	Target enzymes	Probe structure	Reference
1	Serine hydrolases	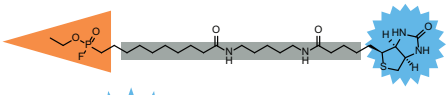	11
2	Lipases	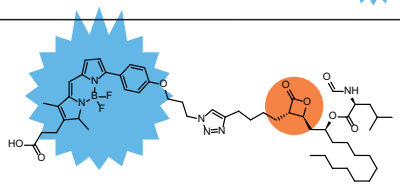	12
3	Caspases	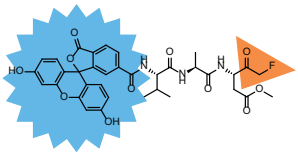	14
4	Deubiquitinases	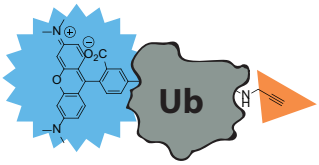	15
5	Proteasome	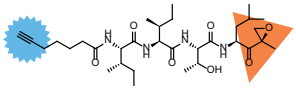	16
6	Kinases	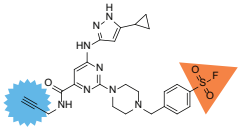	17
7	Cytochrome P450	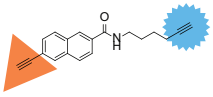	18
8	Glycosidases	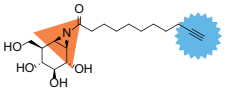	19
9	Metallohydrolases	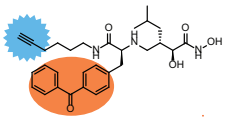	21

activity profile of an ABP.[15] Normally, alkyne moieties are considered unreactive towards nucleophiles. However, when attached to the protein ubiquitin (Ub, probe **4**, **Table 1**), the alkyne is able to function as electrophilic trap.

Threonine proteases. In threonine proteases, a N-terminal threonine acts as the catalytic nucleophile. The secondary alcohol of the threonine is activated by the basic N-terminal amine, via an ordered water molecule in the active site. The proteasome is a multi-subunit protein complex containing several active sites. The natural product epoxomicin is a covalent inhibitor for each of these subunits. Probe **5** (**Table 1**) is based on epoxomicin, containing an epoxyketone electrophilic trap, which reacts with both the threonine nucleophile and the N-terminal amine base in the active site.[16] Probe **5** is equipped with an alkyne tag, which can be used for two-step labeling.

Kinases. Kinases comprise one of the largest enzyme families and are a common target for cancer drugs. Generally, kinases catalyze the phosphorylation of their substrate using ATP. These enzymes lack a nucleophilic catalytic residue and therefore, development of probes for kinases has been challenging. Recently, probe **6** (**Table 1**) was reported as a broad-spectrum kinase ABP.[17] This probe contains a sulfonyl fluoride trap that targets a conserved lysine residue in the ATP-binding site of kinases.

Cytochrome P450s. Cytochrome P450s are a family of enzymes which metabolize a wide variety of substrates, including drug molecules. For this enzyme family alkyne-containing probes have been developed (probe **7**, **Table 1**).[18] P450 enzymes oxidize the alkyne to a highly reactive ketene species, which forms a covalent bond in the active site. Interestingly, probe **7** contains two alkynes, and the enzyme will only oxidize the conjugated alkyne group, leaving the other alkyne group available as a ligation handle.

Glycosidases. Glycosidases catalyze the hydrolysis of glycosidic bonds and thereby this enzyme family degrades a wide variety of substrates: saccharides, glycolipids and glycoproteins. For glycosidases, ABPs have been developed based on the natural product cyclophellitol, an irreversible inhibitor with an epoxide electrophilic trap. Probe **8** is an example of these cyclophellitol inspired probes, with an aziridine trap and an alkyne tag and is used to profile the retaining β-exoglucosidase subfamily of glycosidases.[19]

Photoaffinity probes. Not all enzymes have a suitable nucleophile in the active site that can be targeted with an electrophilic trap. These enzymes can sometimes be labeled with probes bearing a photoreactive trap.[20] These photoaffinity probes form covalent bonds by UV irradiation of the photoreactive group. For example, metallohydrolases have been targeted using probe **9** (**Table 1**).[21] A metal ion in the active site is chelated to the hydroxamine group of the probe and covalent linkage is induced upon UV irradiation of the benzophenone as photoreactive group.

In summary, both the choice of trap and the linker determine the type of enzymes that will be labeled by the probe. The nature of the tag determines the means of detection, which will be discussed in the following sections.

Analytical platforms

The purpose of the second analytical part of an ABPP experiment is to visualize the labeling event.[22] Of note, ABPP does not measure catalytic activity, meaning the turnover of substrate(s) to product(s) in a certain amount of time. Instead, ABPP measures the amount of available active sites of a certain enzyme and thereby reports on the functional state of this protein. In general, the tag of the probe determines the read-out technology to be used (**Table 2**, **Table 3**). Sodium dodecyl sulfate polyacrylamide gel electrophoresis (SDS-PAGE) and liquid chromatography-mass spectrometry (LC-MS) are the most used analytical orthogonal platforms. In the following section the advantages and disadvantages of these analytical platforms will be discussed (**Fig. 2**).

In gel-based experiments the labeled proteins are separated and characterized by molecular weight. First, proteins are denatured using the detergent SDS, loaded on a polyacrylamide gel and subsequently separated using gel electrophoresis (SDS-PAGE). Proteins labeled by one-step fluorescent ABPs are visualized with in-gel fluorescence scanning. Alternatively, ABPs with a biotin can be visualized using streptavidin-horseradish peroxidase (HRP) in a western blot experiment. This technique is robust, simple, has a high throughput and can be performed directly using lysates. To assign the identity of the fluorescently labeled proteins, specific inhibitors or genetic deletion of the gene is required. Disadvantages of the gel-based ABPP include a limited resolution and sensitivity. Also, the identity of the measured proteins sometimes remains ambiguous and the possibility for automation is limited.[23]

Table 2 | Comparison of ABPP analytical platforms.

Analytical platform	Protein (µg)/ sample	Throughput	Sensitivity	Identification	Site of labeling	Native proteome
SDS-PAGE	10	+	-	-	-	+
LC-MS	100	---	+	+	+	+
CE-LIF	0.1	++	++	-	-	+
FluoPol	0.1	+++	-	-	-	-
Enplex	0.001	++++	+	-	-	-
Microarray	1	++	+	+	-	+

For LC-MS-based ABPP experiments proteins are labeled with a biotinylated ABP, enriched using (strept)avidin chromatography (pulldown) and digested with a protease. The resulting peptides are separated with liquid chromatography and measured using mass spectrometry.[16] The measured peptides will allow the identification of the labeled proteins. The peptides are sequenced using MS/MS experiments, and these peptide sequences are searched against a database of protein sequences. If a cleavable linker is used, the site of modification can be identified by releasing the probe-labeled peptide from the avidin bead and measuring the specific probe-peptide conjugate.[24,25] This provides direct evidence that a probe has covalently labeled a protein. LC-MS-based ABPP has high resolution, sensitivity and information content. However, the throughput is low, elaborate sample preparation is needed and pulldown experiments commonly suffer from high background of abundant unlabeled proteins.

To improve the resolution, sensitivity and automation possibilities for SDS-PAGE, Capillary Electrophoresis coupled to Laser-Induced Fluorescence scanning (CE-LIF) has been developed.[26] Proteomes labeled with a fluorescent probe are digested with a protease and the resulting peptides are separated using capillary electrophoresis. The fluorescence signal arising from probe labeled peptides is measured. This distinguishes proteins with similar molecular weight, which co-migrate on a SDS-PAGE gel.

Fluorescence polarization (FluoPol)-ABPP has been developed to perform high-throughput screens and to assess inhibitor kinetics.[27,28] Fluorescence polarization measures the apparent size of a molecule, because a small fluorescent probe rotates quickly in solution resulting in low polarization of light, while

Table 3 | Main advantages and disadvantages of each ABPP analytical platform.

Analytical platform	Advantages	Disadvantages
SDS-PAGE	Robust, simple, low sample requirements	Limited resolution, sensitivity, no identification, no automation
LC-MS	High information content, high resolution and sensitivity	High sample requirements, cost of instrument
CE-LIF	High resolution, sensitivity, automation possible	No identification
FluoPol	High throughput, kinetics	In vitro, enzyme amount required
Enplex	High throughput, multiplexed	Requires immobilised purified enzymes
Microarray	Identification, sensitivity, throughput	Dependent on high quality antibodies

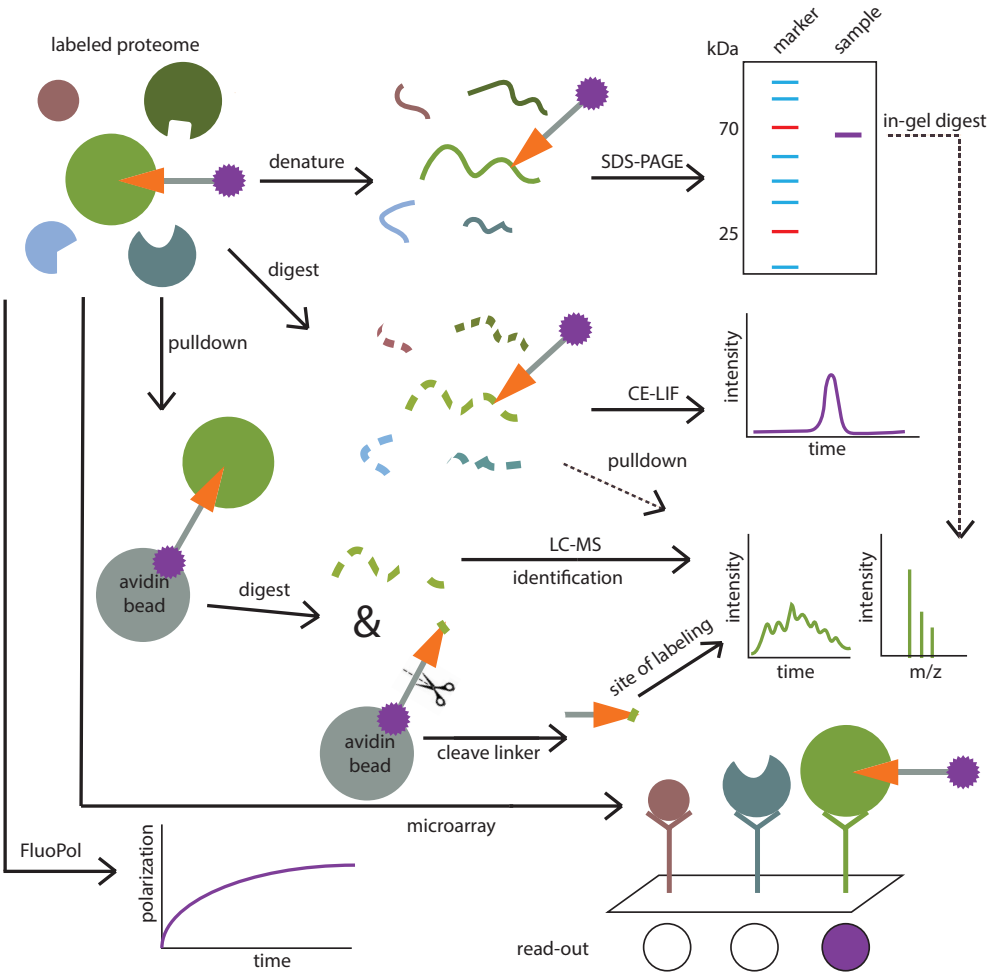

Figure 2 | Visualization of ABPP analytical platforms: SDS-PAGE, CE-LIF, LC-MS, microarray and FluoPol.

a large probe-protein adduct rotates slowly giving rise to a high polarization signal. The advantage of FluoPol compared to substrate assays is that it can be used to find inhibitors for poorly characterized enzymes of which the substrate is unknown. Recently, FluoPol has also been applied in cellular imaging, where free and bound probe could be distinguished, thereby separating the background signal from free fluorescent probes.[29] Interestingly, FluoPol can also be performed with noncovalent probes. A potential disadvantage of FluoPol is the requirement of purified or overexpressed enzyme. Typically, FluoPol assays only measure the potency of inhibitors against one enzyme. Recently, EnPlex was developed, a technique

which makes it possible to assess both potency and selectivity of inhibitors.[30] Multiple purified enzymes are immobilized on colored Luminex beads, with a different color for each enzyme. These beads are mixed, incubated with inhibitor and subsequently labeled with a biotinylated ABP, which is stained with colored streptavidin. The bead mixture is measured by flow cytometry, detecting both the identity (bead color) and activity (streptavidin color) of each enzyme. Due to the requirement of multiple purified enzymes, this platform is elaborate to set up, but once available has the highest throughput.

A technique which has the identification advantage of LC-MS but with higher throughput is microarray ABPP.[31] The probe labeled proteome is incubated with an antibody microarray and a fluorescence signal is measured for the probe labeled proteins. This technique is dependent on high-quality antibodies and prior knowledge of the probe targets is required (there is no discovery possibility as with LC-MS).

Figure 2 and **Tables 2-3** summarize the analytical platforms that can be coupled to ABPP. Various techniques can be combined with each other, such as SDS-PAGE and CE-LIF, which can be coupled to LC-MS to identify the tagged proteins.[32] In short, protein bands from SDS-PAGE can be excised and digested with a protease or using an in-gel digestion and the resulting peptides will be measured by LC-MS. The probe-labeled peptides from CE-LIF can be enriched using anti-fluorophore antibodies and also identified with LC-MS.

Applications

Over the last two decades ABPP has been developed into a mature method. The labeling methods and analytical platforms have become well established. Therefore, ABPP is increasingly applied to answer biological questions by exploiting the unique ability of ABPP to directly report on enzyme activity in living biological systems. Two types of experimental set-ups have been widely used: comparative and competitive ABPP.[33]

In comparative ABPP the active enzyme levels in (at least) two different proteomes are analyzed. These different proteomes can for instance be of two samples of a tissue in which one is in a healthy and the other is in a diseased state (**Fig. 3a**). Alternatively, comparative ABPP can be used to study the effects of pharmacological intervention on the enzyme activity. The goal of comparative ABPP is to highlight any differences or similarities in active protein levels between different biological samples. This information can be used to identify metabolic pathways that are affected in disease states. This may lead to the identification of potential new drug targets. For example, monoacylglycerol lipase was found to be more active in aggressive versus nonaggressive human cancer cell lines, thereby nominating this enzyme as a potential pharmacological target for cancer therapy.[34,35] Comparative ABPP has been used in many biological processes, such as host-virus interactions,[36,37] microbial virulence factors[38] and diet-induced

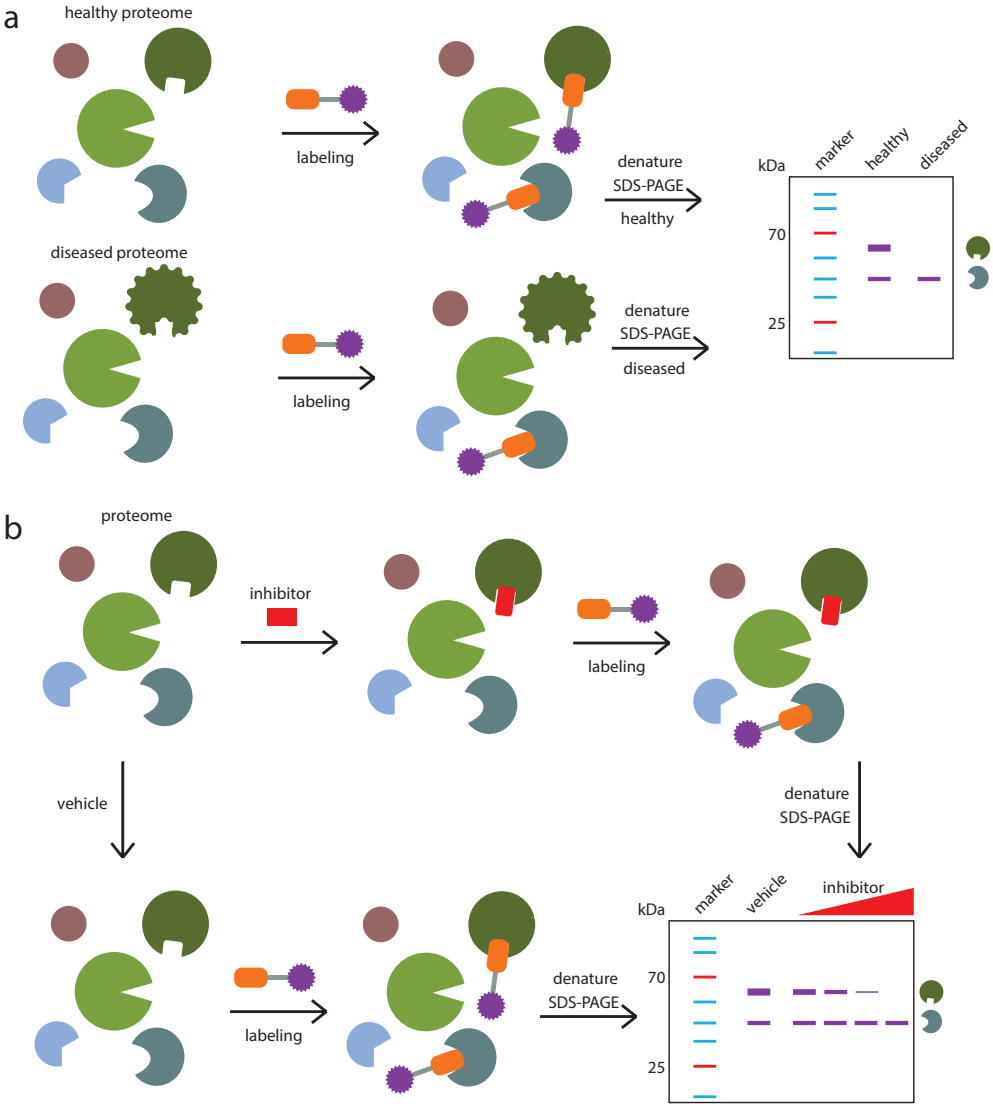

Figure 3 | ABPP experiments. (a) Comparative ABPP. (b) Competitive ABPP.

obesity.[39] Furthermore, ABPP can be used to identify novel enzymes, such as PLA2G4E as a calcium-dependent N-acyltransferase.[40]

Inhibitor potency and selectivity can be simultaneously evaluated in a competitive ABPP experiment using broad-spectrum ABPs (**Fig. 3b**).[41] ABPP efficiently guides the hit and lead optimization process, thereby shortening the drug discovery process. Interestingly, there is also a chance for serendipitous discoveries, such as identifying novel hits for other enzymes. In competitive ABPP a sample is pre-treated with an inhibitor before the ABP is added to label residual enzyme activities. A decrease in fluorescence intensity of the bands will indicate whether the compound interacted with a protein. Competitive ABPP is also an excellent way to confirm target engagement of an enzyme in a cellular or animal model. For example, probe **1** (**Table 1**) was used to screen a library of compounds against a library of enzymes to identify inhibitors for a diverse set of serine hydrolases.[32] Competitive ABPP was also used to guide the discovery and optimization of CNS-active diacylglycerol lipase inhibitors.[42] Recently, ABPP was used to profile the protein interaction landscape in human brain and cortical neurons of BIA 10-2474, an experimental drug which caused the death of volunteer in a phase 1 clinical trial.[43] It was found that BIA 10-2474 inhibited several lipase off-targets, which were not identified by the classical selectivity screening assays. It is therefore recommended that pre-clinical drug discovery should include (competitive) ABPP to profile the drug candidate on human tissues and cells.

Competitive ABPP is, however, restricted to profiling enzyme activities identified by the probe. For an ideal drug target profiling study, the drug candidate itself should be converted into an ABP.[19] This is, however, difficult to realize if the inhibitor does not contain a protein reactive functionality. A combination of broad-spectrum ABPs targeting various enzyme families would therefore be ideal to get a broad overview of the selectivity profile of the drug candidate. Other chemical proteomics techniques such as cellular thermal shift assays (CETSA)[44] and drug affinity responsive target stability (DARTS)[45] can be used to get a proteome-wide selectivity profile, however, these are not necessarily activity-based and should be used only as complementary techniques.

Conclusion

ABPP is a powerful methodology to study enzyme function in a native biological setting. In the future, novel probes will be required to enable further exploration of the enzymatically active subset of the proteome. Furthermore, new analytical platforms should be developed to enhance the sensitivity and resolution of the ABPP technique to detect low abundant enzymes and to study the effects of post-translational modifications on the proteins. Increasing the throughput of ABPP experiments by using automation is another desired feature. Organic chemists should develop novel probes to target novel enzyme classes and

further develop cleavable linkers to identify the site of modification with novel fragmentation techniques such as electron transfer dissociation.[46] Importantly, biologists could benefit a lot from the current ABPP toolbox. Recent examples of online, searchable databases, such as chemicalprobes.org and probes-drugs.org,[47,48] aid scientists in selecting the optimal probes. The ABPP-field could benefit from adding the best probes to these open data resources and making well characterized probes available. ABPP will continue to play an important role in elucidating the function of proteins and the discovery and development of novel drugs.

References

1. van Rooden, E. J., Bakker, A. T., Overkleeft, H. S. & van der Stelt, M. Activity-Based Protein Profiling. *eLS* 1–9 (2018). doi:10.1002/9780470015902.a0023406
2. Simon, G. M. & Cravatt, B. F. Activity-based proteomics of enzyme superfamilies: Serine hydrolases as a case study. *J. Biol. Chem.* **285**, 11051–11055 (2010).
3. Shannon, D. A. & Weerapana, E. Covalent protein modification: The current landscape of residue-specific electrophiles. *Curr. Opin. Chem. Biol.* **24**, 18–26 (2015).
4. Speers, A. E., Adam, G. C. & Cravatt, B. F. Activity-Based Protein Profiling in Vivo Using a Copper (I) -Catalyzed Azide-Alkyne [3 + 2] Cycloaddition. *J. Am. Chem. Soc.* **125**, 4686–4687 (2003).
5. Blum, G., von Degenfeld, G., Merchant, M. J., Blau, H. M. & Bogyo, M. Noninvasive optical imaging of cysteine protease activity using fluorescently quenched activity-based probes. *Nat. Chem. Biol.* **3**, 668–677 (2007).
6. Willems, L. I. *et al.* Bioorthogonal chemistry: Applications in activity-based protein profiling. *Acc. Chem. Res.* **44**, 718–729 (2011).
7. Tornøe, C. W., Christensen, C. & Meldal, M. Peptidotriazoles on Solid Phase: [1 ,2 ,3] -Triazoles by Regiospecific Copper (I) -Catalyzed 1 , 3-Dipolar Cycloadditions of Terminal Alkynes to Azides. *J. Org. Chem.* **67**, 3057–3064 (2002).
8. Patterson, D. M., Nazarova, L. A. & Prescher, J. A. Finding the Right (Bioorthogonal) Chemistry. *ACS Chem. Biol.* **9**, 592–605 (2014).
9. Evans, M. J. & Cravatt, B. F. Mechanism-based profiling of enzyme families. *Chem. Rev.* **106**, 3279–3301 (2006).
10. Nodwell, M. B. & Sieber, S. A. ABPP Methodology: Introduction and Overview. *Top. Curr. Chem.* **324**, 1–42 (2012).
11. Liu, Y., Patricelli, M. P. & Cravatt, B. F. Activity-based protein profiling: The serine hydrolases. *Proc. Natl. Acad. Sci.* **96**, 14694–14699 (1999).
12. Baggelaar, M. P. *et al.* Development of an activity-based probe and in silico design reveal highly selective inhibitors for diacylglycerol lipase-α in brain. *Angew. Chem. Int. Ed.* **52,** 12081–12085 (2013).
13. Kato, D. *et al.* Activity-based probes that target diverse cysteine protease families. *Nat. Chem. Biol.* **1,** 33–38 (2005).
14. Bedner, E., Smolewski, P., Amstad, P. & Darzynkiewicz, Z. Activation of Caspases Measured in Situ by Binding of Fluorochrome-Labeled Inhibitors of Caspases (FLICA): Correlation with DNA Fragmentation. *Exp. Cell Res.* **259**, 308–313 (2000).
15. Ekkebus, R. *et al.* On Terminal Alkynes That Can React with Active-Site Cysteine Nucleophiles in Proteases. *J. Am. Chem. Soc.* **135**, 2867–2870 (2013).
16. Li, N. *et al.* Relative quantification of proteasome activity by activity-based protein profiling and LC-MS/MS. *Nat. Protoc.* **8**, 1155–68 (2013).
17. Zhao, Q. *et al.* Broad-Spectrum Kinase Profiling in Live Cells with Lysine-Targeted Sulfonyl Fluoride Probes. *J. Am. Chem. Soc.* **139**, 680–685 (2017).
18. Wright, A. T. & Cravatt, B. F. Chemical Proteomic Probes for Profiling Cytochrome P450 Activities and Drug Interactions In Vivo. *Chem. Biol.* **14**, 1043–1051 (2007).
19. Kallemeijn, W. W. *et al.* Novel Activity-Based Probes for Broad-Spectrum Profiling of Retaining b -Exoglucosidases In Situ and In Vivo. *Angew. Chem. Int. Ed.* **8**, 12529–12533 (2012).
20. Geurink, P. P., Prely, L. M., Van Der Marel, G. A., Bischoff, R. & Overkleeft, H. S. Photoaffinity Labeling in Activity-Based Protein Profiling. *Top. Curr. Chem.* **324**, 85–114 (2012).
21. Saghatelian, A., Jessani, N., Joseph, A., Humphrey, M. & Cravatt, B. F. Activity-based probes for the

proteomic profiling of metalloproteases. *Proc. Natl. Acad. Sci.* **101**, 10000–10005 (2004).
22. Sieber, S. A. & Cravatt, B. F. Analytical platforms for activity-based protein profiling - exploiting the versatility of chemistry for functional proteomics. *Chem. Commun.* **22**, 2311–2319 (2006).
23. Patricelli, M. P., Giang, D. K., Stamp, L. M. & Burbaum, J. J. Direct visualization of serine hydrolase activities in complex proteomes using fluorescent active site-directed probes. *Proteomics* **1**, 1067–1071 (2001).
24. Weerapana, E., Speers, A. E. & Cravatt, B. F. Tandem orthogonal proteolysis-activity-based protein profiling (TOP-ABPP)-- a general method for mapping sites of probe modification in proteomes. *Nat. Protoc.* **2**, 1414–1425 (2007).
25. Yang, Y., Hahne, H., Kuster, B. & Verhelst, S. H. L. A simple and effective cleavable linker for chemical proteomics applications. *Mol. Cell. Proteomics* **12**, 237–44 (2013).
26. Okerberg, E. S. *et al.* High-resolution functional proteomics by active-site peptide profiling. *Proc. Natl. Acad. Sci.* **102**, 4996–5001 (2005).
27. Bachovchin, D. A., Brown, S. J., Rosen, H. & Cravatt, B. F. Identification of selective inhibitors of uncharacterized enzymes by high-throughput screening with fluorescent activity-based probes. *Nat. Biotechnol.* **27**, 387–394 (2009).
28. Lahav, D. *et al.* A Fluorescence Polarization Activity-Based Protein Profiling Assay in the Discovery of Potent, Selective Inhibitors for Human Nonlysosomal Glucosylceramidase. *J. Am. Chem. Soc.* **139**, 14192–14197 (2017).
29. Dubach, J. M. *et al.* In vivo imaging of specific drug–target binding at subcellular resolution. *Nat. Commun.* **5**, 1–9 (2014).
30. Bachovchin, D. A. *et al.* A high-throughput, multiplexed assay for superfamily-wide profiling of enzyme activity. *Nat. Chem. Biol.* **10**, 656–663 (2014).
31. Sieber, S. A., Mondala, T. S., Head, S. R. & Cravatt, B. F. Microarray platform for profiling enzyme activities in complex proteomes. *J. Am. Chem. Soc*. **126**, 15640–15641 (2004).
32. Bachovchin, D. A. *et al.* Superfamily-wide portrait of serine hydrolase inhibition achieved by library-versus-library screening. *Proc. Natl. Acad. Sci.* **107**, 20941–20946 (2010).
33. Cravatt, B. F., Wright, A. T. & Kozarich, J. W. Activity-Based Protein Profiling: From Enzyme Chemistry to Proteomic Chemistry. *Annu. Rev. Biochem.* **77**, 383–414 (2008).
34. Nomura, D. K., Dix, M. M. & Cravatt, B. F. Activity-based protein profiling for biochemical pathway discovery in cancer. *Nat. Rev. Cancer* **10**, 630–638 (2010).
35. Nomura, D. K. *et al.* Monoacylglycerol Lipase Regulates a Fatty Acid Network that Promotes Cancer Pathogenesis. *Cell* **140**, 49–61 (2010).
36. Blais, D. R. *et al.* Activity-based protein profiling identifies a host enzyme, carboxylesterase 1, which is differentially active during hepatitis C virus replication. *J. Biol. Chem.* **285**, 25602–25612 (2010).
37. Blais, D. R., Nasheri, N., McKay, C. S., Legault, M. C. B. & Pezacki, J. P. Activity-based protein profiling of host-virus interactions. *Trends Biotechnol.* **30**, 89–99 (2012).
38. Puri, A. W. *et al.* Rational design of inhibitors and activity-based probes targeting clostridium difficile virulence factor TcdB. *Chem. Biol.* **17**, 1201–1211 (2010).
39. Sadler, N. C. *et al.* Activity-Based Protein Profiling Reveals Mitochondrial Oxidative Enzyme Impairment and Restoration in Diet-Induced Obese Mice. *PLoS One* **7**, 1–10 (2012).
40. Ogura, Y., Parsons, W. H., Kamat, S. S. & Cravatt, B. F. A calcium-dependent acyltransferase that produces N-acyl phosphatidylethanolamines. *Nat. Chem. Biol.* **12**, 1–5 (2016).
41. Leung, D., Hardouin, C., Boger, D. L. & Cravatt, B. F. Discovering potent and selective reversible inhibitors of enzymes in complex proteomes. *Nat. Biotechnol.* **21**, 687–91 (2003).
42. Ogasawara, D. *et al.* Rapid and profound rewiring of brain lipid signaling networks by acute diacylglycerol lipase inhibition. *Proc. Natl. Acad. Sci.* **113**, 26–33 (2016).

43. van Esbroeck, A. C. M. *et al.* Activity-based protein profiling reveals off-target proteins of the FAAH inhibitor BIA 10-2474. *Science* . **356**, 1084–1087 (2017).
44. Reinhard, F. B. M. *et al.* Thermal proteome profiling monitors ligand interactions with cellular membrane proteins. *Nat. Methods* **12**, 1129–1131 (2015).
45. Lomenick, B. *et al.* Target identification using drug affinity responsive target stability (DARTS). *Proc. Natl. Acad. Sci.* **106**, 21984–21989 (2009).
46. Syka, J. E. P., Coon, J. J., Schroeder, M. J., Shabanowitz, J. & Hunt, D. F. Peptide and protein sequence analysis by electron transfer dissociation mass spectrometry. *Proc. Natl. Acad. Sci.* **101**, 9528–33 (2004).
47. Skuta, C. *et al.* Probes & Drugs portal: an interactive, open data resource for chemical biology. *Nat. Methods* **14**, 759–760 (2017).
48. Arrowsmith, C. H. *et al.* The promise and peril of chemical probes. *Nat. Chem. Biol.* **11**, 536–541 (2015).

Chapter 3

Chemical proteomics analysis of endocannabinoid hydrolase activity in Niemann-Pick Type C mouse brain[1]

Introduction

The endocannabinoid system (ECS) consists of the cannabinoid type 1 and 2 receptors (CB_1R and CB_2R) and their endogenous ligands: the endocannabinoids. The lipids anandamide (AEA) and 2-arachidonoylglycerol (2-AG) are the best characterized endocannabinoids.[2] The enzymes responsible for endocannabinoid biosynthesis and degradation are also part of the ECS, with most endocannabinoid degrading enzymes belonging to the serine hydrolase family (**Fig. 1**).[3] The combined activities of biosynthetic enzymes and degradative enzymes tightly regulate endocannabinoid concentrations in the brain. For example, 2-AG is mainly produced from 1-acyl-2-arachidonoylglycerol by the diacylglycerol lipases, DAGLα and DAGLβ, while it is degraded by monoacylglycerol lipase (MAGL) and to a minor extent by α,β-hydrolase domain-containing protein 6 (ABHD6) and α,β-hydrolase domain-containing protein 12 (ABHD12). Multiple pathways are known for the biosynthesis of anandamide, but they all use N-acylphosphatidylethanolamine (NAPE) as a central precursor, including the serine hydrolase ABHD4 and the β-metallolactamase N-acylphosphatidylethanolamine-phospholipase D (NAPE-PLD). NAPE is synthesized by the calcium-dependent N-acyltransferase PLA2G4E.[4] Fatty acid amide hydrolase (FAAH) terminates anandamide signaling by hydrolysis of its amide bond.

Endocannabinoid hydrolases that are part of the serine hydrolase superfamily can be studied using activity-based protein profiling (ABPP), a method which uses chemical probes for measuring enzyme activity in complex biological samples. Previously, ABPP was used to compare serine hydrolase activity in wildtype and CB_1R knockout mice.[5] Comparative ABPP has also been successfully applied in the identification of new drug targets.[6,7] With ABPP enzyme activities that are deregulated in a certain pathophysiological state can be identified and the relative amount of active enzyme copies as compared to wildtype situations can be quantified. The classical fluorophosphonate (FP)-based probes (FP-TAMRA and FP-biotin)[8] act as broad-spectrum serine hydrolase probes that label the endocannabinoid enzymes

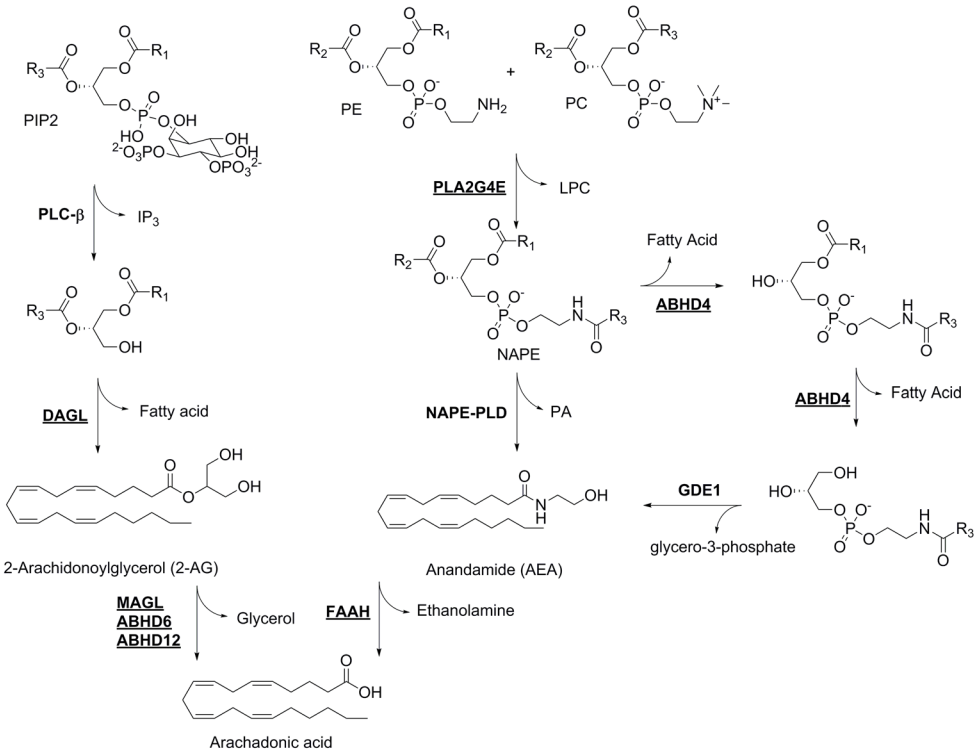

Figure 1 | Pathways for the biosynthesis and degradation of the endocannabinoids 2-AG and AEA. Enzymes with known activity-based probes are underlined. R_1/R_2: alkyl chains, R_3: arachidonoyl. ABHD; α/β-hydrolase domain-containing protein. AEA: anandamide. 2-AG: 2-arachidonoylglycerol. DAG: diacylglycerol. DAGL: diacylglycerol lipase. FAAH: fatty acid amide hydrolase. GDE1: glycerophosphodiesterase 1. LPC: lysophosphatidylcholine. MAGL: monoacylglycerol lipase. NAPE: N-acylphosphatidylethanolamine. PC: phosphatidylcholine. PE: phosphatidylethanolamine. PIP2: phosphatidylinositol 4,5-bisphosphate. PLA2G4E: phospholipase A2 group 4E. PLC: phospholipase C. PLD: phospholipase D.

FAAH, MAGL, PLA2G4E,[4] ABHD6 and ABHD4,[9,8] whereas the tailor-made tetrahydrolipstatin (THL)-based probes (MB064 and MB108) label both DAGL isoforms (alpha and beta) and ABHD4, ABHD6 and ABHD12.[5,10,11,12] Of note, the fluorescent probe DH379[11] targets DAGL and ABHD6.

Evaluation of endocannabinoid hydrolase activity in native tissue may provide insight in the role of the ECS in physiological and disease processes. Interestingly, endocannabinoid levels are elevated during neurodegeneration and neuroinflammation.[13,14,15] For example, endocannabinoid signaling is perturbed in various animal models of neurodegenerative diseases, including stroke,[16] traumatic brain injury,[17] Alzheimer's disease,[18] Huntington's disease,[19] Parkinson's disease[20,21] and multiple sclerosis.[22] It is hypothesized that regulation of ECS activity may provide therapeutic benefit for these type of neurological

diseases.[23]

Niemann-Pick Type C (NPC) is a neurodegenerative lysosomal storage disorder, which is associated with mutations in either of the genes encoding NPC1 or NPC2.[24] Both genes encode lysosomal proteins that are sequentially involved in cholesterol transport out of the lysosomes via a so far unknown mechanism. Defects in the function of the soluble NPC2 or the lysosomal membrane protein NPC1 leads to primary accumulation of cholesterol and secondary storage of sphingomyelin, sphingosine, and glycosphingolipids in lysosomes of multiple cell types, leading to visceral complications such as enlarged liver and spleen combined with progressive neurological disease.[23] There is no treatment available for Niemann-Pick type C patients. Additionally, there is no information available about the status of the ECS in Niemann-Pick. Therefore, endocannabinoid hydrolase activity was measured in the Niemann-Pick type C mouse model using ABPP.

Results

In 95% of the patients afflicted by Niemann-Pick type C, mutations in NPC1 are observed. Therefore, the role of the endocannabinoid system in this disease was investigated by comparison of endocannabinoid hydrolase activity between *Npc1*$^{+\backslash+}$ and *Npc1*$^{-\backslash-}$ mouse brains. First, labeling profiles of MB064, DH379 and FP-TAMRA in wildtype and knockout mouse brains was evaluated (**Fig. 2a**). Membrane and soluble fractions of both wildtype and knockout tissue were labeled with each probe separately, resolved on SDS-PAGE and visualized using in-gel fluorescence scanning. Coomassie staining was used as a protein loading control. The fluorescence intensity of the bands corresponding to DAGLα (~120 kDa), ABHD12 (~50 kDa), ABHD6 (~35 kDa) and FAAH (~60 kDa) were quantified to determine the relative enzyme activity between knockout and wildtype (**Fig. 2b**). Using the FP-TAMRA probe, the two bands corresponding to MAGL (~35 kDa) were observed, but due to band overlap with ABHD6 these cannot be accurately quantified. Labeling of DAGLα significantly decreased in the knockout mice as compared to wildtype, while ABHD6 and ABHD12 activity was the same. FAAH labeling was slightly decreased in the knockout, but this decrease was not statistically significant. In the cytosolic fraction, an increase in intensity of a 75 kDa-band as labeled by MB064 and FP-TAMRA was observed in the knockout brains. As reported previously,[5,29] DAGLα is identified as two separate bands, which can both be labeled with a DAGLα antibody and are absent in DAGLα KO mice (**Fig. 2d**). Remarkably, only the fluorescent band corresponding to the higher molecular weight was significantly decreased in the *Npc1*$^{-/-}$ mice as quantified by two separate probes MB064 and DH379 (**Fig. 2c**). To see if this observation was due to a decrease of protein abundance, a Western blot against DAGLα was performed (**Fig. 2e**). The signal of antibody labeling was quantified (**Fig. 2f**). The same pattern was observed for relative abundance as for relative

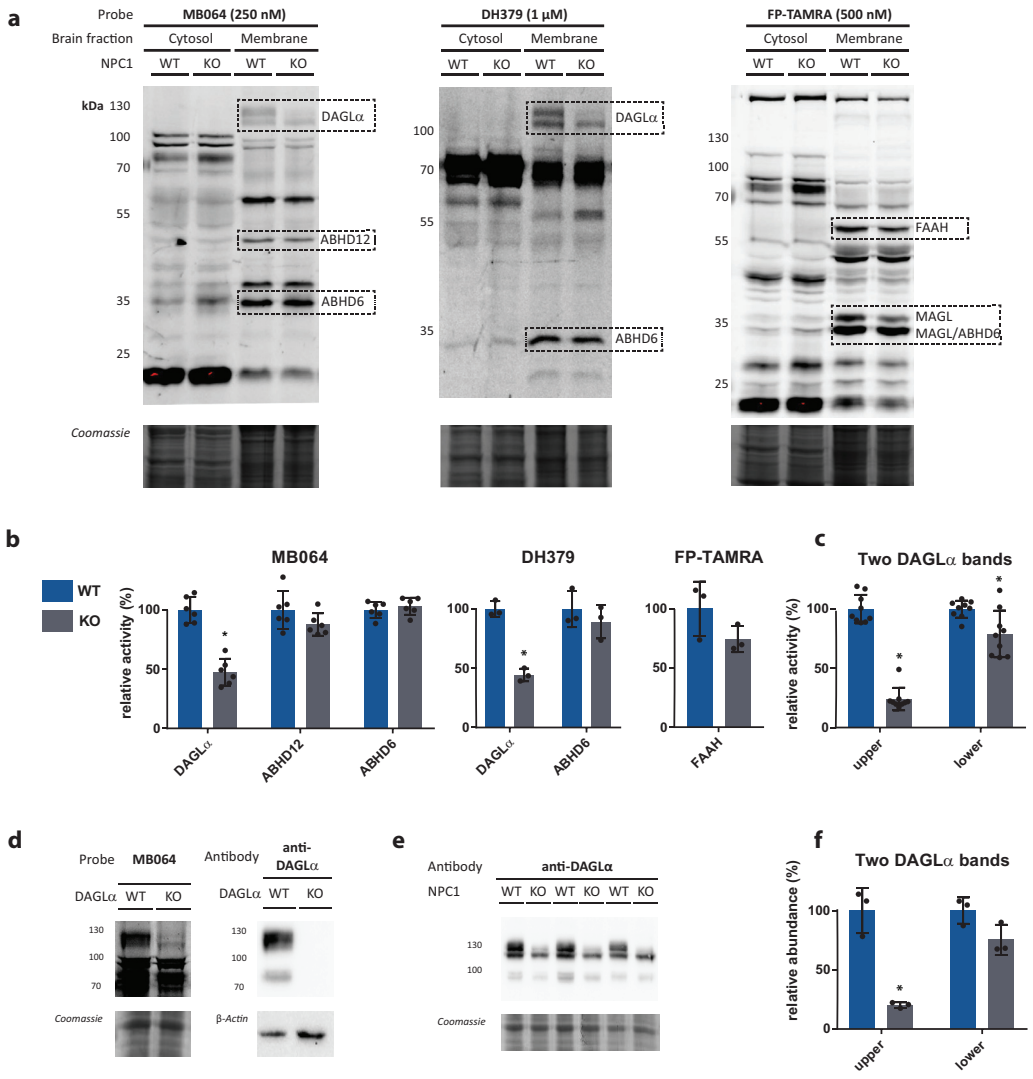

Figure 2 | Gel-based *Npc1*$^{+/+}$ (WT) vs *Npc1*$^{-/-}$ (KO) comparison. (**a**) Enzyme activity in the brain fractions as measured by the probes MB064, DH379 and FP-TAMRA. (**b**) Quantification of relative enzyme activity in WT and KO for probe targets (average WT is set to 100%). N = 3 (mice), n = 2 (MB064) or n = 1 (DH379 and FP-TAMRA). (**c**) Quantification of probe labeling of the two observed bands for DAGLα as measured by MB064 and DH379 (**Fig. 2a**). N = 3, n = 3. (**d**) DAGLα activity and abundance in DAGLα WT and KO mouse brain membrane proteome as measured by the probe MB064 and an anti-DAGLα antibody. (**e**) DAGLα abundance in NPC1 WT and KO mouse brain membrane proteome. (**f**) Quantification of antibody labeling of the two observed bands for DAGLα as measured by anti-DAGLα (blot **Fig. 2e**). Mean ± standard deviation is shown. * P < 0.05 (student's t-test).

activity: only the upper band corresponding to DAGLα is significantly decreased (**Fig. 2c**,**f**).

To study a broader range of serine hydrolases and to confirm the observations from the gel-based assay, a chemical proteomics method was employed using FP-biotin and MB108 to assess the role of the endocannabinoid system in NPC1. The enzymatic activity of 41 hydrolases in NPC1 knockout mouse brain were identified and compared with wildtype mouse brains (**Fig. 3**). In line with the gel-based ABPP, no significant difference in the endocannabinoid hydrolase activity was found (ABHD12, ABHD6, FAAH and MAGL) in NPC1 wildtype versus knockout mice brain proteomes. The activity of endocannabinoid hydrolase ABHD4 is also unaltered in knockout compared to wildtype. Remarkably, and in contrast to the gel-based ABPP results, DAGLα activity in knockout mice brain proteomes was not decreased compared to wildtype mice.

In a control experiment, biotinylated probe MB108 competes with both DAGLα bands labeled by the fluorescent probe MB064. Additionally, DAGL inhibitor DH376 did reduce DAGLα labeling in the chemical proteomics assay (**Fig. 4**). Finally, three hydrolases were significantly increased in knockout mouse brains compared to wildtype brains: retinoid-inducible serine carboxypeptidase (SCPEP1), cathepsin A (CTSA) and palmitoyl-protein thioesterase 1 (PPT1) (**Fig. 3**).

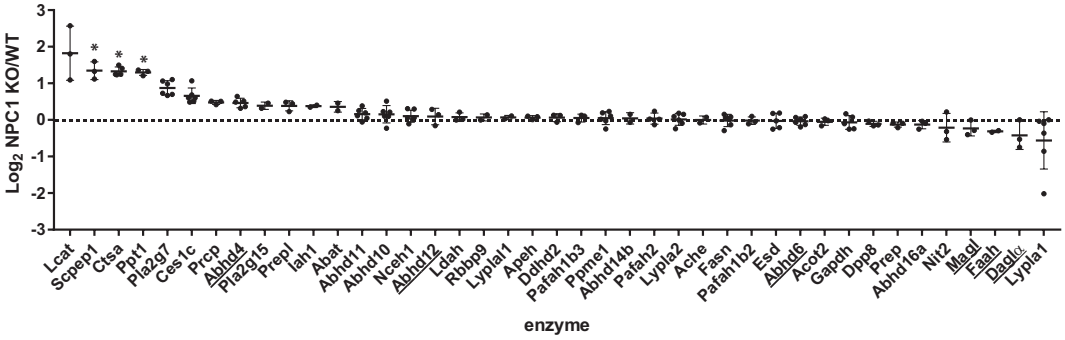

Figure 3 | Chemical proteomics comparison of *Npc1*$^{+/+}$ (WT) vs *Npc1*$^{-/-}$ (KO). Log_2 ratio of enzyme activity in KO brain proteome compared to WT. Activity was measured using FP-biotin or MB108 (both 10 µM, N = 3). The data from both probes was combined for both the cytosolic and membrane fraction. The mean and standard deviation is shown. Endocannabinoid related enzymes are underlined. Statistical analysis by means of student's t-test (each ratio was compared to a log_2 ratio of 0) and the resulting p-values were subjected to Benjamini-Hochberg correction, setting the false discovery rate at 10% (* indicates significant difference).

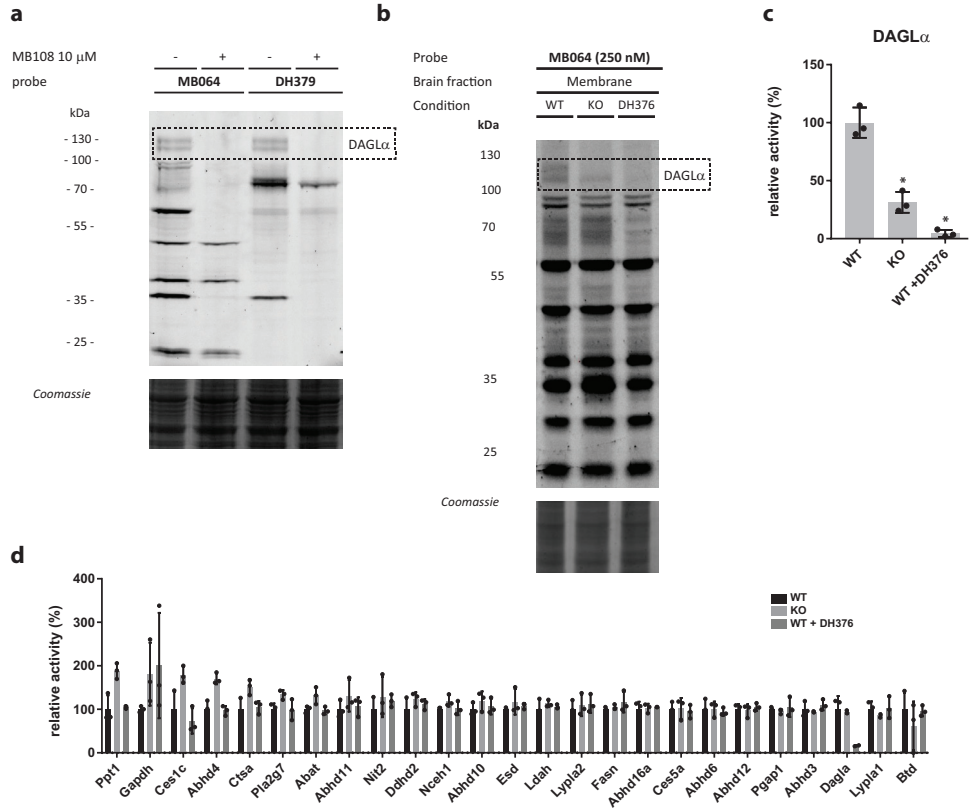

Figure 4 | Control experiments with MB108 and DAGLα inhibitor DH376 in mouse brain membrane proteome. (**a**) Gel-based *Npc1*$^{+/+}$ (WT) pre-treatment with MB108 and labeling with MB064 and DH379. (**b**) Gel-based *Npc1*$^{+/+}$ (WT) vs *Npc1*$^{-/-}$ (KO) comparison and competition with inhibitor DH376. (**c**) Quantification of relative enzyme activity for DAGLα (average WT is set to 100%), N = 3. * P < 0.05 (student's t-test). (**d**) Chemical proteomics comparison of *Npc1*$^{+/+}$ (WT) vs *Npc1*$^{-/-}$ (KO) and competition with DH376 (WT). Activity was measured in the membrane fraction using MB108 (10 µM). Label-free quantification with IsoQuant. Statistical analysis by means of student's t-test (KO and inhibitor conditions compared to WT) and the resulting p-values were subjected to Benjamini-Hochberg correction, setting the false discovery rate at 10% (* indicates significant difference).

Discussion

Niemann-Pick type C mice have previously been studied using activity-based protein profiling with a retaining β-glucosidase probe.[25] This study showed increased activity of the non-lysosomal glucosylceramidase (GBA2) in NPC1 knockout mice (and consistent increased abundance of the protein by Western blot). Importantly, pharmacological inhibition of GBA2 ameliorated the neuropathology of these mice.[25] Miglustat is approved as a drug, and initially thought to work through substrate reduction by inhibiting glucosylceramide synthase.[30] However, as was shown before, the molecular mechanism does not involve glucosylceramide synthase, and it is hypothesized that the therapeutic effect seems at least partly due to off-target inhibition of GBA2 by Miglustat.[25] It has been suggested that accumulation of sterols in lysosomes impaired in NPC1 (or NPC2) causes a more general lysosome dysfunction involving multiple hydrolases, such as lysosomal glucocerebrosidase (GBA).[31] Additionally, mutations in NPC1 or NPC2 genes result in severe progressive neurodegeneration. These observations led to the hypothesis that the hydrolases of the endocannabinoid system (ECS) might play a role in this disease.

Here, ABPP was used to quantify the activity of the endocannabinoid hydrolases FAAH, ABHD6, ABHD12, ABHD4 and MAGL in NPC1 knockout mice and it was found that their activity is not affected in wildtype vs NPC1 knockout mice. DAGLα activity seems to be decreased in the knockout mice based on the gel-based ABPP results. However, a discrepancy was found between the gel-based ABPP assay and the chemical proteomics assay in DAGLα activity between the NPC1 knockout mouse brains compared to wildtype mice. This discrepancy can possibly be caused by technical factors inherent to the two applied methodologies. In the gel-based ABPP assay only the labeling of the upper DAGLα-band was abolished in the NPC1 knockout brain proteome. It could be that the peptides from the protein corresponding to the upper band from the wildtype mouse proteome are not detected in the mass spectrometer due to post-translational modifications, such as phosphorylation, acetylation, methylation, palmitoylation or glycosylation. Peptides with such modifications are not found in this assay. If this would be true, a decrease in DAGLα activity in the NPC1 knockout mice would not be detected. Further experiments, such as direct quantification of 2-AG levels, are required to confirm a decrease in DAGLα activity in Niemann-Pick mice. In addition, it would be interesting to find the origin and role of the altered modification of DAGLα in Niemann-Pick type C. If the gel-based ABPP results are confirmed, it would be worthwhile to test the effects of a pharmacological intervention with DAGLα inhibitors, such as DH376 and DO34,[11] in Niemann-Pick disease models.

Finally, it was found that the activities of three non-endocannabinoid hydrolases, namely, CTSA, PPT1 and SCPEP1, were significantly elevated in NPC1 knockout mouse brains. These enzymes are lysosomal proteins, which is in line with the important role of NPC1 in lysosomes. SCPEP1 shows

homology with CTSA[32] and a study with double knockout of SCPEP1 and CTSA suggests they share the same peptide substrate.[33] Knockout of SCPEP1 in mice resulted in viable mice without lysosomal impairment.[32] Mutations in the CTSA gene cause galactosialidosis in humans[34] and secondary deficiencies of β-galactosidase and neuraminidase. This same phenotype is mirrored in a CTSA knockout mice mouse model.[35] The protective role of the enzyme for galactosidase and neuraminidase is a structural function of the enzyme: mice with catalytic serine-to-alanine mutation have normal levels of β-galactosidase and neuraminidase.[36] CTSA inhibitors have been tested in humans[37] and CTSA is a therapeutic target for the treatment of cardiovascular diseases.[38,39] Thus, it would be interesting to test CTSA inhibitors in Niemann-Pick models. Palmitoyl-protein thioesterase 1 (PPT1) is also a lysosomal enzyme[40] and the dysregulation of this enzyme causes a lysosomal storage and neurodegenerative disorder; infantile neuronal ceroid lipofuscinosis.[37] This enzyme removes palmitoyl modifications from proteins that are being degraded in the lysosome. In PPT1 knockout mice cholesterol catabolism is altered.[41] PPT1 has been proposed to hydrolyze 2-AG and might therefore be involved in the ECS.[42] *In vivo* active inhibitors for PPT1[43] have been identified and could therefore also be tested in Niemann-Pick models. To conclude, no altered activity was found of endocannabinoid hydrolases in a Niemann-Pick type C mouse model using a chemical proteomics assay. Three hydrolases were identified with upregulated activity in NPC1 knockout mice, which might be interesting therapeutic target for future studies.

Experimental

Animals. *Npc1*$^{-/-}$ mice, along with wildtype littermates (*Npc1*$^{+/+}$), were generated as published previously.[25] Briefly, the heterozygous BALB/c Nctr-Npc1^{m1N}/J mice (stock number 003092) were obtained from The Jackson Laboratory (Bar Harbor, USA). Mouse pups were genotyped according to published protocols.[26] The mice were housed at the Institute Animal Core Facility in a temperature- and humidity-controlled room with a 12 h light/dark cycle and given free access to food and water *ad libitum*. All animal protocols were approved by the Institutional Animal Welfare Committee of the Academic Medical Centre Amsterdam in the Netherlands. Animals were first anesthetized with a dose of Hypnorm (0.315 mg/mL fenyl citrate and 10 mg/mL fluanisone) and Dormicum (5 mg/mL midazolam) according to their weight. The given dose was 80 µL/10 g body weight. Blood was collected by a heart puncture followed by cervical dislocation. Brains were dissected, rinsed with phosphate-buffered saline (PBS), snap frozen in liquid N_2 and stored at -80°C for biochemistry. Brain tissue was obtained from six female mice, three wildtype and three knockout.

Preparation of mouse tissue proteome. The mouse brains were cut in half with a scalpel, separating the two hemispheres. The mouse brain halves were slowly thawed on ice. The thawed mouse brain halves were dounce homogenized in 1.5 mL cold (4 °C) lysis buffer (20 mM HEPES pH 7.2, 2 mM DTT, 1 mM $MgCl_2$, 25 U/mL benzonase) and incubated for 15 minutes on ice. The suspension was centrifuged (2500 *g*, 3 min, 4 °C) to remove debris. The supernatant was collected and transferred to an ultracentrifuge tube. The debris was resuspended in 0.25 mL lysis buffer and resubjected to centrifugation. The combined supernatants were collected and subjected to ultracentrifugation

(100,000 *g*, 45 min, 4 °C, Beckman Coulter, Type Ti70 rotor). This yielded the membrane fraction as a pellet and the cytosolic fraction in the supernatant. The supernatant was collected and the membrane fraction was suspended in 1.5 mL storage buffer (20 mM HEPES pH 7.2, 2 mM DTT). The total protein concentration was determined with Quick Start Bradford assay (Bio-Rad). Membranes and supernatant fractions were both diluted to either 1.0 mg/mL or 2.0 mg/mL (for proteomics and gel-based ABPP respectively) and were used directly or flash frozen in liquid nitrogen and stored in aliquots at -80 °C until use.

Gel-based ABPP. Mouse brain cytosol or membrane fraction (2.0 mg/mL) was incubated with activity-based probe MB064 (250 nM), TAMRA-FP (500 nM) or DH379 (1 µM) (20 min, rt, 2.5% DMSO). For the competition experiments with inhibitor DH376, this step was preceded by incubation with 100 nM inhibitor (30 min, rt, 2.5% DMSO). For the competition experiments with probe MB108, this step was preceded by incubation with 10 µM probe (30 min, 37 °C, 2.5% DMSO). Laemlli buffer was added to quench the protein activity and the mixture was allowed to stand at rt for at least five minutes before the samples were loaded and resolved on SDS-PAGE gel (10% acrylamide), together with PageRuler Plus Prestained Protein Ladder (Thermo Scientific). The gels were scanned using a ChemiDoc (Bio-Rad, Cy3 channel: expose 180 sec for MB064, 60 sec for DH379/TAMRA-FP, Cy5 channel 10 sec for marker). After fluorescent scanning, the gels were stained with a Coomassie staining solution (0.25% (w/v) Coomassie Brilliant Blue in 50% MeOH, 10% AcOH, 40% MilliQ (v/v/v)). The gels were scanned after destaining with MilliQ. Both the fluorescence and Coomassie images were analyzed using Image Lab 5.2. The Coomassie gel is used to determine protein loading (automatic lane/band detection, background subtraction not enabled, select whole lane as band). The fluorescence bands are quantified using automatic lane/band detection with background subtraction enabled. Using the Coomassie-corrected gel-fluorescence values the average is calculated for WT and KO and a two-sided student's t-test is performed. The activities of proteins were relatively quantified by setting the average WT at 100%.

Western Blot. After the SDS-PAGE gel was resolved and imaged, proteins were transferred to 0.2 µm polyvinylidene difluoride membranes with a Trans-Blot Turbo™ Transfer system (Bio-Rad). Membranes were washed with TBS (50 mM Tris, 150 mM NaCl) and blocked with 5% milk (w/v, Elk magere melkpoeder, FrieslandCampina) in TBST (50 mM Tris, 150 mM NaCl, 0.05% Tween 20) for 1 h at rt. Membranes were then incubated with the primary antibody anti-DAGLα (1:1000, Cell Signaling Technology, #13626) in 5% BSA (w/v) in TBST (o/n, 4˚C), washed with TBST, incubated with matching secondary antibody HRP-coupled-goat-anti-rabbit (1:5000, Santa Cruz, sc2030) in 5% milk in TBST (1 h, rt) and washed with TBST and TBS. Imaging solution (10 mL Luminol, 100 µL ECL enhancer, 3 µL H_2O_2) was added to develop membranes and chemiluminescence was detected on the ChemiDoc (Bio-Rad) using standard chemiluminescence settings. The signal was normalized to Coomassie staining and quantified with Image Lab 5.2.

Activity-based proteomics. Mouse brain membrane or soluble proteome (245 µL, 1.0 mg/mL) was incubated with 5 µL 0.5 mM MB108 (10 µM) or FP-Biotin (10 µM) for 1 h at rt. The labeling reaction was quenched and excess probe was removed by chloroform/methanol precipitation: 250 µL MilliQ, 666 µL MeOH, 166 µL $CHCl_3$, 150 µL MilliQ added subsequently to each sample with a brief vortex after each addition. After centrifugation (4000 rpm, 10 min) the top and bottom layer surrounding the floating protein pellet was removed. 600 µL MeOH was added and the pellet was resuspended by sonication with a probe sonicator (10 sec, 30% amplitude). After centrifugation (14,000 rpm, 5 min) the methanol was removed and the protein pellet was redissolved in 250 µL 6 M Urea/25 mM

ammonium bicarbonate and allowed to incubate for 15 minutes. 2.5 µL 1 M DTT was added and the mixture was heated to 65 °C for 15 minutes. The sample was allowed to cool to rt (~ 5 min) before 20 µL 0.5 M iodoacetamide was added and the sample was alkylated for 30 minutes in the dark. 70 µL 10% (wt/vol) SDS was added and the proteome was heated for 5 minutes at 65 °C. The sample was diluted with 2 mL PBS. 50 µL of 50% slurry of Avidin-Agarose from egg white (Sigma-Aldrich) was washed with PBS and added to the proteome sample in 1 mL PBS. The beads were incubated with the proteome for 3 h, while rotating. The beads were isolated by centrifugation (2500 *g*, 2 min) and washed with 0.5% (wt/vol) SDS in PBS (1x) and PBS (3x). The proteins were digested overnight with 500 ng sequencing grade trypsin (Promega) in 250 µL on-bead digestion buffer (100 mM Tris pH 8, 100 mM NaCl, 1 mM $CaCl_2$, 2% ACN) at 37 °C with vigorous shaking. The pH was adjusted with formic acid to pH 3 and the beads were removed. The peptides were isotopically labeled by on-stage tip dimethyl labeling. Wildtype and knockout samples were differently labeled with isotopic dimethyl labeling and combined after labeling to allow comparison (wildtype light and knockout heavy). The stage tips were made by inserting C18 material in a 200 µL pipet tip. The stepwise procedure given in the table below was followed for stage tip desalting and dimethyl labeling. The solutions were eluted by centrifugal force and the constitutions of the reagents are given below. For label-free quantification samples, step 6 and 7 are omitted.

Step	Aim	Solution	Centrifugation
1	Conditioning	Methanol (50 µL)	2 min 600 *g*
2	Conditioning	Stage tip solution B (50 µL)	2 min 600 *g*
3	Conditioning	Stage tip solution A (50 µL)	2 min 600 *g*
4	Loading	Load samples on stage tips	2.5 min 800 *g*
5	Washing	Stage tip solution A (100 µL)	2.5 min 800 *g*
6	Dimethyl labeling (5x)	20/20/40/40/30 µL L or M reagent	5 min 400 *g*
7	Washing	Stage tip solution A (100 µL)	2.5 min 800 *g*
8	Elution	Stage tip solution B (100 µL)	2.5 min 800 *g*

Stage tip solution A is 0.5% (vol/vol) FA in H_2O. Stage tip solution B is 0.5% (vol/vol) FA in 80% (vol/vol) ACN in H_2O. Dimethyl labeling reagents: Phosphate buffer (50 mM; pH 7.5) with $NaBH_3CN$ 0.03 M containing either 2% (vol/vol) CH_2O (Light) or CD_2O (Medium). After the final elution step, the desired heavy and light samples were combined and concentrated on a Speedvac to remove the ACN. The residue was reconstituted in 95/3/0.1 H_2O/ACN/FA (vol/vol) before LC/MS analysis. Labelled peptides were measured on an Orbitrap. Label-free peptides were measured on a Synapt mass spectrometer.

Orbitrap. Tryptic peptides were analyzed on a Surveyor nanoLC system (Thermo) hyphenated to a LTQ-Orbitrap mass spectrometer (Thermo) as previously described. Briefly, emitter, trap and analytical column (C18, 120 Å) were purchased from Nanoseparations (Nieuwkoop, The Netherlands) and mobile phases (A: 0.1% formic acid/H_2O, B: 0.1% formic acid/ACN) were made with ULC/MS grade solvents (Biosolve). General mass spectrometric conditions were: electrospray voltage of 1.8-2.5 kV, no sheath and auxiliary gas flow, capillary voltage 40 V, tube lens voltage 155 V and ion transfer tube temperature 150 °C. Polydimethylcyclosiloxane (m/z = 445.12002) and dioctyl phthalate ions (m/z = 391.28429) from the environment were used as lock mass. Some 10 µL of the samples was pressure loaded on the trap column for 5 min with a 10 µL/min flow and separated with a gradient of 35 min

5%–30% B, 15 min 30%–60% B, 5 min A at a flow of 300 µL/min split to 250 nL/min by the LTQ divert valve. Full MS scans (300–2000 m/z) acquired at high mass resolution (60,000 at 400 m/z, maximum injection time 1000 ms, AGC 106) in the Orbitrap was followed by three MS/MS fragmentations in the LTQ linear ion trap (AGC 5x103, max inj time 120 ms) from the three most abundant ions. MS/MS settings were: collision gas pressure 1.3 mT, normalized collision energy 35%, ion selection threshold of 750 counts, activation q = 0.25 and activation time 30 ms. Ions of z < 2 or unassigned were not analyzed and fragmented precursor ions were measured twice within 10 s and were dynamically excluded for 60 s. Data analysis was performed using Maxquant with acetylation (protein N term) and oxidation (M) as variable modifications. The false discovery rate was set at 1% and the peptides were screened against reviewed mouse proteome (Uniprot). Serine hydrolases that were identified in at least two repetitive experiments and for which at least one unique peptide and two peptides in total were identified were considered as valid quantifiable hits. For proteins identified by both probes, the normalized ratios from Maxquant were combined for further analysis. The binary logarithm of each ratio was compared to 0 with a student's t-test. The resulting p-values were subjected to a Benjamini-Hochberg correction, setting the false discovery rate at 10% (q=0.1). Briefly, the p-values of all quantifiable hits were ordered from lowest to highest, and the Benjamini-Hochberg statistic was calculated as q * (position in the list) divided by the number of tests. Subsequently, the proteins for which the p-value is smaller than the BH statistic are controlled for a FDR of q*10%.

Synapt. The peptides were measured as described previously for the NanoACQUITY UPLC System coupled to SYNAPT G2-Si high definition mass spectrometer. A trap-elute protocol, where 1 µL of the digest is loaded on a trap column (C18 100 Å, 5 µM, 180 µM x 20 mm, Waters) followed by elution and separation on the analytical column (HSS-T3 C18 1.8 µM, 75 µM x 250 mm, Waters). The sample is brought onto this column at a flow rate of 10 µL/min with 99.5% solvent A for 2 min before switching to the analytical column. Peptide separation is achieved using a multistep concave gradient based on the gradients used in Distler et al.[27] The column is re-equilibrated to initial conditions after washing with 90% solvent B. The rear seals of the pump are flushed every 30 min with 10% (vol/vol) ACN. [Glu^1]-fibrinopeptide B (GluFib) is used as a lock mass compound. The auxiliary pump of the LC system is used to deliver this peptide to the reference sprayer (0.2 µL/min). A UDMS^e method is set up as described in Distler *et al*.[27] Briefly, the mass range is set from 50 to 2,000 Da with a scan time of 0.6 seconds in positive, resolution mode. The collision energy is set to 4 V in the trap cell for low-energy MS mode. For the elevated energy scan, the transfer cell collision energy is ramped using drift-time specific collision energies.[28] The lock mass is sampled every 30 seconds. Raw data is processed in PLGS (v3.0.3) and ISOQuant v1.5.

Data availability. The mass spectrometry proteomics datasets generated for this study have been deposited to the ProteomeXchange Consortium via the PRIDE[44] partner repository with the dataset identifier PXD008979.

References

1. Eva J. van Rooden, Annelot C. M van Esbroeck, Marc P. Baggelaar, Hui Deng, Bogdan I. Florea, André R. A. Marques, Roelof Ottenhoff, Rolf G. Boot, Herman S. Overkleeft, Johannes M. F. G. Aerts, Mario van der Stelt. Chemical proteomics analysis of endocannabinoid hydrolase activity in Niemann-Pick Type C mouse brain. *Frontiers in Neuroscience*, **2018**, 12:440.
2. Marzo, V. Di, Bifulco, M. & Petrocellis, L. De. The endocannabinoid system and its therapeutic exploitation. *Nat. Rev. Drug Discov.* **3**, 771–784 (2004).
3. Blankman, J. L. & Cravatt, B. F. Chemical probes of endocannabinoid metabolism. *Pharmacol. Rev.* **65**, 849–71 (2013).
4. Ogura, Y., Parsons, W. H., Kamat, S. S. & Cravatt, B. F. A calcium-dependent acyltransferase that produces N-acyl phosphatidylethanolamines. *Nat. Chem. Biol.* **12**, 1–5 (2016).
5. Baggelaar, M. P. *et al.* Chemical Proteomics Maps Brain Region Specific Activity of Endocannabinoid Hydrolases. *ACS Chem. Biol.* **12**, 852–861 (2017).
6. Nomura, D. K., Dix, M. M. & Cravatt, B. F. Activity-based protein profiling for biochemical pathway discovery in cancer. *Nat. Rev. Cancer* **10**, 630–638 (2010).
7. Nomura, D. K. *et al.* Monoacylglycerol Lipase Regulates a Fatty Acid Network that Promotes Cancer Pathogenesis. *Cell* **140**, 49–61 (2010).
8. Liu, Y., Patricelli, M. P. & Cravatt, B. F. Activity-based protein profiling: The serine hydrolases. *Proc. Natl. Acad. Sci.* **96**, 14694–14699 (1999).
9. Simon, G. M. & Cravatt, B. F. Activity-based proteomics of enzyme superfamilies: Serine hydrolases as a case study. *J. Biol. Chem.* **285**, 11051–11055 (2010).
10. Baggelaar, M. P. *et al.* Development of an activity-based probe and in silico design reveal highly selective inhibitors for diacylglycerol lipase-α in brain. *Angew. Chem. Int. Ed.* **52**, 12081–12085 (2013).
11. Ogasawara, D. *et al.* Rapid and profound rewiring of brain lipid signaling networks by acute diacylglycerol lipase inhibition. *Proc. Natl. Acad. Sci.* **113**, 26–33 (2016).
12. Baggelaar, M. P. *et al.* A highly selective, reversible inhibitor identified by comparative chemoproteomics modulates diacylglycerol lipase activity in neurons. *J. Am. Chem. Soc.* **137**, 8851–8857 (2015).
13. Nomura, D. K. *et al.* Endocannabinoid Hydrolysis Generates Brain Prostaglandins That Promote Neuroinflammation. *Science.* **334**, 809–814 (2011).
14. van der Stelt, M. & Di Marzo, V. Cannabinoid Receptors and Their Role in Neuroprotection. *NeuroMolecular Med.* **7**, 37–50 (2005).
15. Chiurchiù, V., van der Stelt, M., Centonze, D. & Maccarrone, M. The endocannabinoid system and its therapeutic exploitation in multiple sclerosis: Clues for other neuroinflammatory diseases. *Prog. Neurobiol.* **160**, 82–100 (2017).
16. Hillard, C. Role of Cannabinoids and Endocannabinoids in Cerebral Ischemia. *Curr. Pharm. Des.* **14**, 2347–2361 (2008).
17. Schurman, L. D. & Lichtman, A. H. Endocannabinoids: A promising impact for traumatic brain injury. *Front. Pharmacol.* **8**, 1–17 (2017).
18. Bisogno, T. & Di Marzo, V. The role of the endocannabinoid system in Alzheimer's disease: facts and hypotheses. *Curr. Pharm. Des.* **14**, 2299–3305 (2008).
19. Maccarrone, M., Battista, N. & Centonze, D. The endocannabinoid pathway in Huntington's disease: A comparison with other neurodegenerative diseases. *Prog. Neurobiol.* **81**, 349–379 (2007).
20. Di Marzo, V., Hill, M. P., Bisogno, T., Crossman, A. R. & Brotchie, J. M. Enhanced levels of endogenous cannabinoids in the globus pallidus are associated with a reduction in movement in an animal model of Parkinson's disease. *FASEB J.* **14**, 1432–1438 (2000).

21. Maccarrone, M. *et al.* Levodopa treatment reverses endocannabinoid system abnormalities in experimental parkinsonism. *J. Neurochem.* **85**, 1018–1025 (2003).
22. Baker, D. *et al.* Endocannabinoids control spasticity in a multiple sclerosis model. *FASEB J.* **15**, 300–302 (2000).
23. Scotter, E. L., Abood, M. E. & Glass, M. The endocannabinoid system as a target for the treatment of neurodegenerative disease. *Br. J. Pharmacol.* **160**, 480–498 (2010).
24. Vanier, M. & Millat, G. Niemann-Pick disease type C. *Clin. Genet.* **64**, 269–281 (2003).
25. Marques, A. R. a *et al.* Reducing GBA2 Activity Ameliorates Neuropathology in Niemann-PickType C Mice. *PLoS One* **10**, 1–18 (2015).
26. Loftus, S. K. *et al.* Murine Model of Niemann-Pick C Disease: Mutation in a Cholesterol Homeostasis Gene. *Science.* **277**, 232–236 (1997).
27. Distler, U., Kuharev, J., Navarro, P. & Tenzer, S. Label-free quantification in ion mobility–enhanced data-independent acquisition proteomics. *Nat. Protoc.* **11**, 795–812 (2016).
28. Distler, U. *et al.* Drift time-specific collision energies enable deep-coverage data-independent acquisition proteomics. *Nat. Methods* **11**, 167–70 (2014).
29. Gao, Y. *et al.* Loss of Retrograde Endocannabinoid Signaling and Reduced Adult Neurogenesis in Diacylglycerol Lipase Knock-out Mice. *J. Neurosci.* **30**, 2017–2024 (2010).
30. Nietupski, J. B. *et al.* Iminosugar-based inhibitors of glucosylceramide synthase prolong survival but paradoxically increase brain glucosylceramide levels in Niemann-Pick C mice. *Mol. Genet. Metab.* **105**, 621–628 (2012).
31. Ferraz, M. J. *et al.* Lyso-glycosphingolipid abnormalities in different murine models of lysosomal storage disorders. *Mol. Genet. Metab.* **117**, 186–193 (2016).
32. Kollmann, K. *et al.* Molecular characterization and gene disruption of mouse lysosomal putative serine carboxypeptidase 1. *FEBS J.* **276**, 1356–1369 (2009).
33. Pan, X. *et al.* Serine Carboxypeptidase SCPEP1 and Cathepsin A Play Complementary Roles in Regulation of Vasoconstriction via Inactivation of Endothelin-1. *PLoS Genet.* **10**, (2014).
34. Galjart, N. J., Gillemans, N., Meijer, D. & D'Azzo, A. Mouse 'Protective Protein'. *J. Biol. Chem.* **265**, 4678–4684 (1990).
35. Korah, N., Smith, C. E., D'Azzo, A., Mui, J. & Hermo, L. Characterization of Cell- and Region-Specific Abnormalities in the Epididymis of Cathepsin A Deficient Mice. *Mol. Reprod. Dev.* **66**, 358–373 (2003).
36. Seyrantepe, V. *et al.* Enzymatic activity of lysosomal carboxypeptidase (cathepsin) a is required for proper elastic fiber formation and inactivation of endothelin-1. *Circulation* **117**, 1973–1981 (2008).
37. Tillner, J. *et al.* Tolerability, safety, and pharmacokinetics of the novel cathepsin A inhibitor SAR164653 in healthy subjects. *Clin. Pharmacol. Drug Dev.* **5**, 57–68 (2016).
38. Schreuder, H. A. *et al.* Crystal structure of cathepsin A, a novel target for the treatment of cardiovascular diseases. *Biochem. Biophys. Res. Commun.* **445**, 451–456 (2014).
39. Petrera, A. *et al.* Cathepsin A inhibition attenuates myocardial infarction-induced heart failure on the functional and proteomic levels. *J. Transl. Med.* **14**, 153 (2016).
40. Lu, J. Y., Verkruyse, L. A. & Hofmann, S. L. The effects of lysosomotropic agents on normal and INCL cells provide further evidence for the lysosomal nature of palmitoyl-protein thioesterase function. *Biochim. Biophys. Acta - Mol. Cell Biol. Lipids* **1583**, 35–44 (2002).
41. Ahtiainen, L. *et al.* Palmitoyl protein thioesterase 1 (Ppt1)-deficient mouse neurons show alterations in cholesterol metabolism and calcium homeostasis prior to synaptic dysfunction. *Neurobiol. Dis.* **28**, 52–64 (2007).
42. Wang, R. *et al.* Identification of palmitoyl protein thioesterase 1 in human thp1 monocytes and macrophages and characterization of unique biochemical activities for this enzyme. *Biochemistry* **52**, 7559–7574 (2013).

43. Cognetta, A. B. *et al.* Selective N-Hydroxyhydantoin Carbamate Inhibitors of Mammalian Serine Hydrolases. *Chem. Biol.* **22**, 928–937 (2015).
44. Vizcaíno, J. A. *et al.* 2016 update of the PRIDE database and its related tools. *Nucleic Acids Res.* **44**, D447–D456 (2016).

Chapter 4

Mapping *in vivo* target interaction profiles of covalent inhibitors using chemical proteomics with label-free quantification[1]

Introduction

Determining target protein engagement and off-target activities of small molecules is an essential step in the drug discovery process. Information on target engagement and off-target profile at a certain concentration will help to select the best compound as a drug candidate (in terms of activity and selectivity) and may guide the dose selection by providing information on full target engagement, while minimizing the risk for untoward off-target interactions by preventing overexposure. Information on target engagement in cellular and animal models, as well as in man can be obtained through a variety of experimental techniques, including direct quantification of substrates and/or products of enzymatic reactions, ligand binding studies using radioactive or fluorescent tracers, cellular thermal shift assays and positron emission tomography.[2–5]

Recently, activity-based protein profiling (ABPP) has emerged as a powerful chemical proteomics technology to map the interactions between small molecules and proteins on a global scale in living systems, including cells, animals and humans.[6–8]

Activity-based Protein Profiling. ABPP is a technique pioneered by the Cravatt laboratory,[6] and that relies on active site-directed chemical probes that react, in a mechanism-based fashion, with the catalytic nucleophile of target proteins in their native biological environment. As a result, a covalent and irreversible bond is formed between the chemical probe and the active site of the target protein. Because this process requires a catalytically active protein, these chemical probes report on the abundance of active enzymes. ABPP enables the possibility to study on-target and off-target activities of drug candidates (and metabolites) in their native physiological context, thereby greatly enhancing the therapeutic relevance of the observed target interaction profile. Generally, an activity-based probe (ABP) consists of an electrophile, a reporter group (a biotin or fluorophore), a linker between the electrophile and reporter group and (in

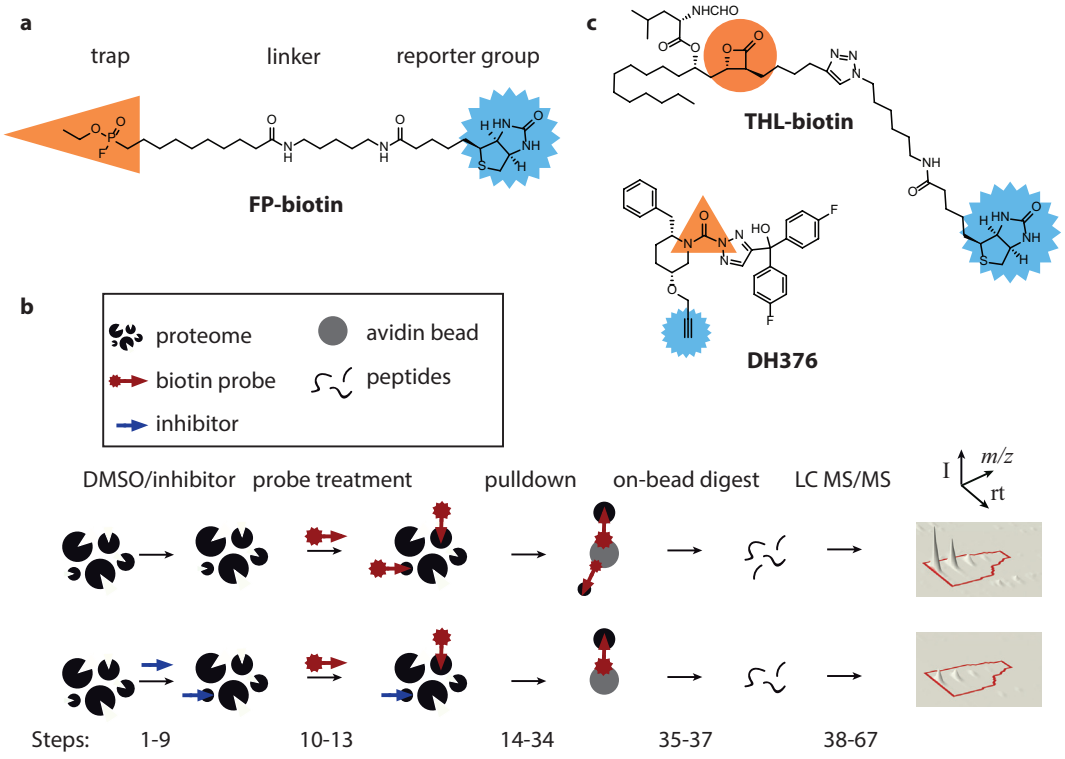

Figure 1 | Chemical proteomics workflow with inhibitor and probes used in this study. (**a**) General activity-based probe (ABP) design, illustrated with FP-biotin. Orange: trap (fluorophosphonate). Blue: reporter group (biotin). (**b**) Workflow of competitive ABPP followed by chemical proteomics: after treatment with inhibitor (or DMSO control), a proteome is labeled with a biotin-containing ABP, enriched using avidin (pulldown), followed by on-bead digestion. The resulting peptides are measured, identified and quantified by LC-MS/MS. Corresponding steps of the Procedure are indicated. (**c**) Structures of the ABP THL-biotin and the inhibitor DH376. Orange: trap. Blue: reporter group.

most cases) a recognition element which targets the probe to a certain enzyme (family). This general design is illustrated with the probe FP-biotin in **Figure 1a**: the fluorophosphonate (FP) is the electrophilic trap and a biotin acts as the reporter group.[6]

A variety of ABPs have been described for different enzyme classes (see **Table 1**).[9,10] An ABP can be specific for one enzyme (tailored probe)[11] or target a group of enzymes sharing recognition or reactivity (broad-spectrum probe).[12] Broad-spectrum probes can be used for competitive ABPP (**Fig. 1b**) to determine target engagement and the selectivity profile of inhibitors. In gel-based competitive ABPP, a fluorescent ABP is incubated with a proteome and the sample resolved and visualized by SDS-PAGE and in-gel fluorescence scanning. Pre-incubation of the proteome with an inhibitor will reduce the

ABP labeling of proteins targeted by the inhibitor.[13] When coupled to a biotin, ABPs enable affinity enrichment using (strept)avidin-beads, proteolytic digestion and identification of the targeted enzymes by high resolution, quantitative liquid chromatography mass spectrometry (LC-MS)-based methods.[14] Compared to gel-based assays, mass spectrometry has the advantage of higher resolution (no band overlap for proteins of similar size), higher dynamic range (proteins of different abundance can be analyzed in parallel) and direct identification of the enriched proteins (bands on a gel have to be validated with genetic knock-out or well-characterized inhibitors). The disadvantage of mass spectrometry based ABPP is the more elaborate sample preparation (typically, a gel-based ABPP experiment can be performed in 3 hours, while a pulldown assay takes 2 days) and the advanced instrumentation required.[15]

Table 1 | Commercially available ABPs for pulldown experiments.

Probe	Enzyme targets	Supplier	Cat. no.
FP-biotin	Serine hydrolases	Santa Cruz Biotechnology	sc-215056A
Desthiobiotin-ATP	Kinases	Thermo Fisher	88311
Desthiobiotin-GTP	GTPases	Thermo Fisher	88315
Biotin-Ahx-SUMO2-VME	SUMO proteases	UbiQ	UbiQ-156
Biotin-ANP-Ub-PA	Deubiquitylating enzymes (DUBs)	UbiQ	UbiQ-077
Biotin-Ahx-Ub-Dha	Ub E1, E2 and E3 ligases	UbiQ	UbiQ-102

Label-free quantification. Quantification of the relative abundance of active proteins using MS-based methods is usually achieved by chemical or metabolic labeling of the proteins by stable heavy isotopes.[16, 17] Recently, label-free quantification approaches have gained interest as a suitable alternative, because they allow for a more simplistic experimental set up avoiding expensive and time consuming labeling steps and do not require analysis of complex mass spectra.[16,18–20] There is no restriction for the number of samples that are to be compared and it is easier to adapt the experimental design. In addition, label-free methods do not require any mixing of samples and, therefore, higher proteome coverage can be achieved. Disadvantages of label-free quantification are the dependency on very stable liquid chromatography separation and spray conditions and the need of technical replicates. Furthermore, data processing time is increased by the requirement of aligning the runs. Label-free quantification has been used extensively in shotgun proteomics, and several examples are reported in the literature of its use in combination with ABPP or affinity-based chemoproteomics.[12,21,22]

Whereas quantification of protein activity in the previous Protocol was performed by dimethyl labeling,[13] now a label-free quantification protocol[18] is described with the use of data-independent

acquisition (DIA) and ion mobility separation (IMS), based on the report of Distler *et al*.[20] In data-dependent acquisition (DDA), peptides above a certain signal intensity threshold are selected for fragmentation. This inherent sampling of high-intensity signals makes it difficult to reproducibly quantify low abundant peptides.[23] DIA is an unbiased method, fragmenting all precursor ions in a certain mass range. However, this approach makes the resulting fragmentation spectra highly complex. In ion mobility separation (IMS), ions are separated in the mass spectrometer according to their mobility in a buffer gas, thereby providing an additional dimension of separation after liquid chromatography.[24] Additionally, precursor ions can be coupled to their fragments on the basis of their drift time in IMS, increasing the number of identified peptides drastically.[25]

Overview of the procedure. The ABPP protocol is demonstrated by identification of the *in vivo* targets of the diacylglycerol lipase inhibitor DH376 in four mouse tissues (brain, kidney, liver and testis) using two biotinylated probes (FP-biotin and THL-biotin (MB108)). In a nutshell, tissue lysates of mice treated with DH376 or vehicle are compared by competitive ABPP (heat-inactivated vehicle samples are used as a control) (**Fig. 1b**). Following tissue lysis (Steps **1**-**9**), enzymes are labeled by incubation with a cocktail of the two biotinylated ABPs (Steps **10**-**13**) and enriched using affinity chromatography (avidin-agarose pulldown, Steps **15**-**34**), and digested with trypsin (Steps **35**-**37**). The resulting tryptic peptides are measured using LC-IMS-MS (liquid chromatography-ion mobility separation-mass spectrometry, Steps **38**-**44**). Label-free quantification is used to compare the different conditions (vehicle vs. heat-inactivated, vehicle vs. inhibitor and the relative enzyme activity across the different tissues) (Steps **45**-**67**). The comparison of these different conditions would not have been possible with dimethyl labeling as a quantification method, due to the lack of multiplicity.

Applications of competitive ABPP. An ABPP protocol is presented that can be used to determine target engagement and selectivity of inhibitors and drug candidates in native proteomes. An earlier version of this protocol has been applied to identify the off-targets of the fatty acid amide inhibitor BIA 10-2474.[26] Competitive ABPP studies are performed with two different activity-based probes: the broad-spectrum serine hydrolase-directed probe fluorophosphonate-biotin (FP-biotin, **Fig. 1a**) and the tailored probe MB108 (THL-biotin, **Fig. 1c**).[27,28] The latter probe preferentially reacts with endocannabinoid hydrolases diacylglycerol lipase α (DAGLα), ABHD6, and ABHD12, as well as with several other enzymes. Together, both probes enabled target engagement assays for FAAH (fatty acid amide hydrolase) and a broad array (>50) of other brain serine hydrolases.[25-31] This competitive ABPP assay confirmed that BIA 10-2474 interacted with FAAH and FAAH2 in human cells.[26] Furthermore, it was discovered that BIA 10-2474 is

not a selective experimental drug, because it inhibits several other lipases, including ABHD6, PNPLA6 and Ces2, which are not targeted by a clinically safe FAAH inhibitor.[26]

Using an adapted version of the protocol, LEI105 (an α-ketoheterocycle)[28] was previously discovered and optimized as a selective and reversible inhibitor for DAGL, an enzyme which catalyzes the conversion of diacylglycerol to the endocannabinoid 2-arachidonoylglycerol (2-AG).[29] Comparative ABPP was used to map the activity of different endocannabinoid hydrolases in various brain regions, both in cannabinoid type 1 receptor knockout and wildtype brain tissue.[30] In addition, competitive ABPP was crucial to identify the first brain active DAGL inhibitor DH376[31,32] (**Fig. 1c)**. Acute pharmacological blockade of DAGL by DH376 resulted in a rapid and dramatic reorganization of the lipid signaling pathways in the brain under normal and neuroinflammatory conditions.[30] Target engagement and selectivity profiling by competitive ABPP using mouse brain proteomes confirmed that DH376 was a selective DAGL inhibitor that only cross-reacted with ABHD6, CES1c and Lipe.[31] ABPP guided the optimal dose selection for further animal studies, showing that DAGLs are involved in modulation of pro-inflammatory prostaglandins and cytokines, lipopolysaccharide-induced anapyrexia and fasting-induced food intake.[31,32]

Limitations and comparison to alternative approaches. For this approach, ABPs are required. For the serine hydrolase (e.g., FP-biotin) and kinase enzyme families, commercial ABPs are available (**Table 1**). THL-biotin and other probes synthesized by our laboratory are available upon request. However, it remains a current limitation of ABPP that organic synthetic expertise is required to synthesize/develop new ABPs.

Competitive ABPP only allows the determination of inhibitor selectivity for the proteins targeted by the ABP. In this protocol, a cocktail of two probes is used to be able to profile more enzymes in parallel. It should, however, be kept in mind that the inhibitor may interact with targets that belong to other protein families. Furthermore, false positive and negative hits are possible. It is, therefore, recommended to confirm off-target activity by orthogonal techniques *in vitro* using recombinant proteins.

There are several alternative methods to study the target interaction profile of covalent inhibitors in living organisms.[2,4] One possibility is to turn the inhibitor of interest into an ABP by attaching a reporter group.[3] The advantage of this approach is that all possible targets may be profiled. It is however important to realize that modification of the inhibitor could influence its activity and the activity of the modified inhibitor should be confirmed in an *in vitro* assay. Several complementary approaches have been developed that rely on the observation that inhibitor binding stabilizes the target protein. The cellular thermal shift assay (CETSA) relies on thermal stabilization of the target proteins by inhibitor binding.[5] Drug affinity responsive target stability (DARTS) is an approach which relies on the assumption that inhibitor targets

are more resistant against proteolysis.[33] Since there is no enrichment step of target proteins in these approaches, detection of low abundance proteins is challenging.

A gel-based approach with fluorescence visualization can also be used for competitive ABPP. This approach has been described in detail in the previous protocol.[13] The main advantage of gel-based ABPP compared to LC-MS methods is the higher throughput of samples. However, LC-MS based ABPP is unrivalled in its depth of analysis, resolution and sensitivity.

Ion mobility separation is a powerful method to increase the analytical depth of the proteomic analysis. Unfortunately, open source software is not yet available to process raw ion mobility data. In this protocol, the vendor software Progenesis is used for data processing. Open source software is published for the label-free data analysis, but this workflow still depends on the vendor software PLGS for raw data processing.[34] For label-free quantification, a very stable liquid chromatography system is required. For the acquisition and processing of high-resolution mass spectrometry data a certain level of expertise is needed.

Since chemical proteomics is a multidisciplinary field in which chemistry, biology and mass spectrometry expertise is needed, this protocol can hopefully serve as a guideline to avoid certain pitfalls.

Experimental design. In the experiment described in this protocol, DH376 is administered to mice and different tissues are collected and lysed. The lysate is separated into membrane and cytosol fractions by centrifugation. The fractionation helps to identify low abundance membrane proteins. Depending on the abundance and distribution of proteins of interest, fractionation can be omitted or elaborated. For example, an elusive calcium-dependent N-acyltransferase was recently reported to be a target of FP-biotin, but only identified by using sucrose gradient fractionation of mouse brain membrane.[35] Comparison of samples to controls is necessary to distinguish specific binders from contaminants and background. In this protocol, heat-inactivated vehicle-treated controls are used to determine if a protein is identified in an activity-based manner. To determine if an enzyme target is enriched compared to the heat-inactivated control, the cut-off values of ANOVA (p) < 0.05 and ratio > 2 are applied. Furthermore, a cocktail of FP-biotin and THL-biotin is used to simultaneously detect multiple serine hydrolases of the endocannabinoid system. This principle of a probe cocktail can also be applied to different ABPs to study enzymatic activities of interest in parallel, thereby minimizing the number of samples. The most cumbersome part of this protocol (which can lead to the highest sample variation) is the methanol-chloroform precipitation (Steps **14**-**21**).[36] This step is necessary to remove excess probe prior to avidin enrichment. This step should be practiced (on any 1.0 mg/mL protein solution), before performing this on valuable samples. The first day of this protocol (up until overnight trypsinolysis in Step **37**) is time-demanding, however there is one optional pause point (step **23**).

This protocol describes the use of LC-IMS-MS with a Synapt G2-Si instrument. The data processing is performed with the commercial software Progenesis, and Top3 quantification is used.[37] Top3 quantification only gives reliable quantification data when low-scoring identified peptides are filtered out. The Benjamini-Hochberg procedure to correct for multiple comparisons, using an FDR of 10% is applied.[38]

Materials

Reagents

- Acetonitrile, ULC/MS grade (Biosolve, cat. no. 012041) **! CAUTION** Acetonitrile is flammable and harmful if inhaled, swallowed or in contact with skin or eyes. Handle in a fume hood and wear labcoat and safety glasses.
- Activity-based probe of interest: In this example FP-Biotin (Santa Cruz Biotechnology, cat. no. sc-215056A) and THL-Biotin (MB108; synthesized as described[27] and available upon request). For an overview of commercially available ABPs, see **Table 1**.
- Ammonium bicarbonate (NH_4HCO_3; Fluka, cat. no. 09830).
- Avidin-Agarose from egg white (Sigma, cat. no. A9207).
- Benzonase Nuclease (Santa Cruz Biotechnology, cat. no. sc-202391).
- Bovine Serum Albumin (BSA; Sigma, cat. no. A9647).
- Bradford reagent (Bio-Rad, cat. no. 500-0006).
- Calcium chloride dihydrate ($CaCl_2 \cdot 2\ H_2O$; Merck Millipore, cat. no. 102382).
- Chloroform (Sigma, cat. no. 32211-M) **! CAUTION** Chloroform is toxic if inhaled and a suspected carcinogen, handle in a fume hood and wear a labcoat and safety glasses.
- DMSO (Sigma, cat. no. 34943-M).
- Dithiothreitol (DTT; BioChemica, cat. no A1101) **! CAUTION** DTT is an eye and skin irritant.
- Empore™ C18 47 mm Extraction Disc (3M Purification Inc., Model 2215).
- Formic acid, LC-MS grade (Actu-all Chemicals, art. nr. 8060128A1) **! CAUTION** Can cause severe burns, handle in a fume hood, wear a labcoat and safety glasses
- [Glu^1]-fibrinopeptide B (GluFib; Waters, product no. 700004729).
- Glycerol 85% (Merck Millipore, cat. no. 104092).
- Hydrochloric acid (HCl; Sigma, cat. no. 30721-M) ! **CAUTION** Can cause severe burns, handle in a fume hood, wear a labcoat and safety glasses.
- HEPES, free acid (Millipore, cat. no. 391340).
- Inhibitor of interest: In this example the diacylglycerol lipase inhibitor DH376 (synthesized as

described[31] and available upon request).

- Iodoacetamide (IAA; Sigma, cat. no. I6125) **! CAUTION** IAA is toxic if swallowed and may cause an allergic reaction.
- Leucine Enkephalin (LeuEnk; Waters, product no. 186006013).
- Magnesium chloride hexahydrate ($MgCl_2 \cdot 6\ H_2O$; Acros Organics, cat. no. 413415000).
- Methanol, reagent grade (Sigma, cat. no. 32213-M) or ULC/MS grade (Biosolve, cat. no. 136841) **! CAUTION** Methanol is flammable and toxic. Handle in a fume hood and wear safety glasses.
- Mice: In the example described in this Protocol, four tissues (brain, kidney, liver and testis) from mice (C57BL/6 mice, Charles River Mice) treated with vehicle or DH376 were used (see Reagent Setup). **! CAUTION** Any experiments involving live mice must conform to relevant Institutional and National regulations. The animal experiments described in this Protocol were conducted in accordance with the ethical committee of Leiden University (DEC#14137).
- Sodium dodecyl sulfate (SDS; MP Biomedicals cat. no. 811032) **! CAUTION** SDS is toxic.
- Sodium chloride (NaCl; Chem-Lab, art. no. CL00.1423).
- Sodium hydroxide (NaOH; Acros Organics, cat. no. 134070010) **! CAUTION** NaOH can cause severe burns, wear a labcoat and safety glasses.
- Tris(hydroxymethyl)aminomethane (Tris; Acros Organics cat. no. 16762).
- Trypsin, sequencing grade (Promega, cat. no. V5111).
- Urea (Sigma, cat. no. 33247).
- Water, ULC/MS grade (Biosolve, cat. no. 232141) and Milli-Q water (see Equipment). ▲ **CRITICAL** Avoid using autoclaved water, because it may contain high chemical background.
- Yeast enolase (Waters, product no. 186002325. SwissProt P00924).

Equipment

- Analytical column (HSS-T3 C18 1.8 μM, 75 μM x 250 mm, Waters).
- Bio-Spin columns (Bio-Rad, cat. no. 7326204).
- Centrifuge for 15 mL tubes, 2500 *g* required. (Heraeus Megafuge 1.0R).
- Centrifuge for 1.5-2 mL tubes, 18,400 *g* required (Eppendorf, 5415D).
- Dounce homogenizer (Wheaton, supplier no. 357422).
- Eppendorf ThermoMixer C.
- Example datasets: The mass spectrometry proteomics data used in this Protocol have been deposited to the ProteomeXchange Consortium via the PRIDE[39] partner repository with the dataset identifier PXD007965.

- Insulin syringe (Terumo, Myjector U-100).
- Microplate, 96-well clear flat bottom (greiner bio-one, cat. no. 655191).
- Milli-Q advantage A10 water purification system (Merck Millipore).
- NanoACQUITY UPLC System (Waters).
- Overhead shaker (Heidolph, Reax 2).
- Pipette, 10 mL (Sarstedt, order no. 86.1254.001).
- Pipette tip, blue (Sarstedt, order no. 70.762.100).
- Pipette tip, yellow (Sarstedt, order no. 70.760.502).
- Pipette tip, grey (Sarstedt, order no. 70.1130.600).
- Probe sonicator (Branson, Digital Sonifier).
- Software: Progenesis (v3.0: http://www.nonlinear.com/progenesis/qi-for-proteomics/), Excel (Microsoft 2010), KNIME (3.2.1: www.knime.com).
- SpeedVac (Eppendorf, concentrator 5301).
- Suction pump (Meyvis B.V.).
- SYNAPT G2-Si high definition mass spectrometer (Waters).
- Tecan GENios Microplate Reader.
- Trap column (C18 100 Å, 5 µM, 180 µM x 20 mm, Waters, P/N 186006527).
- Tube, 15 mL (Sarstedt, order no. 62.554.502).
- Tube, 2 mL (Sarstedt, order no. 72.691).
- Tube, clear 1.5 mL (Sarstedt, order no. 72.690.550).
- Tube, protein low binding (Sarstedt, order no. 72.706.600).
- Ultracentrifuge (Beckman Coulter, optima L-90K).
- Vials, LC-MS (Waters, part no. 600000671CV).
- Vortex mixer.

Reagent setup

All reagents are made with 18.2 MΩ MilliQ water unless indicated otherwise.

▲ CRITICAL

Ammonium bicarbonate buffer Dissolve 198 mg NH_4HCO_3 in water to a final volume of 10 mL for a 250 mM solution. **▲ CRITICAL** Ammonium bicarbonate is thermally unstable. Always prepare this buffer directly before use.

Benzonase stock Prepare a 10 U/µL solution in storage buffer (50% (vol/vol) glycerol, 20 mM Tris pH 8.0, 2 mM $MgCl_2$, 20 mM NaCl). Aliquots of this solution can be stored at -20 °C for at least 6 months.

$CaCl_2$ stock Dissolve 147 mg calcium chloride dehydrate in 1 mL water to prepare a 1 M $CaCl_2$ solution. This solution can be stored at room temperature (18-24 °C) for up to one month.

DTT stock Dissolve 1.54 g DTT in water to a final volume of 10 mL for a 1 M solution. Aliquots can be stored at -20 °C for up to 3 months. Discard after thawing.

FP-Biotin stock Dissolve FP-Biotin in DMSO to a final concentration of 1 mM. Aliquots of this solution can be stored at -20 °C for at least one year.

GFP stock Dissolve 0.1 mg of GluFib in 1 mL water (64 pmol/µL final concentration). Aliquots of this solution can be stored at -20 °C for at least one year.

HCl stock Prepare a 1 mM HCl solution by diluting 37% (wt/vol) HCl (~12 M) into water. Check if pH is 3. This solution can be stored at room temperature for up to one month.

HEPES stock Prepare 1 M HEPES in water and adjust to pH 7.2 with NaOH. This solution can be stored at room temperature for up to one month.

HEPES/DTT buffer For 30 mL buffer, combine 29.4 mL water, 0.6 mL HEPES stock and 60 µL DTT stock (final concentrations 20 mM HEPES, 2 mM DTT). Always prepare this buffer directly before use.

IAA stock Dissolve 92 mg iodoacetamide in 1 mL water for a final concentration of 0.5 M.

▲ **CRITICAL** IAA is light sensitive. Always prepare this solution directly before use.

LC-MS sample solution For 2 mL, combine 1900 µL ULC/MS grade water, 60 µL acetonitrile, 2 µL formic acid and 40 µL yeast enolase stock (final concentrations 3% (vol/vol) acetonitrile, 0.1% (vol/vol) formic acid and 20 fmol/µL enolase). Prepare this solution directly before use.

LeuEnk stock Dissolve 3 mg of LeuEnk in 3 mL water. Aliquots of this solution can be stored at -20 °C for up to one year.

Lockmass solution Prepare 30 mL of a 1:1 (vol:vol) solution of acetonitrile and ULC/MS grade water containing 0.1% (vol/vol) formic acid, add 47 µL GFP stock solution and 6 µL LeuEnk stock solution (final concentrations 200 pg/µL LeuEnk and 100 fmol/µL GFP). This solution can be stored at room temperature for up to one month.

Lysis buffer For lysing 12 tissues, prepare 30 mL lysis buffer by combining 29.2 mL water, 0.6 mL HEPES stock, 60 µL DTT stock, 30 uL $MgCl_2$ stock and 75 µL benzonase (final concentrations 20 mM HEPES, 2 mM DTT, 1 mM $MgCl_2$, 25 U/mL benzonase). Always prepare this buffer fresh before use and keep on ice.

▲ **CRITICAL** Do not add protease inhibitor to the lysis buffer as this might inhibit several of the probe targets.

$MgCl_2$ stock Dissolve 2.0 g of $MgCl_2 \cdot 6\ H_2O$ in water to a final volume of 10 mL for a 1 M solution. This solution can be stored at room temperature for up to one month.

Mobile phase A/weak wash Prepare a 0.1% (vol/vol) formic acid solution in ULC/MS grade water. This solution can be stored at room temperature for up to one month.

Mobile phase B/strong wash Prepare a 0.1% (vol/vol) formic acid solution in ULC/MS grade acetonitrile. This solution can be stored at room temperature for up to one month.

Mouse tissues Mice were injected with 30 mg/kg DH376 (or vehicle) i.p. in 18:1:1 (vol:vol:vol) solution of saline:ethanol:PEG40 ethoxylated castor oil (10 µL/g body weight of mouse). After 2 h, mice were euthanized and tissues were collected. Tissues can be stored at -80 °C for at least two years.

▲ **CRITICAL** The vehicle and inhibitor treated tissues to be compared should be prepared under the same conditions to prevent changes in enzyme activity (arising from different amounts of freeze-thaw cycles for example).

NaCl stock Dissolve 0.58 g of NaCl in water to a final volume of 10 mL for a 1 M solution. This solution can be stored at room temperature for up to one month.

On Bead-Digestion buffer (OB-Dig) For 24 samples, combine 4668 µL water, 600 µL Tris stock, 600 µL NaCl stock, 6 µL $CaCl_2$ stock and 120 µL acetonitrile (final concentrations 100 mM Tris, 100 mM NaCl, 1 mM $CaCl_2$ and 2% (vol/vol) acetonitrile). This buffer should be prepared fresh.

PBS 10x stock Dissolve 68.05 g KH_2PO_4 in 500 mL water (heat to 40 °C dissolve), dissolve 261.23 g K_2HPO_4 in 1500 mL water, mix and add 877 g NaCl, add water to a final volume of 10 L, filter over 0.22 µM filter (final concentrations 150 mM KH_2PO_4, 50 mM KH_2PO_4 and 1.5 M NaCl). This solution can be stored at room temperature for up to three months.

PBS Dilute PBS 10x stock ten times in Milli-Q water (pH should be 7.5). This solution can be stored at room temperature for up to one month.

PBS/SDS Add 50 mL SDS stock to 950 mL PBS (final concentration 0.5% (wt/vol) SDS). This solution can be stored at room temperature for up to one year.

Probe cocktail Mix equal volumetric amounts of FP-Biotin stock and THL-Biotin stock. Aliquots of this solution can be stored at -20 °C for at least one year.

SDS stock Prepare a 10% (wt/vol) SDS solution in water. This solution can be stored at room temperature for up to one year.

Seal wash Prepare a 10% (vol/vol) acetonitrile solution in water (both ULC/MS grade).

StageTip solution A Prepare an 0.5% (vol/vol) formic acid solution in water. This solution can be stored at room temperature for up to one month.

StageTip solution B Prepare an 80% (vol/vol) acetonitrile, 0.5% (vol/vol) formic acid solution in water. This solution can be stored at room temperature for up to one month.

StageTips See equipment setup.

THL-Biotin stock Dissolve THL-Biotin in DMSO to a final concentration of 1 mM. Aliquots of this solution can be stored at -20 °C for at least one year.
Tris stock Prepare 1 M Tris in water and adjust to pH 8 with HCl. This solution can be stored at room temperature for up to one month.
Trypsin solution Dissolve 20 μg of trypsin in 40 μL 1 mM HCl stock (final concentration 0.5 μg/μL). Store this solution at -20 °C for up to one month and avoid freeze-thaw cycles.
Urea buffer Add 1 mL ammonium bicarbonate buffer (250 mM) to 3.6 g urea and adjust with water to a final volume of 10 mL (final concentrations 6 M urea and 25 mM ammonium bicarbonate). This buffer should be prepared fresh.
Yeast enolase stock Dissolve 1 nmol yeast enolase in 1 mL 3% (vol/vol) acetonitrile in water. This solution can be stored at room temperature for at least one year.

Equipment setup
StageTips StageTips are used as a final step in sample preparation. Their preparation and use is described in Nature Protocols by Rappsilber *et al*.[40] Empore™ C18 47 mm Extraction Discs (see Reagents) are used to make the StageTips. Typically, two discs are stacked on top of each other to make StageTips with two layers of column material, inserted in a yellow pipette tip. It is recommended to make all the StageTips required for one experiment at once to achieve a more consistent back-pressure. The C18 material should be pressed into the pipette tips with as little pressure as possible.
NanoUPLC The LC-MS method is based on the approach described by Distler *et al*.[20] A summary of changes in approach is given here. DMSO is not added to the LC solvents. Therefore, a lower source temperature is used (80 °C instead of 100 °C). Because the affinity chromatography step (pulldown) makes the samples less complex, this gradient is shorter. A trap-elute protocol is used, where the digest is loaded on a trap column followed by elution and separation on the analytical column. The sample is brought onto this column at a flow rate of 10 μL/min with 99.5% solvent A for 2 min before switching to the analytical column. Peptide separation is achieved using a multistep concave gradient based on the gradients used in Distler *et al*.[20] The column is re-equilibrated to initial conditions after washing with 90% solvent B. The detailed protocol is specified below:

Time (min)	Gradient composition (%B)	Flow rate (nL/min)
0.0	1.0	400
2.4	1.0	400
4.2	5.0	300
10.2	7.6	300
15.6	10.3	300
21.0	13.1	300
25.8	16.1	300
30.6	19.2	300
35.4	22.4	300
40.2	25.7	300
45.0	29.1	300
49.8	32.6	300
54.0	36.2	300
58.2	40.0	300
58.8	90.0	400
60.3	90.0	600
61.2	90.0	600
61.5	1.0	400
70.8	1.0	400

The rear seals of the pump are flushed every 30 min with 10% (vol/vol) ACN. [Glu[1]]-fibrinopeptide B (GluFib) is used as a lock mass compound. The auxiliary pump of the LC system is used to deliver this peptide to the reference sprayer (0.2 μL/min).

MS acquisition method A UDMS[e] method is set up as described in Distler *et al*.[20] Briefly, the mass range is set from 50 to 2,000 Da with a scan time of 0.6 seconds in positive, resolution mode. The collision energy is set to 4 V in the trap cell for low-energy MS mode. For the elevated energy scan, the transfer cell collision energy is ramped using drift-time specific collision energies.[34] The lock mass is sampled every 30 seconds.

Procedure

Tissue lysis ● TIMING ~4 h for 12 tissues

▲ **CRITICAL** Steps **1-9** are performed on ice to prevent protease activity. Make sure to cool centrifuges (4 °C) and dounce homogenizer (on ice).

1| Thaw the tissue on ice (~0.5 h) and cool the lysis buffer on ice.
▲ **CRITICAL STEP** The vehicle and inhibitor treated tissues to be compared should be prepared under the same conditions to prevent changes in enzyme activity (arising from different amounts of freeze-thaw cycles for example).

2| Manually lyse the tissue in 2 mL pre-cooled lysis buffer using a dounce homogenizer. The amount of strokes required depends on both the type of tissue and the size. Typically, for brain (soft tissue) and heart (though tissue) 5 and 25 strokes are used for complete homogenization. Transfer the lysed tissue to a 2 mL tube.

3| Incubate the homogenized tissue on ice for 15 min.

4| Pellet cell debris by centrifugation (3 min, 2500*g*, 4 °C) and transfer the supernatant to an ultracentrifuge tube. Balance pairs of samples using an analytical balance and if necessary, adjust the weight by adding lysis buffer.

5| Separate the lysate into membrane and cytosol fractions by ultracentrifugation (45 min, 100,000*g*, 4 °C).
▲ **CRITICAL STEP** Depending on the abundance and distribution of proteins of interest, this fractionation step can be omitted or elaborated (Experimental Design).
! CAUTION The tubes should be undamaged, properly balanced and sealed. The rotor should be undamaged, clean and dry.

6| Collect the supernatant into a tube as cytosolic fraction.

7| Resuspend the pellet (membrane fraction) in 1-2 mL HEPES/DTT buffer (amount depends on the size of the pellet, typically 1 mL for kidney and testis, 1.5 mL for brain and 2 mL for liver gives sufficient protein concentration) by pipetting up and down. After transferring to a 2 mL tube, use an insulin syringe to suck up the membrane fraction and push it through the needle

once for homogenization.

8| According to the manufacturer's protocol (Bulletin #4110065, Bio-Rad), perform the Bradford assay to determine the protein concentration. Usually, approximately the following protein amounts are obtained:

Tissue	Protein yield cytosol (mg)	Protein yield membrane (mg)
Brain	~6	~5
Kidney	~8	~5
Liver	~30	~20
Testis	~4	~3

9| Dilute the samples to 1.0 mg/mL using HEPES/DTT buffer, aliquot into 0.245 mL fractions, snap freeze in liquid nitrogen and store at -80 °C.

▲ **CRITICAL STEP** To retain enzyme activity and prevent protein degradation it is important that the lysates are snap frozen and freeze-thaw cycles are avoided.

■ **PAUSE POINT** The lysates can be stored at -80 °C for at least six months. For some enzymes, freshly prepared lysate may give better probe labeling.

Probe incubation ● TIMING **~2 h**

10| Thaw the lysates on ice (~1 h) and transfer 245 µL of the protein sample (1.0 mg/mL) into each clear 1.5 mL tube. Prepare one tube for each inhibitor-treated sample, two tubes for each vehicle sample.

11| In order to prepare heat-inactivated control samples, incubate one of the vehicle-treated samples for 5 min at 100 °C. It is advised to add 25 µL 10% (wt/vol) SDS (final concentration is 1% (wt/vol) SDS) to prevent protein precipitation in this step.

12| Add 5 µL of probe cocktail to each sample and vortex briefly. The same protocol can be used when the probes are tested separately, the only modification being the use of 50% less avidin beads in **Step 28**.

13| Incubate the samples for 30 min at 37 °C while shaking (300 rpm), followed by a short spin down.

Methanol/chloroform precipitation ● TIMING **~1.5 h for 24 samples**

! CAUTION Perform steps **1**-**21** in a fume hood and discard the supernatants obtained in steps **18** and **21** into halogenated organic waste.

14| Add 250 µL water to each sample for a final volume of 500 µL.

▲ **CRITICAL STEP** The ratios between water, MeOH and $CHCl_3$ are important. It is therefore required to adjust the volume to 500 µL also when using a different volume of protein sample.

15| Add 666 µL MeOH and briefly vortex.

16| Add 166 µL $CHCl_3$ and briefly vortex.

17| Add 150 µL water and briefly vortex, this should result in a cloudy suspension (**Fig. 2-1**).

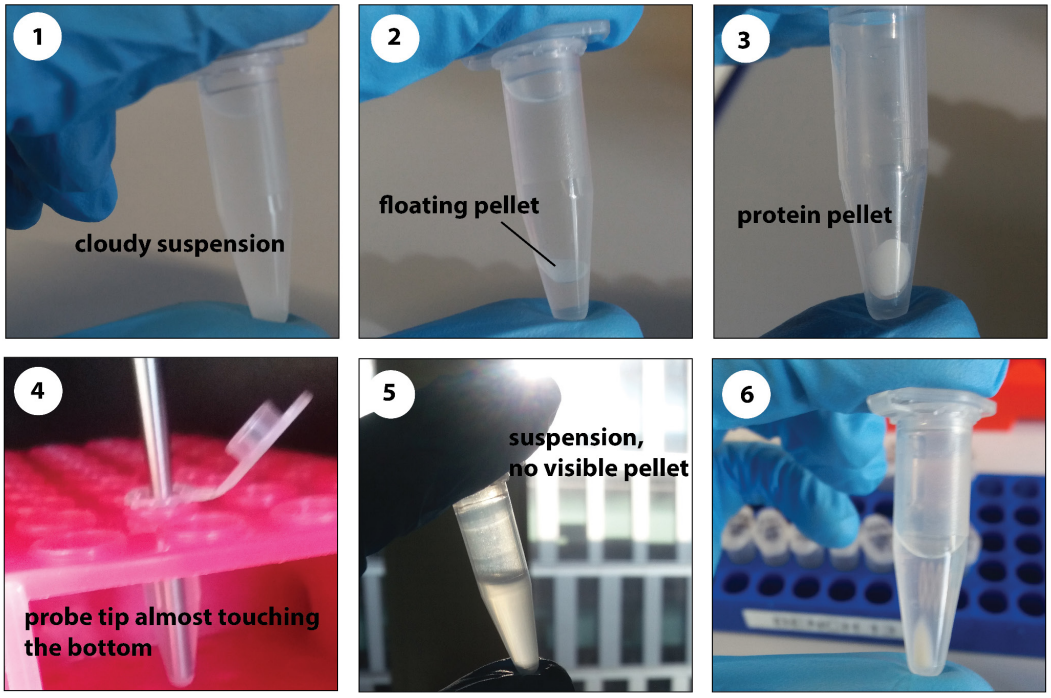

Figure 2 | Cartoon of a successfully performed methanol/chloroform precipitation (Steps **14**-**21**).

18| Pellet the precipitated protein by centrifugation (10 min, 1500*g* at room temperature), this should result in a floating pellet (**Fig. 2-2**). Remove the upper and lower layer without disturbing the floating pellet (this works best by holding the tube at a 45° angle to stick the protein pellet against the side, **Fig. 2-3**).

▲ **CRITICAL STEP** Handle the samples carefully to prevent disrupting the protein pellet.

? TROUBLESHOOTING

19| Add 600 µL MeOH to the pellet.

20| Resuspend the pellet by sonication with a probe sonicator (10 sec, 30% amplitude), this should result in a suspension without any visible protein pellet (**Fig. 2-5**)

▲ **CRITICAL STEP** The tip of the probe sonicator should be positioned just above the bottom of the tube (**Fig. 2-4**).

21| Pellet the protein by centrifugation (5 min, 18,400*g* at room temperature) (**Fig. 2-6**) and remove the supernatant.

▲ **CRITICAL STEP** Close the tubes after removing the supernatant to prevent the pellet from drying out, as this makes redissolving difficult.

Reduction, alkylation and avidin enrichment ● **TIMING ~5 h**

▲ **CRITICAL** The incubation times of steps **24**-**27** can be used to perform steps **28**-**31**.

22| Add 250 µL urea buffer to each sample.

23| Resuspend the pellet by thoroughly pipetting up and down with a yellow pipette tip (~10 times, pipettor set to ~200 uL)

? TROUBLESHOOTING

■ **PAUSE POINT** The solubilized protein samples can be stored at -80 °C for at least one month.

24| Add 2.5 µL DTT stock, vortex briefly, spin down briefly and incubate for 15 min at 65 °C while shaking (600 rpm).

25| Let samples cool down to room temperature (at least 5 min).

26| Add 20 µL IAA stock, vortex briefly and incubate for 30 min at room temperature in the dark

(for example, in a drawer or wrapped in aluminum foil).

27| Add 70 µL SDS stock, vortex briefly and incubate for 5 min at 65 °C.

28| For 24 samples, remove 2.4 mL avidin beads from a 50% slurry (100 µL slurry per sample) divide over four 15 mL tubes (600 µL per tube). Be sure to properly homogenize the slurry before pipetting. When testing the individual probes (Step **12**), 50 µL slurry can be used per sample.

29| Wash the beads three times with 10 mL PBS. Pellet the beads by centrifugation (2 min, 2500 *g*) and remove the supernatant with a suction pump.

▲ **CRITICAL STEP** Be careful not to suck up the beads.

30| Resuspend the beads in 6 mL PBS per tube.

31| For 24 samples, prepare 24 tubes (15 mL) with 2 mL PBS and 1 mL beads from step **30**. Add each individual sample from step **27** to one of these tubes.

32| Incubate the samples while rotating at low speed using an overhead shaker for at least 3 h at room temperature.

Wash beads ● **TIMING ~1.5 h** for 24 samples

▲ **CRITICAL** This step can be performed twice as fast with two people – one adding buffer and centrifuging and the other removing the supernatant.

33| Pellet the beads by centrifugation (2 min, 2500 *g* at room temperature) and remove the supernatant.

▲ **CRITICAL STEP** Be careful not to suck up the beads.

34| Wash the beads once with 6 mL PBS/SDS, followed by three times with 6 mL PBS. Pellet beads by centrifugation (2 min, 2500 *g* at room temperature) after each washing step and remove the supernatant.

▲ **CRITICAL STEP** Be careful not to suck up the beads.

On-bead digestion ● TIMING ~0.5 h + overnight digestion

35| Add 250 µL OB-Dig buffer to the beads and transfer to a 1.5 mL low binding tube.

▲ **CRITICAL STEP** Make sure to transfer all the beads, pipette up and down to homogenize and do not push the pipette tip to the bottom of the tube as this will result in leaving the beads in the tube.

36| Add 1 µL (500 ng) trypsin solution per sample. The trypsin stock can also be diluted (24 µL in 6 mL OB-Dig buffer) to be able to pipette larger volumes (250 µL) – this might improve consistency.

37| Digest overnight at 37 °C with vigorous shaking (950 rpm).

Sample preparation ● TIMING ~3 h

38| Spin down briefly and add 12.5 µL formic acid, briefly vortex and spin down.

39| Remove the beads by filtering the sample through a biospin column by centrifugation (2 min, 600 *g* at room temperature) and collect the flow-through in a 2 mL tube.

40| Condition the StageTips (see Equipment Setup), load the sample and wash the sample following the scheme below. The flow-through from conditioning, loading and washing can be discarded. Elution should be done in a low binding tube.

▲ **CRITICAL STEP** Centrifugation speed and duration are merely estimates. Solutions should have entirely run through without drying of the column.

Step	Aim	Solution	Centrifugation
1	Conditioning	Methanol (50 µL)	2 min 300 *g*
2	Conditioning	Stage tip solution B (50 µL)	2 min 300 *g*
3	Conditioning	Stage tip solution A (50 µL)	2 min 300 *g*
4	Loading	Load samples on stage tips	2 min 600 *g*
5	Washing	Stage tip solution A (100 µL)	2 min 600 *g*
6	Switch to low binding tube		
7	Elution	Stage tip solution B (100 µL)	2 min 600 *g*

41| Evaporate the solvent in a SpeedVac.

■ **PAUSE POINT** Store the samples at -20 °C until required.

42| Reconstitute sample in 50 µL of LC-MS sample solution.

43| Prepare a QC sample by pooling 2 µL from each sample.

LC-IMS-MS analysis ● TIMING ~1 h per sample per replicate

44| Inject 1 µL of a sample onto the UPLC-IMS-MS system (see Equipment Setup) and perform at least duplicate LC-MS analysis of each sample.

▲ CRITICAL STEP To prevent drift in instrument performance influencing the results, make sure to randomize the measurement of biological replicates and perform technical replicates of QC samples to check the variation in LC-MS performance. It is recommend to run a QC sample after every 24 MS runs.[20]

? TROUBLESHOOTING

Data processing and analysis ● TIMING ~5 h per 16 runs

45| Open Progenesis QI for proteomics. Create new label-free experiment. Choose Data type "Profile data" and Machine type "High resolution mass spectrometer". Choose an experiment folder (use the same name as the experiment name).

46| Import data: select the .raw folder of each LC-MS run that must be compared. If samples are fractionated (step 5), analyze the fractions separately using the processing parameters specified below. Perform lock mass calibration with lock mass *m/z* 785.8426. Perform MS^E identification workflow (the default energy thresholds and elution start 10 min and elution end 65 min were used in this example. The optimal settings depend on the instrument and the LC gradient). Non-default settings are indicated with an asterisk:

47| Perform automatic processing while the raw data is importing. Assess all runs in the experiment for suitability as alignment reference. Automatically align the runs and perform peak picking with the default parameters. Set the parameters to identify peptides. Use the DataBank Editor to select the FASTA file (**Box 1**) and add with parsing rules: UNIPROT. Select trypsin as digest reagent, 2 missed cleavages, max protein mass 250 kDa, modifications carbamidomethyl C (fixed) and oxidation M (variable). Search tolerance parameters: set FDR to less than 1% and ion matching requirements: at least 2 fragments/peptide, 5 fragments/protein and 1 peptide/protein. Protein quantitation: select relative quantitation using Hi-N with N =3 and use protein grouping. Depending on the sample complexity and number of runs being compared, processing may take up to one hour per sample.

Parameter	Value
Lock mass m/z	785.8426
Low energy threshold	150 counts
Elevated energy threshold	30 counts
Elution start	Run start
Elution end	Run end
Alignment reference	Assess all runs in the experiment for suitability
Automatic alignment	Yes
Peak picking	Yes
FASTA file	See **Box 1***
Digest reagent	trypsin
Missed cleavages	Max 2*
Modifications	Fixed carbamidomethyl C, variable oxidation M
FDR less than	1%*
Fragments/peptide	2*
Fragments/protein	5*
Peptides/protein	1
Quantitation method	Relative quantitation using Hi-N
Number of peptides to measure per protein (N)	3
Protein grouping	Yes

Box 1 | Database generation
For an excellent tutorial on the bioinformatics behind protein identification, see Vaudel *et al*.[41] Here are the steps to generate the database used in this study to search for protein identifications in Progenesis:

1. Go to www.uniprot.org.[42] Under "Proteomes" search for "Mus musculus" and select the mouse proteome (ID UP000000589).
2. View all proteins, select the reviewed proteins and download as an uncompressed FASTA (canonical) file. ▲ **CRITICAL STEP** For this study only the reviewed part of the mouse proteome was selected, because the unreviewed (TrEMBL) database contains many duplicate proteins. This makes identification of unique peptides more difficult. If your organism of interest is not as extensively reviewed as the mouse proteome however, or if you are searching for novel, unknown proteins, it might be better to use the unreviewed proteome.
3. Add expected contaminants to the database: trypsin, yeast enolase (peptide standard added to all samples) and avidin (from the on-bead digestion). Search the Uniprot database (accessions P00761, P00924 and P02701), go to the "sequence" tab and click the "FASTA" button. Paste this sequence into the mouse proteome fasta file.

48| Review alignment: check if the automatic alignment algorithm has allocated vectors and make sure the part of the chromatogram where peptides elute has good alignment quality.

? TROUBLESHOOTING

49| Filtering: select ions with charges 2, 3, 4, 5, 6 and 7+ and delete non-matching peptide ions (roughly 20-25%).

50| Review normalization: check if certain samples deviate from the normalization reference.

51| Experiment design setup: choose between-subject design. Create separate designs for vehicle vs heat and vehicle vs inhibitor.

52| QC metrics: use the QC metrics to quickly identify possible errors in sample preparation or acquisition due to the visualization of complex data across the separate runs.

53| Refine identifications: use PLGS score less than 6.0 as batch deletion criterion and delete matching search results (only peptides with a score of 6.0 or more should be used for protein quantitation).

▲ CRITICAL STEP This step is crucial to obtain reliable quantitative data. The search algorithm tries to identify as many peptides as possible, and the low-scoring peptides are very unreliable, resulting in unreliable quantified proteins.

54| Review proteins: export protein measurements for each experimental design setup. The protein data is exported as .csv files and the analysis can be continued with Excel, for example (step **57**). For proteins of interest, view peptide measurements. Each peptide has a unique identifier which can be used to find the spectrum and chromatogram in "Review peak picking". The fragmentation spectrum can be found in "Identify peptides".

55| Check if the data clusters according to the experimental conditions using PCA under Protein statistics.

56| Repeat steps **45-55** for each fraction. Open Progenesis and go to "Combine analysed fractions". Select "Recombine analysed fractions". Import data and recombine samples. Go to "Experiment design setup" and select the sample grouping. Go to "review proteins" and export protein

measurements. Check if the data clusters according to the experimental conditions using PCA under Protein statistics.

57| Use Excel to open the "vehicle-vs-heat" .csv file created in step **56**. Save as .xlsx file (for data management, extend the file name with "-analysis", and keep the .csv file as "raw" data from Progenesis).

58| Insert a column and extract the gene name from description using (for example) the following Excel formula (K4 is the cell containing the description in this example):

=MID(K4,SEARCH("GN=",K4)+3,SEARCH("PE=",K4)-SEARCH("GN=",K4)-4)

Applying this formula to the string "Fatty-acid amide hydrolase 1 OS=Mus musculus GN=Faah PE=1 SV=1" should return "Faah".

59| Delete proteins with 0 unique peptides or a peptide count < 2. Calculate the average normalized abundance for the vehicle and heat treated control samples. Use these values to calculate the ratio of vehicle/heat.

60| Select the proteins with Anova(p) < 0.05 and ratio > 2 (enriched in vehicle).

61| Use Excel to open the "vehicle-vs-inhibitor" .csv file created in step **56**. Save as .xlsx file (for data management, extend the file name with "-analysis", and keep the .csv file as "raw" data from Progenesis).

62| Extract the gene names as in step **58**. Copy the gene names from the proteins selected in step **60** and paste into a second sheet called "heat-filtered".

63| Use the option "Advanced filter" (under Data > Sort & Filter > Advanced). Select the first sheet as "List range" and the heat-filtered genes as "Criteria range" to only show the proteins that are enriched compared to the heat-inactivated control.

64| Filter this selection again using the putative targets list. A small database of putative probe targets from previous experiments using these probes was generated,[28,30] a phylogenetic tree of α,β-

hydrolase fold proteins combined with annotated catalytic nucleophiles in Uniprot.[42]

65| Apply the Benjamini-Hochberg correction with a FDR of 10% (q = 0.1): (1) List all anova(p) values from lowest to highest. (2) Calculate the B-H statistic as q * position in the list / number of tests. The choice of q is arbitrary (the lower the value the stricter the correction), but decide on this value before performing the analysis! (3) Select all proteins with a p value smaller than the B-H statistic (with q = 0.1, these are now corrected for a FDR of 10%).

66| For each protein, calculate the average normalized abundance of vehicle and inhibitor treated samples, percentage of inhibition (inhibitor / vehicle * 100%) and the error of ratio using the following formula (with x = average inhibitor, y = average vehicle and σ = standard deviation).

$$\text{error of ratio} = \frac{x}{y} \cdot \sqrt{\left(\frac{\sigma_x}{x}\right)^2 + \left(\frac{\sigma_y}{y}\right)^2}$$

67| Repeat steps **57**-**66** for each tissue.

68| To compare the relative activity of each probe target across the different tissues, select the proteins from each tissue from step **65.** Calculate the average normalized abundance for brain, kidney, liver and testis (as described in step **66**). Calculate the relative intensity of each protein by dividing the average intensity of each tissue by the maximum intensity of that protein. Use hierarchical clustering (node in KNIME 3.2.1, agglomerative algorithm, Euclidian distance function, single linkage type) (**Fig. 2**).

● TIMING

Steps **1**-**9**, tissue lysis: ~4 h for 12 tissues.
Steps **10**-**37**; pulldown: ~11 h for 24 samples + overnight digestion.
Steps **38**-**43**, sample preparation: ~3 h
Step **44**, LC-IMS-MS analysis: ~1 h per sample per replicate
Steps **45**-**68**, data processing and analysis: depends highly on number of runs and sample complexity (~5 h per 16 runs)
Box 1, database generation: ~5 min.

? TROUBLESHOOTING

Table 2 | Troubleshooting advice.

Step	Problem	Possible reason	Solution
18	The protein pellet breaks	The protein concentration was too low	Use more protein per sample (250 – 2000 µg)
23	The protein does not redissolve	The pellet has dried out The protein amount was too high	Add urea directly after removing methanol Use more urea buffer
44	Low signal Loss in sensitivity	Unsuccessful pulldown The column or instrument was contaminated	Optimize the protein amount, probe concentration and amount of beads Replace the trap and/or analytical column, clean the instrument
48	Poor alignment	The algorithm did not place vectors correctly Samples are too different	Choose a mix sample as alignment reference Minimize differences arising from sample preparation If the alignment quality is poor, you can consider manually placing vectors. However, this is very time-consuming and makes the acquired results irreproducible. It can help automatic alignment to select a QC sample (mix of samples being compared) as an alignment reference in step **47**.

Anticipated results

Probe cocktail. In previous studies using FP- and THL-based biotinylated probes,[28,30] a separate sample for each probe was prepared, duplicating the amount of samples. The Venn diagram in **Figure 3** summarizes the result of comparing the identified probe targets in samples of mouse brain membrane proteome treated with THL-biotin or FP-biotin separately, or mixed (probe cocktail; twice the amount of avidin beads used). All proteins identified in the samples treated with each probe separately are also identified in the probe cocktail sample. Furthermore, several putative probe targets are identified only in the probe cocktail sample. A possible explanation for this observation could be that these enzymes are shared probe targets for which both probes have a low potency. The additive effect of peptides being picked up by two probes might push these hits over the detection threshold. Depending on the experimental design and enzymes of interest, it can be worthwhile to combine biotinylated probes for one pulldown.

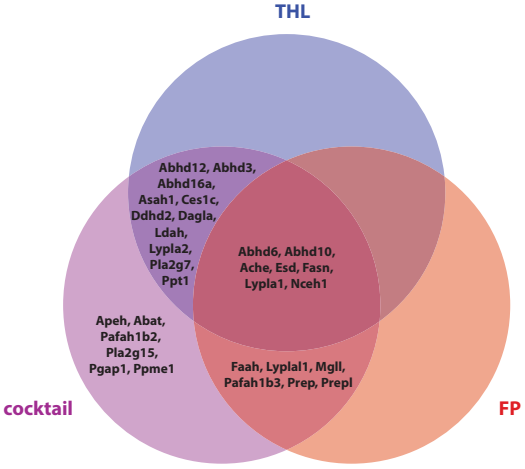

Figure 3 | Venn diagram of putative probe targets identified in mouse brain membrane proteome with THL-biotin (blue), FP-biotin (red) or a mix of both (cocktail; purple).

Competitive ABPP. Using this label-free quantitative proteomics protocol, it is confirmed that DH376 inhibits Dagla and Abhd6 *in vivo* and identify several novel off-targets (**Fig. 4**). Using heat-inactivated controls is helpful in separating probe targets from background binders. Combining this heat-filter with a putative probe target filter (Step **64**), 81 proteins are identified that are picked up by the probe cocktail in an activity-based manner across four murine tissues. The results of the competitive ABPP experiment are summarized in **Figure 4**.

In the brain, the known targets of DH376 are found to be inhibited: Dagla and Abhd6. Ces1c, a carboxylesterase, is inhibited in all four tissues (**Fig. 5a**). Several other carboxylesterases with high sequence

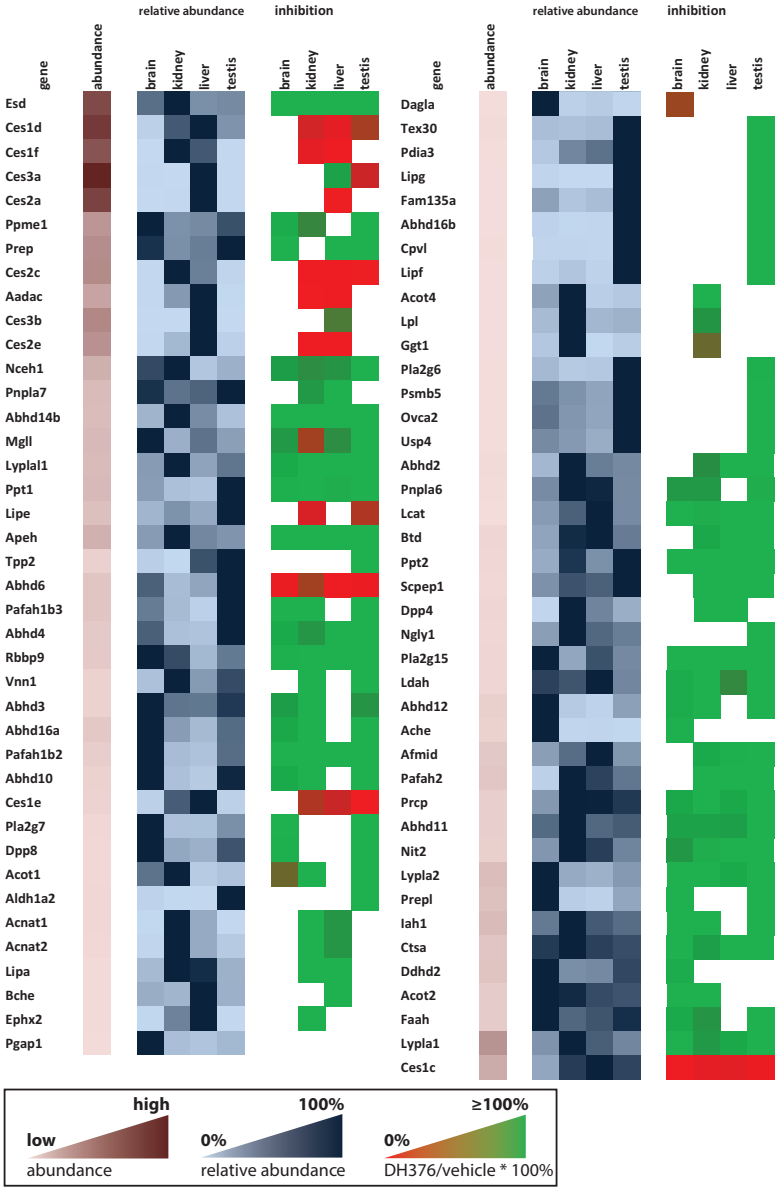

Figure 4 | Results of the competitive ABPP experiment in mice with DH376 and the probe cocktail, with hierarchical clustering of probe targets. Highest normalized abundance is shown in brown. The relative abundance of each protein in each tissue is shown in blue. The inhibition by DH376 is shown in red (inhibition) and green (no inhibition). The animal experiments were conducted in accordance with the ethical committee of Leiden University (DEC no. 14137).

similarity, i.e. Ces1d, Ces1e, Ces1f, Ces2a and Ces2c, were also identified as novel targets of DH376 in the other tissues. Further off-targets are Aadac and Lipe (both involved in triglyceride hydrolysis). An apparent discrepancy in the activity profile of DH376 between different tissues was observed for monoglyceride lipase (Mgll). DH376 inhibited Mgll in the kidney, but not in the other three tissues (**Fig. 5a**). In **Figure 5b**, the peptides used for quantification of brain Dagla, Abhd6, Ces1c and Mgll show consistent inhibition profiles. However, only one Mgll peptide was significantly different between the vehicle and inhibitor treated kidney samples (**Fig. 5b**) Combined with results obtained via an orthogonal method of measuring Mgll inhibition[31] this finding is denoted as a false positive. In a similar vein, Acot1 seems to be significantly inhibited in the brain, but not in the kidney and testis. Therefore, this might also be a false positive. These observations indicate that quality controls at the level of peptide quantification (in conjunction with orthogonal assays) will aid to establish the selectivity profile. Finally, the generation of the *in vivo* off-target profile of inhibitors using label-free quantitative activity-based proteomics will help to understand the *in vivo* mode of action of pharmacological tool compounds and guide the dose selection of drug candidates.

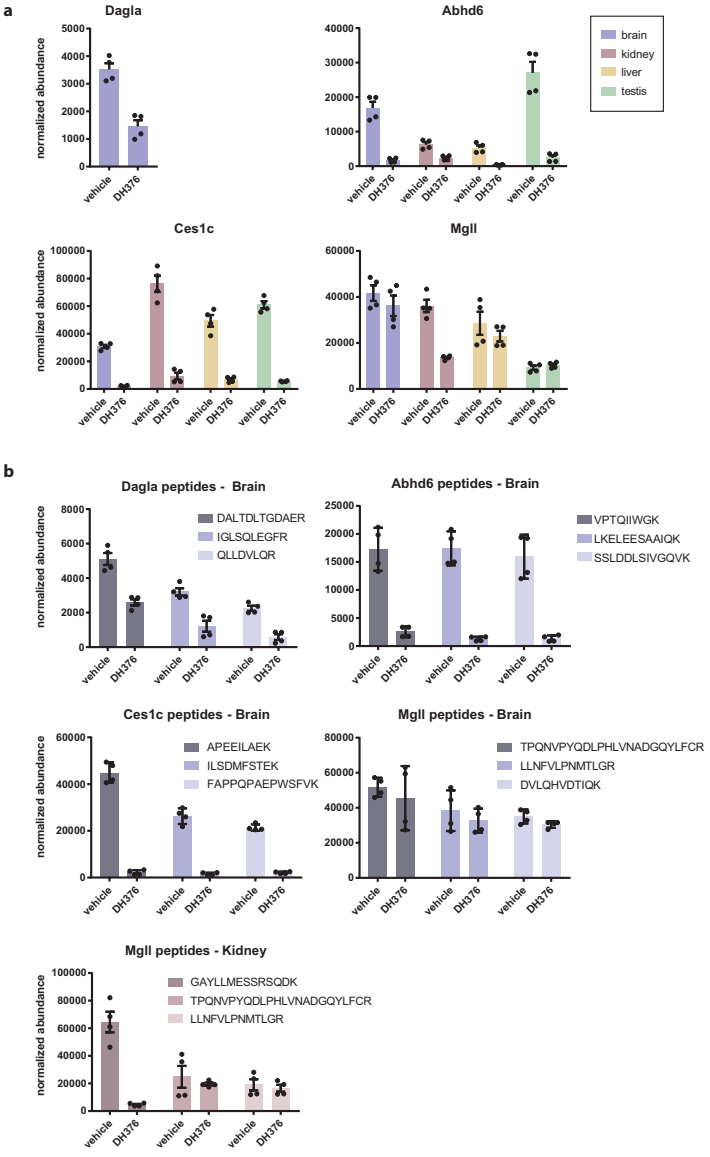

Figure 5 | Protein and peptide abundance data for selected probe targets. (**a**) Normalized protein abundance for Dagla, Abhd6, Ces1c and Mgll in different conditions. The normalized protein abundance is calculated from the averaged normalized abundance of the top three most abundant peptides of each protein. (**b**) Normalized abundance of peptides used in quantification of brain Dagla, Abhd6, Ces1c, Mgll and kidney Mgll. Individual data points, mean and standard deviation are shown. The peptide ion abundances are normalized between runs in Progenesis (see step **50**).

References

1. Eva J van Rooden, Bogdan I Florea, Hui Deng, Marc P Baggelaar, Annelot C M van Esbroeck, Juan Zhou, Herman S Overkleeft & Mario van der Stelt. Mapping *in vivo* target interaction profiles of covalent inhibitors using chemical proteomics with label-free quantification. *Nat.Protoc.* **13**, 752-767 (2018).
2. Ziegler, S., Pries, V., Hedberg, C. & Waldmann, H. Target identification for small bioactive molecules: Finding the needle in the haystack. *Angew. Chem. Int. Ed.* **52**, 2744–2792 (2013).
3. Bunnage, M. E., Piatnitski Chekler, E. L. & Jones, L. H. Target validation using chemical probes. *Nat. Chem. Biol.* **9**, 195–199 (2013).
4. Simon, G. M., Niphakis, M. J. & Cravatt, B. F. Determining target engagement in living systems. *Nat. Chem. Biol.* **9**, 200–205 (2013).
5. Jafari, R. *et al.* The cellular thermal shift assay for evaluating drug target interactions in cells. *Nat. Protoc.* **9**, 2100–2122 (2014).
6. Liu, Y., Patricelli, M. P. & Cravatt, B. F. Activity-based protein profiling: The serine hydrolases. *Proc. Natl. Acad. Sci.* **96**, 14694–14699 (1999).
7. Rix, U. & Superti-Furga, G. Target profiling of small molecules by chemical proteomics. *Nat. Chem. Biol.* **5**, 616–624 (2009).
8. Niphakis, M. J. & Cravatt, B. F. Enzyme Inhibitor Discovery by Activity-Based Protein Profiling. *Annu. Rev. Biochem.* **83**, 341–377 (2014).
9. Cravatt, B. F., Wright, A. T. & Kozarich, J. W. Activity-Based Protein Profiling: From Enzyme Chemistry to Proteomic Chemistry. *Annu. Rev. Biochem* **77**, 383–414 (2008).
10. Willems, L. I., Overkleeft, H. S. & Kasteren, S. I. Van. Current Developments in Activity-Based Protein Profiling. *Bioconjug. Chem.* **25**, 1181–1191 (2014).
11. Marques, A. R. *et al.* A specific activity-based probe to monitor family GH59 galactosylceramidase - the enzyme deficient in Krabbe disease. *ChemBioChem* **18**, 402–412 (2017).
12. Zhao, Q. *et al.* Broad-Spectrum Kinase Profiling in Live Cells with Lysine-Targeted Sulfonyl Fluoride Probes. *J. Am. Chem. Soc.* **139**, 680–685 (2017).
13. Li, N. *et al.* Relative quantification of proteasome activity by activity-based protein profiling and LC-MS/MS. *Nat. Protoc.* **8**, 1155–68 (2013).
14. Speers, A. E. & Cravatt, B. F. Activity-Based Protein Profiling (ABPP) and Click Chemistry (CC)-ABPP by MudPIT Mass Spectrometry. *Curr. Protoc. Chem. Biol* **1**, 29–41 (2009).
15. Sieber, S. A. & Cravatt, B. F. Analytical platforms for activity-based protein profiling - exploiting the versatility of chemistry for functional proteomics. *Chem. Commun.* **22**, 2311–2319 (2006).
16. Bantscheff, M., Lemeer, S., Savitski, M. M. & Kuster, B. Quantitative mass spectrometry in proteomics: Critical review update from 2007 to the present. *Anal. Bioanal. Chem.* **404**, 939–965 (2012).
17. Rauniyar, N. & Yates, J. R. Isobaric Labeling-Based Relative Quantification in Shotgun Proteomics. *J. Proteome Res.* **13,** 5293–5309 (2014).
18. Neilson, K. a. *et al.* Less label, more free: Approaches in label-free quantitative mass spectrometry. *Proteomics* **11**, 535–553 (2011).
19. Filiou, M. D., Martins-de-Souza, D., Guest, P. C., Bahn, S. & Turck, C. W. To label or not to label: Applications of quantitative proteomics in neuroscience research. *Proteomics* **12**, 736–747 (2012).
20. Distler, U., Kuharev, J., Navarro, P. & Tenzer, S. Label-free quantification in ion mobility–enhanced data-independent acquisition proteomics. *Nat. Protoc.* **11**, 795–812 (2016).
21. Kleiner, P., Heydenreuter, W., Stahl, M., Korotkov, V. S. & Sieber, S. A. A Whole Proteome Inventory of Background Photocrosslinker Binding. *Angew. Chem. Int. Ed.* **56**, 1396–1401 (2017).
22. Yang, W. S. *et al.* Regulation of ferroptotic cancer cell death by GPX4. *Cell* **156**, 317–331 (2014).

23. Doerr, A. DIA mass spectrometry. *Nat. Methods* **12**, 35 (2015).
24. Baker, E. S. *et al.* An LC-IMS-MS platform providing increased dynamic range for high-throughput proteomic studies. *J. Proteome Res.* **9**, 997–1006 (2010).
25. Bond, N. J., Shliaha, P. V., Lilley, K. S. & Gatto, L. Improving Qualitative and Quantitative Performance for MS^E -based Label-free Proteomics. *J. Proteome Res.* **12**, 2340–2353 (2013).
26. van Esbroeck, A. C. M. *et al.* Activity-based protein profiling reveals off-target proteins of the FAAH inhibitor BIA 10-2474. *Science.* **356**, 1084–1087 (2017).
27. Baggelaar, M. P. *et al.* Development of an activity-based probe and in silico design reveal highly selective inhibitors for diacylglycerol lipase-α in brain. *Angew. Chem. Int. Ed.* **52**, 12081–12085 (2013).
28. Baggelaar, M. P. *et al.* A highly selective, reversible inhibitor identified by comparative chemoproteomics modulates diacylglycerol lipase activity in neurons. *J. Am. Chem. Soc.* **137**, 8851–8857 (2015).
29. Bisogno, T. *et al.* Cloning of the first sn1-DAG lipases points to the spatial and temporal regulation of endocannabinoid signaling in the brain. *J. Cell Biol.* **163**, 463–468 (2003).
30. Baggelaar, M. P. *et al.* Chemical Proteomics Maps Brain Region Specific Activity of Endocannabinoid Hydrolases. *ACS Chem. Biol.* **12**, 852–861 (2017).
31. Ogasawara, D. *et al.* Rapid and profound rewiring of brain lipid signaling networks by acute diacylglycerol lipase inhibition. *Proc. Natl. Acad. Sci.* **113**, 26–33 (2016).
32. Deng, H. *et al.* Triazole Ureas Act as Diacylglycerol Lipase Inhibitors and Prevent Fasting-Induced Refeeding. *J. Med. Chem.* **60**, 428–440 (2017).
33. Lomenick, B. *et al.* Target identification using drug affinity responsive target stability (DARTS). *Proc. Natl. Acad. Sci.* **106**, 21984–21989 (2009).
34. Distler, U. *et al.* Drift time-specific collision energies enable deep-coverage data-independent acquisition proteomics. *Nat. Methods* **11**, 167–70 (2014).
35. Ogura, Y., Parsons, W. H., Kamat, S. S. & Cravatt, B. F. A calcium-dependent acyltransferase that produces N-acyl phosphatidylethanolamines. *Nat. Chem. Biol.* **12**, 1–5 (2016).
36. Wessel, D. & Flügge, U. I. A method for the quantitative recovery of protein in dilute solution in the presence of detergents and lipids. *Anal. Biochem.* **138**, 141–143 (1984).
37. Silva, J. C., Gorenstein, M. V, Li, G.-Z., Vissers, J. P. C. & Geromanos, S. J. Absolute Quantification of Proteins by $LCMS^E$: A Virtue of Parallel MS Acquisition. *Mol. Cell. Proteomics* **5**, 144–156 (2005).
38. Choi, M. *et al.* ABRF Proteome Informatics Research Group (iPRG) 2015 Study: Detection of differentially abundant proteins in label-free quantitative LC-MS/MS experiments. *J. Proteome Res.* **16**, 945–957 (2017).
39. Vizcaíno, J. A. *et al.* 2016 update of the PRIDE database and its related tools. *Nucleic Acids Res.* **44**, D447–D456 (2016).
40. Rappsilber, J., Mann, M. & Ishihama, Y. Protocol for micro-purification, enrichment, pre-fractionation and storage of peptides for proteomics using StageTips. *Nat. Protoc.* **2**, 1896–1906 (2007).
41. Vaudel, M. *et al.* Shedding light on black boxes in protein identification. *Proteomics* **14**, 1001–1005 (2014).
42. Wasmuth, E. V & Lima, C. D. UniProt: the universal protein knowledgebase. *Nucleic Acids Res.* **45**, 1–12 (2016).

Chapter 5

Design and synthesis of quenched activity-based probes for diacylglycerol lipase and α,β-hydrolase domain containing protein 6[1]

Introduction

The endocannabinoid signaling system (ECS) consists of the cannabinoid receptors, their endogenous ligands, i.e. 2-arachidonoylglycerol (2-AG) and anandamide (AEA), and the enzymes regulating the levels of these ligands.[2] The endocannabinoid system is involved in a wide array of neurophysiological processes, including nociception, cognitive function and appetite. Enzymes involved in the ECS are consequently potential therapeutic targets for an array of human disorders, including pain, neurodegenerative diseases and obesity.[3–5] The endocannabinoid 2-AG is synthesized from diacylglycerol (DAG) by hydrolysis catalyzed by either *sn*-1-diacylglycerol lipase α or β (DAGLα and DAGLβ).[6] The DAG lipases belong to the serine hydrolase superfamily and selectively hydrolyze the *sn*-1 ester within diacylglycerols. DAGLα is mainly responsible for the generation of 2-AG in the central nervous system, whereas DAGLβ mostly acts in the periphery.[7] To date, isoform selective inhibitors have not been reported. DAGLα inhibitors have potential as drug candidates for obesity as well as neurodegenerative disorders.[8] Most of the reported covalent DAGL inhibitors also target α,β-hydrolase domain containing protein 6 (ABHD6).[9,10] ABHD6 is thought to control 2-AG levels postsynaptically.[11] The enzyme responsible for catalyzing the bulk 2-AG in the brain, monoacylglycerol lipase (MAGL), acts at presynaptic sites. To gain a better understanding of the regulation of 2-AG levels, it is necessary to study the activity of these enzymes in their native environment.

Activity-based protein profiling (ABPP) is a method to study native enzyme activity.[12] Activity-based probes (ABPs) form a covalent bond with active enzymes and thus report on the amount of active enzyme present in a biological system at a given time. Various fluorescent ABPs for DAGL and ABHD6, such as DH379[13] and HT-01,[9] have been reported.

Quenched ABPs (qABPs) have been developed to decrease the fluorescent signal arising from an unbound fluorescent probe.[14] A qABP consists of an electrophilic trap, a recognition element, a

fluorophore (F) and a complementary quencher (Q) (**Fig. 1a**). The quencher is part of the leaving group, which disassociates after the formation of the enzyme-probe complex. Bogyo and co-workers were the first to synthesize a qABP and developed a set of qABPs for cathepsins.[15–19] To date various enzyme classes, including kinases,[20] serine proteases[21] and cysteine proteases such as legumain[22] and caspases,[23] have been targeted with qABPs. However, metabolic serine hydrolases have not yet been studied with qABPs. In this chapter, the synthesis and characterization of qABPs for the metabolic serine hydrolases DAGL and ABHD6 is described.

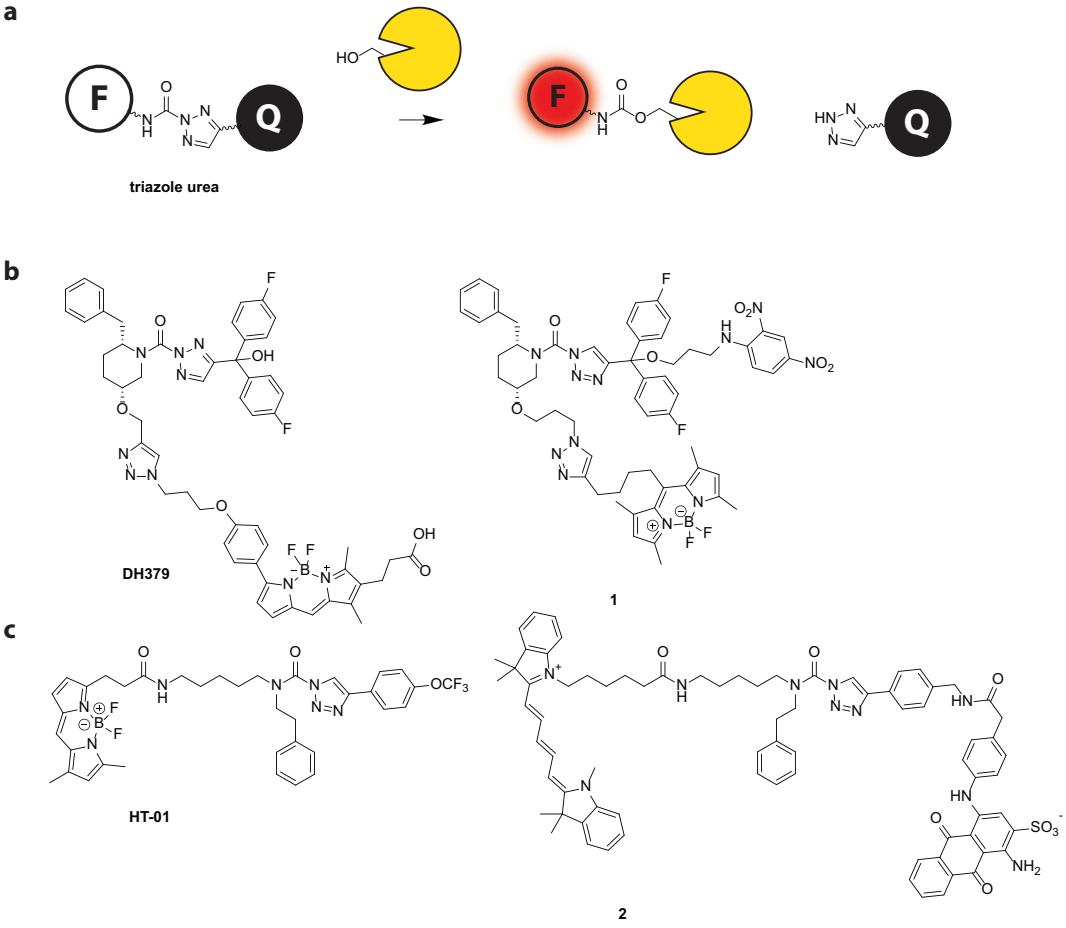

Figure 1. qABP design for DAGL and ABHD6. (a) General design of a triazole urea as qABP for serine hydrolases. (F) is the fluorophore and (Q) is the quencher. (b) Probe DH379 and probe **1**. (c) Probe HT-01 and probe **2**.

Results and discussion

The design of the qABPs **1** and **2** is based on triazole ureas, DH379 and KT-01, respectively, both of which are ABPs for the serine hydrolases targeted in the here-reported studies. DH379 targets DAGLα, DAGLβ and ABHD6, while KT-01 labels DAGLβ and ABHD6 (**Fig. 1**).[9,24] Both ABPs contain a triazole urea as an electrophilic trap, which is commonly used for serine hydrolases (**Fig. 1a**).[13,25] BODIPY-FL[26] and 2,4-DNA[27–31] were chosen as a fluorophore-quencher pair for probe **1**,[20,32] while Cy5 and cAB40 were selected as a fluorophore-quencher pair for qABP **2**.[33]

Synthesis of probe 1. The synthesis of probe **1** and DAGL inhibitor **3**, an azide analogue of inhibitor DH376, started with the nucleophilic addition of lithium TMS-acetylene onto 4,4'-difluorophenyl ketone (**4**) (**Scheme 1**), followed by deprotection in basic solution to give alcohol **5**. Copper(I)-catalyzed [2+3] azide-alkyne cycloaddition (CuAAC) of **5** with hydrazoic acid, formed *in situ* from methanol and TMS-N_3 in DMF,[34,35] gave triazole **6** in moderate yield. Next, piperidine **7**, which was synthesized as previously reported[13], was deprotected with acid and the resulting amine was treated with triphosgene and reacted with **6**. The two regioisomers thus formed were separated by column chromatography yielding inhibitor **3**. To obtain probe **1**, alkylation of alcohol **5** led to azide **8**, the azide in which was reduced by treatment with triphenylphosphine and water to give **9**. A nucleophilic aromatic substitution reaction between amine **9** and 2,4-dinitrofluorobenzene yielded the desired alkyne **10**, which contains dinitroaniline as a quencher. CuAAC of alkyne **10** with pivaloyloxymethyl-azide (POM-N_3) gave the POM-protected triazole, which was deprotected in basic solution to give compound **11**.[36] Similarly as described above for triazole **6**, triphosgene coupling of **11** with **7** gave intermediate **12** after separation of two regioisomers by column chromatography. A CuAAC reaction between azide **12** and acetylene-functionalized BODIPY-FL[26] furnished probe **1**.

Synthesis of probe 2. The qABP **2** is based on the fluorescent ABP HT-01 (**Fig. 1c**). Reduction of commercially available 4-ethynylbenzaldehyde (**13**) with sodium borohydride gave alcohol **14**, which was subsequently mesylated to provide **15** (**Scheme 2**). Next, nucleophilic substitution of the mesylate with phthalimide yielded compound **16**. A CuAAC reaction between alkyne **16** and TMS-azide resulted in triazole **17**. Separately, N-Boc-cadaverine (**18**) was nosylated and alkylated using phenethylbromide. Subsequent deprotection with ethylenediamine resulted in amine **19**. This amine was treated with triphosgene and coupled to triazole **17**, resulting in a mixture of two regioisomers, which were separated by column chromatography to give the N1 isomer **20**. The Cy5-analogue of HT-01 **21** was made by deprotecting **20** with TFA and coupling the resulting amine to a Cy5 activated ester. To make the probe **2**, the phthalimide **20** was deprotected with ethylenediamine. Amine **22** was coupled to the cAB40 quencher and amide product **23** was deprotected by TFA, followed by coupling to Cy5, yielding the final product **2**.

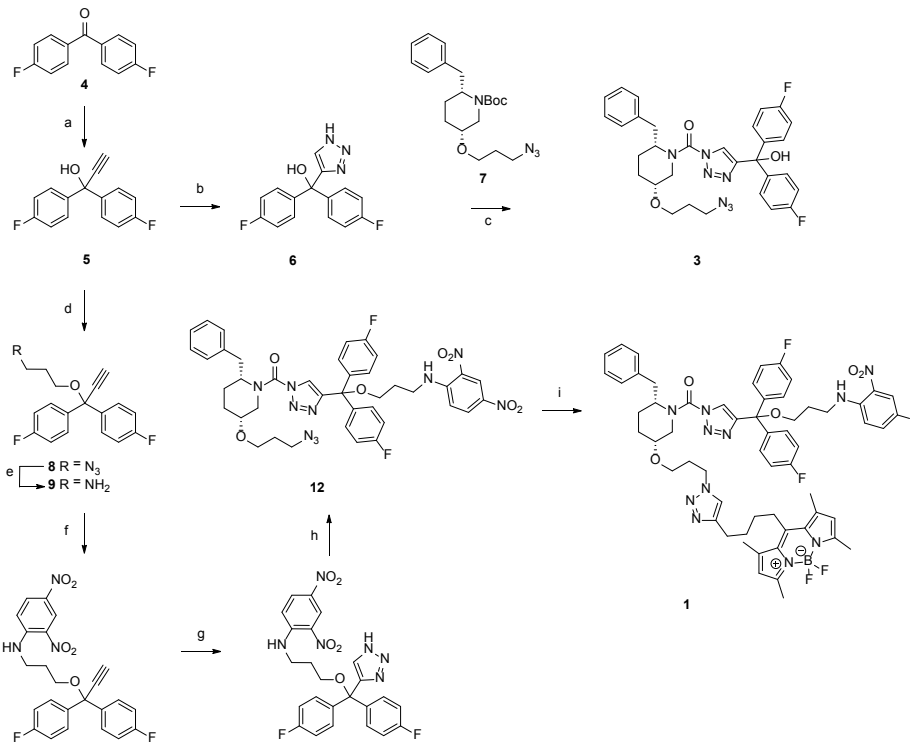

Scheme 1. Synthesis of probe **1**. Reagents and conditions: (a) *i*. TMS-acetylene, *n*-BuLi, THF, -10 - 0 °C; *ii*. KOH, MeOH/THF, 0 °C, 74%; (b) TMS-N_3, NaAsc, $CuSO_4$, DMF/MeOH, 60 °C, 59%; (c) *i*. **7**, 40% TFA in DCM; *ii*. Triphosgene, DIPEA, THF, 0 °C; *iii*. **6**, DIPEA, THF, 60 °C; (d) NaH, 3-azidopropanol tosylate, DMF, 0 °C - rt, 64%; (e) PPh_3, H_2O/THF, 60 °C, 100%; (f) 2,4-dinitrofluorobenzene, NEt_3, DMF, 95%; (g) *i*. POM-azide, CuBr, TBTA, THF/H_2O; *ii*. KOH, MeOH, 67%; (h) *i*. **7**, 40% TFA in DCM; *ii*. Triphosgene, DIPEA, THF, 0 °C; *iii*. **11**, DIPEA, THF, 60 °C; (i) NaAsc, $CuSO_4$, DMF, MeOH, BODIPY-FL.[26]

Spectroscopic characterization. The absorbance spectrum of probe **1** was compared to BODIPY-FL. In ethanol, the probe and the parent BODIPY have identical absorbance maxima (**Table 1**). In aqueous solution the maximal absorbance of the probe is shifted towards the red (approximately 10 nm) while the parent BODIPY does not display such a redshift (**Table 1**). Similar shifts in absorbance profiles have been previously observed in comparable systems[27,28,37] and are indicative of a ground state complex. This suggests that the fluorescence of the probe is quenched to a certain extent by ground state complex formation. Probe **2** is also slightly redshifted in water compared to ethanol. To determine the amount of quenching, the fluorescence quantum yield was assessed, which is defined as the ratio of the number of photons emitted to the number of photons absorbed by a fluorophore. Fluorescence quantum yields of qABPs **1** and **2** were determined relative to their parent fluorophores, i.e. BODIPY-FL and Cy5 (**Table 1**).

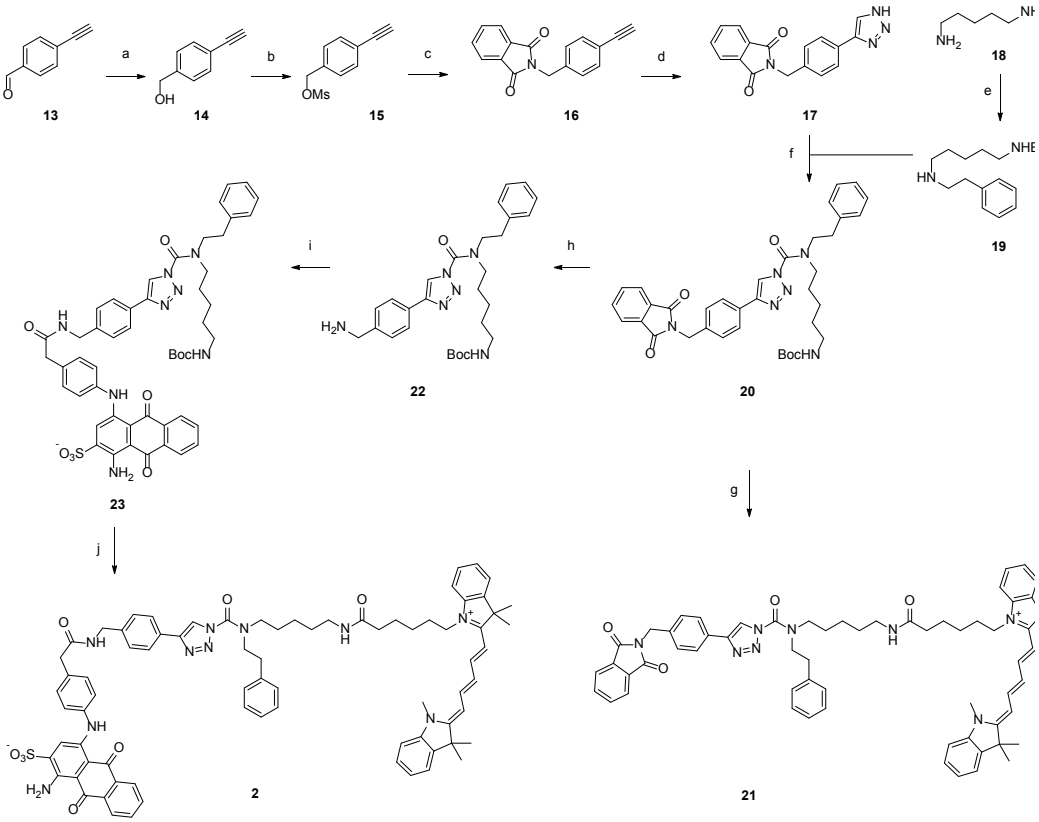

Scheme 2. Synthesis of qABP **2** and control compound **21**. Reagents and conditions: (a) $NaBH_4$, EtOH, 99%; (b) DCM, Et_3N, MsCl, 0 °C, 94%; (c) potassium phthalimide, DMF, 92%; (d) TMS-N_3, CuI, DMF/MeOH (5/1), reflux, 64%; (e) *i*. NsCl, Et_3N, THF; *ii*. $Ph(CH_2)_2Br$, Cs_2CO_3, ACN, 80 °C; *iii*. PhSH, Cs_2CO_3, ACN, 71%; (f) *i*. triphosgene, DIPEA, THF; *ii*. **17**, DMAP, DIPEA, THF, 27%; (g) *i*. TFA/DCM. *ii*. Cy5-OSu, DIPEA, DMF, 44%; (h) ethylenediamine, EtOH, 50%; (i) HCTU, DIPEA, cAB40, DMF, 53%; (j) *i*. 10% TFA/DCM; *ii*. Cy5-NHS, DIPEA, DMF, 10%.

Table 1. λ_{max} (absorbance maximum) and $\Phi^{relative}$ (relative quantum yield) of probe **1** and **2**.

Compound	λ_{max} in EtOH (nm)	λ_{max} in H_2O (nm)	$\Phi^{relative}$ in EtOH
BODIPY-FL	497	497	1.0*
Probe **1**	497	505	0.34*
Cy5	644	639	1.0**
Probe **2**	644	650	0.081**

*relative to BODIPY-FL, **relative to Cy5

Probe **1** has a relative quantum yield of 0.34 (± 3-fold quenched). Probe **2** has a relative quantum yield of 0.081 (± 12-fold quenched).

Biological characterization of probe 1. To determine whether qABP **1** inhibits human DAGLα, a colorimetric assay was performed with para-nitrophenyl butyrate as surrogate substrate and membranes of HEK293T cells overexpressing recombinant human DAGLα.[38,39] Compound **3**, an azide analogue of DH376, was used as positive control and showed good inhibitory activity (IC_{50} = 5 nM), comparable to DH376 (**Table 2**). Intermediate **12**, containing only a quencher, retained high inhibitory activity, whereas qABP **1** was approximately ten-fold less active. Of note, probe **1** is about as active as the ABP DH379.

Table 2. Activity of DAGLα inhibitors in surrogate substrate assay.

Compound	pIC_{50} DAGLα
3	8.3 ± 0.07
DH376	8.7 ± 0.1
12	8.4 ± 0.04
1	7.4 ± 0.2
DH379	7.4 ± 0.05

To investigate whether qABP **1** could covalently label human DAGLα, a gel-based activity-based protein profiling (ABPP) assay was employed for rapid and efficient visualization of endogenous serine hydrolase activity in native biological samples. Recombinant human DAGLα was over-expressed in HEK293T cells, which were lysed and treated with varying concentrations of qABP **1**. The proteins were resolved by SDS-PAGE and labeled proteins were visualized by in-gel fluorescence scanning. Human DAGLα was dose-dependently labeled by probe **1** (**Fig. 2a**) and could be out-competed by the selective DAGL inhibitor, LEI105 (**Fig. 2b**).[40]

Biological characterization of probe 2. To test whether probe **2** labeled ABHD6, lysates from two cell lines were used: human osteosarcoma U2OS cells stably overexpressing ABHD6 fused to green fluorescent protein (GFP) as well as wildtype mouse neuroblastoma Neuro2A (N2A) with endogenous ABHD6 expression. In the U2OS lysates, a strong signal was visible at approximately 70 kDa, corresponding to the MW of the ABHD6-GFP fusion protein (**Fig. 3a**). Incubation of wildtype N2A lysates with probe **2** resulted in fluorescent labeling of several proteins, including a protein at 35 kDa, which was also labeled by the well-characterized ABHD6 probe DH379 (**Fig. 3b**). These results suggest that probe **2** covalently labels mouse and human ABHD6.

Finally, live U2OS-ABHD6-GFP cells were treated with **2**, lysed and remaining ABHD6 activity was

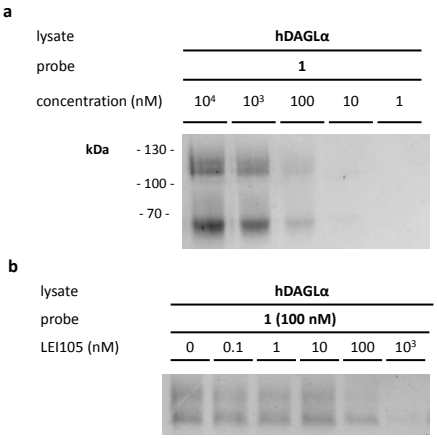

Figure 2. Activity-based protein profiling with probe **1**. (a) Lysate of recombinant human DAGLα over-expressed in HEK293T cells, treated with probe **1** (30 min, rt). (b) Competition of human DAGLα labeling by probe **1** with LEI105 (30 min pre-incubation with LEI105, followed by 20 min incubation with probe, rt).

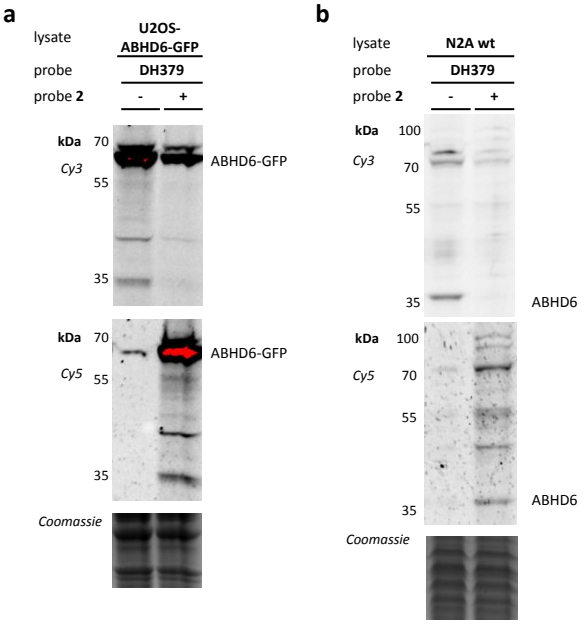

Figure 3. Activity-based protein profiling with probe **2**. (a) ABPP on U2OS-ABHD6-GFP lysate with probe DH379 (Cy3 signal, 1 μM, 20 min, rt), with or without pre-incubation with probe **2** (Cy5 signal, 10 μM, 30 min, 37 °C). (b) ABPP on N2A lysate with probe DH379 (Cy3 signal, 1 μM, 20 min, rt), with or without pre-incubation with probe **2** (Cy5 signal, 10 μM, 30 min, 37 °C). Gels with coomassie staining (lower panels) are shown as protein loading controls.

visualized post-lysis with DH379. Almost no fluorescent signal from **2** was detected and no decrease in ABHD6 activity was observed with DH379 labeling (**Fig. 4a**), which suggested that probe **2** has limited cell permeability. Of note, control compound **21** was able to reduce ABHD6 activity *in situ* (**Fig. 4b**), which suggested that the reduced cell permeability is caused by the quencher.

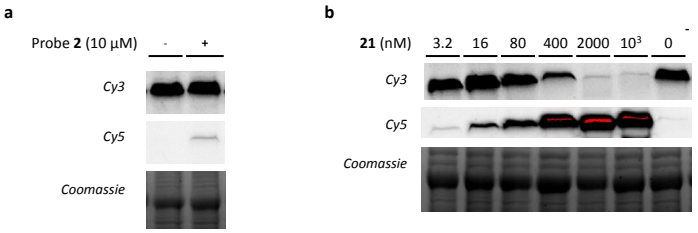

Figure 4. *In situ* treatment of U2OS-ABHD6-GFP. (a) Probe **2**-treated cells (Cy5 signal, 1 h, 37 °C), lysed and labeled with DH379 (Cy3 signal, 20 min, 1 µM, rt). (b) Probe **21**-treated cells (Cy5 signal, 1 h, 37 °C), lysed and treated with DH379 (Cy3 signal, 20 min, 1 µM, rt). Gels with coomassie staining (lower panels) are shown as protein loading controls.

Conclusions

The qABPs **1** and **2** were successfully synthesized. Probe **1** showed characteristics of static quenching in aqueous solution and showed activity in a surrogate substrate assay using recombinant human DAGLα. Probe **1** could dose-dependently label human DAGLα in a gel-based activity-based protein profiling assay. Probe **2** did label endogenously expressed mouse ABHD6, but was not able to label ABHD6 in live cells. Further optimization of fluorescent properties and cell permeability of the probes is required to apply them in biological studies.

Experimental Section

Chemistry

General methods. Reagents were purchased from Sigma Aldrich, Acros or Merck and used without further purification unless noted otherwise. Reactions under dry conditions were performed using oven or flame-dried glassware and dry solvents, which were dried for a minimum of 24 h over activated molecular sieves of appropriate (3 - 4Å) pore size. Traces of water were removed from starting compounds by co-evaporation with toluene. All moisture sensitive reactions were performed under an argon or nitrogen atmosphere. Flash chromatography was performed using SiliCycle silica gel type SilicaFlash P60 (230 – 400 mesh). HPLC purification was performed on a preparative LC-MS system (Agilent 1200 series) with an Agilent 6130 Quadruple MS detector. TLC analysis was performed on Merck silica gel 60/Kieselguhr F254, 0.25 mm. Preparative TLC was performed on UNIPLATE Alumina GF 1000 µm plates. Compounds were visualized using UV-irradiation, a $KMnO_4$

stain (K_2CO_3 (40 g), $KMnO_4$ (6 g), H_2O (600 mL) and 10% NaOH (5 mL)). A stain for organic azides was used as follows: i. 10% PPh_3 in toluene, heating; ii. Ninhydrin in EtOH/AcOH, heating.[41] ^{1}H- and ^{13}C-NMR spectra were recorded on a Bruker AV-400 MHz spectrometer at 400 (^{1}H) and 100 (^{13}C) MHz using $CDCl_3$, CD_3OD or $(CD_3)_2SO$ as solvent, unless stated otherwise. Spectra were analyzed using MestReNova 11.0.3. Chemical shift values are reported in ppm with tetramethylsilane or solvent resonance as the internal standard ($CDCl_3$, δ 7.26 for ^{1}H, δ 77.16 for ^{13}C; CD_3OD, δ 3.31 for ^{1}H, δ 49.00 for ^{13}C; $(CD_3)_2SO$, δ 2.50 for ^{1}H, δ 39.52 for ^{13}C). Data are reported as follows: chemical shifts (δ), multiplicity (s = singlet, d = doublet, dd = double doublet, td = triple doublet, t = triplet, q = quartet, m = multiplet, br = broad), coupling constants J (Hz), and integration. LC-MS analysis was performed on a Finnigan Surveyor HPLC system with a Gemmi C18 50x4.60 mm column (detection at 200-600 nm), coupled to a Finnigan LCQ Adantage Max mass spectrometer with ESI. The applied buffers were H_2O, MeCN and 1.0% TFA in H_2O (0.1% TFA end concentration). High resolution mass spectra (HRMS) were recorded by direct injection on a q-TOF mass spectrometer (Synapt G2-Si) equipped with an electrospray ion source in positive mode with leu-enkephalin (m/z = 556.2771) as an internal lock mass. The instrument was calibrated prior to measurement using the MS/MS spectrum of glu-1-fibrinopeptide B. IR spectra were recorded on a Shimadzu FTIR-8300 and are reported in cm^{-1}. Optical rotations were measured on a Propol automatic polarimeter (Sodium D-line, λ = 589 nm). Molecules shown are drawn using Chemdraw v16.0.

General procedure for the CuAAC reaction. To a solution of 1 eq. of azide and 1.0 to 1.5 eq. of BODIPY alkyne (red or green) in minimal DMF was added a freshly prepared solution of 0.15 eq. NaAsc and 0.05 eq. of $CuSO_4$ in H_2O. The resulting solution was stirred o/n. The reaction mixture was diluted with EtOAc and H_2O and extracted with EtOAc (3x). The combined organic layers were washed with H_2O (5x), brine, dried ($MgSO_4$), filtered and concentrated.

Pivaloyloxymethyl-azide (POM-N_3, scheme 1). This procedure was adapted from literature.[42] To a solution of NaN_3 (0.44 g, 6.6 mmol) in H_2O (3.5 mL) was added POM-Cl (0.85 mL, 6 mmol). The resulting mixture was stirred vigorously at 90 °C o/n. The reaction mixture was diluted with water and extracted with DCM (3x). The combined organic layers were carefully concentrated to yield a colorless liquid (0.92 g, 5.9 mmol, 98%). ^{1}H NMR (400 MHz, $CDCl_3$) δ 5.14 (s, 2H), 1.26 (s, 9H). ^{13}C NMR (100 MHz, $CDCl_3$) δ 178.22, 74.52, 39.11, 27.13. IR: 2102.41 (-N_3), 1737.86 (C=O).

3-Azidopropanol tosylate (scheme 1). To a solution of 3-bromopropanol (1.2 mL, 13.8 mmol) in water (40 mL) was added NaN_3 (1.8 g, 27.6 mmol). The resulting reaction mixture was stirred at 80 °C for 3 days, allowed to cool to rt and extracted with EtOAc (5x). The combined organic layers were washed with brine, dried (Na_2SO_4), filtered and carefully concentrated. The residue was dissolved in DCM and NEt_3 (3.8 mL, 27.6 mmol) was added. The resulting solution was cooled to 0 °C before addition of tosyl chloride (4.0 g, 21 mmol) and stirred o/n. The reaction mixture was diluted with H_2O and extracted with DCM (3x). The combined organic layers were dried (Na_2SO_4), filtered and concentrated over celite. Purification of the residue by silica gel column chromatography (9:1 PE:DCM) yielded a colorless liquid (2.3 g, 9 mmol, 65%), which discolored slightly upon storage at rt. ρ = ~1.5 g/mL. TLC: R_f = 0.3 (1:9 DCM:pentane). IR: 2095 (-N_3). ^{1}H NMR (400 MHz, $CDCl_3$) δ 7.83 (d, J = 8.2 Hz, 2H), 7.40 (d, J = 8.0 Hz, 2H), 4.14 (t, J = 5.9 Hz, 2H), 3.41 (t, J = 6.5 Hz, 2H), 2.49 (s, 3H), 1.92 (p, J = 6.2 Hz, 2H). ^{13}C NMR (100 MHz, $CDCl_3$) δ 145.28, 132.90, 130.17, 128.14, 67.20, 47.48, 28.66, 21.91.

1-Amino-4-((4-(carboxymethyl)phenyl)amino)-9,10-dioxo-9,10-dihydroanthracene-2-sulfonate (cAB40, scheme 2). To a solution of bromaminic acid (2 g, 5 mmol) and 4-aminophenyl acetic acid

(674 mg, 4.45 mmol) in water (75 mL) were added Na_2CO_3 (795 mg, 7.5 mmol) and $CuSO_4$ (120 mg, 0.75 mmol). The reaction mixture was refluxed for 16 h, washed with DCM (3 x 50 mL) and concentrated. MeOH was added to the residue and after filtration the filtrate was concentrated and purification of the residue by reversed phase silica gel column chromatography (H_2O > 1:4 MeOH:H_2O) yielded cAB40 as a blue solid (650 mg, 1.4 mmol, 32%). ^{1}H NMR (400 MHz, CD_3OD) δ 8.34 - 8.32 (m, 2H), 8.26 (s, 1H), 7.88 - 7.77 (m, 2H), 7.36 (d, J = 8.4 Hz, 2H), 7.26 (d, J = 8.4 Hz, 2H), 3.62 (s, 2H). LC-MS *m/z*: 452.9 $[M+2H]^+$.

1,1-*bis*(4-Fluorophenyl)prop-2-yn-1-ol (5). To a cooled (-10 °C) solution of ethynyltrimethylsilane (1.55 mL, 11 mmol) in dry THF (20 mL) was slowly added *n*-BuLi (2.5 M, 4.5 mL, 11 mmol) and stirred for 1 h. Subsequently, a solution of 4,4'-difluorobenzophenone (4, 2.18 g, 10 mmol) in dry THF (16 mL) was added in 15 minutes. The resulting solution was stirred at -10 °C for 1 h and then 0 °C for 1 h. The reaction mixture was quenched by the addition of KOH (2 M in MeOH, large excess) and stirred o/n, poured into H_2O, adjusted to pH 6 - 7 with 1 M HCl and extracted with EtOAc (3x). The combined organic layers were dried ($MgSO_4$), filtered and concentrated. Purification of the residue by silica gel column chromatography (1:19 EtOAc:pentane) yielded a yellow oil (1.81 g, 7.4 mmol, 74%). TLC: R_f = 0.42 (1:9 EtOAc:pentane). IR: 3298 (CC-H), 1601, 1504, 1221, 1157. ^{1}H NMR (400 MHz, $CDCl_3$) δ 7.60 – 7.50 (m, 4H), 7.07 – 6.96 (m, 4H), 2.90 (s, 1H), 2.79 (s, 1H). ^{13}C NMR (100 MHz, $CDCl_3$) δ 163.76, 127.99 (d, J = 8.3 Hz), 115.35 (d, J = 21.7 Hz), 76.10.

4,4'-(1-(3-Azidopropoxy)prop-2-yne-1,1-diyl)*bis*(fluorobenzene) (8). To a cooled (0 °C) solution of alkyne **5** (0.29 g, 1.2 mmol) in dry DMF (10 mL) was added NaH (60% dispersion in mineral oil, 55 mg, 1.3 mmol) and the reaction mixture was stirred for 30 minutes. Next, 3-azidopropanol tosylate (0.44 g, 1.8 mmol) was added dropwise. The resulting yellow solution was stirred o/n at rt, diluted with EtOAc and H_2O and extracted with EtOAc (3x). The combined organic layers were washed with H_2O (3x), brine, dried ($MgSO_4$), filtered and concentrated over celite. Purification of the residue by silica gel column chromatography (1% EtOAc in pentane) yielded a colorless viscous oil (0.25 g, 0.77 mmol, 64%). TLC: R_f = 0.57 (1:19 EtOAc:pentane). IR: 3297 (CC-H), 2095 (N_3). ^{1}H NMR (400 MHz, $CDCl_3$) δ 7.54 – 7.43 (m, 4H), 7.09 – 6.94 (m, 4H), 3.54 (d, J = 5.9 Hz, 2H), 3.46 (t, J = 6.8 Hz, 2H), 2.92 (s, 1H), 1.99 – 1.84 (m, 2H). ^{13}C NMR (100 MHz, $CDCl_3$) δ 162.44 (d, J = 247.1 Hz), 138.85, 128.50 (d, J = 8.2 Hz), 115.27 (d, J = 21.6 Hz), 82.82, 79.17, 78.23, 61.55, 48.74, 29.33. LC-MS *m/z*: 328 $[M+H]^+$.

3-((1,1-*bis*(4-Fluorophenyl)prop-2-yn-1-yl)oxy)propan-1-amine (9). To a solution of **8** (0.25 g, 0.77 mmol) in 1:10 H_2O:THF was added PPh_3 (0.45 g, 1.7 mmol). The reaction mixture was stirred at 60 °C o/n, concentrated, diluted with EtOAc and H_2O, basified with 1 M NaOH and extracted with EtOAc (3x). The combined organic layers were washed with brine, dried ($MgSO_4$), filtered and concentrated. Purification of the residue by silica gel column chromatography (10% methanolic solution of 3% NH_3 in DCM) yielded a colorless film (234 mg, 0.77 mmol, 100%). TLC: R_f = 0.27 (1:9 MeOH:DCM). ^{1}H NMR (400 MHz, $CDCl_3$) δ 7.57 – 7.42 (m, 4H), 7.07 – 6.92 (m, 4H), 3.52 (t, J = 6.1 Hz, 2H), 2.91 (s, 1H), 2.86 (t, J = 6.9 Hz, 2H), 1.86 (s, 2H), 1.84 – 1.74 (m, 2H). ^{13}C NMR (100 MHz, $CDCl_3$) δ 162.35 (d, J = 246.9 Hz), 139.02 (d, J = 3.1 Hz), 128.45 (d, J = 8.2 Hz), 115.19 (d, J = 21.6 Hz), 83.03, 79.03, 78.05, 62.55, 39.48, 33.35. LC-MS m/z: 301.6 $[M+H]^+$.

***N*-(3-((1,1-*bis*(4-Fluorophenyl)prop-2-yn-1-yl)oxy)propyl)-2,4-dinitroaniline (10)**. To a solution of **9** (234 mg, 0.77 mmol) in DMF (5 mL) was added NEt_3 (0.2 mL, 1.5 mmol) and 2,4-dinitrofluorobenzene (100 µL, 0.77 mmol). The reaction mixture was stirred o/n, diluted with Et_2O and brine and extracted with Et_2O (3x). The combined organic layers were washed with H_2O (5x), brine, dried ($MgSO_4$), filtered

and concentrated to yield a viscous yellow oil (341 mg, 0.73 mmol, 95%). TLC: R_f = 0.33 in (2:8 EtOAc:pentane). IR: 3366 (N-H), 3292 (CC-H). ^{1}H NMR (400 MHz, $CDCl_3$) δ 9.10 (d, J = 2.7 Hz, 1H), 8.62 (t, J = 5.5 Hz, 1H), 8.24 (dd, J = 9.5, 2.7 Hz, 1H), 7.54 – 7.43 (m, 4H), 7.05 – 6.92 (m, 5H), 3.62 (m, 4H), 2.96 (s, 1H), 2.10 (m, 2H). ^{13}C NMR (100 MHz, $CDCl_3$) δ 162.40 (d, J = 247.4 Hz), 148.39, 138.52 (d, J = 3.0 Hz), 136.01, 130.39, 128.46 (d, J = 8.2 Hz), 124.38, 115.25 (d, J = 21.6 Hz), 114.03, 82.62, 79.40, 78.55, 61.70, 40.91, 28.89.

***bis*(4-Fluorophenyl)(1*H*-1,2,3-triazol-4-yl)methanol (6)**. To a degassed solution of alkyne **5** (1.2 g, 5 mmol) in 1:5 MeOH:DMF (20 mL) was added sequentially trimethylsilyl azide (1 mL, 7.4 mmol), $CuSO_4$ (1 M in water, 0.5 mL, 0.5 mmol) and NaAsc (1 M, 1.5 mL, 1.5 mmol). After prolonged heating (5 days) and several new portions of TMS-N_3 (3 x 1 mL), the reaction was quenched with H_2O. The reaction mixture was filtered over celite, concentrated, diluted with H_2O and extracted with Et_2O (3x). The combined organic layers were washed with H_2O (3x), brine, dried (Na_2SO_4), filtered and concentrated. Purification of the residue by silica gel column chromatography (10 > 30% EtOAc in pentane) yielded a white solid with yellow discoloration. This solid was recrystallized from $CHCl_3$ to yield the title compound (835 mg, 2.91 mmol, 59%). TLC: R_f = 0.54 (1:1 EtOAc:pentane). IR: 3192 (N-H), 1601, 1504. ^{1}H NMR (400 MHz, CD_3OD) δ 7.58 (s, 1H), 7.42 – 7.29 (m, 4H), 7.18 – 6.79 (m, 4H). ^{13}C NMR (100 MHz, $(CD_3)_2SO$) δ 161.11 (d, J = 243.3 Hz),143.12, 128.96 (d, J = 8.2 Hz), 114.38 (d, J = 21.3 Hz), 75.14. LC-MS *m/z*: 287.8 $[M+H]^+$.

***N*-(3-(*bis*(4-Fluorophenyl)(1*H*-1,2,3-triazol-4-yl)methoxy)propyl)-2,4-dinitroaniline (11)**. To a degassed solution of **10** (110 mg, 0.24 mmol) and POM-azide (60 µL, 0.35 mmol) in THF:H_2O 10:3 (6.5 mL) was added CuBr (6.1 mg, 42 µmol) and the resulting suspension was sonicated shortly before being stirred at 60 °C for 4 days. The reaction mixture was allowed to cool to rt before KOH (2 M in MeOH) was added and the resulting solution was stirred for 30 minutes, concentrated, diluted with EtOAc and H_2O and extracted with EtOAc (3x). The combined organic layers were washed with a basic solution of 1 M EDTA (basified with NH_3(aq.), 2x), brine, dried ($MgSO_4$), filtered and concentrated. Purification of the residue by silica gel column chromatography (1:4 EtOAc: pentane) yielded a yellow film (81 mg, 0.167 mmol, 67%). TLC: R_f = 0.33 (1:1 EtOAc:pentane). IR: 3362 (N-H aniline), 3100 (N-H triazole). ^{1}H NMR (400 MHz, $(CD_3)_2SO$) δ 15.03 (s, 1H), 8.94 – 8.74 (m, 2H), 8.22 (dd, J = 9.7, 2.8 Hz, 1H), 7.50 (s, 1H), 7.39 (m, 4H), 7.21 (d, J = 9.5 Hz, 1H), 7.12 (m, 4H), 3.64 – 3.49 (m, 2H), 3.26 (m, 2H), 2.00 – 1.81 (m, 2H). ^{13}C NMR (100 MHz, $(CD_3)_2SO$) δ 161.18 (d, J = 245.2 Hz), 148.10, 140.21, 134.71, 130.00, 129.4 (d, J = 8 Hz), 123.72, 115.28, 114.73 (d, J = 21.3 Hz), 61.24, 40.30, 28.50. LC-MS *m/z*: 510.8 $[M+H]^+$.

***tert*-Butyl (2*R*,5*R*)-5-(3-azidopropoxy)-2-benzylpiperidine-1-carboxylate (7)**. To a cooled (0 °C) solution of *tert*-butyl (2*R*,5*R*)-2-benzyl-5-hydroxypiperidine-1-carboxylate[24] (80 mg, 0.27 mmol) in dry DMF was added NaH (33 mg, 0.82 mmol) and stirred for 30 minutes. Subsequently, 3-azidopropanol tosylate (280 mg, 1.1 mmol) was added dropwise and the solution stirred at rt o/n. The mixture was diluted with Et_2O, poured into water and extracted with Et_2O (3x). The combined organic layers were washed with H_2O (2x), brine, dried (Na_2SO_4), filtered and concentrated. Purification of the residue by silica gel column chromatography (7.5% Et2O in PE) yielded a colorless oil (66 mg, 0.18 mmol or 65%). TLC: R_f = 0.44 (1:9 Et2O:pentane). $[\alpha]_D$= -3.5. IR: 2096 (-N_3), 1689 (Boc). ^{1}H NMR (400 MHz, $CDCl_3$) δ 7.37 – 7.07 (m, 5H), 4.57 – 4.05 (m, 2H), 3.62 (m, 2H), 3.41 (m, 2H), 3.26 (m, 1H), 3.04 – 2.81 (m, 1H), 2.69 (m, 2H), 1.94 (m, 1H), 1.85 (m, 2H), 1.60 (m, 3H), 1.36 (m, 9H). ^{13}C NMR (100 MHz, $CDCl_3$) δ 129.29, 128.55, 126.37, 79.72, 74.87, 65.35, 52.26, 48.56, 42.51, 36.03, 29.63, 28.31, 26.18. LC-MS *m/z*: 274.7 (M-Boc), 374.5 $[M+H]^+$.

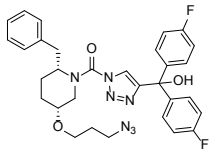

3

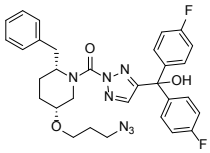

24

((2*R*,5*R*)-5-(3-Azidopropoxy)-2-benzylpiperidin-1-yl)(4-(*bis*(4-fluorophenyl)(hydroxy)methyl)-1*H*-1,2,3-triazol-1-yl)methanone (3) and ((2*R*,5*R*)-5-(3-azidopropoxy)-2-benzylpiperidin-1-yl)(4-(*bis*(4-fluorophenyl)(hydroxy)methyl)-2*H*-1,2,3-triazol-2-yl)methanone (24). **7** (46 mg, 0.12 mmol) was dissolved in 40% TFA in DCM and stirred for 15 minutes before the volatiles were removed under reduced pressure and coevaporated with toluene. The thus obtained TFA salt was dissolved in THF, treated with DIPEA (0.1 mL, 0.6 mmol) and cooled to 0 °C before triphosgene (18 mg, 0.06 mmol) was added. The resulting solution was stirred for 30 minutes at 0 °C. The reaction mixture was quenched with ice cold H_2O and extracted with EtOAc (3x). The combined organic layers were washed with H_2O, brine, dried (Na_2SO_4), filtered and concentrated. The crude carbamoyl chloride was dissolved in THF, treated with DIPEA (0.1 mL, 0.6 mmol), DMAP (16 mg, 0.12 mmol), **6** (35 mg, 0.12 mmol) and stirred at 60 °C for 2 h. The reaction mixture was quenched with sat. aq. NH_4Cl and extracted with EtOAc (3x). The combined organic layers were washed with H_2O (2x), brine, dried (Na_2SO_4), filtered and concentrated. Purification of the residue by silica gel column chromatography (15 > 20% EtOAc in PE), to yield two regioisomers. N1 isomer, apolar fractions, **3**: TLC: R_f = 0.60 (3:7 EtOAc:pentane). HRMS *m/z* calculated for $C_{31}H_{31}F_2N_7O_3$ $[M+Na]^+$: 610.2349, found: 610.2358. N2 isomer, polar fractions, **24**: R_f = 0.43 (3:7 EtOAc:pentane). HRMS *m/z* calculated for $C_{31}H_{31}F_2N_7O_3$ $[M+Na]^+$: 610.2349, found: 610.2350.

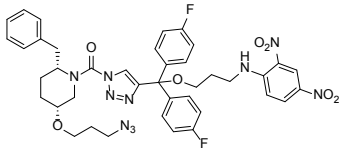

12

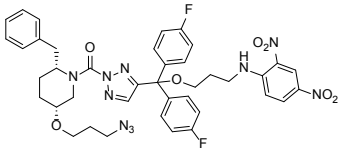

25

((2*R*,5*R*)-5-(3-Azidopropoxy)-2-benzylpiperidin-1-yl)(4-((3-((2,4-dinitrophenyl)amino)propoxy)*bis*(4-fluorophenyl)methyl)-1*H*-1,2,3-triazol-1-yl)methanone (12) and ((2*R*,5*R*)-5-(3-azidopropoxy)-2-benzylpiperidin-1-yl)(4-((3-((2,4-dinitrophenyl)amino)propoxy)*bis*(4-fluorophenyl)methyl)-2*H*-1,2,3-triazol-2-yl)methanone (25). Following the procedure for the preparation of **3**, but from triazole **11** at 100 µmol scale. Purification by silica gel column chromatography (20 > 25% EtOAc in PE). Yellow film, 74% yield as a mixture of N1 and N2-isomers. N1, apolar fractions, **12**: TLC: R_f = 0.38 (3:7 EtOAc:pentane). HRMS *m/z* calculated for $C_{40}H_{40}F_2N_{10}O_7$ $[M+Na]^+$: 833.2942, found: 833.2947. N2, polar fractions, **25**: TLF: R_f = 0.26 (3:7 EtOAc:pentane). HRMS *m/z* calculated for $C_{40}H_{40}F_2N_{10}O_7$ $[M+Na]^+$: 833.2942, found: 833.2956.

((2*R*,5*R*)-2-Benzyl-5-(3-(4-(4-(5,5-difluoro-1,3,7,9-tetramethyl-5*H*-4λ4,5λ4-dipyrrolo[1,2-*c*:2',1'-*f*][1,3,2]diazaborinin-10-yl)butyl)-1*H*-1,2,3-triazol-1-yl)propoxy)piperidin-1-yl)(4-((3-((2,4-dinitrophenyl)amino)propoxy)bis(4-fluorophenyl)methyl)-1*H*-1,2,3-triazol-1-yl)methanone (1). This compound was obtained by the general procedure for the CuAAC reaction on

a 38 µmol scale. Purification of the residue by silica gel column chromatography (50 > 60% EtOAc in PE). TLC: R_f = 0.25 (3:2 EtOAc:pentane). N1 isomer, **1**, HRMS *m/z* calculated for $C_{59}H_{63}BF_4N_{12}O_7$ $[M+H]^+$: 1139.5045, found: 1139.5076.

((2*R*,5*R*)-2-Benzyl-5-(3-(4-(4-(5,5-difluoro-1,3,7,9-tetramethyl-5*H*-4λ4,5λ4-dipyrrolo[1,2-*c*:2',1'-*f*][1,3,2]diazaborinin-10-yl)butyl)-1*H*-1,2,3-triazol-1-yl)propoxy)piperidin-1-yl)(4-((3-((2,4-dinitrophenyl)amino)propoxy)bis(4-fluorophenyl)methyl)-2*H*-1,2,3-triazol-2-yl)methanone (26). This compound was obtained by the general procedure for the CuAAC reaction on a 35 µmol scale. Purification of the residue by silica gel column chromatography (50 > 60% EtOAc in PE). TLC: R_f = 0.25 (3:2 EtOAc:pentane). N2 isomer, **26**, HRMS *m/z* calculated for $C_{59}H_{63}BF_4N_{12}O_7$ $[M+H]^+$: 1139.5045, found: 1139.5067.

(4-Ethynylphenyl)methanol (14). To a solution of 4-ethynylbenzaldehyde (**13**, 390 mg, 3 mmol) in EtOH (6 mL) was added $NaBH_4$ (390 mg, 10.3 mmol). The reaction mixture was stirred for 10 min, quenched with water and extracted with DCM. The organic layer was washed with brine, dried ($MgSO_4$), filtered, and concentrated to yield **14** (389 mg, 3 mmol, 99%) as a yellow oil. TLC: R_f = 0.61 (6:4 pentane:EtOAc). ^{1}H NMR (400 MHz, $CDCl_3$) δ 7.48 (d, J = 8.2 Hz, 2H), 7.31 (d, J = 8.1 Hz, 2H), 4.68 (s, 2H), 3.08 (s, 1H), 1.90 (s, 1H). ^{13}C NMR (100 MHz, $CDCl_3$) δ 141.67, 132.42, 126.85, 121.38, 83.59, 77.36, 64.94.

4-Ethynylbenzyl methanesulfonate (15). To a cooled (0 °C) solution of **14** (373 mg, 2.82 mmol) in dry DCM (15 mL) were added Et_3N (0.59 mL, 4.23 mmol) and MsCl (262 µL, 3.38 mmol). The reaction mixture was stirred for 45 minutes, washed with water, extracted with DCM, dried ($MgSO_4$), filtered and concentrated to yield **15** (558 mg, 2.7 mmol, 94%). TLC: R_f = 0.66 (6:4 pentane:EtOAc). ^{1}H NMR (400 MHz, $CDCl_3$) δ 7.53 (d, J = 8.3 Hz, 2H), 7.38 (d, J = 8.3 Hz, 2H), 5.23 (s, 2H), 4.57 (s, 1H), 3.14 (s, 1H), 2.94 (s, 3H). ^{13}C NMR (100 MHz, $CDCl_3$) δ 134.07, 132.70, 128.74, 123.37, 82.93, 78.57, 70.80, 38.47. LC-MS *m/z*: 211.0 $[M+H]^+$.

2-(4-Ethynylbenzyl)isoindoline-1,3-dione (16). To a cooled (0 °C) solution of **15** (546 mg, 2.6 mmol) in dry DMF (10 mL) was added phthalimide potassium salt (722 mg, 3.9 mmol). The reaction mixture was stirred on ice for 2 h and at rt o/n. After addition of water, the product precipitated. The suspension was filtered and the solid was dissolved in DCM, washed with HCl (0.1 M), brine, dried ($MgSO_4$), filtered and concentrated to yield **16** (625 mg, 2.4 mmol, 92%). ^{1}H NMR (400 MHz, $CDCl_3$) δ 7.85 (m, 2H), 7.72 (m, 2H), 7.44 (d, J = 8.4 Hz, 2H), 7.38 (d, J = 8.4 Hz, 2H), 4.84 (s, 2H), 3.06 (s, 1H). ^{13}C NMR (100 MHz, $CDCl_3$) δ 137.10, 134.25, 132.58, 132.15, 128.69, 123.58, 77.63, 41.43.

2-(4-(1*H*-1,2,3-Triazol-4-yl)benzyl)isoindoline-1,3-dione (17). To a degassed solution of **16** (102 mg, 0.4 mmol) and TMS-azide (79 µL, 0.6 mmol) in DMF:MeOH (4:0.8 mL) was added CuI (5 mg, 25 µmol). The reaction mixture was refluxed o/n, concentrated and purification of the residue by silica gel column chromatography (6:4 pentane:EtOAc) yielded **17** (78 mg, 0.26 mmol, 64%). ^{1}H NMR (400 MHz, $CDCl_3$) δ 8.05 – 7.66 (m, 6H), 7.52 (m, 2H), 7.00 (s, 1H), 4.89 (s, 2H). LC-MS *m/z*: 305.2 $[M+H]^+$.

***tert*-Butyl (5-((2-nitro-*N*-phenethylphenyl)sulfonamido)pentyl)carbamate**. To a solution of *N*-Boc-cadaverine (372 mg, 1.84 mmol) in THF (8 mL) were added 2-nitrobenzenesulfonyl chloride (408 mg, 1.84 mmol) and Et_3N (0.38 mL, 2.76 mmol). The cloudy reaction mixture was stirred for 75 minutes, quenched with water (40 mL) and extracted with EtOAc (3 x 20 mL). The combined organic layers were washed with water (60 mL), brine (60 mL), dried ($MgSO_4$), filtered and concentrated. The residue was

dissolved in CH_3CN (16 mL) and Cs_2CO_3 (1798 mg, 5.52 mmol) and phenethylbromide (0.38 mL, 2.76 mmol) were added. The solution was stirred at 80 °C for 6 h. Another equivalent of phenethylbromide (0.38 mL, 2.76 mmol) was added and stirred at 80 °C o/n. The mixture was poured into water (50 mL) and extracted with EtOAc (3 x 25 mL). The combined organic layers were washed with water (50 mL), brine (50 mL), dried ($MgSO_4$), filtered, and concentrated. Purification of the residue by silica gel column chromatography (2:8 > 3:7 EtOAc:pentane) yielded the title compound (781 mg, 1.6 mmol, 87%) as a yellow oil. TLC: R_f = 0.75 (1:1 pentane:EtOAc). ^{1}H NMR (400 MHz, $CDCl_3$) δ 7.95 (d, J = 7.6 Hz, 1H), 7.67 - 7.58 (m, 3H), 7.26 - 7.15 (m, 5H), 4.52 (br s, 1H), 3.50 (t, J = 8.0 Hz, 2H), 3.33 (t, J = 7.6 Hz, 2H), 3.07 - 3.06 (m, 2H), 2.84 (t, J = 8.0 Hz, 2H), 1.57 (m, 2H), 1.49-1.43 (m, 11H), 1.27 (m, 2H). ^{13}C NMR (100 MHz, $CDCl_3$) 156.06, 148.10, 138.11, 133.67, 133.48, 131.69, 130.73, 128.84, 128.69, 126.75, 124.24, 79.07, 48.87, 47.68, 40.35, 35.19, 29.69, 28.51, 27.82, 23.75. LC-MS *m/z*: 492.1 $[M+H]^+$.

***tert*-Butyl (5-(phenethylamino)pentyl)carbamate (19)**. To a solution of *tert*-butyl (5-((2-nitro-*N*-phenethylphenyl)sulfonamido)pentyl)carbamate (781 mg, 1.59 mmol) in CH_3CN (15 mL) were added Cs_2CO_3 (1.57 g, 4.77 mmol) and PhSH (244 µL, 2.38 mmol). The reaction mixture was stirred o/n, poured into water (100 mL) and extracted with DCM (3 x 50 mL). The combined organic layers were dried ($MgSO_4$), filtered and concentrated. Purification of the residue by silica gel column chromatography (1:9 MeOH:DCM > 1:9 MeOH:DCM + 1% Et_3N) yielded **19** (400 mg, 1.3 mmol, 82%) as a clear oil. ^{1}H NMR (400 MHz, $CDCl_3$) δ 7.33 – 7.27 (m, 2H), 7.21 (dt, J = 5.9, 1.4 Hz, 3H), 4.66 (br s, 1H), 3.74 (br s, 1H), 3.09 (m, 2H), 3.00 – 2.84 (m, 4H), 2.68 (m, 2H), 1.56 (m, 2H), 1.44 (s, 11H), 1.40 – 1.23 (m, 2H). LC-MS *m/z*: 307.2 $[M+H]^+$.

***tert*-Butyl (5-(4-(4-((1,3-dioxoisoindolin-2-yl)methyl)phenyl)-*N*-phenethyl-1*H*-1,2,3-triazole-1-carboxamido)pentyl)carbamate (20)**. To a cooled (0 °C) solution of **19** (98 mg, 0.32 mmol) in dry THF (3 mL) were added DIPEA (167 µL, 0.96 mmol) and triphosgene (47 mg, 0.16 mmol). The reaction mixture was stirred on ice for 1 h, quenched with water and extracted with EtOAc (3 x 15 mL). The combined organic layers were washed with brine, dried ($MgSO_4$), filtered and concentrated. The residue was dissolved in dry THF (3 mL) and DMAP (39 mg, 0.32 mmol), DIPEA (167 µL, 0.96 mmol) and **17** (97 mg, 0.32 mmol) were added and stirred at 60 °C for 3 h. The reaction was quenched by the addition of NH_4Cl (sat. aq.), extracted with EtOAc (3 x 15 mL), washed with water, brine, dried ($MgSO_4$), filtered and concentrated. Purification of the residue by silica gel column chromatography (7:3 pentane:EtOAc) yielded **20** (55 mg, 86 µmol, 27%). ^{1}H NMR (400 MHz, $CDCl_3$) δ 8.39 (s, 1H), 7.86 (m, 2H), 7.80 (m, 2H), 7.71 (m, 2H), 7.51 (m, 2H), 7.31 – 7.07 (m, 5H), 4.88 (s, 2H), 4.63 (s, 1H), 3.96 (m, 1H), 3.73 (m, 1H), 3.63 – 3.45 (m, 2H), 3.23 – 2.90 (m, 3H), 1.84 – 1.66 (m, 2H), 1.66 – 1.53 (m, 1H), 1.43 (s, 9H). ^{13}C NMR (100 MHz, $CDCl_3$) δ 156.15, 146.11, 136.85, 134.17, 132.15, 129.32, 128.99, 128.81, 126.80, 126.70, 126.51, 126.26, 123.52, 121.17, 120.95, 51.35, 49.21, 41.42, 40.38, 35.14, 33.58, 29.86, 28.51, 26.99, 24.06, 23.71. LC-MS *m/z*: 637.2 $[M+H]^+$. HRMS *m/z* calculated for $C_{36}H_{40}N_6O_5$ $[M+H]^+$: 637.3133, found: 637.3134.

***tert*-Butyl (5-(4-(4-(aminomethyl)phenyl)-*N*-phenethyl-1*H*-1,2,3-triazole-1-carboxamido)pentyl) carbamate (22)**. To a solution of **20** (27 mg, 0.04 mmol) in EtOH (1 mL) was added ethylene diamine (4.3 µL, 0.06 mmol). The reaction mixture was stirred o/n, concentrated and purification of the residue by silica gel column chromatography (1:9 MeOH:DCM > 1:9 MeOH:DCM + 1% Et_3N) yielded **22** (10 mg, 20 µmol, 50%). A side reaction was nucleophilic addition on the urea by the ethylenediamine, requiring the deprotection to be stopped before full conversion was reached. ^{1}H NMR (400 MHz, $CDCl_3$) δ 8.38 (s, 1H), 7.71 (m, 2H), 7.30 (m, 2H), 7.29-7.12 (m, 5H), 4.60 (br s, 1H), 3.99 (s, 2H), 3.72 - 3.39 (m, 4H),

3.16 - 3.00 (m, 4H), 1.75 (br s, 2H), 1.55 - 1.43 (m, 11H), 1.34 - 1.23 (m, 2H). LC-MS *m/z*: 507.0 $[M+H]^+$.

1-Amino-4-((4-(2-((4-(1-((5-((*tert*-butoxycarbonyl)amino)pentyl)(phenethyl)carbamoyl)-1*H*-1,2,3-triazol-4-yl)benzyl)amino)-2-oxoethyl)phenyl)amino)-9,10-dioxo-9,10-dihydroanthracene-2-sulfonate (23). To a solution of cAB40 (8.5 mg, 0.02 mmol) and HCTU (7.7 mg, 0.02 mmol) in dry DMF (1 mL) was added DIPEA (3.6 µL, 0.02 mmol). The reaction mixture was stirred for 15 min before addition of **22** (10 mg in 1 mL DMF, 0.02 mmol). The reaction mixture was stirred for 3 h, concentrated and purification of the residue by silica gel column chromatography (5:5:1 DCM:pentane:MeOH + 1% AcOH) yielded **23** (10 mg, 11 µmol, 53%) as a blue solid. ^{1}H NMR (500 MHz, $CDCl_3$/CD_3OD) δ 8.31 (t, J = 9.0 Hz, 2H) 8.27 (s, 1H), 7.84 - 7.74 (m, 4H), 7.35 - 7.13 (m, 12H), 4.46 (br s, 2H), 3.67 - 3.57 (m, 4H), 3.37 (s, 2H), 3.16 - 2.99 (m, 6H), 1.77 (br s, 2H), 1.43 - 1.33 (m, 11H), 1.31 - 1.26 (m, 2H). ^{13}C NMR (125 MHz, $CDCl_3$/CD_3OD) 183.97, 172.03, 140.92, 138.67, 134.53, 134.07, 133.09, 132.80, 131.04, 130.46, 128.90, 128.76, 128.13, 126.44, 126.31, 126.15, 124.29, 123.43, 54.73, 51.37, 46.77, 43.18, 42.86, 42.64, 29.58, 28.34. LC-MS *m/z*: 940.93 $[M+H]^+$.

1-Amino-4-((4-(2-((4-(1-((5-(6-(3,3-dimethyl-2-((1*E*,3*E*)-5-((*Z*)-1,3,3-trimethylindolin-2-ylidene)penta-1,3-dien-1-yl)-3*H*-indol-1-ium-1-yl)hexanamido)pentyl)(phenethyl)carbamoyl)-1*H*-1,2,3-triazol-4-yl)benzyl)amino)-2-oxoethyl)phenyl)amino)-9,10-dioxo-9,10-dihydroanthracene-2-sulfonate (2). A solution of **23** (9 mg, 9.6 µmol) in DCM (9 mL) and TFA (1 mL) was stirred for 45 min. The solvent was evaporated and co-evaporated with toluene. The crude was dissolved in dry DMF (5 mL), Cy5-OSu ester (5.5 mg, 9.6 µmol) and DIPEA (5.2 µL, 0.03 mmol) were added and the reaction mixture was stirred for 4 h, concentrated and purified by semi-preparative HPLC to yield **2** (1.3 mg, 1.0 µmol, 10%) as a blue solid. HRMS *m/z* calculated for $C_{77}H_{80}N_{10}O_8S$ $[M+H]^+$: 1305.5954, found: 1305.5941.

1-(6-((5-(4-(4-((1,3-Dioxoisoindolin-2-yl)methyl)phenyl)-*N*-phenethyl-1*H*-1,2,3-triazole-1-carboxamido)pentyl)amino)-6-oxohexyl)-3,3-dimethyl-2-((1*E*,3*E*)-5-((*Z*)-1,3,3-trimethylindolin-2-ylidene)penta-1,3-dien-1-yl)-3*H*-indol-1-ium (21). A solution of **20** (21 mg, 0.035 mmol) in DCM (0.9 mL) and TFA (0.1 mL) was stirred for 1 h. The solvent was evaporated and co-evaporated with toluene. The crude was dissolved in dry DMF (11 mL), Cy5-OSu ester (19 mg, 0.035 mmol) and DIPEA (11.9 µL, 0.09 mmol) were added and the reaction mixture was stirred o/n, poured into H_2O and extracted with EtOAc (3x). The combined organic layers were washed with water, brine, dried (Na_2SO_4), filtered and concentrated. Purification of the residue by silica gel column chromatography (EtOAc > 1:19 MeOH:DCM) yielded the title compound (15 mg, 15 µmol, 44%) as a blue solid. ^{1}H NMR (500 MHz, $CDCl_3$) δ 8.40 (s, 1H), 7.98 – 7.65 (m, 7H), 7.50 (m, 2H), 7.45 – 6.93 (m, 15H), 6.66 (s, 1H), 6.28 (s, 1H), 4.88 (s, 2H), 4.10 (s, 2H), 3.94 (s, 1H), 3.86 – 3.62 (m, 2H), 3.56 (s, 4H), 3.40 – 3.12 (m, 2H), 3.12 – 2.91 (m, 2H), 2.49 (s, 1H), 2.00 – 1.50 (m, 22H), 1.50 – 1.20 (m, 7H).^{13}C NMR (125 MHz, $CDCl_3$) δ 173.51, 172.29, 168.17, 142.96, 142.00, 141.27, 140.69, 134.21, 132.20, 129.31, 129.15, 128.79, 128.76, 126.28, 125.60, 124.89, 123.56, 122.18, 111.20, 110.19, 52.23, 51.33, 49.49, 49.33, 48.95, 44.87, 41.46, 29.83, 28.18, 27.04, 26.50, 25.43, 25.22. HRMS *m/z* calculated for $C_{63}H_{69}N_8O_4^+$ $[M]^+$: 1001.5436, found: 1001.5449.

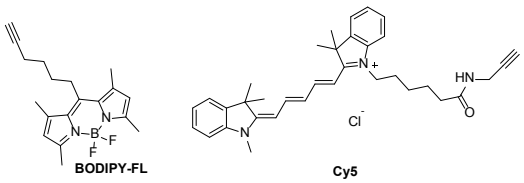

Spectroscopic characterization. UV-VIS spectra (400 - 700 nm) were recorded on a Shimadzu PharmaSpec UV-1700 UV-Visible spectrophotometer in a cuvette with 1 cm light path. Fluorescence spectra were recorded on a Shimadzu RF-5301PC spectrofluorophotometer in a quartz cuvette with four polished windows with a light path of 1 cm. The spectrofluorophotometer was set at high sensitivity and to record spectra with a 1 nm sampling interval. For BODIPY-FL and probe **1**, the wavelength of excitation was set to 497 nm and emission spectra were recorded from 500 – 700 nm with a slit width of 1.5 nm. For Cy5 and probe **2**, the wavelength of excitation was set to 646 nm and emission spectra were recorded from 650 - 800 nm with a slit width of 3 nm. Absorbance and fluorescence spectra were recorded at five concentrations in 2 mL of 96% EtOH. The slopes of the absorbance versus fluorescence plot were used to determine the relative fluorescence quantum yields (gradient probe divided by gradient parent fluorophore).

Biological assays

Surrogate substrate assay. The surrogate substrate assay was performed as published previously,[39] with the following adaptions: 100 µL per well as final volume and an endpoint measurement of the absorbance. Briefly, the assay was performed in a transparent flat bottomed 96 wells plate. The membranes used in these experiments were derived from HEK293T cells overexpressing human DAGLα. The assay was performed in 50 mM HEPES buffered to pH 7.0. Inhibitors were incubated for 20 min at rt, followed by addition of p-nitrophenol butyrate. The final p-nitrophenol butyrate concentration was 300 µM. The amount of hydrolysis of p-nitrophenol butyrate was determined from the absorbance at 420 nm after 30 min incubation at rt. All measurements were performed with 5% DMSO present and a final protein concentration of 0.2 mg/mL. Negative controls consisted of mock transfected membranes or 10 µM Orlistat inhibited hDAGLα membranes. All measurements were performed in duplo (N=2, n=2).

Cell culture. Cells were cultured at 37 °C under 7% CO2 in DMEM containing phenol red, GlutaMax, 10% (v/v) New Born Calf Serum (Thermo Fisher), penicillin and streptomycin (200 µg/mL each; Duchefa). For selection and maintenance of stable expression cell lines, complete DMEM was supplemented with G418 (0.4 mg/mL). Medium was refreshed every 2-3 days and cells were passaged twice a week at 80-90% confluence by resuspension in fresh medium (Neuro2A, HEK293T) or by trypsinization (U2OS).

Plasmids. The hDAGLα plasmid was constructed as described before.[39] Briefly, full length human cDNA of hDAGL-α was purchased from Biosource and cloned into mammalian expression vector pcDNA3.1, containing genes for ampicillin and neomycin resistance. A FLAG-linker was made from primers and cloned into the vector at the C-terminus of hDAGL-α. The plasmid was grown in XL-10 Z-competent cells and prepped (Maxi Prep, Qiagen). The sequences were confirmed by sequence analysis at the Leiden Genome Technology Centre.

Transfection. HEK293T cells were grown to ~70% confluency in 15 cm dishes. Prior to transfection, culture medium was refreshed (15 mL). A 3:1 (m:m) mixture of polyethyleneimine (PEI, 60 µg/well) and plasmid DNA (20 µg/well) was prepared in serum free culture medium and incubated for 10 min at rt. Transfection was performed by dropwise addition of the PEI/DNA mixture (2 mL/well) to the cells. 24 h post-transfection, the medium was refreshed and after 48 h cells were harvested.

U2OS_ABHD6-GFP stable expression. Full-length human cDNA of ABHD6 (Source Bioscience) was cloned into mammalian expression vector pcDNA3.1, containing genes for ampicillin and neomycin resistance. The inserts were cloned in frame with a C-terminal FLAG- and GFP-tag. Plasmids were isolated from transformed XL-10 Z-competent cells (Maxi Prep kit: QiaGen) and sequenced at the Leiden Genome Technology Center. Sequences were analyzed and verified (CLC Main Workbench). One day prior to transfection U2OS cells were seeded to a 6 wells plates (~0.5 million cells/well). Prior to transfection, culture medium was aspirated and a minimal amount of medium was added. A 3:1 (m/m) mixture of polyethyleneimine (PEI) (3.75 µg/well) and plasmid DNA (11.25 µg/well) was prepared in serum free culture medium and incubated (15 min, rt). Transfection was performed by dropwise addition of the PEI/DNA mixture to the cells. After 24 h, transfection efficiency was determined by fluorescence microscopy and transfection medium was exchanged for selection medium containing 800 µg/mL G418. 48 h after transfection single cells were seeded to 96 wells plates in 100 µL selection medium. After 14 days, plates were inspected for cell growth, clones were checked for ABHD6-GFP expression by fluorescence microscopy (GFP channel). From here on, cells were grown in maintenance medium containing 400 µg/mL G418, and expanded in 12- and 6-wells plates and 10 cm dishes.

Inhibitor treatment. The medium was aspirated and 0.5 mL serum-free medium containing the inhibitor was added. After incubation for 1 h at 37 °C, medium was removed and PBS added, removed, trypsin buffer was added, quenched with 1 mL medium and the cells were harvested by pipetting. After centrifugation (5 min, 1000 *g*), the medium was removed, the cells were resuspended in PBS, centrifuged again (5 min, 1000 *g*) and the pellets flash frozen with N_2 (l) and stored at - 80 °C.

Whole cell lysate preparation. Cell pellets were thawed on ice, resuspended in cold lysis buffer (20 mM HEPES pH 7.2, 2 mM DTT, 250 mM sucrose, 1 mM $MgCl_2$, 2.5 U/mL benzonase) and incubated on ice (15-30 min). The cell lysate was diluted to 2 mg/mL (Neuro2A) in cold storage buffer (20 mM Hepes, pH 7.2, 2 mM DTT). Protein concentrations were determined by a Quick Start™ Bradford Protein Assay (Bio-Rad) and diluted samples were flash frozen with N_2 (l) and stored at -80 °C until further use.

Activity-based protein profiling. Cell lysate (15 µL, 2.0 mg/mL) was pre-incubated with vehicle or inhibitor (0.375 µL 40 x inhibitor stock, 30 min, rt or 37 °C) followed by an incubation with the activity-based probe (1 µM DH379 or 100 nM **1**, 20 min, rt). Final concentrations for the inhibitors are indicated in the main text and figure legends. Reactions were quenched with 4x Laemmli buffer (5 µL, 240 mM Tris (pH 6.8), 8% (w/v) SDS, 40% (v/v) glycerol, 5% (v/v) β-mercaptoethanol, 0.04% (v/v) bromophenol blue). 10 or 20 µg per reaction was resolved on a 10% acrylamide SDS-PAGE gel (180 V, 75 min). Gels were scanned using Cy2, Cy3 and Cy5 multichannel settings on a ChemiDoc MP (Bio-Rad) and stained with Coomassie after scanning. Fluorescence was normalized to Coomassie staining and quantified with Image Lab v5.2.1 (Bio-Rad). IC50 curves were fitted with Graphpad Prism® v7 (Graphpad Software Inc.).

References

1. Eva J. van Rooden, Maurits Kohsiek, Roy Kreekel, Annelot C. M. van Esbroeck, Adrianus M. C. H. van den Nieuwendijk, Antonius P. A. Janssen, Richard J. B. H. N. van den Berg, Herman S. Overkleeft, Mario van der Stelt. Design and synthesis of quenched activity-based probes for diacylglycerol lipase and α,β-hydrolase domain containing protein 6. *Chemistry - An Asian Journal*, **2018**, doi: 10.1002/asia.201800452.
2. Katona, I. & Freund, T. F. Multiple Functions of Endocannabinoid Signaling in the Brain. *Annu. Rev. Neurosci.* **35**, 529–558 (2012).
3. Kohnz, R. A. & Nomura, D. K. Chemical approaches to therapeutically target the metabolism and signaling of the endocannabinoid 2-AG and eicosanoids. *Chem. Soc. Rev.* **43**, 6859–6869 (2014).
4. Blankman, J. L. & Cravatt, B. F. Chemical probes of endocannabinoid metabolism. *Pharmacol. Rev.* **65**, 849–71 (2013).
5. Di Marzo, V. Targeting the endocannabinoid system: To enhance or reduce? *Nat. Rev. Drug Discov.* **7**, 438–455 (2008).
6. Bisogno, T. *et al.* Cloning of the first sn1-DAG lipases points to the spatial and temporal regulation of endocannabinoid signaling in the brain. *J. Cell Biol.* **163**, 463–468 (2003).
7. Reisenberg, M., Singh, P. K., Williams, G. & Doherty, P. The diacylglycerol lipases: structure, regulation and roles in and beyond endocannabinoid signalling. *Philos. Trans. R. Soc. B Biol. Sci.* **367**, 3264–3275 (2012).
8. Di Marzo, V. Endocannabinoid signaling in the brain: Biosynthetic mechanisms in the limelight. *Nat. Neurosci.* **14**, 9–15 (2011).
9. Hsu, K.-L. *et al.* DAGLβ inhibition perturbs a lipid network involved in macrophage inflammatory responses. *Nat. Chem. Biol.* **8**, 999–1007 (2012).
10. Marrs, W. R. *et al.* The serine hydrolase ABHD6 controls the accumulation and efficacy of 2-AG at cannabinoid receptors. *Nat. Neurosci.* **13**, 951–7 (2010).
11. Savinainen, J. R., Saario, S. M. & Laitinen, J. T. The serine hydrolases MAGL, ABHD6 and ABHD12 as guardians of 2-arachidonoylglycerol signalling through cannabinoid receptors. *Acta Physiol.* **204**, 267–276 (2012).
12. Li, N., Overkleeft, H. S. & Florea, B. I. Activity-based protein profiling: An enabling technology in chemical biology research. *Curr. Op. in Chem. Biol.* 227–233 (2012).
13. Ogasawara, D. *et al.* Rapid and profound rewiring of brain lipid signaling networks by acute diacylglycerol lipase inhibition. *Proc. Natl. Acad. Sci.* **113**, 26–33 (2016).
14. Lee, S., Park, K., Kim, K., Choi, K. & Kwon, I. C. Activatable imaging probes with amplified fluorescent signals. *Chem. Commun.* **0**, 4250-4260 (2008).
15. Blum, G. *et al.* Dynamic imaging of protease activity with fluorescently quenched activity-based probes. *Nat. Chem. Biol.* **1**, 203–209 (2005).
16. Blum, G., von Degenfeld, G., Merchant, M. J., Blau, H. M. & Bogyo, M. Noninvasive optical imaging of cysteine protease activity using fluorescently quenched activity-based probes. *Nat. Chem. Biol.* **3**, 668–677

(2007).

17. Verdoes, M. *et al.* A nonpeptidic cathepsin s activity-based probe for noninvasive optical imaging of tumor-associated macrophages. *Chem. Biol.* **19**, 619–628 (2012).
18. Verdoes, M. *et al.* Improved quenched fluorescent probe for imaging of cysteine cathepsin activity. *J. Am. Chem. Soc.* **135**, 14726–14730 (2013).
19. Garland, M., Yim, J. J. & Bogyo, M. A Bright Future for Precision Medicine: Advances in Fluorescent Chemical Probe Design and Their Clinical Application. *Cell Chem. Biol.* **23**, 122–136 (2016).
20. Zhang, Q., Liu, H. & Pan, Z. A general approach for the development of fluorogenic probes suitable for no-wash imaging of kinases in live cells. *Chem. Commun.* **50**, 15319–15322 (2014).
21. Serim, S., Baer, P. & Verhelst, S. H. L. Mixed alkyl aryl phosphonate esters as quenched fluorescent activity-based probes for serine proteases. *Org. Biomol. Chem.* **13**, 2293–9 (2015).
22. Edgington, L. E. *et al.* Functional imaging of legumain in cancer using a new quenched activity-based probe. *J. Am. Chem. Soc.* **135**, 174–182 (2013).
23. Shaulov-Rotem, Y. *et al.* A novel quenched fluorescent activity-based probe reveals caspase-3 activity in the endoplasmic reticulum during apoptosis. *Chem. Sci.* **7**, 1322–1337 (2016).
24. Deng, H. *et al.* Triazole Ureas Act as Diacylglycerol Lipase Inhibitors and Prevent Fasting-Induced Refeeding. *J. Med. Chem.* **60**, 428–440 (2017).
25. Adibekian, A. *et al.* Click-generated triazole ureas as ultrapotent in vivo-active serine hydrolase inhibitors. *Nat. Chem. Biol.* **7**, 469–478 (2011).
26. Verdoes, M. *et al.* Acetylene functionalized BODIPY dyes and their application in the synthesis of activity based proteasome probes. *Bioorganic Med. Chem. Lett.* **17**, 6169–6171 (2007).
27. Sadhu, K. K., Mizukami, S., Watanabe, S. & Kikuchi, K. Turn-on fluorescence switch involving aggregation and elimination processes for β-lactamase-tag. *Chem. Commun.* **46**, 7403 (2010).
28. Sadhu, K. K., Mizukami, S., Watanabe, S. & Kikuchi, K. Sequential ordering among multicolor fluorophores for protein labeling facility via aggregation-elimination based β-lactam probes. *Mol. Biosyst.* **7**, 1766 (2011).
29. Li, H., Kang, J., Ding, L., Lü, F. & Fang, Y. A dansyl-based fluorescent film: Preparation and sensitive detection of nitroaromatics in aqueous phase. *J. Photochem. Photobiol. A: Chem.* **197**, 226–231 (2008).
30. Focsaneanu, K.-S. *et al.* Potential analytical applications of differential fluorescence quenching: pyrene monomer and excimer emissions as sensors for electron deficient molecules. *Photochem. Photobiol. Sci.* **4**, 817 (2005).
31. Johnston, M. *et al.* Assay and inhibition of diacylglycerol lipase activity. *Bioorganic Med. Chem. Lett.* **22**, 4585–4592 (2012).
32. Farber, S. A. Genetic Analysis of Digestive Physiology Using Fluorescent Phospholipid Reporters. *Science.* **292**, 1385–1388 (2001).
33. Jernigan, F. E. & Lawrence, D. S. A broad spectrum dark quencher: construction of multiple colour protease and photolytic sensors. *Chem. Commun.* **49**, 6728–30 (2013).
34. Haase, J. *Large-Scale Preparation and Usage of Azides*. *Organic Azides: Syntheses and Applications* (2010).

(Eds.: S. Bräse, K. Banert). Wiley-VCH, Weinheim, **2010**, chapter 2.

35. Woudenberg, R. C. Anhydrous proton conducting materials for use in high temperature polymer electrolyte membrane fuel cells. (2007).
36. Blencowe, C. A., Thornthwaite, D. W., Hayes, W. & Russell, A. T. Self-immolative base-mediated conjugate release from triazolylmethylcarbamates. *Org. Biomol. Chem.* **13**, 8703–8707 (2015).
37. Bullok, K. E. *et al.* Biochemical and in vivo characterization of a small, membrane-permeant, caspase-activatable far-red fluorescent peptide for imaging apoptosis. *Biochemistry* **46**, 4055–4065 (2007).
38. Pedicord, D. L. *et al.* Molecular characterization and identification of surrogate substrates for diacylglycerol lipase alpha. *Biochem. Biophys. Res. Commun.* **411**, 809–814 (2011).
39. Baggelaar, M. P. *et al.* Development of an activity-based probe and in silico design reveal highly selective inhibitors for diacylglycerol lipase-α in brain. *Angew. Chem. Int. Ed.* **52**, 12081–12085 (2013).
40. Baggelaar, M. P. *et al.* A highly selective, reversible inhibitor identified by comparative chemoproteomics modulates diacylglycerol lipase activity in neurons. *J. Am. Chem. Soc.* **137**, 8851–8857 (2015).
41. Cegielska, B. & Kacprzak, K. M. Simple and Convenient Protocol for Staining of Organic Azides on TLC Plates by Ninhydrin. A New Application of an Old Reagent. *Chem. Analityczna* **54**, 807–812 (2009).
42. England, K. S. *et al.* Optimisation of a triazolopyridine based histone demethylase inhibitor yields a potent and selective KDM2A (FBXL11) inhibitor. *Med. Chem. Commun.* **5**, 1879–1886 (2014).

Chapter 6

Two-step activity-based protein profiling of diacylglycerol lipase[1]

Introduction

Endocannabinoids are key regulators of neurotransmitter release in the central nervous system (CNS). They are involved in virtually every aspect of brain function, including modulation of synaptic plasticity and (patho)physiological processes, such as anxiety, fear and neuroinflammation.[2] 2-Arachidonoylglycerol (2-AG) is one of the most important endocannabinoids and activates the cannabinoid CB_1 and CB_2 receptors. 2-AG is synthesized by two diacylglycerol lipases (DAGLα (120 kDa) and DAGLβ (70 kDa)).[3] Both enzymes belong to the family of serine hydrolases, which share the same catalytic Ser-His-Asp triad to hydrolyze the *sn*-1 ester of 1-acyl-2-arachidonoylglycerides to generate 2-AG. A method to measure endogenous DAGL activity in biological samples is therefore important to understand endocannabinoid physiology.

Activity-based protein profiling (ABPP) is a powerful technique for monitoring enzyme activity in living systems using chemical probes.[4] These activity-based probes (ABPs) covalently and irreversibly bind to the active site of an enzyme and this interaction can be subsequently monitored using different techniques depending on the reporter group.[5] Several fluorescent ABPs have been reported to study the two isoforms of DAGLs. For example, HT-01 (**Fig. 1**), a DAGL probe based on 1,2,3-triazole urea inhibitors developed by the Cravatt laboratory, was used to study endogenous DAGLβ in (primary) macrophages.[6] In addition, DH379 (**Fig. 1**), based on the potent DAGL inhibitor DH376, was developed as a tailored fluorescent probe for DAGLα and DAGLβ.[7] However, reporter groups may affect the affinity and selectivity of the probes as well as cell permeability and metabolic stability. These issues are avoided by ligation of the reporter group to the probe after covalent binding of the target. Bioorthogonal chemistry enables the design of chemical probes with a minimalist handle for the conjugation of a reporter group after the probe target has been bound.[8] These two-step bioorthogonal probes also provide flexibility, as different reporter groups can be attached to the same probe. Different pairs of bioorthogonal reactants are

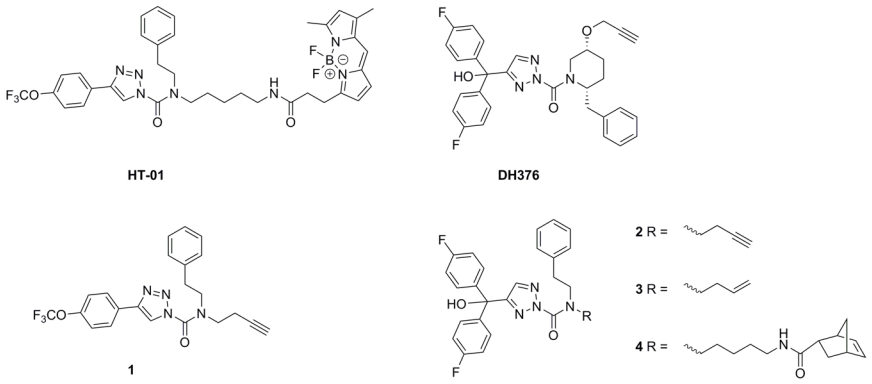

Figure 1. Design of two-step labeling probes **1** - **4** based on HT-01 and DH376.

currently available.[9] For two-step activity-based probes, the most popular pair is the azide-alkyne couple. These handles are reacted using the copper(I)-catalyzed azide-alkyne cycloaddition (CuAAC), often called "click" reaction. Both azides and alkynes are compact handles, chemically stable and synthetically accessible. An example of a two-step bioorthogonal probe for DAGL is DH376, which carries an alkyne handle (**Fig. 1**).

The CuAAC is relatively slow and requires toxic Cu(I) as a catalyst, therefore the inverse electron-demand Diels-Alder (IEDDA) ligation is sometimes used as an alternative. The reactants are an electron-rich dienophile and electron poor diene, usually a tetrazine. Tetrazines attached to fluorophores can serve as both the bioorthogonal reactive group and the fluorescence quencher, creating fluorescence "turn-on" reporters ideal for imaging.[10,11] An additional advantage is that no catalyst is required for the IEDDA.

Seven different two-step ABPs (**1** - **4**, **21** - **23**) are reported for DAGLs based on the scaffolds of HT-01 and DH376 (**Fig. 1**). Probe **1** is based on the HT-01 scaffold and has an alkyne handle. Probes **2** - **4** are hybrid probes of DH376 and HT-01. Probes **3** and **4** were designed to enable the use of the IEDDA reaction,[12,13] employing an alkene and a more strained norbornene, respectively. Probes **21** - **23** are triazole regioisomers of probes **1** - **3**, respectively.

Results and discussion

Synthesis. The synthesis of the triazole urea probes **1 – 4** started with the synthesis of the triazole scaffolds **6** and **8**, which are subsequently converted to the triazole ureas by coupling to an amine using triphosgene.[14] For the synthesis of probe **1**, 4-trifluoromethoxyphenylacetylene (**5**) was reacted with TMS-N_3 under Cu^I-catalyzed [2+3] cycloaddition conditions to give triazole **6** (**Scheme 1**).

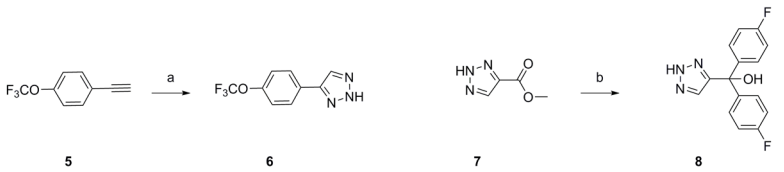

Scheme 1. Synthesis of triazoles. Reagents and conditions: (**a**) TMS-N_3, CuI, DMF/MeOH, 100 °C, o/n, 27%; (**b**) 4-fluorophenylmagnesium bromide, THF, 74%.

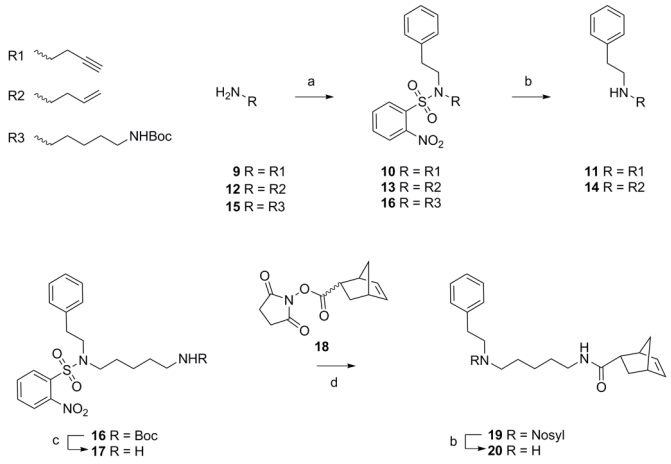

Scheme 2. Synthesis of amines. Reagents and conditions: (**a**) *i*. NsCl, Et_3N, THF; ii. $Ph(CH_2)_2Br$, Cs_2CO_3, CH_3CN, 80 °C, **10**: 93%; **13**: 70%; **16**: 92%; (**b**) PhSH, Cs_2CO_3, CH_3CN, **11**: 74%; **14**: 81%; **20**: 41%; (**c**) TFA/DCM 1:9, 100%; (**d**) DIPEA, DMF, 33%.

The triazole scaffold of compounds **2** - **4** was synthesized by performing a Grignard reaction on ester **7** to yield triazole **8**.

The amine building blocks (**11**, **14**, **20**), which were used to construct the urea warheads, were synthesized using the following reaction sequences (**Scheme 2**). 1-Amino-3-butyne (**9**) was first nosylated and reacted with phenethyl bromide to yield **10**, which was subsequently deprotected to give **11** in 69% yield over three steps. Amines **14** and **16** were synthesized in a similar fashion from 3-butenylamine (**12**) and N-Boc-cadaverine (**15**), respectively. The Boc-group of **16** was removed with acid to yield **17**, which was coupled to the activated norbornene ester **18** to give the amide **19** as the endo-isomer. Removal of the nosyl group yielded amine **20**.

With the triazoles (**6**, **8**) and amines (**11**, **14** and **20**) in hand, the final compounds (probes **1** - **4**) were obtained using a triphosgene coupling (**Scheme 3**).[14] The amines were first converted to the corresponding carbamoyl chlorides and subsequently reacted with the triazoles. Generally, this yielded two regioisomers:

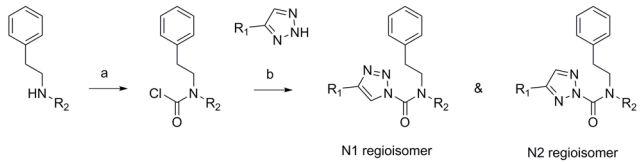

Scheme 3. Triphosgene coupling for synthesis of triazole ureas. Reagents and conditions: (**a**) triphosgene, DIPEA, THF, 0 °C; (**b**) DIPEA, DMAP, THF, 60 °C. **1**: 37%; **21**: 41%; **22**: 33%; **2**: 40%; **23**: 29%; **3**: 11%; **4**: 37% (Table 2).

N1 and N2.

To assign the separate compounds as either N1-regioisomer or N2-regioisomer, it was anticipated that the NMR chemical shift of the triazole carbon could be used (**Table 1**, **2**). To this end, theoretical chemical shifts were computed with density functional theory (DFT) for simplified structures of the triazole urea scaffold (**Table 1**). For structures with either a phenyl or a methyl directly attached to the triazole, the chemical shift in DMSO was calculated for the lowest energy conformer of either the N1 or N2 regioisomer. This resulted in theoretical chemical shift differences of approximately 10 ppm between the triazole carbon of the regioisomers with a shift of ±125 ppm for the N1 regioisomers and ±135 ppm for the N2 regioisomers.

Next, the experimental chemical shifts of the regioisomeric pairs (**1** & **21**, **2** & **22**, **3** & **23** and **4**) were measured (**Table 2**). In line with the theoretical calculations, the experimental chemical shift differed ~10 ppm between the two separated isomers. The triazole proton is highly characteristic (broad, downfield peak) and HSQC experiments were used to confidently assign the triazole carbon peak in the ^{13}C aromatic region. For the polar regioisomers (slower migration on TLC, left column of **Table 1**) the chemical shift is ~125 ppm and the same carbon in the apolar regioisomers (right column of **Table 1**) is shifted downfield to around 135 ppm. This trend is observed for each pair of regioisomers (**Table 2**; the corresponding apolar regioisomer of probe **4** was not obtained in sufficient yield for NMR analysis). The compounds (**Table 2**) can therefore be assigned as N1 or N2 isomers depending on their chemical shift. This assignment is in agreement with earlier reported regioisomers of other triazole ureas as determined with a crystal structure[6] or NMR measurements.[7,15]

Table 1. Computed values of the ^{13}C shift of the triazole carbon (indicated with the red circle). Simplified structures of N1 and N2 regioisomers for DFT calculations are shown.

Structure	Theoretical δ (ppm)
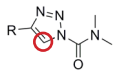	122 (R = Ph) 124 (R = Me)
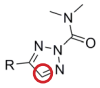	135 (R = Ph) 138 (R = Me)

Table 2. Final compounds obtained from triphosgene couplings (Scheme 3) and the ^{13}C NMR chemical shift of the triazole carbon of 1,2,3-triazole urea regioisomers (measured in DMSO).

Entry	Structure	^{13}C ppm	Entry	Structure	^{13}C ppm
1	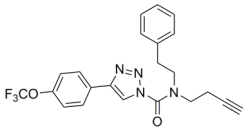	126	**21**	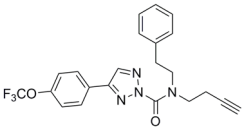	134
22	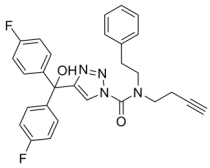	123	**2**	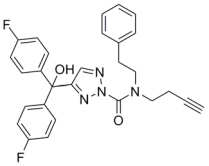	135
23	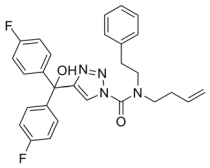	123	**3**	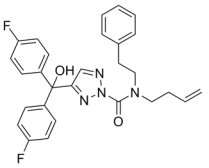	135
			4	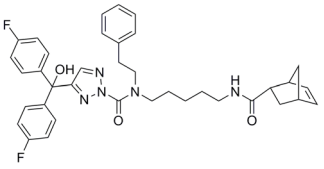	135

Biochemical analysis

The potency and selectivity of the probes **1** - **4** and their regioisomers (**21** - **23**) were initially screened in mouse membrane proteomes using competitive ABPP with MB064 (**Fig. 2**).

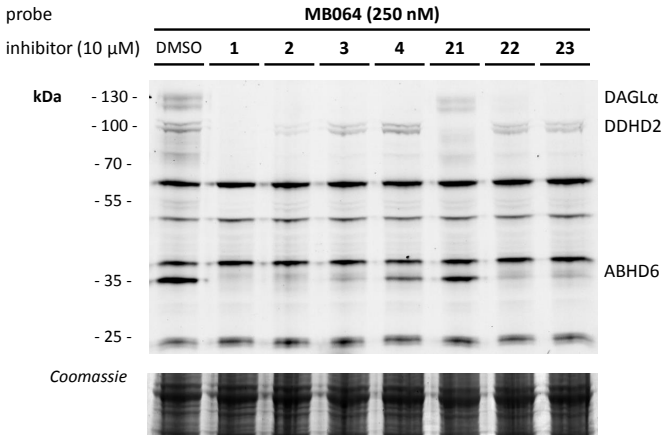

Figure 2. Activity-based protein profiling of probes **1** – **4** and their regioisomers (**21** - **23**) in mouse brain membrane proteome in competition with probe MB064.

Probe **1** (10 µM) inhibited DAGLα, DDHD domain-containing protein 2 (DDHD2) and ABHD6, as judged from the disappearing bands on the gel. Its regioisomer **21** was inactive against DAGLα and ABHD6, but did inhibit DDHD2. Probe **2** (and the regioisomer **22**) also inhibited DAGLα, DDHD2 and ABHD6. Probe **3** (and the regioisomer **23**) showed a similar labeling pattern as probe **2**, but were less active against DDHD2. The norbornene-substituted probe **4** was highly potent and selective for DAGLα in mouse brain, therefore this probe was further profiled in mouse brain proteome against ABPs MB064, FP-TAMRA and DH379 (**Fig. 3a**,**b**). Probe **4** showed a dose-dependent inhibition of DAGLα and DAGLβ with a pIC_{50} of 8.3 ± 0.3 and 8.6 ± 0.1, respectively. In addition, *in situ* experiments were performed with probe **4** (**Fig. 3c**) using the human cell line U2OS transiently transfected with recombinant human DAGLα. Live cells were treated with **4** and post-lysis labeled with MB064. Probe **4** was able to cross the cell membrane and label human DAGLα, albeit with a ten-fold lower potency compared to *in vitro* mouse brain proteome (**Fig. 3f**). Of note, probe **4** also inhibited the post-lysis labeling of endogenous ABHD6 with pIC_{50} of 8.5 ± 0.3. This discrepancy between *in situ* and *in vitro* potency has been previously observed for other covalent, irreversible serine hydrolase inhibitors.[7,16]

Finally, *in situ* two-step labeling was performed with fluorogenic BODIPY-tetrazine **24** (**Fig. 4**, see experimental for synthesis).[11] U2OS cells were transfected with either human DAGLα or catalytically

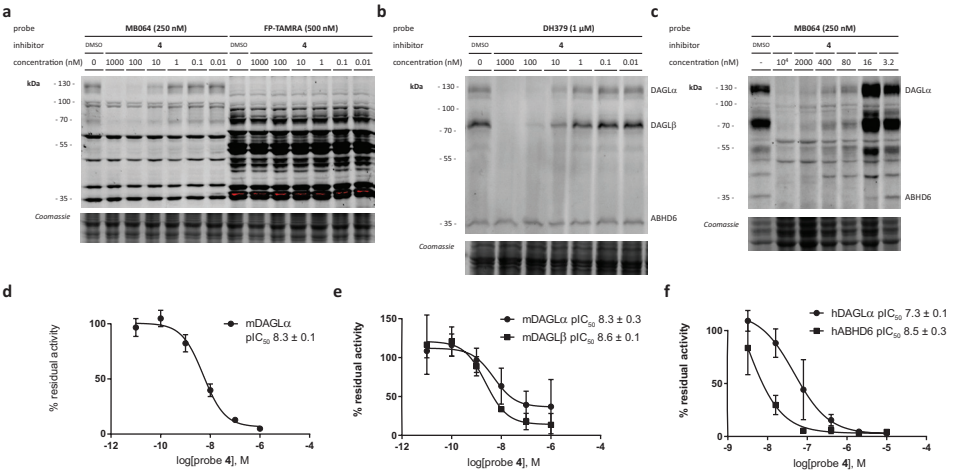

Figure 3. Activity-based protein profiling of probe **4** in mouse brain membrane proteome against (**a**) MB064 and FP-TAMRA and (**b**) DH379. (**c**) *In situ* treatment of U2OS cells transfected with DAGLα. (**d**) Quantification of residual DAGLα activity as measured with MB064 in mouse brain. (**e**) Quantification of residual DAGLα and DAGLβ activity as measured with DH379 in mouse brain. (**f**) Quantification of residual DAGLα and ABHD6 activity as measured with MB064 in U2OS-DAGLα cells.

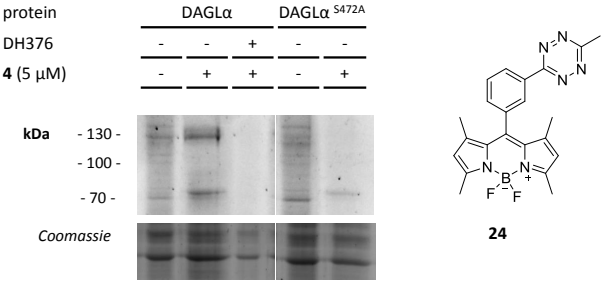

Figure 4. *In situ* two-step labeling of DAGLα overexpressed in U2OS cells with probe **4** and BODIPY-tetrazine **24** (10 µM).

inactive DAGLα^{S472A}. Cells were pre-treated with DH376 as a negative control. Treatment of cells expressing DAGLα or DAGLα^{S472A} with tetrazine **24** only showed some background labeling (**Fig. 4**), whereas treatment with norbornene probe **4**, followed by *in situ* treatment with tetrazine **24**, resulted in a strong fluorescent band just below 130 kDa, which was prevented by pre-treatment of cells with DH376 and absent in the DAGLα^{S472A} control. This experiment demonstrated that norbornene probe **4** reacted with the catalytic serine of DAGLα in live cells and can be labeled with a tetrazine fluorophore.

Conclusion

Norbornene probe **4** was successfully synthesized as a two-step ABP for visualization of DAGLα using an IEDDA ligation in living cells. The IEDDA reaction is complementary to the CuAAC reaction for labeling DAGLα, but is preferred for *in situ* imaging of enzyme activity. However, additional probes with improved activity and selectivity should be made to study endogenous DAGL activity. For live cell imaging, fluorogenic tetrazines with longer wavelengths than **24** are required.[17] It is envisioned that live cell imaging of DAGL activity will enable the study of this endocannabinoid enzyme's localization and processing during differentiation and other cellular processes.

Experimental

Synthesis

General methods. Reagents were purchased from Sigma Aldrich, Acros or Merck and used without further purification unless noted otherwise. Reactions under dry conditions were performed using oven or flame-dried glassware and dry solvents, which were dried for a minimum of 24 h over activated molecular sieves of appropriate pore size (3 - 4Å). Traces of water were removed from starting compounds by co-evaporation with toluene. All moisture sensitive reactions were performed under an argon or nitrogen atmosphere. Flash chromatography was performed using SiliCycle silica gel type SilicaFlash P60 (230 – 400 mesh). HPLC purification was performed on a preparative LC-MS system (Agilent 1200 series) with an Agilent 6130 Quadruple MS detector. TLC analysis was performed on Merck silica gel 60/Kieselguhr F254, 0.25 mm. Compounds were visualized using UV-irradiation and/or a $KMnO_4$ stain (K_2CO_3 (40 g), $KMnO_4$ (6 g), H_2O (600 mL) and 10% NaOH (5 mL)). ^{1}H- and ^{13}C-NMR spectra were recorded on a Bruker AV-400 MHz spectrometer at 400 (^{1}H) and 100 (^{13}C) MHz using $CDCl_3$, CD_3OD or $(CD_3)_2SO$ as solvent, unless stated otherwise. Spectra were analyzed using MestReNova 11.0.3. Chemical shift values are reported in ppm with tetramethylsilane or solvent resonance as the internal standard ($CDCl_3$, δ 7.26 for ^{1}H, δ 77.16 for ^{13}C; CD_3OD, δ 3.31 for ^{1}H, δ 49.00 for ^{13}C; $(CD_3)_2SO$, δ 2.50 for ^{1}H, δ 39.52 for ^{13}C). Data are reported as follows: chemical shifts (δ), multiplicity (s = singlet, d = doublet, dd = double doublet, td = triple doublet, t = triplet, q = quartet, m = multiplet, br = broad), coupling constants J (Hz), and integration. LC-MS analysis was performed on a Finnigan Surveyor HPLC system with a Gemmi C18 50x4.60 mm column (detection at 200-600 nm), coupled to a Finnigan LCQ Adantage Max mass spectrometer with ESI. The applied buffers were H_2O, MeCN and 1.0% TFA in H_2O (0.1% TFA end concentration). High resolution mass spectra (HRMS) were recorded by direct injection on a q-TOF mass spectrometer (Synapt G2-Si) equipped with an electrospray ion source in positive mode with leu-enkephalin H^+ (m/z = 556.2771) as an internal lock mass. The instrument was calibrated prior to measurement using the MS/MS spectrum of [glu^1]-fibrinopeptide B. Molecules shown are drawn using ChemDraw v16.0.

4-(4-(Trifluoromethoxy)phenyl)-2*H*-1,2,3-triazole (6).
To a solution of 4-trifluoromethoxyphenylacetylene (**5**, 0.61 mL, 4.0 mmol) in a mixture of DMF (27 mL) and MeOH (5.3 mL) were added CuI (75 mg, 0.4 mmol) and azidotrimethylsilane (0.8 mL, 6 mmol). The reaction mixture was stirred at 100 °C o/n, quenched with brine (20 mL), extracted with DCM (3 x 50 mL), dried ($MgSO_4$), filtered and concentrated. Purification of the residue by silica gel

column chromatography (1:4 EtOAc:pentane) yielded the title compound (0.25 g, 1.1 mmol, 27%). ^{1}H NMR (400 MHz, MeOD) δ 8.25 – 8.11 (br s, 1H), 7.93 (d, J = 8.8 Hz, 2H), 7.34 (d, J = 7.9 Hz, 2H).^{13}C NMR (100 MHz, MeOD) δ 150.30, 130.44, 128.56, 123.18, 122.56, 120.64. LC-MS m/z: 230.1 $[M+H]^+$.

Methyl 1*H*-1,2,3-triazole-5-carboxylate (7). This protocol is based on literature procedure.[18] A mixture of azidotrimethylsilane (2.6 mL, 20 mmol) and methyl propiolate (1.8 mL, 20 mmol) was heated for 4 h at 90 °C, concentrated and coevaporated with MeOH to yield the title compound (1.74 g, 14 mmol, 68%). ^{1}H NMR (400 MHz, CD_3OD) δ 8.36 (s, 1H), 3.92 (s, 3H). ^{13}C NMR (100 MHz, CD_3OD) δ 162.61, 139.63, 131.92, 52.53.

***bis*(4-Fluorophenyl)(2*H*-1,2,3-triazol-4-yl)methanol (8)**. To a cooled (0 °C) solution of **7** (0.69 g, 5.4 mmol) in THF (70 mL) was added 4-fluorophenylmagnesium bromide (2.0 M in THF, 9.5 mL, 19 mmol). The reaction mixture was stirred for 2 h at rt, quenched with NH_4Cl (sat. aq.) and extracted with DCM. The combined organic layers were washed with brine, dried ($MgSO_4$), filtered and concentrated. Purification of the residue by silica gel column chromatography (20 > 40% EtOAc in pentane) yielded the title compound (1.2 g, 4.0 mmol, 74%). ^{1}H NMR (300 MHz, CD_3OD) δ 7.58 (s, 1H), 7.40 – 7.29 (m, 4H), 7.09 – 6.97 (m, 4H). ^{13}C NMR (75 MHz, CD_3OD) δ 174.84, 165.07, 130.38, 130.27, 115.64, 115.35, 103.14, 103.12, 100.62.

***N*-(But-3-yn-1-yl)-2-nitro-*N*-phenethylbenzenesulfonamide (10)**. This protocol is based on literature procedure.[6] To a solution of 1-amino-3-butyne (**9**, 0.52 g, 7.5 mmol) in DCM (30 mL) were added *O*-nitrophenylsulfonyl chloride (1.7 g, 7.5 mmol) and Et_3N (1.6 mL, 11 mmol). The reaction mixture was stirred for 4 h, poured into H_2O and extracted with EtOAc. The combined organic layers were washed with H_2O, brine, dried (Na_2SO_4), filtered and concentrated. The residue was dissolved in CH_3CN (60 mL) and Cs_2CO_3 (7.3 g, 23 mmol) and phenethyl bromide (3.0 mL, 22 mmol) were added. The reaction mixture was stirred at 80 °C for 2 h, poured into H_2O and extracted with EtOAc. The combined organic layers were washed with H_2O, brine, dried (Na_2SO_4), filtered and concentrated. Purification of the residue by silica gel column chromatography (0 > 25% EtOAc in pentane) yielded the title compound (2.5 g, 7.0 mmol, 93%). ^{1}H NMR (400 MHz, $CDCl_3$) δ 7.95 (dd, J = 7.6, 1.7 Hz, 1H), 7.71 – 7.57 (m, 3H), 7.27 – 7.14 (m, 5H), 3.64 – 3.50 (m, 4H), 2.93 – 2.83 (m, 2H), 2.46 (td, J = 7.2, 2.7 Hz, 2H), 2.00 (t, J = 2.7 Hz, 1H). ^{13}C NMR (100 MHz, $CDCl_3$) δ 147.99, 137.81, 133.73, 133.25, 131.88, 130.62, 128.79, 128.66, 126.75, 124.29, 80.66, 70.74, 49.58, 46.46, 35.07, 19.09.

***N*-(But-3-en-1-yl)-2-nitro-*N*-phenethylbenzenesulfonamide (13)**. To a solution of 3-butenylamine hydrochloride (**12**, 0.23 g, 2.1 mmol) in THF (8.4 mL) were added *O*-nitrophenylsulfonyl chloride (0.46 g, 2.1 mmol) and DIPEA (0.5 mL, 3 mmol). The reaction mixture was stirred o/n, poured into H_2O and extracted with EtOAc. The combined organic layers were washed with H_2O, brine, dried ($MgSO_4$), filtered and concentrated. The residue was dissolved in CH_3CN (17 mL) and Cs_2CO_3 (2.1 g, 6.3 mmol) and phenethyl bromide (1.4 mL, 11 mmol) were added. The reaction mixture was stirred at 80 °C for 2 h, poured into H_2O and extracted with EtOAc. The combined organic layers were washed with H_2O, brine, dried ($MgSO_4$), filtered and concentrated. Purification of the residue by silica gel column chromatography (5 > 30% EtOAc in pentane) yielded the title compound (0.53 g, 1.5 mmol, 70%). ^{1}H NMR (400 MHz, $CDCl_3$) δ 7.96 (dd, J = 7.5, 1.8 Hz, 1H), 7.71 – 7.57 (m, 3H), 7.30 – 7.14 (m, 5H), 5.70 (ddt, J = 17.1, 10.2, 6.8 Hz, 1H), 5.12 – 4.99 (m, 2H), 3.58 – 3.50 (m, 2H), 3.46 – 3.38 (m, 2H), 2.90 – 2.82 (m, 2H), 2.32 (q, J = 7.2 Hz, 2H). ^{13}C NMR (100 MHz, $CDCl_3$) δ 138.08, 134.26, 133.72, 133.54, 131.74, 130.79, 128.86, 128.73, 126.79, 124.28, 117.62, 49.01, 47.17, 35.15, 32.80.

***N*-Phenethylbut-3-yn-1-amine (11)**. To a solution of **10** (2.5 g, 7.0 mmol) in CH_3CN (70 mL) were added Cs_2CO_3 (6.8 g, 21 mmol) and benzenethiol (1.2 mL, 12 mmol). The reaction mixture was stirred o/n, quenched with $NaHCO_3$ (sat. aq., 200 mL) and extracted with DCM (2 x 150 mL). The combined organic layers were dried (Na_2SO_4), filtered and concentrated. Purification of the residue by silica gel column chromatography (neutralized column with Et_3N, 0 > 10% MeOH in DCM) yielded the title compound (0.90 g, 5.2 mmol, 74%). ^{1}H NMR (400 MHz, $CDCl_3$) δ 7.32 – 7.25 (m, 2H), 7.21 (m, 3H), 2.89 (dd, J = 8.4, 6.5 Hz, 2H), 2.80 (m, 4H), 2.36 (td, J = 6.7, 2.6 Hz, 2H), 1.95 (t, J = 2.6 Hz, 1H), 1.47 (s, 1H). ^{13}C NMR (100 MHz, $CDCl_3$) δ 139.93, 128.75, 128.50, 126.21, 82.41, 69.56, 50.68, 47.87, 36.42, 19.58.

***N*-Phenethylbut-3-en-1-amine (14)**. To a solution of **13** (0.54 g, 1.5 mmol) in CH_3CN (15 mL) were added Cs_2CO_3 (1.5 g, 4.5 mmol) and benzenethiol (0.23 mL, 2.3 mmol). The reaction mixture was stirred o/n, quenched with $NaHCO_3$ (sat. aq.) and extracted with DCM. The combined organic layers were dried ($MgSO_4$), filtered and concentrated. Purification of the residue by silica gel column chromatography (1 > 20% MeOH in DCM) yielded the title compound (0.21 g, 1.2 mmol, 81%). ^{1}H NMR (300 MHz, CD_3OD) δ 7.34 – 7.12 (m, 5H), 5.75 (ddt, J = 17.1, 10.2, 6.8 Hz, 1H), 5.12 – 4.83 (m, 3H), 2.81 (m, 4H), 2.65 (t, J = 7.2 Hz, 2H), 2.24 (q, J = 7.1 Hz, 2H). ^{13}C NMR (75 MHz, CD_3OD) δ 140.73, 136.92, 129.65, 129.55, 127.31, 117.04, 51.81, 49.36, 36.48, 34.50.

***tert*-Butyl (5-((2-nitro-*N*-phenethylphenyl)sulfonamido)pentyl)carbamate (16)**. To a solution of N-Boc-cadaverine (15, 0.70 g, 3.5 mmol) in THF (14 mL) were added 2-nitrobenzenesulfonyl chloride (0.77 g, 3.5 mmol) and Et_3N (0.73 mL, 5.2 mmol). The reaction mixture was stirred for 1.5 h, poured into H_2O (60 mL) and extracted with EtOAc (3x 30 mL). The combined organic layers were washed with H_2O, brine, dried ($MgSO_4$), filtered and concentrated. The residue was dissolved in CH_3CN (28 mL) and Cs_2CO_3 (3.4 g, 10 mmol) and phenethyl bromide (2.2 mL, 16 mmol) were added. The reaction mixture was stirred at 80 °C o/n, poured into H_2O (70 mL) and extracted with EtOAc (3 x 35 mL). The combined organic layers were washed with H_2O, brine, dried ($MgSO_4$), filtered and concentrated. Purification of the residue by silica gel column chromatography (20 > 30% EtOAc in pentane) yielded the title compound (1.6 g, 3.2 mmol, 92%). ^{1}H NMR (400 MHz, $CDCl_3$) δ 7.95 (dd, J = 7.4, 1.9 Hz, 1H), 7.71 – 7.57 (m, 3H), 7.29 – 7.23 (m, 2H), 7.22 – 7.13 (m, 3H), 4.53 (br s, 1H), 3.54 – 3.45 (t, J = 8.0 Hz, 2H), 3.33 (t, J = 7.6 Hz, 2H), 3.07 (d, J = 6.4 Hz, 2H), 2.93 – 2.79 (t, J = 8.0 Hz, 2H), 1.57 (p, J = 7.6 Hz, 2H), 1.44 (m, 11H), 1.33 – 1.20 (m, 2H). ^{13}C NMR (100 MHz, $CDCl_3$) δ 156.08, 148.12, 138.13, 133.69, 133.50, 131.72, 130.75, 128.87, 126.77, 124.26, 79.07, 48.90, 47.71, 40.39, 35.22, 29.72, 27.85, 23.78. LC-MS m/z: 391.9 (M-Boc), 513.9 $[M+Na]^+$.

***N*-(5-Aminopentyl)-2-nitro-*N*-phenethylbenzenesulfonamide (17)**. To a solution of **16** (0.72 g, 1.5 mmol) in DCM (13.5 mL) was added TFA (1.4 mL). The reaction mixture was stirred for 1 h, concentrated and co-evaporated with toluene (3 x) to yield the title compound as TFA adduct (0.74 mg, 1.5 mmol, 100%). ^{1}H NMR (400 MHz, $CDCl_3$) δ 7.84 (dd, J = 7.4, 1.8 Hz, 1H), 7.69 – 7.54 (m, 3H), 7.29 – 7.07 (m, 5H), 6.4 (br s, 2H), 3.46 (t, J = 7.9 Hz, 2H), 3.32 (t, J = 7.2 Hz, 2H), 2.97 (s, 2H), 2.79 (t, J = 7.9 Hz, 2H), 1.66 (t, J = 7.7 Hz, 2H), 1.57 (q, J = 7.4 Hz, 2H), 1.34 (q, J = 7.8 Hz, 2H). ^{13}C NMR (100 MHz, $CDCl_3$) δ 148.06, 137.93, 133.81, 133.19, 132.07, 130.29, 128.85, 128.74, 126.84, 124.37, 49.14, 47.56, 40.11, 35.07, 27.49, 26.75, 23.01. LC-MS m/z: 391.9 $[M+H]^+$, 782.8 $[2M + H]^+$.

2,5-Dioxopyrrolidin-1-yl (1*S*,4*S*)-bicyclo[2.2.1]hept-5-ene-2-carboxylate (18). To a solution of 5-norbornene-2-carboxylic acid (Sigma Aldrich, mixture of endo and exo, predominantly endo, 0.60 mL, 4.9 mmol) in DCE (50 mL) were added EDC (3.8 g, 20 mmol) and N-hydroxysuccinimide (2.3 g, 20

mmol). The reaction mixture was stirred o/n, washed with 1 M HCl (3 x 40 mL), dried ($MgSO_4$), filtered and concentrated. Purification of the residue by silica gel column chromatography (30% EtOAc in pentane) yielded the title compound as a 1 : 0.3 mixture of endo and exo isomers (1.1 g, 4.5 mmol, 92%). TLC: R_f = 0.45 (1:2 EtOAc:pentane). NMR assignment for major isomer: ^{1}H NMR (400 MHz, $CDCl_3$) δ 6.24 (dd, J = 5.7, 3.1 Hz, 1H), 6.12 (dd, J = 5.7, 2.9 Hz, 1H), 3.40 (m, 1H), 3.25 (dt, J = 9.0, 3.8 Hz, 1H), 2.99 (d, J = 1.6 Hz, 1H), 2.80 (s, 4H), 2.04 – 1.98 (m, 1H), 1.53 – 1.48 (m, 2H), 1.39 – 1.32 (m, 1H). ^{13}C NMR (100 MHz, $CDCl_3$) δ 169.99, 138.15, 132.17, 49.66, 46.46, 42.53, 40.61, 29.57, 25.61.

(1*S*,2*S*,4*S*)-*N*-(5-((2-Nitro-*N*-phenethylphenyl)sulfonamido)pentyl)bicyclo[2.2.1]hept-5-ene-2-carboxamide (19). To a solution of **18** (0.34 g, 1.5 mmol) in DMF (10 mL) were added **17** (0.74 g, 1.5 mmol) and DIPEA (0.76 mL, 4.4 mmol). The reaction mixture was stirred for 2 h, poured into a 1:1 mixture of 1 M HCl and brine (100 mL) and extracted with Et_2O (2 x 50 mL). The combined organic layers were washed with brine (3 x 50 mL), dried ($MgSO_4$), filtered and concentrated. Purification of the residue by silica gel column chromatography (1:1 pentane:EtOAc) yielded two stereoisomers: endo and exo. Title compound **19** (endo isomer): 0.23 g, 0.46 mmol, 33%. ^{1}H NMR (400 MHz, $CDCl_3$) δ 7.94 (dd, J = 7.5, 1.4 Hz, 1H), 7.72 – 7.56 (m, 3H), 7.31 – 7.10 (m, 5H), 6.23 (dd, J = 5.7, 3.1 Hz, 1H), 5.96 (dd, J = 5.8, 2.8 Hz, 1H), 5.51 (s, 1H), 3.55 – 3.45 (m, 2H), 3.34 (t, J = 7.4 Hz, 2H), 3.16 (dt, J = 13.2, 6.6 Hz, 3H), 2.94 – 2.79 (m, 4H), 1.98 – 1.86 (m, 1H), 1.58 (p, J = 7.5 Hz, 2H), 1.52 – 1.41 (m, 3H), 1.35 – 1.26 (m, 4H). ^{13}C NMR (100 MHz, $CDCl_3$) δ 174.57, 148.13, 138.08, 137.87, 133.63, 133.54, 132.39, 131.76, 130.69, 128.84, 128.72, 126.79, 124.29, 50.14, 48.92, 47.62, 46.31, 44.91, 42.84, 39.27, 35.18, 30.05, 29.10, 27.70, 23.71.
Exo isomer: 0.14 g, 0.26 mmol, 18%. ^{1}H NMR (400 MHz, $CDCl_3$) δ 7.98 – 7.91 (m, 1H), 7.72 – 7.56 (m, 3H), 7.29 – 7.14 (m, 5H), 6.18 – 6.05 (m, 2H), 5.61 (s, 1H), 3.55 – 3.44 (m, 2H), 3.40 – 3.32 (m, 2H), 3.28 – 3.19 (m, 2H), 2.91 (dd, J = 3.0, 1.4 Hz, 2H), 2.88 – 2.80 (m, 2H), 2.01 – 1.85 (m, 4H), 1.71 (d, J = 8.3 Hz, 1H), 1.60 (t, J = 7.4 Hz, 2H), 1.55 – 1.48 (m, 2H), 1.33 (dd, J = 5.9, 2.9 Hz, 2H). ^{13}C NMR (100 MHz, $CDCl_3$) δ 175.87, 138.29, 138.09, 136.20, 133.66, 133.54, 131.77, 130.76, 128.86, 128.74, 126.81, 124.31, 48.90, 47.59, 47.37, 46.46, 44.83, 41.71, 39.41, 35.17, 30.64, 29.83, 27.69, 23.69.

(1*S*,2*S*,4*S*)-*N*-(5-(Phenethylamino)pentyl)bicyclo[2.2.1]hept-5-ene-2-carboxamide (20). To a solution of **19** (0.23 g, 0.46 mmol) in CH_3CN (6 mL) were added Cs_2CO_3 (0.45 g, 1.4 mmol) and thiophenol (70 µL, 0.70 mmol). The reaction mixture was stirred o/n, quenched with $NaHCO_3$ (sat. aq., 10 mL) and extracted with DCM (3 x 30 mL). The combined organic layers were dried ($MgSO_4$), filtered and concentrated. Purification of the residue by silica gel column chromatography (silica neutralized with Et_3N, 1:19 MeOH:DCM) yielded the title compound (62 mg, 0.19 mmol, 41%). ^{1}H NMR (400 MHz, $CDCl_3$) δ 7.32 – 7.27 (m, 2H), 7.26 – 7.18 (m, 3H), 6.21 (dd, J = 5.7, 3.1 Hz, 1H), 5.94 (dd, J = 5.7, 2.8 Hz, 1H), 5.90 (t, J = 6.3 Hz, 1H), 4.30 (s, 2H), 3.24 – 3.11 (m, 3H), 3.05 (m, 2H), 2.96 – 2.76 (m, 4H), 1.91 (ddd, J = 11.7, 9.3, 3.7 Hz, 1H), 1.72 (p, J = 7.5 Hz, 2H), 1.55 – 1.23 (m, 8H). ^{13}C NMR (100 MHz, $CDCl_3$) δ 174.24, 139.99, 137.75, 132.33, 128.75, 128.53, 126.23, 51.21, 50.09, 49.68, 46.29, 44.87, 42.79, 39.36, 36.30, 29.98, 29.67, 29.61, 24.68.

***N*-(But-3-yn-1-yl)-*N*-phenethyl-4-(4-(trifluoromethoxy)phenyl)-1*H*-1,2,3-triazole-1-carboxamide (1) and *N*-(but-3-yn-1-yl)-*N*-phenethyl-4-(4-(trifluoromethoxy)phenyl)-2*H*-1,2,3-triazole-2-carboxamide (21)**. To a cooled (0 °C) solution of **11** (85 mg, 0.49 mmol) in THF (5 mL) were added DIPEA (0.26 mL, 1.5 mmol) and triphosgene (77 mg, 0.26 mmol). The reaction mixture was stirred at 0 °C for 1 h, quenched with H_2O and extracted with EtOAc. The combined organic layers were washed with brine, dried ($MgSO_4$), filtered and concentrated. The residue was dissolved in THF (5 mL) and DIPEA (0.26 mL, 1.5 mmol), DMAP (61 mg, 0.5 mmol) and **6** (0.12 g, 0.5 mmol) were added. The

reaction mixture was stirred for 4 h at 60 °C, quenched with NH_4Cl (sat. aq.) and extracted with EtOAc. The combined organic layers were washed with brine (2x), dried (Na_2SO_4), filtered and concentrated. Purification of the residue by silica gel column chromatography (5 > 10% EtOAc in pentane) yielded the title compounds. LC-MS m/z: 428.9 $[M+H]^+$. **1** (apolar): 79 mg, 0.18 mmol, 37%. ^1H NMR (400 MHz, $(CD_3)_2SO$, 90 °C) δ 8.85 (s, 1H), 8.10 – 8.02 (m, 2H), 7.49 – 7.39 (m, 2H), 7.35 – 7.15 (m, 5H), 3.85 (dd, J = 8.6, 6.6 Hz, 2H), 3.70 (t, J = 7.0 Hz, 2H), 3.00 (t, J = 7.6 Hz, 2H), 2.75 (d, J = 2.2 Hz, 1H), 2.65 – 2.56 (m, 2H). ^{13}C NMR (150 MHz, $(CD_3)_2SO$, 20 °C) δ 148.89, 148.25, 144.66, 144.54, 138.51, 138.09, 128.92, 128.89, 128.74, 128.50, 127.48, 126.46, 126.40, 123.00, 122.65, 122.56, 121.68, 120.95, 119.25, 117.55, 81.43, 81.23, 73.30, 72.95, 51.19, 50.00, 48.15, 47.11, 34.24, 32.61, 18.19, 16.51. HRMS *m/z* calculated for $C_{22}H_{19}F_3N_4O_2$ $[M+Na]^+$: 451. 1352, found: 451.1360. **21** (polar): 84 mg, 0.20 mmol, 41%. ^1H NMR (400 MHz, $(CD_3)_2SO$, 90 °C) δ 8.57 (s, 1H), 8.11 – 8.01 (m, 2H), 7.53 – 7.43 (m, 2H), 7.38 – 7.12 (m, 5H), 3.77 (dd, J = 8.9, 6.5 Hz, 2H), 3.63 (t, J = 7.1 Hz, 2H), 2.99 (t, J = 7.7 Hz, 2H), 2.73 (s, 1H), 2.59 (td, J = 7.0, 2.7 Hz, 2H). ^{13}C NMR (150 MHz, $(CD_3)_2SO$, 20 °C) δ 149.37, 149.35, 148.94, 147.14, 138.53, 138.04, 134.06, 133.99, 128.85, 128.59, 128.42, 128.26, 128.09, 126.39, 122.58, 121.72, 120.88, 119.18, 117.48, 81.42, 81.09, 73.05, 72.83, 51.08, 50.09, 48.15, 47.21, 34.32, 32.56, 18.22, 16.44. HRMS *m/z* calculated for $C_{22}H_{19}F_3N_4O_2$ $[M+Na]^+$: 451.1352, found: 451.1355.

4-(bis(4-Fluorophenyl)(hydroxy)methyl)-*N*-(but-3-yn-1-yl)-*N*-phenethyl-1*H*-1,2,3-triazole-1-carboxamide (22) and 4-(bis(4-fluorophenyl)(hydroxy)methyl)-*N*-(but-3-yn-1-yl)-*N*-phenethyl-2H-1,2,3-triazole-2-carboxamide (2). To a cooled (0 °C) solution of **11** (78 mg, 0.45 mmol) in THF (5 mL) were added DIPEA (0.26 mL, 1.5 mmol) and triphosgene (77 mg, 0.26 mmol). The reaction mixture was stirred at 0 °C for 1.5 h, quenched with H_2O and extracted with EtOAc. The combined organic layers were washed with brine, dried ($MgSO_4$), filtered and concentrated. The residue was dissolved in THF (5 mL) and DIPEA (0.26 mL, 1.5 mmol), DMAP (61 mg, 0.5 mmol) and **8** (0.13 g, 0.45 mmol) were added. The reaction mixture was stirred for 4 h at 60 °C, quenched with NH_4Cl (sat. aq.) and extracted with EtOAc. The combined organic layers were washed with brine (2x), dried (Na_2SO_4), filtered and concentrated. Purification of the residue by silica gel column chromatography (12 > 20% EtOAc in pentane) yielded the title compounds. LC-MS *m/z*: 487.0 $[M+H]^+$. **22** (apolar): 72 mg, 0.15 mmol, 33%. ^1H NMR (400 MHz, $(CD_3)_2SO$, 90 °C) δ 8.01 (s, 1H), 7.48 – 7.36 (m, 4H), 7.31 – 7.07 (m, 8H), 6.59 (d, J = 2.2 Hz, 1H), 3.79 (dd, J = 8.7, 6.6 Hz, 2H), 3.67 (t, J = 7.0 Hz, 2H), 2.95 (t, J = 7.6 Hz, 2H), 2.72 (s, 1H), 2.58 (td, J = 7.0, 2.7 Hz, 2H). ^{13}C NMR (100 MHz, $(CD_3)_2SO$, 90 °C) δ 162.08, 159.66, 152.82, 148.60, 142.09, 137.78, 128.63, 128.54, 128.20, 127.92, 125.91, 123.23, 113.99, 113.77, 80.84, 74.67, 72.04, 50.17, 47.24, 33, 17. HRMS *m/z* calculated for $C_{28}H_{24}F_2N_4O_2$ $[M+Na]^+$: 509.1760, found: 509.1760. **2** (polar): 88 mg, 0.18 mmol, 40%. ^1H NMR (400 MHz, $(CD_3)_2SO$, 90 °C) δ 7.97 (s, 1H), 7.43 – 7.34 (m, 4H), 7.30 – 7.06 (m, 8H), 6.77 (s, 1H), 3.69 (dd, J = 8.8, 6.7 Hz, 2H), 3.53 (t, J = 7.2 Hz, 2H), 2.89 (d, J = 7.9 Hz, 2H), 2.69 (d, J = 1.8 Hz, 1H), 2.46 (s, 2H). ^{13}C NMR (100 MHz, $(CD_3)_2SO$, 90 °C) δ 162.13, 159.71, 155.41, 149.02, 141.64, 137.83, 134.78, 128.53, 128.45, 128.13, 127.87, 125.84, 114.09, 113.87, 80.79, 74.98, 71.92, 65.99, 50.10, 47.48. HRMS *m/z* calculated for $C_{28}H_{24}F_2N_4O_2$ $[M+Na]^+$: 509.1760, found: 509.1766.

4-(*bis*(4-Fluorophenyl)(hydroxy)methyl)-*N*-(but-3-en-1-yl)-*N*-phenethyl-1*H*-1,2,3-triazole-1-carboxamide (23) and 4-(*bis*(4-fluorophenyl)(hydroxy)methyl)-*N*-(but-3-en-1-yl)-*N*-phenethyl-2*H*-1,2,3-triazole-2-carboxamide (3). To a cooled (0 °C) solution of **14** (0.11 g, 0.62 mmol) in THF (6.2 mL) were added DIPEA (0.3 mL, 1.7 mmol) and triphosgene (96 mg, 0.32 mmol). The reaction mixture was stirred at 0 °C for 1 h, quenched with H_2O and extracted with EtOAc. The combined organic layers were washed with brine, dried ($MgSO_4$), filtered and concentrated. The residue was dissolved in THF (6.2 mL) and DIPEA (0.3 mL, 1.7 mmol), DMAP (76 mg, 0.62 mmol) and **8** (0.18 g, 0.62 mmol) were

added. The reaction mixture was stirred o/n at 60 °C, quenched with NH_4Cl (sat. aq.) and extracted with EtOAc. The combined organic layers were washed with brine (2x), dried (Na_2SO_4), filtered and concentrated. Purification of the residue by silica gel column chromatography (10 > 25% EtOAc in pentane) yielded the title compounds. **23** (apolar): 89 mg, 0.18 mmol, 29%. NMR assignment major rotamer: ^{1}H NMR (400 MHz, $(CD_3)_2SO$) δ 7.8 (s, 1H), 7.49 – 6.83 (m, 13H), 5.94 – 5.52 (m, 1H), 5.25 – 4.91 (m, 2H), 3.81 – 3.45 (m, 4H), 3.07 – 2.79 (m, 2H), 2.38 (dd, J = 50.6, 8.3 Hz, 2H). ^{13}C NMR (100 MHz, $(CD_3)_2SO$) δ 162.89, 160.47, 153.62, 149.41, 142.99, 138.98, 138.45, 135.55, 135.15, 129.53, 129.45, 129.16, 128.88, 126.88, 124.26, 123.84, 117.75, 117.63, 115.05, 114.84, 75.36, 51.23, 50.45, 49.25, 47.86, 34.71, 33.06, 31.59, 21.20. HRMS *m/z* calculated for $C_{28}H_{26}F_2N_4O_2$ $[M+H]^+$: 489.2097, found: 489.2098. **3** (polar): 32 mg, 65 µmol, 11%. ^{1}H NMR (400 MHz, $(CD_3)_2SO$) δ 8.03 (s, 1H), 7.40 – 6.87 (m, 13H), 5.62 (m, 1H), 5.25 – 4.76 (m, 2H), 3.68 – 3.48 (m, 3H), 3.30 (s, 1H), 2.84 (d, J = 78.8 Hz, 2H), 2.26 (dd, J = 109.5, 7.4 Hz, 2H). ^{13}C NMR (100 MHz, $(CD_3)_2SO$) δ 162.91, 160.48, 156.10, 149.90, 142.60, 138.98, 138.38, 135.60, 135.04, 129.42, 129.34, 128.98, 128.82, 126.82, 117.59, 117.45, 115.14, 114.93, 75.68, 50.93, 50.42, 49.08, 48.16, 34.65, 33.09, 32.73, 31.52, 29.47. HRMS *m/z* calculated for $C_{28}H_{26}F_2N_4O_2$ $[M+Na]^+$: 511.1916, found: 511.1924.

***N*-(5-((1*S*,2*S*,4*S*)-bicyclo[2.2.1]hept-5-ene-2-carboxamido)pentyl)-4-(bis(4-fluorophenyl)(hydroxy)methyl)-*N*-phenethyl-2*H*-1,2,3-triazole-2-carboxamide (4)**. To a cooled (0 °C) solution of **20** (36 mg, 0.11 mmol) in THF (1 mL) were added DIPEA (58 µL, 0.33 mmol) and triphosgene (15 mg, 0.05 mmol). The reaction mixture was stirred for 1.5 h, quenched with H_2O (10 mL) and extracted with EtOAc (2 x 10 mL). The combined organic layers were washed with brine (2 x 10 mL), dried (Na_2SO_4), filtered and concentrated. The residue was dissolved in THF (2 mL) and DIPEA (58 µL, 0.33 mmol), DMAP (15 mg, 0.11 mmol) and **8** (33 mg, 0.11 mmol) were added. The reaction mixture was stirred for 3.5 h at 60 °C, quenched with NH_4Cl (sat. aq., 10 mL) and extracted with EtOAc (2 x 10 mL). The combined organic layers were washed with H_2O (10 mL), brine (10 mL), dried (Na_2SO_4), filtered and concentrated. Purification of the residue by silica gel column chromatography (3:2 PE:EtOAc) yielded the title compound as the lower TLC spot (26 mg, 0.04 mmol, 37%). ^{1}H NMR (400 MHz, $(CD_3)_2SO$, 80 °C) δ 7.95 (s, 1H), 7.37 (m, 4H), 7.29 – 7.07 (m, 9H), 6.07 (dd, J = 5.7, 3.0 Hz, 1H), 5.81 (dd, J = 6.0, 2.7 Hz, 1H), 3.70 (t, J = 7.6 Hz, 1H), 3.59 (s, 1H), 3.45 (s, 1H), 3.30 (s, 1H), 3.07 – 2.71 (m, 6H), 1.73 (ddd, J = 12.6, 9.4, 3.8 Hz, 1H), 1.66 – 1.15 (m, 13H). ^{13}C NMR (100 MHz, $(CD_3)_2SO$, 80 °C) δ 162.19, 159.76, 155.28, 149.18, 148.63, 142.22, 141.79, 136.26, 134.59, 131.87, 128.71, 128.61, 128.53, 128.30, 128.22, 128.02, 127.96, 126.02, 125.95, 114.21, 114.11, 113.99, 113.90, 49.01, 45.26, 43.19, 41.79, 38.02, 28.55, 28.50, 28.47, 28.29, 23.21. HRMS *m/z* calculated for $C_{37}H_{39}F_2N_5O_3$ $[M+Na]^+$: 662.2913, found: 662.2923.

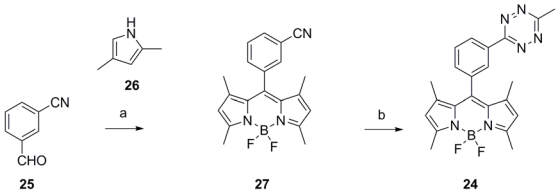

Scheme 4. Synthesis of BODIPY-tetrazine. Reagents and conditions: (**a**) *i*. TFA (catalytic), DCM; *ii*. DDQ; *iii*. DIPEA, $BF_3{\cdot}OEt_2$; 42%; (b) *i*. $Zn(OTf)_2$, CH_3CN, NH_2NH_2, 60 °C; *ii*. $NaNO_2$; 0.3%.

3-(5,5-Difluoro-1,3,7,9-tetramethyl-5*H*-4λ4,5λ4-dipyrrolo[1,2-c:2',1'-f][1,3,2]diazaborinin-10-yl) benzonitrile (27). This protocol is based on literature procedure.[11] To a solution of 3-formylbenzonitrile (**25**, 0.81 g, 6.1 mmol) and 2,4-dimethylpyrrole (**26**, 1.4 mL, 13 mmol) in DCM (160 mL) were added four drops of TFA. After stirring at rt for 30 min, a solution of DDQ (1.4 g, 6.1 mmol) in DCM (160 mL) was added, followed by DIPEA (12.5 mL, 73 mmol) and $BF_3{\cdot}OEt_2$ (12.5 mL, 100 mmol). The reaction was stirred o/n, diluted with water and extracted with DCM. The combined organic layers were dried ($MgSO_4$), filtered and concentrated. The residue was purified by column chromatography (75 > 100% toluene in pentane) to yield the title compound (0.89 g, 2.6 mmol, 42%). ^{1}H NMR (400 MHz, $CDCl_3$) δ 7.89 – 7.51 (m, 4H), 6.01 (s, 2H), 2.56 (s, 6H), 1.36 (s, 6H). ^{13}C NMR (100 MHz, $CDCl_3$) δ 156.70, 142.63, 138.09, 136.65, 132.92, 132.83, 131.91, 131.13, 130.27, 121.94, 117.99, 113.65, 14.82, 14.77.

5,5-Difluoro-1,3,7,9-tetramethyl-10-(3-(6-methyl-1,2,4,5-tetrazin-3-yl)phenyl)-5H-4λ4,5λ4-dipyrrolo[1,2-c:2',1'-f][1,3,2]diazaborinine (24). Adapted from literature procedure, omitted DMF as a co-solvent.[11] To a suspension of **27** (175 mg, 0.5 mmol) and $Zn(OTf)_2$ (91 mg, 0.25 mmol) in CH_3CN (0.26 mL) in a sealed microwave tube under argon was added hydrazine (0.8 mL, 25 mmol). The reaction mixture was stirred at 60 °C o/n and allowed to cool down to rt before addition of $NaNO_2$ (0.7 g in 5 mL H_2O). The mixture was acidified with 1 M HCl and extracted with DCM. The combined organic layers were dried ($MgSO_4$), filtered and concentrated. The residue was purified with column chromatography (0 > 0.5% CH_3CN in toluene, followed by 4:1 pentane:EtOAc) 0.3% isolated yield after preparative HPLC. NMR data agrees with literature values.[11] 1H NMR (500 MHz, $(CD_3)_2SO$) δ 8.70 – 8.57 (m, 1H), 8.41 – 8.32 (m, 1H), 7.88 (t, J = 7.8 Hz, 1H), 7.75 (dt, J = 7.7, 1.4 Hz, 1H), 6.22 (s, 2H), 3.01 (s, 3H), 2.48 (s, 6H), 1.41 (s, 6H). HRMS *m/z* calculated for $C_{22}H_{21}BF_2N_6$ $[M+H]^+$: 419.1962, found: 419.1962.

Computational methods

The triazole urea structures were initially optimized by a conformer distribution search included in the Spartan 10 program.[19] The conformer distribution was calculated in the gas phase at the DFT level of theory using B3LYP as hybrid functional and 6-31G(d) as basis set. The resulting structure library was further refined using the Gaussian 09 program revision A.02,[20] with the use of the ωB97XD long-range corrected hybrid functional and 6-311+G(d,p) as basis set. Optimization was done in gas-phase and subsequently corrections for solvent effects were done by use of a polarizable continuum model (PCM), using DMSO as solvent parameter. Gas-phase free energies were computed using the quasi-harmonic approximation in the gas phase according to the work of Truhlar - the quasi-harmonic approximation is the same as the harmonic oscillator approximation except that vibrational frequencies lower than 100 cm^{-1} were raised to 100 cm^{-1} as a way to correct for the breakdown of the harmonic oscillator model for the free energies of low-frequency vibrational modes. The denoted free Gibbs energy was calculated using Equation (1) in which ΔE_{gas} is the gas-phase energy (electronic energy), ΔG^T_{gas} (T = 298.15 K and pressure = 1 atm.) is the sum of corrections from the electronic energy to free Gibbs energy in the harmonic oscillator approximation also including zero-point-vibrational energy, and ΔG^T_{solv} is their corresponding free solvation Gibbs energy.

$$\Delta G^T_{\text{in solution}} = \Delta E_{gas} + \Delta G^T_{gas} + \Delta G^{solv} = \Delta E_{gas} \qquad (1)$$

All found minima were checked for negative frequencies. Based on the lowest energy structures according to the optimization described above, the chemical shifts were calculated with the use of the Gauge-Independent Atomic Orbital (GIAO) method using WC04/6-311+G(2d,p) and a PCM model with as solvent DMSO. No additional scaling was used for the denoted chemical shifts.

Biochemical methods

Mouse brain membrane proteome. Mouse brains (C57Bl/6) were isolated according to guidelines approved by the ethical committee of Leiden University (DEC#13191), frozen in N_2 (l), and stored at -80 °C until use. Tissues were thawed on ice, dounce homogenized in appropriate volumes (2-4 mL) of cold lysis buffer (20 mM HEPES, pH 7.2, 2 mM DTT, 250 mM sucrose, 1 mM $MgCl_2$, 2.5 U/mL benzonase) and incubated on ice (15 min), followed by two low-speed spins (3 min, 1,400–2,500 *g*, 4 °C) to remove debris. The supernatant fraction was collected for further use. The membrane and cytosolic fractions of cell or tissue lysates were separated by ultracentrifugation (93,000 *g*, 45 min, 4 °C). The supernatant was collected (cytosolic fraction) and the membrane pellet was resuspended in cold storage buffer (20 mM HEPES, pH 7.2, 2 mM DTT) by thorough pipetting and passage through an insulin needle. Protein concentrations were determined by a Quick Start™ Bradford Protein Assay and samples were diluted to 2.0 mg/mL with cold storage buffer, aliquoted, flash frozen in N_2 (l) and stored at -80 °C until further use.

SDS-PAGE. Mouse brain proteome or cell lysate (15 µL, 2.0 or 1.0 mg/mL, membrane fraction or whole lysate) was pre-incubated with vehicle or inhibitor (0.375 µL 40 x inhibitor stock, 30 min, rt) followed by an incubation with the activity-based probe (0.375 µL 40 x probe stock, 20 min, rt). Final concentrations for the inhibitors are indicated in the main text and figure legends. Reactions were quenched with 4x Laemmli buffer (5 µL, 240 mM Tris (pH 6.8), 8% (w/v) SDS, 40% (v/v) glycerol, 5% (v/v) β-mercaptoethanol, 0.04% (v/v) bromophenol blue). 10 or 20 µg per reaction was resolved on a 10% acrylamide SDS-PAGE gel (180 V, 75 min). Gels were scanned using Cy2, Cy3 and Cy5 multichannel settings on a ChemiDoc MP (Bio-Rad) and stained with Coomassie after scanning. Fluorescence was normalized to Coomassie staining and quantified with Image Lab v5.2.1 (Bio-Rad). IC_{50} curves were fitted with Graphpad Prism® v7 (Graphpad Software Inc.).

Cell culture. U2OS cells were cultured at 37 °C under 7% CO_2 in DMEM containing phenol red, stable glutamine, 10% (v/v) New Born Calf Serum (Thermo Fisher), and penicillin and streptomycin (200 µg/mL each; Duchefa). Medium was refreshed every 2-3 days and cells were passaged twice a week at 80-90% confluence by trypsinization, followed by resuspension in fresh medium. Cells lines were purchased from ATCC and were regularly tested for mycoplasma contamination. Cultures were discarded after 2-3 months of use.

Plasmids. The DAGLα and DAGLα-S472A plasmids (both containing a FLAG tag) were constructed as described before.[21] Briefly, full length human cDNA of hDAGL-α was purchased from Biosource and cloned into mammalian expression vector pcDNA3.1, containing genes for ampicillin and neomycin resistance. A FLAG-linker was made from primers and cloned into the vector at the C-terminus of hDAGL-α. Two step PCR mutagenesis was performed to substitute the active site serine for an alanine in the hDAGL-α-FLAG, to obtain hDAGL-α-S472A-FLAG. All plasmids were grown in XL-10 Z-competent cells and prepped (Maxi Prep, Qiagen). The sequences were confirmed by sequence analysis at the Leiden Genome Technology Centre.

Transfection. U2OS cells were grown to ~70% confluency in 6-well plates. Prior to transfection, culture medium was aspirated and 1 mL medium was added per well. A 3:1 (m:m) mixture of polyethyleneimine (PEI, 4.5 µg/well) and plasmid DNA (1.5 µg/well) was prepared in serum free culture medium and incubated for 10 min at rt. Transfection was performed by dropwise addition of the PEI/DNA mixture (200 µL/well) to the cells. 24 h post-transfection, the medium was refreshed

and after 48 h cells were harvested or used for *in situ* treatments.

***In situ* tetrazine labeling**. 48 h after transfection, the cells were washed with serum free medium (3 x 1 mL). The cells were treated with either DMSO as vehicle or DH376 (2.5 μM final concentration, 0.05% DMSO) for 1 h at 37 °C, followed by either vehicle or 4 (5 μM final concentration, 1 h 37 °C, 0.1% DMSO). The cells were washed with serum-free medium and treated with either vehicle or tetrazine 24 (10 μM final concentration, 0.1% DMSO) for 1 h at 37 °C. The cells were subsequently washed with PBS and harvested by scraping into PBS. The cells were pelleted by centrifugation (5 min, 1000 *g*), the supernatant was discarded and cell pellets were frozen in N_2 (l) and stored at -80 °C until sample preparation for SDS-PAGE. Cell pellets were thawed on ice, resuspended in cold lysis buffer (20 mM HEPES, pH 7.2, 2 mM DTT, 250 mM sucrose, 1 mM $MgCl_2$, 2.5 U/mL benzonase) and incubated on ice (15-30 min). Protein concentrations were determined by a Quick Start™ Bradford Protein Assay. The cell lysate was diluted to 1 mg/mL in cold storage buffer (20 mM HEPES, pH 7.2, 2 mM DTT) before being prepared for SDS-PAGE analysis as described above.

References

1. E. J. van Rooden, R. Kreekel, T. Hansen, A. P. A. Janssen, A. C. M. van Esbroeck, H. den Dulk, R. J. B. H. N. van den Berg, J. D. C. Codée and M.van der Stelt. *Org. Biomol. Chem*., **2018**, doi: 10.1039/C8OB01499J.
2. Pacher, P. The Endocannabinoid System as an Emerging Target of Pharmacotherapy. *Pharmacol. Rev.* **58**, 389–462 (2006).
3. Bisogno, T. *et al.* Cloning of the first sn1-DAG lipases points to the spatial and temporal regulation of endocannabinoid signaling in the brain. *J. Cell Biol.* **163**, 463–468 (2003).
4. Barglow, K. T. & Cravatt, B. F. Activity-based protein profiling for the functional annotation of enzymes. *Nat. Methods* **4**, 822–827 (2007).
5. Sieber, S. A. & Cravatt, B. F. Analytical platforms for activity-based protein profiling - exploiting the versatility of chemistry for functional proteomics. *Chem. Commun.* **22**, 2311–2319 (2006).
6. Hsu, K.-L. *et al.* DAGLβ inhibition perturbs a lipid network involved in macrophage inflammatory responses. *Nat. Chem. Biol.* **8**, 999–1007 (2012).
7. Ogasawara, D. *et al.* Rapid and profound rewiring of brain lipid signaling networks by acute diacylglycerol lipase inhibition. *Proc. Natl. Acad. Sci.* **113**, 26–33 (2016).
8. Willems, L. I. *et al.* Bioorthogonal chemistry: Applications in activity-based protein profiling. *Acc. Chem. Res.* **44**, 718–729 (2011).
9. Patterson, D. M., Nazarova, L. A. & Prescher, J. A. Finding the Right (Bioorthogonal) Chemistry. *ACS Chem. Biol.* **9**, 592–605 (2014).
10. Lee, Y., Cho, W., Sung, J., Kim, E. & Park, S. B. Mono-chromophoric Design Strategy for Tetrazine-based Colorful Bioorthogonal Probes with a Single Fluorescent Core Skeleton. *J. Am. Chem. Soc.* **140**, 974-983 (2018).
11. Carlson, J. C. T., Meimetis, L. G., Hilderbrand, S. A. & Weissleder, R. BODIPY-tetrazine derivatives as superbright bioorthogonal turn-on probes. *Angew. Chem. Int. Ed.* **52**, 6917–6920 (2013).
12. Carboni, R. A. & Lindsey, R. V. Reactions of Tetrazines with Unsaturated Compounds. A New Synthesis of Pyridazines. *J. Am. Chem. Soc.* **81**, 4342–4346 (1959).
13. Oliveira, B. L., Guo, Z. & Bernardes, G. J. L. Inverse electron demand Diels–Alder reactions in chemical biology. *Chem. Soc. Rev.* **46**, 4895–4950 (2017).
14. Eckert, H. & Forster, B. Triphosgene, a Crystalline Phosgene Substitute. *Angew. Chem. Int. Ed.* **26**, 894–895 (1987).
15. Deng, H. *et al.* Triazole Ureas Act as Diacylglycerol Lipase Inhibitors and Prevent Fasting-Induced Refeeding. *J. Med. Chem.* **60**, 428–440 (2017).
16. van Esbroeck, A. C. M. *et al.* Activity-based protein profiling reveals off-target proteins of the FAAH inhibitor BIA 10-2474. *Science.* **356**, 1084–1087 (2017).
17. Wieczorek, A., Werther, P., Euchner, J. & Wombacher, R. Green- to far-red-emitting fluorogenic tetrazine probes – synthetic access and no-wash protein imaging inside living cells. *Chem. Sci.* **8**, 1506–1510 (2017).
18. Taherpour, A. A. & Kheradmand, K. One-Pot Microwave-Assisted Solvent Free Synthesis of Simple Alkyl 1,2,3-Triazole-4-carboxylates by Using Trimethylsilyl Azide. *J. Heterocycl. Chem.* **46**, 131–133 (2009).
19. Kong, J. Spartan '10. Wavefunction Inc. (2004).
20. Frisch, M. J. *et al.* Gaussion 09, Revision A.02. (2016).
21. Baggelaar, M. P. *et al.* Development of an activity-based probe and in silico design reveal highly selective inhibitors for diacylglycerol lipase-α in brain. *Angew. Chem. Int. Ed.* **52**, 12081–12085 (2013).

Chapter 7

Summary and future prospects

In **Chapter 1**, the endocannabinoid system (ECS) and its therapeutic potential are introduced. The endocannabinoid system consists of the cannabinoid CB_1 and CB_2 receptors and their endogenous ligands: 2-arachidonoylglycerol (2-AG) and anandamide (AEA). The enzymes regulating the levels of 2-AG and AEA are interesting targets for the development of small molecule therapeutics, which are currently lacking. Activity-based protein profiling (ABPP) is a powerful method to aid in drug discovery and in particular for the ECS. Activity-based probes are available for the majority of endocannabinoid enzymes: the diacylglycerol lipases (DAGLs), monoacylglycerol lipase (MAGL), several α/β hydrolase domain containing proteins (ABHD4, 6 and 12), phospholipase A2 group IVE (PLA2G4E), fatty acid amide hydrolase (FAAH) and N-acylethanolamine-hydrolyzing acid amidase (NAAA).

The activity-based protein profiling methodology is reviewed in **Chapter 2**. ABPP is a methodology to study a subset of the enzymatically active proteome. ABPP relies on chemical probes that covalently react with active enzymes. The targeted proteins can subsequently be analyzed via a fluorescent or biotin reporter tag of the probe. If the reporter group interferes with target affinity or selectivity, then a two-step probe with a small ligation handle, suited for bioorthogonal chemistry, can be used to introduce a reporter group after the probe has reacted with the target. A diverse set of probes has been developed for many enzyme classes, including serine hydrolases, proteases, deubiquitinases, glycosidases, cytochrome P450s and kinases. Different analytical techniques are currently available to visualize, identify and quantify probe-labeled proteins. Depending on the goal and type of the experiment, available protein amount, throughput and sensitivity requirements, a suitable analytical platform can be chosen. ABPP has well-developed applications in discovering new drug targets and in profiling inhibitors for potency and selectivity. ABPP will, therefore, continue to aid research both in fundamental biology and drug discovery.

ABPP is applied in **Chapter 3** for the search for new drug targets. The endocannabinoid system is considered to be an endogenous protective system in various neurodegenerative diseases. Niemann-Pick Type C is a neurodegenerative lysosomal storage disease in which the role of the endocannabinoid system

has not been studied yet. In **Chapter 3**, serine hydrolase activity in brain proteomes of a Niemann-Pick type C mouse model was measured by ABPP and compared to wild type mice. DAGLα, ABHD4, ABHD6, ABHD12, FAAH and MAGL activities were quantified. Chemical proteomics showed that three lysosomal serine hydrolase activities (retinoid-inducible serine carboxypeptidase, cathepsin A and palmitoyl-protein thioesterase 1) were increased in Niemann-Pick C1 protein (NPC1) knockout mouse brain compared to wild type brain, whereas no difference in endocannabinoid hydrolase activity was observed. These targets might be interesting therapeutic targets for future validation studies. With SDS-PAGE and Western blot, differences in DAGLα protein abundance and activity levels were observed. This proteoform of DAGLα was not measured by the mass spectrometry based method. It was hypothesized that the peptides from this proteoform escape detection in the LC-MS measurement.

In **Chapter 3**, two different mass spectrometry methods were used for relative quantification of probe-labeled enzymes. The first uses dimethyl labeling, in which tryptic peptides are modified with isotopically labeled formaldehyde. These labeled peptides were measured on an Orbitrap mass spectrometer. The second method is label-free, where tryptic peptides are measured unmodified on a Synapt mass spectrometer and alignment software is used to compare the signal of each peptide in different samples. The optimized protocol for this label-free method is described in **Chapter 4**.

Chapter 4 consists of a protocol for identifying the *in vivo* selectivity profile of covalent inhibitors using ABPP with label-free quantitative proteomics as exemplified by experimental data on the diacylglycerol lipase inhibitor DH376 in mouse brain, liver, kidney and testes. The stages of the protocol include tissue lysis, probe incubation, enrichment, sample preparation, liquid chromatography-mass spectrometry measurement, processing and data analysis. The results include evidence of target engagement in a native proteome and the identification of potential off-targets for the inhibitor under investigation. The advantages of label-free quantification methods include high proteome coverage and the ability to analyze multiple samples at the same time.

In the protocol described in **Chapter 4**, enzymes labeled with a biotinylated probe are purified using avidin enrichment. After enrichment and washing steps, trypsin is added to the avidin beads and the resulting peptides are measured. However, the probe-modified peptides will remain on the beads. Identifying these probe-modified peptides is necessary to determine how the probe reacts with its target enzymes. A powerful method to characterize both the probe-labeled proteins and their site of modification is using a cleavable linker.[1–5] Additionally, cleavable linkers can be used for top-down proteomics. To be able to measure the probe-modified peptides or intact proteins, an acid cleavable linker with a mass-tag for enhanced signal intensity in MS was designed (**Fig. 1a**).[6] After bioorthogonal ligation with the probe-labeled enzymes and avidin enrichment, the linker can be cleaved with acid. The liberated

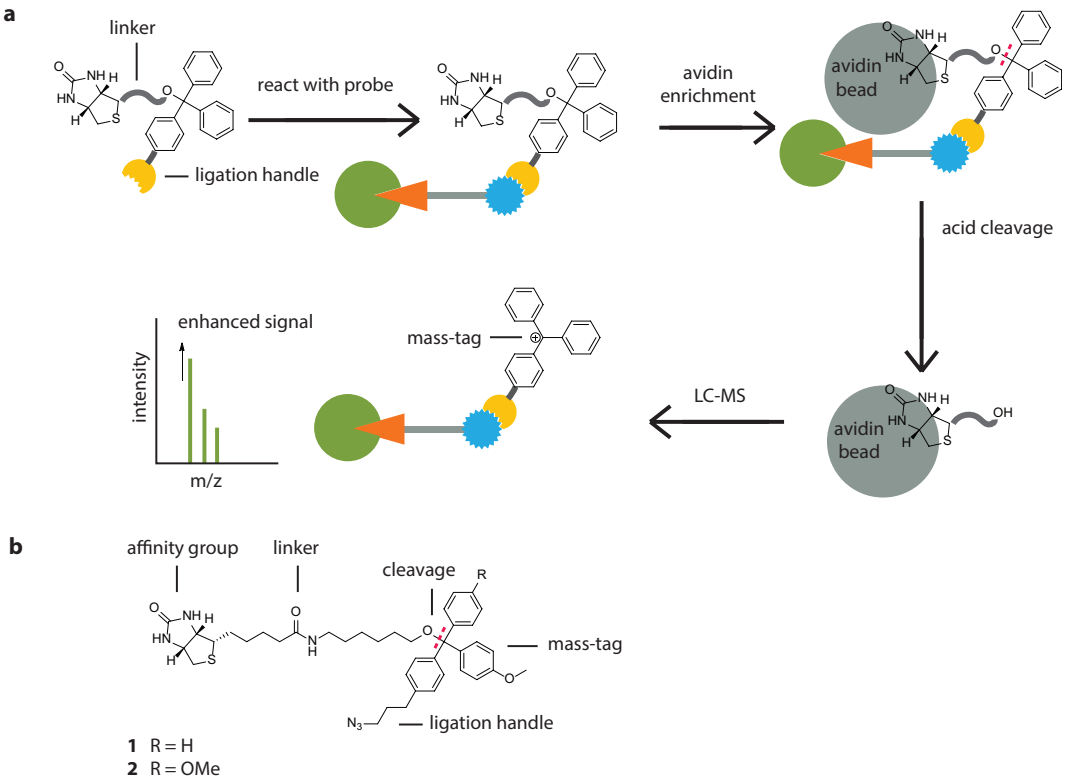

Figure 1. Design of the cleavable trityl-based mass-tag affinity handle. (a) Workflow for the reagent: a trityl moiety as mass-tag and cleavable linker, designed with a biotin moiety and a ligation handle for bioorthogonal chemistry to react with probes. After avidin enrichment, the trityl core is cleaved with acid and the released probe can be measured with LC-MS. The trityl mass-tag will increase the signal intensity. (b) Design of the mass-tag reagents **1** and **2**.

enzymes can either be measured intact or digested with trypsin to provide the probe-labeled peptide. This dual functionality linker is based on the trityl (triarylmethyl) group, which is used extensively in organic chemistry as a protecting group.[7] Para and ortho electron donating groups stabilize the cation and increase signal enhancement in MS. Therefore, two triarylmethyl ethers were designed, monosubstituted (1) or disubstituted (2) with para-methoxys (**Fig. 1b**). An azide was chosen as bioorthogonal ligation handle.

Synthesis. The linker with affinity group was synthesized by conversion of biotin **3** to the activated ester **4**, followed by amide bond formation with an alkyl linker to yield biotin alcohol **5**[8] (**Scheme 1**). The synthesis of the mass-tag started with the reduction of 3-(4-bromophenyl)propionic acid (**6**) with sodium borohydride to alcohol **7**. The hydroxyl group was protected by conversion to the

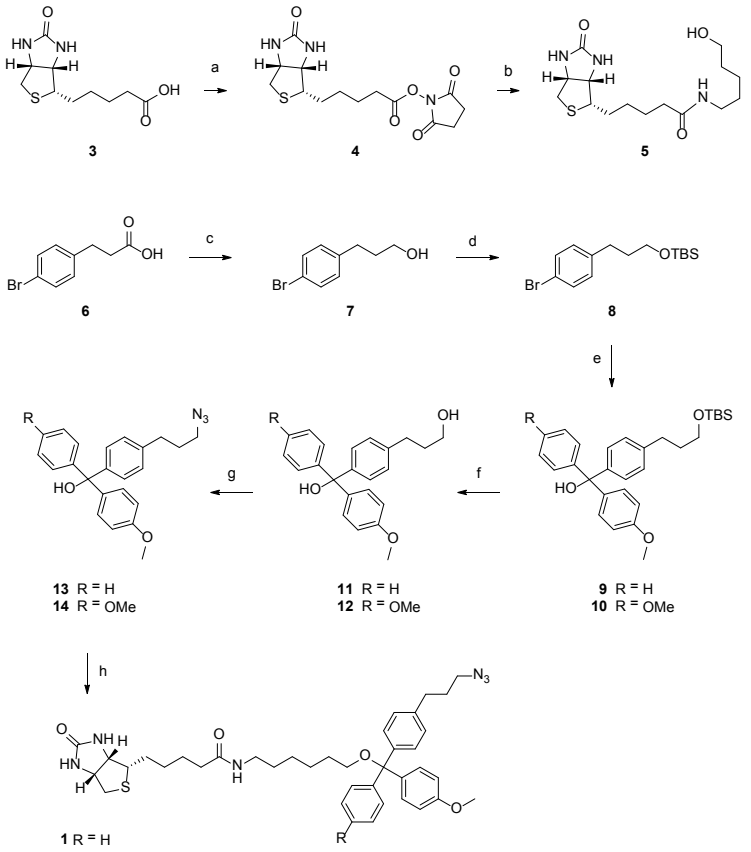

Scheme 1. Synthesis of the trityl-based mass-tag affinity handles **1** and **2**. Reagents and conditions: (a) NHS, DCC, DMF, 88%; (b) 6-amino-1-hexanol, DMF, 85%; (c) $NaBH_4$, $BF_3{\cdot}Et_2O$, THF, 0 °C > rt, 100%; (d) TBDMS-Cl, imidazole, DMF, 87%; (e) *i*. *n*-BuLi, THF, -78 °C > 0 °C; *ii*. For **9**: 4-methoxybenzophenone, -78 °C > rt, 77%; for **10**: 4,4-dimethoxybenzophenone, -78 °C > rt, 73%; (f) TBAF, THF, 100%; (g) DPPA, DBU, 55 °C, 65% (**13**) and 19% (**14**); (h) **5**, DMF, HCl, molecular sieves 4Å, 14% (**1**) and 20% (**2**).

tert-butyldimethylsilyl ether **8**.[9] The triphenylmethyl core was synthesized from **8** by first forming an organolithium reagent, followed by nucleophilic addition to benzophenone (4-methoxybenzophenone for **9** and 4,4-dimethoxybenzophenone for **10**). The lithium-bromine exchange of **8** did not proceed at -78 °C. However, adding **8** at -78 °C to a solution of *n*-BuLi and allowing the reaction mixture to warm to 0 °C,[10] and subsequently cooling to -78 °C for benzophenone addition, before stirring at rt, resulted in good yields of **9** and **10**.[11] Compounds **9** and **10** were easily visualized on TLC by spraying with H_2SO_4, forming a bright orange spot.[12] Fluorine induced deprotection of **9**[9] was followed by azide substitution of the alcohol **11** by diphenyl phosphoryl azide (DPPA).[13] For **13** a sharp peak at 2093 cm^{-1} was observed in

the IR spectrum, characteristic of azides.[14] The trityl ether **1** was finally formed by mixing the trityl alcohol **13** and biotin alcohol **5** with dry HCl and activated molsieves. Trityl ether **2** was synthesized from **10** with the same procedures, in an overall yield of 4%.

Evaluation. As a model for an acetylene functionalized protein, the free cysteine[15] of bovine serum albumin (BSA) was alkylated with either iodoacetamide or iodoacetamide-alkyne (IAA-alkyne, see Experimental).[16] The resulting functionalized BSA was reacted with different azides using the CuAAC: Cy5-N_3, biotin-N_3, azides **1** and **2** (**Fig. 2**). A clear Cy5 signal is visible at the expected molecular weight of BSA (~69 kDa). To visualize biotinylated protein, a blot with streptavidin-HRP was performed. A chemiluminescent signal is visible for biotin-N_3 at the same height as the fluorescent signal. However, no

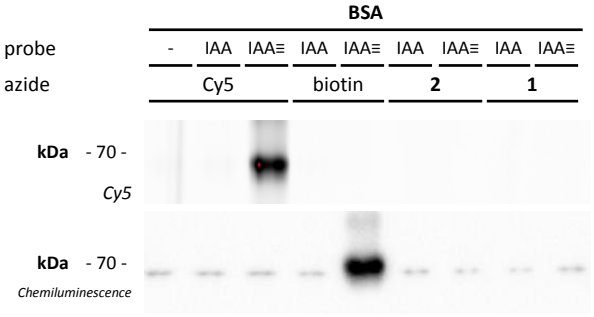

Figure 2. Gel analysis of the CuAAC reaction with BSA-alkyne and different azides. IAA: iodoacetamide. IAA≡: IAA-alkyne.

signal is visible for BSA reacted with azides **1** and **2**.

From the SDS-PAGE experiments, it is clear that the CuAAC reaction does not work for these compounds. Different bioorthogonal chemistries could therefore be considered when designing the next generation compounds,[17] such as the inverse electron-demand Diels-Alder reaction with tetrazines and strained alkenes.[18] A potential route for the synthesis of a mass-tag **16** with a tetrazine ligation handle is presented in **Scheme 2**.

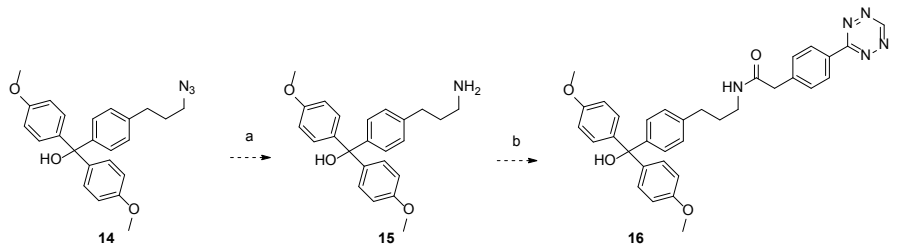

Scheme 2. Synthesis of a mass-tag with a tetrazine ligation handle. Reagents and conditions: (a) PPh_3, H_2O; (b) tetrazine-OSu.

A more stable cation used as a mass-tag is the triphenylcyclopropenyl ion.[19] It is the smallest aromatic ring: a three-membered ring containing two electrons.[20] The first derivative of these aromatic rings was synthesized in 1957 by Breslow.[21] Phenyl substituents are not required for the stability of the cation,[22] therefore a smaller mass-tag can be obtained. Two potential synthetic routes to incorporate the tag between an azide and a biotin are shown in **Scheme 3**.

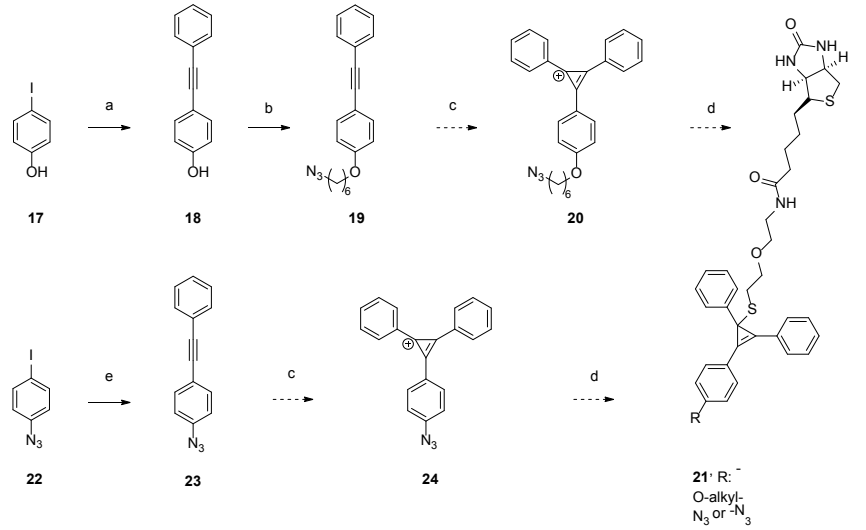

Scheme 3. Proposed synthesis of a mass-tag generating a triphenylcyclopropenyl cation. Reagents and conditions: (a) phenylacetylene, $Pd(OAc)_2$, PPh_3, CuI, Et_3N, THF, 84%; (b) *i*. NaH, DMF *ii*. 1-azido-6-bromohexane (**29**), 87%; (c) *i*. benzene, KOtBu, α,α-dichlorotoluene. *ii*. HBF_4 (aq); (d) biotin-SH; (e) phenylacetylene, MTBE, Et_3N, $Pd(OAc)_2$, PPh_3, CuI, 53%.

Top-down activity-based proteomics. Currently, most proteomics methods use peptide-based bottom-up approaches, where proteins are digested with trypsin before analysis.[26] The activity-based proteomics methods used in **Chapter 3** and **Chapter 4** are examples of a bottom-up approach. The main reason for using this approach is that peptides are more easily separated than intact proteins. Separation of complex proteomes is needed for high proteome coverage. However, bottom-up proteomics suffers from severable draw-backs. For instance, quantification of proteins is inherently problematic due to shared peptides between different proteins (the protein inference problem[27]). Additionally, using peptides for identification of post-translational modifications (PTMs) makes it impossible to assign combinations of PTMs to various proteoforms. A more intuitive approach to proteomics is a top-down approach, where the intact proteins themselves are measured.[28] For example, this method was recently used for characterizing proteoforms of histones with multiple PTMs.[29] Several methods described in this thesis are top-down proteomics techniques, such as SDS-PAGE and Western blotting. Mass spectrometry based top-down proteomics will be standard in the future due to technological advances in intact protein separation. Activity-based proteomics is at an advantage compared to abundance-based proteomics, because biotinylated probes already enable a purification step using avidin chromatography. By using cleavable linkers instead of on-bead digestion to detach the probe-labeled enzymes from avidin beads, the proteins remain intact. For more separating power, reverse-phase chromatography or SDS-PAGE can be used.[30] Top-down activity-based proteomics will enable the identification of active proteoforms and their post-translational modifications.

In **Chapter 5** the synthesis and characterization of the first reported quenched activity-based probes for metabolic serine hydrolases is described. The probes contain a triazole urea electrophilic trap to covalently attach to a catalytic serine. The first probe was active against DAGLα, contains a BODIPY-FL and 2,4-dinitroaniline as fluorophore-quencher pair and was approximately threefold quenched. The second probe contained a Cy5 fluorophore and cAB40 quencher and was more efficiently quenched (± 12-fold). This probe was able to label endogenous ABHD6 *in vitro*, but not did not penetrate the cells. To improve the quenching efficiency of these probes, a possible starting point could be minimalist quenched probes, with only an electrophilic trap, a fluorophore and quencher. Besides the triazole ureas described in **Chapter 5**, another possible electrophilic trap for such minimalist probes is a mixed alkyl aryl phosphonate ester (**Fig. 3a**). This electrophilic trap has been previously used in quenched serine proteases probes.[31] To tune quenching efficiency, various linker lengths and fluorophore-quencher pairs could be synthesized. To decide on a suitable starting point for linker length, computational chemistry can be used. By calculating the lowest energy conformation of the molecule in solution the distance between fluorophore and quencher can be predicted. The optimal distance for FRET energy transfer

for the fluorophore/quencher pair can then be chosen as a starting point for synthesis. To limit the steric bulk of the qABPs, a quencher should function as a leaving group, e.g. dinitrophenol as an aryl on a phosphonate[32] or sulfonate (**Fig. 3b**). Using a successfully quenched minimalist probe as starting point, more selective probes could be designed. For example, fluorescent diaryl phosphonate probes have a small recognition element which provides selectivity for different serine proteases.[33]

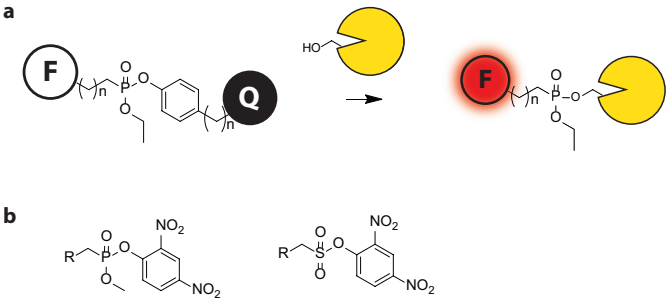

Figure 3. Design of broad-spectrum qABPs for serine hydrolases. (a) General design for mixed alkyl aryl phosphonate esters. F: fluorophore; Q: quencher. (b) 2,4-dinitrophenyl quencher as aryl on phosphonate or sulfonate probes.

In **Chapter 6**, triazole urea probes for diacylglycerol lipase (DAGL) were designed with different bio-orthogonal handles: an alkyne, alkene or norbornene. Two regioisomers of each triazole urea were generated and characterized using NMR analysis supported by DFT calculations. The selectivity of the probes was assessed with activity-based protein profiling and norbornene probe **4** was selected as the most selective DAGL-probe. This probe was potent against endogenous DAGLα (IC_{50} = 5 nM) and was successfully applied as a two-step activity-based probe for labeling of DAGLα using a bioorthogonal ligation in living cells. The inverse electron-demand Diels-Alder reaction has several advantages to surpass the CuAAC reaction as the "go-to" reaction for bioorthogonal chemistry, but improvements are required to make more compact reactants than trans-cyclooctene and aromatic substituted tetrazines. Cyclopropene as a strained alkene is promising in this regard, with possibilities to modify the ring making the reaction faster. Tetrazine chemistry is currently being actively explored.[34] Additionally, minimalist linkers containing the bioorthogonal handles will become more synthetically accessible and commercially available.

To conclude, this thesis described several new strategies and tools for activity-based protein profiling to improve the drug discovery process. A new label-free quantification method for activity-based proteomics was developed. This method allowed the comparison of multiple samples within the same experiment, as exemplified by mapping the *in vivo* off-target interaction landscape of the diacylglycerol lipase inhibitor DH376 in various tissues. Furthermore, this method resulted in the identification of three potential drug targets for Niemann-Pick Type C disease. Additionally, new quenched and two-step probes were developed for cellular profiling of diacylglycerol lipases. It is anticipated that these novel tools and strategies will help to bring forward new treatment opportunities for diseases in which aberrant 2-arachidonoylglycerol signaling plays a role.

Experimental

Synthesis

General remarks. Reagents were purchased from Sigma Aldrich, Acros or Merck and used without further purification unless noted otherwise. Some reactions were performed using oven or flame-dried glassware and dry solvents. All moisture sensitive reactions were performed under an argon or nitrogen atmosphere. Traces of water were removed from starting compounds by co-evaporation with toluene. ^{1}H- and ^{13}C-NMR spectra were recorded on a Bruker AV 400 MHz spectrometer at 400 (^{1}H) and 100 (^{13}C) MHz using $CDCl_3$, CD_3OD or $(CD_3)_2SO$ as solvent, unless stated otherwise. Spectra were analyzed using MestReNova 11.0.3. Chemical shift values are reported in ppm with tetramethylsilane or solvent resonance as the internal standard ($CDCl_3$, δ 7.26 for ^{1}H, δ 77.16 for ^{13}C; CD_3OD, δ 3.31 for ^{1}H, δ 49.00 for ^{13}C; $(CD_3)_2SO$, δ 2.50 for ^{1}H, δ 39.52 for ^{13}C). Data are reported as follows: chemical shifts (δ), multiplicity (s = singlet, d = doublet, dd = double doublet, td = triple doublet, t = triplet, q = quartet, m = multiplet, br = broad), coupling constants J (Hz), and integration. LC-MS analysis was performed on a Finnigan Surveyor HPLC system with a Gemmi C18 50x4.60 mm column (detection at 200-600 nm), coupled to a Finnigan LCQ Adantage Max mass spectrometer with ESI. The applied buffers were H_2O, MeCN and 1.0% TFA in H_2O (0.1% TFA end concentration). High resolution mass spectra (HRMS) were recorded by direct injection on a q-TOF mass spectrometer (Synapt G2-Si) equipped with an electrospray ion source in positive mode with leu-enkephalin (*m/z* = 556.2771) as an internal lock mass. The instrument was calibrated prior to measurement using the MS/MS spectrum of Glu-1-fibrinopeptide B. HPLC purification was performed on a preparative LC-MS system (Agilent 1200 series) with an Agilent 6130 Quadruple MS detector. IR spectra were recorded on a Shimadzu FTIR-8300 and are reported in cm^{-1}. Flash chromatography was performed using SiliCycle silica gel type SilicaFlash P60 (230 – 400 mesh). TLC analysis was performed on Merck silica gel 60/Kieselguhr F254, 0.25 mm. Compounds were visualized using UV-irradiation, a KMnO4 stain (K_2CO_3 (40 g), $KMnO_4$ (6 g), H_2O (600 mL) and 10% NaOH (5 mL)) or a H_2SO4 stain (20% H_2SO_4 in EtOH). Molecules shown are drawn using Chemdraw v16.0.

2,5-Dioxopyrrolidin-1-yl-5-((3a*S*,4*S*,6a*R*)-2-oxohexahydro-1*H*-thieno[3,4-d]imidazol-4-yl) pentanoate (4). To a solution of biotin (0.224 g, 1 mmol) and N-hydroxysuccinimide (0.12 g, 1.0 mmol) in DMF (7.3 mL) was added N,N'-dicyclohexylcarbodiimide (0.27 g, 1.3 mmol). The reaction mixture was stirred o/n, during which a white precipitate formed. The mixture was filtered and the filtrate was

concentrated. The white powder that was obtained was triturated with Et_2O, then filtered and left to dry to the air. The final product (0.30 g, 0.88 mmol, 88% yield) was a white powder, contaminated with dicyclohexylurea. ^{1}H NMR (300 MHz, $(CD_3)_2SO$) δ 6.41 (d, J = 18.9 Hz, 2H), 4.30 (dd, J = 7.7, 4.9 Hz, 1H), 4.20 – 4.09 (m, 1H), 3.09 (dd, J = 7.8, 4.7 Hz, 1H), 2.92 – 2.81 (m, 1H), 2.73 – 2.52 (m, 3H), 1.76 – 1.50 (m, 4H), 1.54 – 1.34 (m, 2H), 1.34 – 1.10 (m, 1H), 1.14 – 0.94 (m, 1H). ^{13}C NMR (75 MHz, $CDCl_3$) δ 170.32, 168.98, 162.71, 61.01, 59.19, 55.27, 39.95, 30.02, 27.87, 25.48, 25.36, 24.51.

N-(6-Hydroxyhexyl)-5-((3a*S*,4*S*,6a*R*)-2-oxohexahydro-1*H*-thieno[3,4-d]imidazol-4-yl)pentanamide (5). To a solution of **4** (0.30 g, 0.88 mmol) in DMF (8.8 mL) was added 6-amino-1-hexanol (0.12 g, 1.1 mmol) and the reaction mixture was stirred o/n and concentrated. Purification of the residue by silica gel column chromatography (10% MeOH in DCM) yielded the title compound (0.26 g, 0.75 mmol, 85%). ^{1}H NMR (300 MHz, $CDCl_3$) δ 4.49 (dd, J = 7.9, 4.9 Hz, 1H), 4.30 (dd, J = 7.9, 4.4 Hz, 1H), 3.54 (t, J = 6.5 Hz, 2H), 3.35 (s, 2H), 3.26 – 3.12 (m, 3H), 3.03 – 2.82 (m, 1H), 2.75 – 2.63 (m, 1H), 2.20 (t, J = 7.3 Hz, 2H), 1.82 – 1.27 (m, 14H). ^{13}C NMR (75 MHz, $CDCl_3$) δ 175.95, 63.38, 62.87, 61.62, 57.02, 41.04, 40.31, 36.82, 33.57, 30.43, 29.79, 29.51, 27.84, 26.96, 26.64.

3-(4-Bromophenyl)propan-1-ol (7). To a cooled (0 °C) suspension of 3-(4-bromophenyl)propionic acid (13.32 g , 58 mmol) in dry THF (120 mL) was added $NaBH_4$ (4.4 g, 116 mmol), followed by dropwise addition of $BF_3{\cdot}Et_2O$ (14.6 mL, 116 mmol). The reaction mixture was warmed to rt and stirred o/n. The reaction was cooled to 0 °C and carefully quenched by dropwise addition of 1 M HCl. The aqueous layer was extracted with Et_2O (3x). The combined organic layers were dried ($MgSO_4$), filtered and concentrated. Purification of the residue by silica gel column chromatography (20 > 50% EtOAc in pentane) afforded the title compound as a clear oil (12.8 g, 58 mmol, 100%). ^{1}H NMR (400 MHz, $CDCl_3$) δ 7.39 (d, J = 8.4 Hz, 2H), 7.07 (d, J = 8.3 Hz, 2H), 3.66 (t, J = 6.4 Hz, 2H), 2.74 – 2.57 (m, 2H), 2.23 (s, 1H), 1.86 (dt, J = 13.9, 6.5 Hz, 2H). ^{13}C NMR (100 MHz, $CDCl_3$) δ 140.81, 131.53, 130.30, 119.68, 62.10, 34.03, 31.52.

(3-(4-Bromophenyl)propoxy)(*tert*-butyl)dimethylsilane (8). To a solution of **7** (12.8 g, 58 mmol) in dry DMF (250 mL) were added TBDMS-Cl (10.5 g, 69.6 mmol) and imidazole (9.86 g, 145 mmol) and the mixture was stirred o/n. H_2O (400 mL) was added and the aqueous layer was extracted with Et_2O (3 x 250 mL). The combined organic layers were washed with H_2O (200 mL), brine (200 mL), dried ($MgSO_4$), filtered and concentrated. Purification of the residue by silica gel column chromatography (1:99 EtOAc:pentane) afforded the title compound (16.6 g, 50.4 mmol, 87%). ^{1}H NMR (400 MHz, $CDCl_3$) δ 7.39 (d, J = 8.3 Hz, 2H), 7.07 (d, J = 8.3 Hz, 2H), 3.61 (t, J = 6.2 Hz, 2H), 2.69 – 2.59 (m, 2H), 1.86 – 1.72 (m, 2H), 0.91 (s, 9H), 0.05 (s, 6H). ^{13}C NMR (100 MHz, $CDCl_3$) δ 141.34, 131.43, 130.40, 119.50, 62.19, 34.39, 31.64, 26.09, 18.47, -5.14.

(4-(3-((*tert*-Butyldimethylsilyl)oxy)propyl)phenyl)(4-methoxyphenyl)(phenyl)methanol (9). To a cooled (-78 °C) solution of *n*-BuLi (1.6 M in hexanes, 7.5 mL, 12 mmol) was added dropwise a solution of **8** (3.29 g, 10 mmol) in Et_2O (80 mL) in 20 min. The reaction mixture was allowed to warm to 0 °C and stirred for 1 h. The reaction mixture was cooled to -78 °C before dropwise addition of a solution of 4-methoxybenzophenone (2.12 g, 10 mmol) in THF (40 mL) in 15 min. The reaction mixture was allowed to gradually warm up to rt and stirred for 30 min. The reaction was quenched with H_2O and diluted with EtOAc. The organic layer was washed with sat. aq. $NaHCO_3$, H_2O, brine, dried ($MgSO_4$), filtered and concentrated. Purification of the residue by silica gel column chromatography (1% Et_3N, 2 > 10% EtOAc in pentane) afforded the title compound (3.6 g, 7.7 mmol, 77%). ^{1}H NMR (300 MHz, $CDCl_3$) δ 7.41 – 7.13 (m, 11H), 6.88 (d, J = 8.8 Hz, 2H), 3.83 (s, 3H), 3.72 (t, J = 6.3 Hz, 2H), 3.00 (s, 1H),

2.85 – 2.66 (m, 2H), 1.92 (dt, J = 13.7, 6.4 Hz, 2H), 1.00 (s, 9H), 0.14 (s, 6H). ^{13}C NMR (75 MHz, $CDCl_3$) δ 158.62, 147.35, 144.66, 141.18, 139.48, 129.28, 128.04, 127.92, 127.88, 127.11, 125.48, 113.20, 81.65, 62.47, 55.25, 34.38, 31.73, 26.08, 18.42, -5.14.

(4-(3-((*tert*-Butyldimethylsilyl)oxy)propyl)phenyl)*bis*(4-methoxyphenyl)methanol (10). To a cooled (-78 °C) solution of *n*-BuLi (1.6 M in hexanes, 7.5 mL, 12 mmol) was added dropwise a solution of **8** (3.29 g, 10 mmol) in Et_2O (90 mL) in 20 min. The reaction mixture was allowed to warm to 0 °C and stirred for 25 min. The reaction mixture was cooled to -78 °C before dropwise addition of a solution of 4,4'-dimethoxybenzophenone (2.42 g, 10 mmol) in THF (40 mL) in 15 min. The reaction mixture was allowed to gradually warm up to rt and stirred o/n. The reaction was quenched with H_2O and diluted with EtOAc. The organic layer was washed with sat. aq. $NaHCO_3$, H_2O, brine, dried ($MgSO_4$), filtered and concentrated. Purification of the residue by silica gel column chromatography (1% Et_3N, 5 > 10% EtOAc in pentane) afforded the title compound (3.2 g, 7.3 mmol, 73%). ^{1}H NMR (400 MHz, $CDCl_3$) δ 7.21 – 7.09 (m, 8H), 6.86 – 6.80 (m, 4H), 3.80 (s, 6H), 3.63 (t, J = 6.4 Hz, 2H), 2.67 (m, 3H), 1.89 – 1.76 (m, 2H), 0.90 (s, 9H), 0.04 (s, 6H). ^{13}C NMR (100 MHz, $CDCl_3$) δ 158.68, 144.88, 141.25, 139.72, 129.22, 128.09, 127.85, 113.24, 81.46, 62.55, 55.39, 34.44, 31.78, 26.11, 18.49, -5.11.

3-(4-(Hydroxy(4-methoxyphenyl)(phenyl)methyl)phenyl)propan-1-ol (11). To a solution of **9** (3.6 g, 7.7 mmol) in THF (7.7 mL) was added TBAF (1.0 M in THF, 23 mL, 23 mmol). The reaction mixture was stirred over the weekend, diluted with EtOAc and washed with H_2O, brine, dried ($MgSO_4$), filtered and concentrated. Purification of the residue by silica gel column chromatography (1% Et_3N, 20 > 70% EtOAc in pentane) afforded the title compound (2.7 g, 7.7 mmol, 100%).^{1}H NMR (400 MHz, $CDCl_3$) δ 7.41 – 7.21 (m, 6H), 7.23 – 7.01 (m, 6H), 6.90 – 6.74 (m, 2H), 3.79 (s, 3H), 3.66 (t, J = 6.4 Hz, 2H), 2.82 (s, 1H), 2.77 – 2.64 (m, 2H), 1.95 – 1.81 (m, 2H), 1.36 (s, 1H). ^{13}C NMR (100 MHz, $CDCl_3$) δ 158.73, 147.29, 144.86, 140.84, 139.43, 129.29, 128.07, 128.04, 127.98, 127.92, 127.23, 81.70, 62.42, 55.38, 34.20, 31.73.

3-(4-(Hydroxybis(4-methoxyphenyl)methyl)phenyl)propan-1-ol (12). To a solution of **10** (0.32 g, 0.73 mmol) in THF (3 mL) was added TBAF (1.0 M in THF, 1.5 mL, 1.5 mmol). The reaction mixture was stirred for 2 h, diluted with EtOAc and washed with H_2O, dried ($MgSO_4$), filtered and concentrated. Purification of the residue by silica gel column chromatography (1% Et_3N, 50 > 70% EtOAc in pentane) afforded the title compound (0.24 g, 0.73 mmol, 100%).^{1}H NMR (400 MHz, $CDCl_3$) δ 7.32-7.13 (m, 8H), 6.81 (m, 4H), 3.77 (s, 6H), 3.63 (t, J = 6.5 Hz, 2H), 2.96 (s, 1H), 2.77 – 2.57 (m, 2H), 1.95 – 1.76 (m, 2H), 1.64 (s, 1H). ^{13}C NMR (100 MHz, $CDCl_3$) δ 158.60, 145.07, 140.69, 139.67, 129.19, 127.97, 127.94, 113.20, 81.37, 62.32, 55.33, 34.14, 31.69.

(4-(3-Azidopropyl)phenyl)(4-methoxyphenyl)(phenyl)methanol (13). To a solution of **11** (697 mg, 2 mmol) in DMF (4 mL) was added DPPA (517 µL, 2.4 mmol), DBU (359 µL, 2.4 mmol) and NaN_3 (195 mg, 3 mmol). The reaction mixture was stirred o/n at 55 °C. H_2O and Et_2O were added, the organic layer was seperated and washed with brine, dried ($MgSO_4$), filtered and concentrated. Purification of the residue by silica gel column chromatography (20% EtOAc, 1% Et_3N in pentane) afforded the title compound (0.48 g, 1.3 mmol, 65%). ^{1}H NMR (400 MHz, $CDCl_3$) δ 7.39 – 7.08 (m, 16H), 6.86 – 6.78 (m, 2H), 3.79 (s, 3H), 3.28 (t, J = 6.8 Hz, 2H), 2.79 (s, 1H), 2.68 (t, J = 8.4, 6.8 Hz, 2H), 1.90 (dq, J = 8.7, 6.9 Hz, 2H). ^{13}C NMR (100 MHz, $CDCl_3$) δ 158.75, 147.23, 145.14, 139.85, 139.36, 129.98, 129.28, 128.13, 128.08, 127.99, 127.90, 127.26, 125.72, 120.22, 113.30, 81.68, 55.36, 50.76, 32.43, 30.42. IR: sharp peak at 2093 cm^{-1} (N_3).

(4-(3-Azidopropyl)phenyl)bis(4-methoxyphenyl)methanol (14). To a solution of **12** (757 mg, 2 mmol) in DMF (4 mL) was added DPPA (517 µL, 2.4 mmol), DBU (359 µL, 2.4 mmol) and NaN_3 (195 mg, 3 mmol). The reaction mixture was stirred o/n at 55 °C. H_2O and Et_2O were added, the organic layer was washed with brine, dried ($MgSO_4$), filtered and concentrated. Purification of the residue by silica gel column chromatography (10 > 20% EtOAc, 1% Et_3N in pentane) afforded the title compound (0.15 g, 0.38 mmol, 19%). ^{1}H NMR (400 MHz, $CDCl_3$) δ 7.26 – 7.07 (m, 8H), 6.81 (m, 4H), 3.77 (s, 6H), 3.27 (t, J = 6.8 Hz, 2H), 2.82 (s, 1H), 2.68 (t, J = 7.6 Hz, 2H), 1.89 (p, J = 6.9 Hz, 2H). ^{13}C NMR (100 MHz, $CDCl_3$) δ 158.64, 145.36, 139.70, 139.59, 129.17, 128.03, 128.00, 113.22, 81.35, 55.32, 50.73, 32.40, 30.39. IR: sharp peak at 2093 (-N_3).

N-(6-((4-(3-Azidopropyl)phenyl)(4-methoxyphenyl)(phenyl)methoxy)hexyl)-5-((3a*S*,4*S*,6a*R*)-2-oxohexahydro-1*H*-thieno[3,4-d]imidazol-4-yl)pentanamide (1). To a solution of **5** (34 mg, 0.10 mmol) in DMF (1 mL) were added activated molecular sieves (4 Å, 180 mg), **13** (75 mg, 0.2 mmol) in 2 x 0.2 mL DMF and HCl (4 M in dioxane, 250 µL). The reaction mixture was stirred over the weekend. Et_3N (0.3 mL) was added to the reaction mixture. Purification of the residue by silica gel column chromatography (2 > 5 % (1:9 NH_4OH (30% aq.) : MeOH) in DCM) afforded the title compound (10 mg, 14 µmol, 14%). ^{1}H NMR (400 MHz, CD_3OD) δ 7.46 – 7.08 (m, 11H), 6.84 (d, J = 8.9 Hz, 2H), 4.44 (dd, J = 7.8, 4.6 Hz, 1H), 4.26 (dd, J = 7.9, 4.4 Hz, 1H), 3.77 (s, 3H), 3.33 – 3.25 (m, 6H), 3.15 (ddt, J = 9.2, 6.8, 3.0 Hz, 3H), 3.04 (t, J = 6.4 Hz, 2H), 2.99 (s, 1H), 2.92 – 2.84 (m, 2H), 2.71 – 2.62 (m, 3H), 2.18 (t, J = 7.3 Hz, 2H), 1.93 – 1.23 (m, 20H).^{13}C NMR (100 MHz, CD_3OD) δ 175.92, 166.08, 160.04, 146.55, 143.98, 141.05, 137.45, 131.39, 129.82, 129.45, 128.79, 128.67, 127.74, 113.94, 87.20, 64.37, 63.35, 61.59, 57.03, 55.70, 51.79, 41.05, 40.32, 36.81, 33.32, 31.64, 31.01, 30.36, 29.78, 29.50, 27.82, 27.19, 26.95. HRMS *m/z* calculated for $C_{39}H_{50}N_6O_4S$ $[M + Na]^+$ 721.3506, found 721.3506.

N-(6-((4-(3-Azidopropyl)phenyl)*bis*(4-methoxyphenyl)methoxy)hexyl)-5-((3a*S*,4*S*,6a*R*)-2-oxohexahydro-1*H*-thieno[3,4-d]imidazol-4-yl)pentanamide (2). To a solution of **5** (68 mg, 0.20 mmol) in DMF (2 mL) were added activated molecular sieves (4 Å, 150 mg), **14** (162 mg, 0.4 mmol) in 2 x 0.4 mL DMF and HCl (4 M in dioxane, 50 µL). The reaction mixture was stirred o/n. Et_3N (0.1 mL) was added to the reaction mixture. Purification of the residue by silica gel column chromatography (2 > 5 % (1:9 NH_4OH (30% aq.) : MeOH) in DCM) afforded the title compound (30 mg, 41 µmol, 20%). ^{1}H NMR (400 MHz, CD_3OD) δ 7.36 – 7.23 (m, 6H), 7.10 (d, J = 8.3 Hz, 2H), 6.86 – 6.76 (m, 4H), 4.42 (dd, J = 7.8, 4.4 Hz, 1H), 4.25 (dd, J = 7.9, 4.4 Hz, 1H), 3.74 (s, 6H), 3.26 (t, J = 6.7 Hz, 2H), 3.19 – 3.09 (m, 3H), 3.03 (t, J = 6.4 Hz, 2H), 2.98 (s, 1H), 2.90 – 2.82 (m, 2H), 2.65 (dd, J = 14.8, 8.1 Hz, 3H), 2.18 (t, J = 7.3 Hz, 2H), 1.84 (dt, J = 14.2, 6.8 Hz, 2H), 1.76 – 1.22 (m, 16H).^{13}C NMR (100 MHz, CD_3OD) δ 175.86, 165.86, 159.88, 144.51, 140.81, 138.00, 131.08, 129.55, 128.76, 113.93, 86.90, 64.29, 63.33, 61.56, 57.01, 55.69, 51.78, 41.06, 40.32, 36.81, 33.31, 31.62, 31.05, 30.37, 29.77, 29.49, 27.84, 27.20, 26.95. HRMS *m/z* calculated for $C_{40}H_{52}N_6O_5S$ $[M+Na]^+$ 751.3612, found 751.3614.

4-(Phenylethynyl)phenol (18). This procedure was adapted from literature procedures.[23] A mixture of PPh_3 (52 mg, 0.2 mmol), CuI (10 mg, 0.05 mmol), 4-iodophenol (2.2 g, 10 mmol) and phenylacetylene (1.3 mL, 12 mmol), THF (10 mL) and triethylamine (6.9 mL) was sonicated with nitrogen bubbling though. $Pd(OAc)_2$ (22 mg, 0.1 mmol) was added and after stirring for 1 h, the reaction mixture was diluted with Et_2O, washed with sat. aq. NH_4Cl, H_2O, dried ($MgSO_4$), filtered and concentrated. Purification of the residue by silica gel column chromatography (5 > 10% EtOAc in pentane) yielded the product (1.6 g, 8.4 mmol, 84%). ^{1}H NMR (400 MHz, $CDCl_3$) δ 7.54 – 7.48 (m, 2H), 7.45 – 7.40 (m, 2H), 7.38 – 7.28 (m, 3H), 6.88 – 6.72 (m, 2H), 4.90 (s, 1H). ^{13}C NMR (100 MHz, $CDCl_3$) δ 155.68, 133.42, 131.59, 128.46, 128.13, 123.61, 115.82, 115.63, 89.30, 88.21.

1-((6-Azidohexyl)oxy)-4-(phenylethynyl)benzene (19). To a solution of **18** (0.49 g, 2.5 mmol) in DMF (25 mL) was added NaH (60 % dispersion in mineral oil, 100 mg, 2.5 mmol). After stirring for 1 h, 1-azido-6-bromohexane (**29**, 0.42 g, 2.1 mmol) was added and the reaction mixture was stirred o/n, cooled to 0 °C, quenched with H_2O, extracted with Et_2O, dried ($MgSO_4$), filtered and concentrated. Purification of the residue by silica gel column chromatography (5% Et_2O in pentane) yielded the product (0.48 g, 1.5 mmol, 71%). ^{1}H NMR (400 MHz, $CDCl_3$) δ 7.56 – 7.43 (m, 4H), 7.40 – 7.28 (m, 3H), 6.99 – 6.81 (m, 2H), 3.96 (t, J = 6.4 Hz, 2H), 3.28 (t, J = 6.9 Hz, 2H), 1.80 (dq, J = 8.0, 6.4 Hz, 2H), 1.63 (p, J = 7.0 Hz, 2H), 1.58 – 1.38 (m, 4H). ^{13}C NMR (100 MHz, $CDCl_3$) δ 159.21, 133.16, 131.55, 128.42, 128.03, 123.72, 115.31, 114.61, 89.55, 88.14, 67.88, 51.49, 29.19, 28.92, 26.63, 25.80. IR: 2089 ($-N_3$).

1-Azido-4-(phenylethynyl)benzene (23). A mixture of 1-azido-4-iodobenzene (0.5 M in MTBE, 5 mL, 2.5 mmol), phenylacetylene (0.33 mL, 3 mmol) and triethylamine (1.7 mL) was sonicated with nitrogen bubbling though. $Pd(OAc)_2$ (5.6 mg, 0.025 mmol), PPh_3 (13 mg, 0.05 mmol) and CuI (2.4 mg, 0.013 mmol) were added and after 1.5 h the reaction mixture was diluted with Et_2O, washed with sat. aq. NH_4Cl, H_2O, dried ($MgSO_4$), filtered and concentrated. Purification of the residue by silica gel column chromatography (0 > 1% Et_2O in pentane) yielded the product (0.29 g, 1.3 mmol, 53%). ^{1}H NMR (400 MHz, $CDCl_3$) δ 7.56 – 7.47 (m, 4H), 7.40 – 7.29 (m, 3H), 7.02 – 6.94 (m, 2H). ^{13}C NMR (100 MHz, $CDCl_3$) δ 140.04, 133.20, 131.68, 128.50, 128.47, 123.20, 119.94, 119.19, 89.83, 88.81. IR: 2126 ($-N_3$).

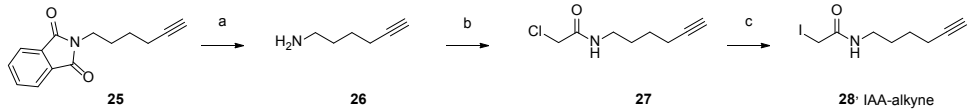

Scheme 4. Synthesis of IAA-alkyne (**28**). Reagents and conditions: (a) hydrazine hydrate, EtOH, 98%; (b) chloroacetic anhydride, N-methyl morpholine, 29%; (c) NaI, acetone, 56%.

5-Hexynylamine (26). To a suspension of N-(5-hexynyl)phtalimide (**25**, 1.1 g, 5.0 mmol) in EtOH (20 mL) was added hydrazine hydrate (1.2 mL, 20 mmol). The reaction mixture was refluxed for 1 h and cooled to rt. Sat. aq. $NaHCO_3$ was added and the pH of the aqueous layer was adjusted to 10 with NaOH (10 M), before being extracted with EtOAc (5 x 50 mL). The combined organic layers were acidified with 1 M HCl and concentrated to yield the title compound as a HCl salt (0.66 g, 4.9 mmol, 98%). ^{1}H NMR (400 MHz, MeOD) δ 2.98 (t, 2H), 2.32 - 2.28 (m, 3H), 1.90 - 1.77 (m, 2H), 1.67 - 1.59 (m, 2H).

2-Chloro-N-(hex-5-yn-1-yl)acetamide (27). To a cooled (0 °C) solution of **26** (654 mg, 4.9 mmol) in DCM (25 mL) was added N-methyl morpholine (2.2 mL, 20 mmol), followed by portionwise addition of chloroacetic anhydride (1.7 g, 10 mmol). The reaction was stirred o/n at rt, diluted with Et_2O (250 mL), washed with HCl (3 M), NaOH (1 M, 3x), brine, dried ($MgSO_4$), filtered and concentrated. Purification of the residue by silica gel column chromatography (10 > 50% EtOAc in petroleum ether) yielded the title compound (0.24 g, 1.4 mmol, 29%). ^{1}H NMR (300 MHz, $CDCl_3$) δ 6.69 (s, 1H), 4.01 (s, 2H), 3.29 (q, J = 6.8 Hz, 2H), 2.19 (td, J = 6.8, 2.6 Hz, 2H), 1.94 (t, J = 2.6 Hz, 1H), 1.75 – 1.42 (m, 4H). ^{13}C NMR (75 MHz, $CDCl_3$) δ 165.96, 83.86, 68.93, 42.70, 39.33, 28.39, 25.57, 18.07.

N-(Hex-5-yn-1-yl)-2-iodoacetamide (28, IAA-alkyne). To a solution of **27** (0.24 g, 1.4 mmol) in acetone (5.6 mL) was added NaI (0.43 g, 2.9 mmol) and the reaction mixture was stirred o/n.

The solvent was removed and purification of the residue by silica gel column chromatography (3:7 EtOAc:PE) afforded the title compound (210 mg, 0.79 mmol, 56%). ^{1}H NMR (400 MHz, $CDCl_3$) δ 6.76 (s, 1H), 3.73 (s, 2H), 3.35 – 3.25 (m, 2H), 2.24 (td, J = 6.9, 2.7 Hz, 2H), 1.99 (t, J = 2.6 Hz, 1H), 1.73 – 1.54 (m, 4H). ^{13}C NMR (100 MHz, $CDCl_3$) δ 167.51, 83.99, 68.95, 39.90, 28.30, 25.61, 18.14, -0.13.

1-Azido-6-bromohexane (29). To a heated (50 °C) solution of 1,6-dibromohexane (2.3 mL, 15 mmol) in DMF (20 mL) was added NaN_3 (0.65 g, 10 mmol). The reaction mixture was stirred at 55 °C o/n, cooled to rt, diluted with Et_2O and washed with NaOH (1 M), brine, dried ($MgSO_4$), filtered and concentrated. Purification of the residue by silica gel column chromatography (0 > 3% Et_2O in PE) yielded the product (0.42 g, 2.1 mmol, 21%). NMR ($CDCl_3$) corresponded to literature.[24]

Biochemical methods

General. Cy5-N_3 was synthesized according to previously published procedures[36] and biotin-N_3 was purchased from Bio-Connect Life Sciences. All buffers and solutions were prepared using Millipore water (deionized using a MilliQ A10 Biocel, with a 0.22 µm filter) and analytical grade reagents and solvents. Bio-Rad Imagelab v5.2.1 was used for gel analysis.

Click conditions.[15] To a solution of bovine serum albumin (0.1 g/L in 100 mM phosphate buffer (pH 8), 16.25 µL, 1.6 µg) was added IAA-alkyne **29** (200 µM in DMSO, 1 µL) or IAA (200 µM in DMSO, 1 µL) and the reaction mixture was incubated for 1 h at rt. Subsequently, to each sample, one of the different azides was added: Cy5-N_3, biotin-N_3, **1** or **2** (0.8 mM, 1 µL), followed by 0.75 µL of a premixed CuSO4/THPTA solution: CuSO4 (8 mM, 5 µL) and THPTA (20 mM, 10 µL). Finally, sodium ascorbate (100 mM, 1 µL) was added and the mixture was incubated for 1 h at 37 °C.
SDS-PAGE. The samples were denatured with Laemmli buffer (final concentrations: 60 mM Tris (pH 6.8), 2% (w/v) SDS, 10% (v/v) glycerol, 1.25% (v/v) β-mercaptoethanol, 0.01% (v/v) bromophenol blue) and resolved on a 10% acrylamide SDS-PAGE gel (180 V, 75 min). The Cy3/Cy5 channels were scanned on the ChemiDoc (Bio-Rad) before proteins were transferred to a 0.2 µm polyvinylidene difluoride membrane by Trans-Blot Turbo™ Transfer system (Bio-Rad). The membrane was washed with TBS (50 mM Tris, 150 mM NaCl) and TBST (TBS, 0.05% Tween 20) before blocking with 5% milk (w/v, Elk magere melkpoeder, FrieslandCampina) in TBST for 1 h, washed with TBST (3x), incubated with Streptavidin-HRP (Invitrogen), diluted 1:4000 in 5% BSA (TBST), washed with TBST (3x), washed with TBS and developed in the dark with 10 mL luminol, 100 µL ECL enhancer and 3 µL H_2O_2 (30%). The signal was detected on the ChemiDoc (Bio-Rad) using standard chemiluminescence settings.

References

1. Speers, A. E. & Cravatt, B. F. A tandem orthogonal proteolysis strategy for high-content chemical proteomics. *J. Am. Chem. Soc.* **127**, 10018–10019 (2005).
2. Fonović, M., Verhelst, S. H. L., Sorum, M. T. & Bogyo, M. Proteomics evaluation of chemically cleavable activity-based probes. *Mol. Cell. Proteomics* **6**, 1761–1770 (2007).
3. Leriche, G., Chisholm, L. & Wagner, A. Cleavable linkers in chemical biology. *Bioorganic Med. Chem.* **20**, 571–582 (2012).
4. Rudolf, G. C., Heydenreuter, W. & Sieber, S. A. Chemical proteomics: Ligation and cleavage of protein modifications. *Curr. Opin. Chem. Biol.* **17**, 110–117 (2013).
5. Szychowski, J. *et al.* Cleavable biotin probes for labeling of biomolecules via azide-alkyne cycloaddition. *J. Am. Chem. Soc.* **132**, 18351–18360 (2010).
6. Li, Y. *et al.* Derivatization reagents in liquid chromatography/electrospray ionization tandem mass spectrometry for biomedical analysis. *Biomed. Chromatogr.* **20**, 597–604 (2006).
7. Wuts, P. G. M. & Greene, T. W. *Greene's Protective Groups in Organic Synthesis, Fourth Edition*, 152. (2007).
8. Susumu, K. *et al.* Enhancing the stability and biological functionalities of quantum dots via compact multifunctional ligands. *J. Am. Chem. Soc.* **129**, 13987–13996 (2007).
9. Corey, E. J. & Venkateswarlu, A. Protection of Hydroxyl Groups as tert-Butyldimethylsilyl Derivatives. *J. Am. Chem. Soc.* **94**, 6190–6191 (1972).
10. Bailey, W. F., Luderer, M. R. & Jordan, K. P. Effect of solvent on the lithium-bromine exchange of aryl bromides: Reactions of n-butyllithium and tert-butyllithium with 1-bromo-4-tert-butylbenzene at 0 °C. *J. Org. Chem.* **71**, 2825–2828 (2006).
11. Geurink, P. P. *et al.* Design of peptide hydroxamate-based photoreactive activity-based probes of zinc-dependent metalloproteases. *Eur. J. Org. Chem.* 2100–2112 (2010).
12. Deno, N. C., Jaruzelski, J. J. & Schriesheim, A. Carbonium Ions. I. An Acidity Function (C0) Derived from Arylcarbonium Ion Equilibria. *J. Am. Chem. Soc.* **77**, 3044–3051 (1955).
13. Thompson, A. S., Humphrey, G. R., DeMarco, A. M., Mathre, D. J. & Grabowski, E. J. J. Direct conversion of activated alcohols to azides using diphenyl phosphorazidate. A practical alternative to Mitsunobu conditions. *J. Org. Chem.* **58**, 5886–5888 (1993).
14. Lieber, E., Rao, C. N. R., Chao, T. S. & Hoffman, C. W. W. Infrared Spectra of Organic Azides. *Anal. Chem.* **29**, 916–918 (1957).
15. Hong, V., Presolski, S. I., Ma, C. & Finn, M. G. Analysis and optimization of copper-catalyzed azide-alkyne cycloaddition for bioconjugation. *Angew. Chem. Int. Ed.* **48**, 9879–9883 (2009).
16. Backus, K. M. *et al.* Proteome-wide covalent ligand discovery in native biological systems. *Nature* **534**, 570–4 (2016).
17. Patterson, D. M., Nazarova, L. A. & Prescher, J. A. Finding the Right (Bioorthogonal) Chemistry. *ACS Chem. Biol.* **9**, 592–605 (2014).
18. Elliott, T. S., Bianco, A., Townsley, F. M., Fried, S. D. & Chin, J. W. Tagging and Enriching Proteins Enables Cell-Specific Proteomics. *Cell Chem. Biol.* **23**, 805–815 (2016).
19. Topolyan, A. P. *et al.* A triphenylcyclopropenylium mass tag: synthesis and application to ultrasensitive LC/MS analysis of amines. *Analyst* **141**, 3289–3295 (2016).
20. Breslow, R. & Yuan, C. The sym-Triphenylcyclopropenyl Cation, a Novel Aromatic System. *J. Am. Chem. Soc.* **80**, 5991–5994 (1958).
21. Breslow, R. Synthesis of the s-Triphenylcyclopropenyl Cation. *J. Am. Chem. Soc.* **79**, 5318 (1957).
22. Breslow, R., Lockhart, J. & Chang, H. W. The Diphenylcyclopropenyl Cation. Synthesis and Stability. *J. Am. Chem. Soc.* **83**, 2375–2379 (1961).
23. Phetrak, N. *et al.* Regioselectivity of Larock Heteroannulation: A Contribution from Electronic Properties

of Diarylacetylenes. *J. Org. Chem.* **78**, 12703 (2013).
24. Coutrot, F. & Busseron, E. Controlling the chair conformation of a mannopyranose in a large-amplitude [2] rotaxane molecular machine. *Chem. - A Eur. J.* **15**, 5186–5190 (2009).
25. Xu, R. & Breslow, R. 1,2,3-Triphenylcyclopropenium Bromide. *Org. Synth.* **74**, 72 (1997).
26. Aebersold, R. & Mann, M. Mass spectrometry-based proteomics. *Nature* **422**, 198–207 (2003).
27. Nesvizhskii, A. I. & Aebersold, R. Interpretation of Shotgun Proteomic Data. *Mol. Cell. Proteomics* **4**, 1419–1440 (2005).
28. Catherman, A. D., Skinner, O. S. & Kelleher, N. L. Top Down Proteomics: Facts and Perspectives. *Biochem. Biophys. Res. Commun.* **445**, 683–693 (2014).
29. Zhou, M., Paša-Tolić, L. & Stenoien, D. L. Profiling of Histone Post-Translational Modifications in Mouse Brain with High-Resolution Top-Down Mass Spectrometry. *J. Proteome Res.* **16**, 599–608 (2017).
30. Takemori, N. *et al.* Top-down/Bottom-up Mass Spectrometry Workflow Using Dissolvable Polyacrylamide Gels. *Anal. Chem.* **89**, 8244-8250 (2017).
31. Serim, S., Baer, P. & Verhelst, S. H. L. Mixed alkyl aryl phosphonate esters as quenched fluorescent activity-based probes for serine proteases. *Org. Biomol. Chem.* **13**, 2293–9 (2015).
32. Cevasco, G. & Thea, S. Kinetic Study on the Alkaline Hydrolysis of Some Tetracoordinate P″ Esters of 2,4-Dinitrophenol. J. Chem. Soc. PerkinTrans. 2. 1103–1105 (1994).
33. Edgington-Mitchell, L. E. *et al.* Fluorescent diphenylphosphonate-based probes for detection of serine protease activity during inflammation. *Bioorganic Med. Chem. Lett.* **27,** 254–260 (2017).
34. Wieczorek, A., Werther, P., Euchner, J. & Wombacher, R. Green- to far-red-emitting fluorogenic tetrazine probes – synthetic access and no-wash protein imaging inside living cells. *Chem. Sci.* **8**, 1506–1510 (2017).
35. Patterson, D. M., Nazarova, L. A. & Prescher, J. A. Finding the Right (Bioorthogonal) Chemistry. *ACS Chem. Biol.* **9**, 592–605 (2014).
36. Kvach, M. V. *et al.* A convenient synthesis of cyanine dyes: Reagents for the labeling of biomolecules. *Eur. J. Org. Chem.* 2107–2117 (2008).

Samenvatting

Het doel van het onderzoek dat de basis vormt voor dit proefschrift was om ons begrip van het endocannabinoïde system te verbeteren door gebruik te maken van de *activity-based proteomics* methode.

In **hoofdstuk 1** wordt het endocannabinoïde systeem geïntroduceerd. Het endocannabinoïde systeem bestaat uit twee cannabinoïde receptoren, hun liganden en de enzymen die de hoeveelheid van deze liganden reguleren. De cannabinoïde receptoren zijn ontdekt als de doelwitten van THC, de psychoactieve stof in marijuana. De endogene liganden van deze receptoren zijn de lipides 2-arachidonoylglycerol en anandamide. Het endocannabinoïde systeem reguleert verschillende neurologische processen en daarom zijn de endocannabinoïde enzymen interessante doelwitten voor nieuwe medicijnen. Voor dit proefschrift zijn de enzymen diacylglycerol lipase (DAGL) en het α/β hydrolase domein met proteïne 6 (ABHD6) nader bestudeerd.

Activity-based protein profiling (ABPP) is een krachtige methode in de zoektocht naar nieuwe medicijnen, vooral voor het endocannabinoïde systeem. De ABPP methode wordt uitgelegd in **hoofdstuk 2**. ABPP is een methode om het enzymatisch actieve deel van eiwitten te bestuderen. Deze methode gebruikt chemische *probes* die covalent reageren met actieve enzymen. Een label op de *probe* (zoals een fluorofoor of biotine) maakt het mogelijk om de doelenzymen te meten. Als het label voor analyse de affiniteit voor het doelenzym vermindert, dan kan een zogenaamde twee-staps *probe* worden gebruikt. Twee-staps *probes* hebben geen label maar een kleine bioorthogonale groep, die kan worden gebruikt om, nadat het doelenzym is gebonden, een label voor analyse te introduceren. Een scala aan *probes* is ontwikkeld voor verschillende type enzymen, waaronder serine hydrolases, proteases, deubiquitinases, glycosidases, cytochroom P450s en kinases. *Activity-based probes* (ABPs) zijn beschikbaar voor de meerderheid van de enzymen in het endocannabinoïde systeem.

Verschillende technieken zijn beschikbaar om *probe*-gebonden enzymen te visualiseren, identificeren en kwantificeren. Afhankelijk van het doel en type experiment, de beschikbare hoeveelheid eiwit, de hoeveelheid monsters en de eisen voor gevoeligheid, kan een geschikt analyseplatform worden gekozen. ABPP kan zo niet alleen worden toegepast om nieuwe doelwitten voor medicijnen te ontdekken, maar ook voor het bepalen van de sterkte en selectiviteit van remmers.

De ABPP methode wordt in **hoofdstuk 3** toegepast in de zoektocht naar nieuwe doelwitten voor medicijnen. Het endocannabinoïde systeem wordt beschouwd als een verdedigingssysteem in verschillende neurodegeneratieve ziektes. De ziekte van Niemann-Pick Type C is een neurodegeneratieve lysosomale stapelingsziekte waarin de rol van het endocannabinoïde systeem nog niet is onderzocht. In **hoofdstuk 3** is de serine hydrolase activiteit in hersenen van een Niemann-Pick Type C muismodel gemeten met ABPP en vergeleken met gezonde muizen. Er is geen verschil gevonden in een van de enzymen van het endocannabinoïde systeem. Met een gevoelige massaspectrometrie methode zijn evenwel drie enzymen gevonden waarvan de activiteit is verhoogd in de hersenen van het Niemann-Pick Type C muismodel vergeleken met die van gezonde muizen. Deze enzymen zijn interessant voor verdere validatie studies.

In dit onderzoek zijn twee verschillende massaspectrometrie methodes gebruikt voor de relatieve kwantificatie van *probe*-gelabelde enzymen. De eerste methode maakt gebruik van dimethyl labels, waarbij peptides worden gemodificeerd met isotoop gelabelde formaldehyde. Deze gelabelde peptides werden gemeten op een Orbitrap massaspectrometer. De tweede methode is label-vrij, waarbij peptides worden gemeten op een Synapt massaspectrometer en speciale software wordt gebruikt om het signaal van elk peptide te vergelijken in de verschillende monsters.

Hoofdstuk 4 bestaat uit een geoptimaliseerd protocol waarmee de selectiviteit van een remmer kan worden bepaald in een levend systeem. De ABPP methode wordt gebruikt met label-vrije kwantificatie. Als voorbeeld is de diacylglycerol lipase remmer DH376 toegediend aan muizen en vervolgens is de resterende enzymactiviteit in het brein, de lever, de nieren en de testes gemeten. Het protocol beschrijft het maken van lysaat van de organen, de incubatie met een *probe*, de verrijking van met *probe* gebonden enzymen, de voorbereiding van het monster, de metingen met behulp van chromatografie en massaspectrometrie, de verwerking van de ruwe data en de data analyse. De resultaten zijn 1) bewijs dat de remmer het doelenzym bindt in een levend systeem en 2) de identificatie van andere enzymen die worden geremd. Label-vrije kwantificatie blijkt zo dus de mogelijkheid te bieden om meerdere monsters onderling te vergelijken en het identificeren van meer peptides per eiwit, wat een verbetering is ten opzichte van eerder gebruikt technieken.

In **hoofdstuk 5** worden de synthese en het karakteriseren van de eerste gerapporteerde *quenched activity-based probe* voor een metabolische serine hydrolase beschreven. Een *quenched probe* is minder fluorescent totdat deze bindt aan het doelenzym. De *probes* bevatten een triazool urea als electrofiele val om covalent te binden aan de katalytische serine van het enzym. De eerste *probe* is actief tegen DAGLα, bevat een BODIPY-FL en 2,4-dinitroanaline als fluorophoor en *quencher* en is ongeveer driemaal minder fluorescent. De tweede probe bevat een Cy5 fluorophoor en cAB40 quencher en was 12-maal minder fluorescent. Deze *probe* kon endogeen ABHD6 labelen in lysaat, maar bleek niet in een cel te kunnen

doordringen.

In **hoofdstuk 6** zijn tweestaps *probes* voor DAGLα omschreven met verschillende groepen geschikt voor bioorthogonale chemie: een alkyn, alkeen of norborneen. Er zijn twee regio-isomeren van elke *probe* gemaakt en gekarakteriseerd met NMR analyse, ondersteund met DFT berekeningen. De selectiviteit van de *probes* is bekeken met ABPP en de norborneen *probe* is geselecteerd als de meest selectieve *probe* voor DAGL. Deze *probe* is een potente remmer van endogeen DAGLα en is succesvol gebruikt als tweestaps probe om DAGL te labelen met een fluorophoor in levende cellen.

Met dit alles beschrijft dit proefschrift verschillende nieuwe strategieën en verbeterd gereedschap voor de ABPP methode om de zoektocht naar nieuwe medicijnen te ondersteunen. In de loop van het onderzoek is een nieuwe label-vrije kwantificatie methode voor ABPP ontwikkeld. Dankzij deze methode kunnen meerdere monsters onderling worden vergeleken in hetzelfde experiment. Dit wordt geïllustreerd door de doelenzymen van de diacylglycerol lipase remmer DH376 in kaart te brengen in verschillende organen. Met deze methode is het gelukt nieuwe potentiële medicijn doelenzymen te identificeren voor de ziekte van Niemann-Pick Type C. Verder zijn nieuwe probes ontwikkeld, *quenched* en tweestaps, voor diacylglycerol lipases. Te verwachten valt dat deze label-vrije methode en dit nieuwe gereedschap zullen helpen in de ontwikkeling van nieuwe medicijnen voor ziektes waarin afwijkende 2-arachidonoylglycerol signalering een rol speelt.

List of publications

Mapping *in vivo* target interaction profiles of covalent inhibitors using chemical proteomics with label-free quantification

E. J. van Rooden, B. I. Florea, H. Deng, M. P. Baggelaar, J. Zhou, H. S. Overkleeft, and M. van der Stelt. *Nature Protocols,* **13**, 752-767 (2018).

Activity-Based Protein Profiling

E. J. van Rooden, A. T. Bakker, H. S. Overkleeft, and M. van der Stelt. *eLS,* **2018**, 1–9. doi:10.1002/9780470015902.a0023406.

Chemical proteomics analysis of endocannabinoid hydrolase activity in Niemann-Pick Type C mouse brain

E. J. van Rooden, A. C. M van Esbroeck, M. P. Baggelaar, H. Deng, B. I. Florea, A. R. A. Marques, R.Ottenhoff, R. G. Boot, H. S. Overkleeft, J. M. F. G. Aerts and M. van der Stelt. *Frontiers in Neuroscience*, **2018**, 12:440.

Design and synthesis of quenched activity-based probes for diacylglycerol lipase and α,β-hydrolase domain containing protein 6

E. J. van Rooden, M. Kohsiek, R. Kreekel, A. C. M. van Esbroeck, A. M. C. H. van den Nieuwendijk, A. P. A. Janssen, R. J. B. H. N. van den Berg, H. S. Overkleeft and M. van der Stelt. *Chemistry - An Asian Journal*, **2018**, doi: 10.1002/asia.201800452.

Two-step activity-based protein profiling of diacylglycerol lipase

E. J. van Rooden, R. Kreekel, T. Hansen, A. P. A. Janssen, A. C. M. van Esbroeck, H. den Dulk, R. J. B. H. N. van den Berg, J. D. C. Codée and M. van der Stelt. *Org. Biomol. Chem*., **2018**, doi: 10.1039/C8OB01499J.

A selective photoaffinity probe enables assessment of catnabinoid CB2 receptor expression and ligand engagement in human cells

M. Soethoudt, S. C. Stolze, M. V. Westphal, L. van Stralen, A. Martella, E. J. van Rooden, W. Guba, Z. V. Varga, H. Deng, S. I. van Kasteren, U. Grether, A. P. IJzerman, P. Pacher, E. M. Carreira, H. S. Overkleeft, A. Ioan-Facsinay, L. H. Heitman and M. van der Stelt. *J. Am. Chem. Soc.* **2018**, doi:10.1021/jacs.7b11281

Asymmetric Synthesis of Lysine Analogues with Reduced Basicity, and their Incorporation into Proteasome Inhibitors

G. de Bruin, E. J. van Rooden, D. Ward, C. Wesseling, A. M. C. H. van den Nieuwendijk, C. A. A. van Boeckel, C. Driessen, A. F. Kisselev, B. I. Florea, M. van der Stelt, and H. S. Overkleeft. *European J. Org. Chem.* **2017**, *39*, 5921–5934.

Chemical Proteomics Maps Brain Region Specific Activity of Endocannabinoid Hydrolases

M. P. Baggelaar, A. C. M. van Esbroeck, E. J. van Rooden, B. I. Florea, H. S. Overkleeft, G. Marsicano, F. Chaouloff, and M. van der Stelt. *ACS Chem. Biol.* **2017**, *12*, 852–861.

Towards broad spectrum activity-based glycosidase probes: synthesis and evaluation of deoxygenated cyclophellitol aziridines

S. P. Schröder, J. W. van de Sande, W. W. Kallemeijn, C.-L. Kuo, M. Artola, E. J. van Rooden, J. Jiang, T. J. Beenakker, B. I. Florea, W. A. Offen, G. Davies, A. J. Minnaard, H. Aerts, J. D. Codee, G. van der Marel, and H. S. Overkleeft. *Chem. Commun.* **2017**, *53*, 12528–12531.

Chemical Swarming: Depending on Concentration, an Amphiphilic Ruthenium Polypyridyl Complex Induces Cell Death via Two Different Mechanisms

B. Siewert, V. H. S. van Rixel, E. J. van Rooden, S. L. Hopkins, M. J. B. Moester, F. Ariese, M. A. Siegler, and S. Bonnet. *Chem. - A Eur. J.* **2016**, *22*, 10960–10968.

Synthesis of 6-Hydroxysphingosine and α-Hydroxy Ceramide Using a Cross-Metathesis Strategy

P. Wisse, M. A. R. de Geus, G. Cross, A. M. C. H. van den Nieuwendijk, E. J. van Rooden, R. J. B. H. N. van den Berg, J. M. F. G. Aerts, G. A. van der Marel, J. D. C. Codée, and H. S. Overkleeft. *J. Org. Chem.* **2015**, *80*, 7258–7265.

The novel β2-selective proteasome inhibitor LU-102 synergizes with bortezomib and carfilzomib to overcome proteasome inhibitor resistance of myeloma cells

M. Kraus, J. Bader, P. P. Geurink, E. S. Weyburne, A. C. Mirabella, T. Silzle, T. B. Shabaneh, W. A. van der Linden, G. de Bruin, S. R. Haile, E. van Rooden, C. Appenzeller, N. Li, A. F. Kisselev, H. Overkleeft, and C. Driessen. *Haematologica.* **2015**, *100*, 1350–1360.

Structure-based design of β1i or β5i specific inhibitors of human immunoproteasomes

G. de Bruin, E. M. Huber, B. T. Xin, E. J. van Rooden, K. Al-Ayed, K. B. Kim, A. F. Kisselev, C. Driessen, M. van der Stelt, G. A. van der Marel, M. Groll, and H. S. Overkleeft. *J. Med. Chem*. **2014**, *57*, 6197–6209.

Curriculum Vitae

Nederlands

Eva Jacoba van Rooden werd op 21 april 1990 geboren te Leiden, Nederland. Ze behaalde haar diploma aan het Stedelijk Gymnsasium Leiden in 2008. In hetzelfde jaar startte zij haar bachelor *Life Science & Technology* aan de Universiteit Leiden en TU Delft. Haar eindstage heeft zij verricht bij de vakgroep *Bio-organic Synthesis* aan de universiteit Leiden. Hier heeft zij onderzoek gedaan naar een stereoselectieve aldol reactie in de synthese route van het natuurproduct cyclophellitol. Tijdens haar studie was zij hoofddocent scheikunde bij Stiching Studiebegeiding Leiden.

In 2012 startte zij met de master *Chemistry* aan de Universiteit Leiden. Tijdens haar onderzoeksproject, in de groep van prof. dr. H. S. Overkleeft, heeft zij zich gericht op de synthese en karaktarisatie van covalente proteasoom remmers. Tijdens een buitenlandstage aan de ETH Zürich in de groep van prof. dr. Donald Hilvert heeft zij onderzoek gedaan naar de dynamiek van een eiwitmantel. In 2014 behaalde zij haar master diploma *cum laude*.

In maart 2014 begon zij als promovenda aan de Universiteit Leiden in de vakgroep Bio-organische Synthese. Na een jaar vervolgde ze het onderzoek in de nieuwe vakgroep Moleculaire Fysiologie, onder begeleiding van prof. dr. Mario van der Stelt. Zij heeft haar onderzoek gepresenteerd op posters op CHAINS in Veldhoven (2014 en 2017), het Reedijk symposium in Leiden (2017) en op een ABPP congres in Oxford (2015).

Curriculum Vitae

English

Eva Jacoba van Rooden was born on April 21st 1990 in Leiden, the Netherlands. She graduated high school in 2008 at *Stedelijk Gymnsasium Leiden*. In the same year she started her bachelor Life Science & Technology at Leiden University and Delft University of Technology. She did an internship in the Bio-organic synthesis group at Leiden University, where she researched a stereoselective aldol reaction in the synthesis route of the natural product cyclophellitol. During her studies she was a chemistry teacher at *Stiching Studiebegeiding Leiden*.

In 2012 she started the master Chemistry at Leiden University. During her research internship in the group of prof. dr. H. S. Overkleeft, she synthesized and characterized covalent proteasome inhibitors. During an internship at ETH Zurich in the group of prof. dr. Donald Hilvert she researched the dynamics of a protein container. In 2014 she received her master of science with honors.

In March 2014 she started as a PhD candidate at Leiden University in the Bio-organic Synthesis group. After a year she continued this research in the new group Molecular Physiology, under the supervision of prof. dr. Mario van der Stelt. She presented parts of her research as poster presentations at CHAINS in Veldhoven (2014 and 2017), the Reedijk symposium in Leiden (2017) and at the annual ABPP meeting in Oxford (2015).